University of Tennessee, Knoxville
TRACE: Tennessee Research and Creative Exchange

Doctoral Dissertations | Graduate School

5-2013

Experimental and Theoretical Investigations of Lube Oil Performance and Engine Friction

William Fredrick Rohr
wrohr@utk.edu

Follow this and additional works at: https://trace.tennessee.edu/utk_graddiss

 Part of the Tribology Commons

Recommended Citation

Rohr, William Fredrick, "Experimental and Theoretical Investigations of Lube Oil Performance and Engine Friction. " PhD diss., University of Tennessee, 2013.
https://trace.tennessee.edu/utk_graddiss/1774

This Dissertation is brought to you for free and open access by the Graduate School at TRACE: Tennessee Research and Creative Exchange. It has been accepted for inclusion in Doctoral Dissertations by an authorized administrator of TRACE: Tennessee Research and Creative Exchange. For more information, please contact trace@utk.edu.

To the Graduate Council:

I am submitting herewith a dissertation written by William Fredrick Rohr entitled "Experimental and Theoretical Investigations of Lube Oil Performance and Engine Friction." I have examined the final electronic copy of this dissertation for form and content and recommend that it be accepted in partial fulfillment of the requirements for the degree of Doctor of Philosophy, with a major in Mechanical Engineering.

Ke Nguyen, Major Professor

We have read this dissertation and recommend its acceptance:

Jay I. Frankel, Roberto S. Benson, David K. Irick

Accepted for the Council:

Carolyn R. Hodges

Vice Provost and Dean of the Graduate School

(Original signatures are on file with official student records.)

Experimental and Theoretical Investigations of Lube Oil Performance and Engine Friction

A Dissertation

Presented for the

Doctor of Philosophy Degree

The University of Tennessee, Knoxville

William Fredrick Rohr

May 2013

Copyright © 2013 by William Fredrick Rohr

All rights reserved.

DEDICATION

To my father, Kim, and my mother, Vicky, for their unwavering support.

ACKNOWLEDGEMENTS

I would like to thank my advisor, Dr. Ke Nguyen, for his patience and wisdom throughout the course of the project. I would also like to thank my co-advisor, Dr. Bruce Bunting, for his technical guidance and support. I express appreciation for the feedback and input from my graduate committee members, Dr. Jay Frankel, Dr. Roberto Benson, and Dr. David Irick, and thank them for their time and effort. I would like to thank Jun Qu at the Oak Ridge National Lab for allowing me to use the falling ball viscometer and showing me how to use the device. Furthermore, I would like to thank Dr. Jim Szybist, Scott Eaton, and Adam Youngquist for their help in the initial phase of my project. In addition, I would like to thank my colleagues Will Brookshear, Vitaly Prikhodko, Mike Bunce, and Scott Curran for their friendship and support.

This work was supported by the Department of Energy and conducted at ORNL under contract number DE-AC05-00OR22725. I would like to thank the DOE Vehicle Technologies, Fuel Program, and Lubricants Subs-Program for contributing financially to this project. Finally, I thank the Massachusetts Institute of Technology for loaning the line contact friction rig.

ABSTRACT

The feasibility of using a motored small, single-cylinder 517 cc Hatz 1D50 diesel engine to evaluate lube oil performance and engine friction at conditions typical for a fired engine is investigated in the present study. In addition a commercial engine modeling software, AVL Excite Power Unit, is used to predict the effects of lube oil formulations on the engine friction of the same engine. The motored engine can be operated with and without compression and with and without the engine oil pump. Lube oil performance is evaluated for 19 different lube oils by using either instantaneous motoring torque (motoring torque over an engine cycle) or friction mean effective pressure (fmep). For the latter, lube oil performance is evaluated by plotting fmep as a function of lube oil dynamic viscosity calculated using the Vogel's equation with the mid-stroke cylinder liner temperature. Furthermore, the contribution of engine components such as piston/rings/liner assembly, connecting rod, journal bearings, valve train, and oil pump to the total engine friction is determined by removing components from the engine. For the model, the engine friction is estimated only for two different lube oil formulations via a friction coefficients measured with a line contact friction rig.

Lube oil performance is examined for several different base oils, commercial oils with additives, and commercial oils without additives by comparing the motoring torque over a range of viscosities. Engine friction represented by either peak instantaneous torque or fmep is found to decrease with decreasing viscosity; whereas the effect of additives is to increase friction observed as an increase in peak instantaneous torque or fmep. The contribution of several engine components to the total engine friction is also examined by comparing the fmep obtained for different engine configurations. The piston, piston rings, and journal bearings are found to contribute the most to total engine friction, followed by the valve train, and finally the oil pump. The fmeps for two

different oils, a 15W40 base oil and a commercial 15W40 oil, predicted by the simulation are generally lower than those for the motored Hatz engine and highly dependent on the modified Stribeck curve.

TABLE OF CONTENTS

LIST OF TABLES

LIST OF FIGURES

CHAPTER 1
INTRODUCTION

Automobiles, first introduced in 1886, have become a common part of modern life with just over a billion vehicles in operation worldwide in 2010 or roughly 1 vehicle for every 7 people [1-3]. The overwhelming majority of automobiles are powered by internal combustion engines (ICE) which are approximately 43% efficient and use fossil fuels that produce pollution when burned [4, 5]. According to the reports published by the U.S. environmental protection agency (EPA) in 2009, passenger vehicles consume approximately 40% of all U.S. oil and contribute 20% of all U.S. CO_2 emissions [6]. Because of the prevalence of automobiles and the associated inefficiencies and pollution, the U.S. government has been mandating the auto industry to produce vehicles with better fuel economy since the 1970's through the Corporate Average Fuel Economy (CAFE) standard and gas guzzler tax [7, 8]. The Obama administration is further increasing fuel efficiency standards by setting standards of 35.5 equivalent miles per gallon (mpg) by 2016 and 54.5 mpg by 2025, as shown in Figure 1.1 [9-11]. This is a dramatic increase in fuel efficiency from the 2009 average U.S. light duty short wheel base fuel efficiency of 23.8 mpg and passenger car domestic new vehicle fuel efficiency of 32.9 mpg [12]. Meeting these fuel efficiency goals requires many improvements and new designs of the automobile. One method to increase fuel economy is the reduction of engine friction. Friction accounts for as much as 15% of engine losses and a 10% reduction of these losses would lead to a 1.5% reduction in fuel consumption [13]. This increase in fuel efficiency is a small part of the fuel efficiency goals set by the U.S. government. However, improved lube oils can be quickly implemented to existing vehicles to have an immediate effect; whereas, new vehicle and engine designs will take time to be introduced into the market [14].

Also, It is likely that new engines will be designed to use lower viscosity oils to reduce friction losses, i.e., lowering lube oil viscosity from 10W40 to 0W10 has shown a 4% improvement in fuel economy [15].

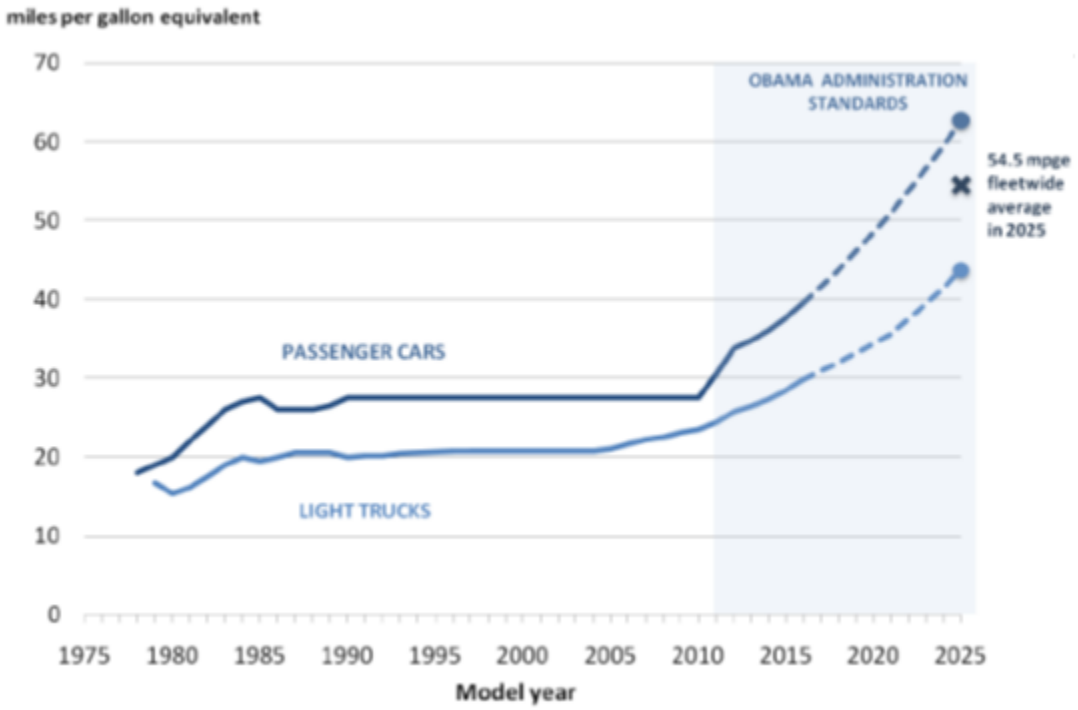

Figure 1.1: Historical and future CAFE fuel efficiency standards [9, 16]

1.1 Engine lubrication and lube oil properties

The lubricant used in an engine is vital as it serves many functions such as: separating surfaces in relative movement, flushing away particles, cooling the engine, and reducing wear and friction [17, 18]. The lube oil must perform all these functions while remaining stable for long durations. The performance of the oil is optimized through complex oil formulations, fitting the correct viscosity

range for the engine application, and understanding how the oil performs over the range of engine conditions expected. Because of all these demands, the engine lubricant has become complex over the past 100 years.

The friction coefficient for a lubricating oil and the materials the oil separates is usually described using the Stribeck diagram, in which the friction coefficient, *f*, is plotted as a function of the Stribeck number, ηU/P; where η is the dynamic viscosity of the oil, U is the relative speed between lubricated surfaces, and P is pressure or load between the surfaces. Lubricated friction is divided into three regimes: boundary, mixed, and hydrodynamic lubrication. Boundary lubrication is characterized by surface to surface contact at lower values of the Stribeck number, during which the friction coefficient is predominately determined by the contacting surfaces. Here, the friction coefficient is a constant and relatively large value of approximately 0.1 [19, 20]. Mixed lubrication occurs as the surfaces begin to separate but there is still some intermittent surface to surface contact. During mixed lubrication, the friction coefficient drops sharply to a minimum, on the order of 0.001 to 0.0002 [19, 20]. As the pressure in the oil produced by speed and viscosity overcomes load, hydrodynamic lubrication occurs and there is complete separation of the two surfaces by a fluid film. In this regime, the coefficient of friction increases in a log linear rate and is a function of hydrodynamic lubrication laws.

The typical internal combustion engine consists of a slider-crank mechanism used to compress gases in the combustion chamber, a valve train to open and close valves for cylinder gas exchange, a fuel delivery system, and various supporting equipment such as oil and water pumps. The slider-crank mechanism consists of the crankshaft, connecting rod or conrod, piston, and piston pin. The crankshaft and connecting rod are supported by journal bearings which experience large loads due to the downward force during combustion.

However, the speed within the bearing is relatively steady over an engine cycle and hydrodynamic lubrication is predominant during normal steady state operation. For the piston to perform the task of compressing air and contain the combustion gasses, a tight seal between the piston and liner is required. This seal is made by small clearances between the piston/liner and with flexible rings housed in grooves on the piston. The piston experiences a range of speeds and loads during a cycle causing all forms of lubrication to be present. The valve train operates at relatively slow speeds and some high loads causing mostly boundary lubrication. The load, relative surface speed, and lubricant viscosity at each surface interaction determine the mode of friction causing the various engine components to operate in different modes of lubrication. Because of this, each component contributes differently to total engine friction. The piston/ring/liner assembly has the highest friction and the journal bearings have the second highest [21]. The percent contribution of each component to total engine friction also changes with engine speed and temperature. The variety of friction modes from component to component and over engine conditions is the major problem faced when studying engine friction.

1.2 Engine friction measurement

The internal combustion engine operates in all regimes of lubrication and many of the frictional interactions are significantly influenced by compression and combustion. This makes the measurement of engine friction and particularly friction measurement at specific locations within the engine difficult. The measurement of engine friction can be categorized into three methods: fired engine tests, motored engine tests, and engine component tests. Fired engine tests measure friction in a fully functional engine with combustion. These tests are complex and costly requiring highly accurate cylinder pressure and torque measurements to calculate total engine friction. Motored engine tests measure

friction as the torque required to spin the engine. These tests offer the ability to examine the friction contribution of various components within the engine but actual engine conditions are lost. Engine component tests measure friction through setups designed to simulate engine components, a reciprocating piston in a fixed liner for example. These engine component tests offer great insight to friction mechanisms over the conditions in which they are performed but actual engine conditions are again lost and even more so than in motored engine tests.

Motored engine friction does not include some combustion effects which are vital to engine friction. These include: cylinder pressure loading on the piston, the piston and cylinder liner temperatures, and the exhaust blowdown phase at the start of the exhaust process [22]. Lower cylinder pressures reduce the load from the piston rings on the liner surface and thus lower rubbing friction. The lack of combustion causes lower engine temperatures and changes the temperature relationship between engine components, affecting lube oil viscosity and changing friction properties. Exhaust gases are denser than air therefore motored pumping loads are less. On the other hand, motored engine friction tests allow for component removal to isolate the frictional contribution of various components. By motoring an engine, and sequentially dismantling it, each component of the mechanical and accessory friction contributions can be determined [22]. While this method offers insight to the contribution of various components, the same general problems with motored tests, such as actual engine conditions not being represented, affect this method as well. In fact these problems can be magnified by removing components. In component removal methods the accuracy is affected by the different engine conditions between the two tests such as cylinder pressure, lubricant oil pressure and temperature, and other operating variables [23].

1.3 Theoretical modeling of engine friction

Theoretical modeling of engine friction began as early as 1886 when Osborne Reynolds first developed the equation for hydrodynamic lubrication in a journal bearing [24]. Theoretical engine friction models typically focus on particular friction regimes, such as boundary, mixed, and hydrodynamic, and can be divided primarily into empirical or Reynolds equation based models. Empirical models typically calculate friction mean effective pressure as a function several engine parameters and coefficients derived from experimental engine data [22, 25]. On the other hand, Reynolds based simulations calculate friction over an engine cycle from the pressure field in the oil film [20-27].

Both of the types of models have varying complexity. The simpler models consider components as rigid and viscosity as constant. Whereas, the more complex models consider oil temperature changes due to friction, changes in viscosity caused by temperature, pressure, and shear rate, and even deformation of the components [28]. Modeling engine friction becomes complex when all these changes and all the engine components are considered together. Therefore, models have been developed to focus on specific types of friction or conditions and are used in conjunction to find total fiction. In more complex component models, sub-models are used to break the complexity into more manageable parts and reduce computational time [29].

1.4 Scope of Investigation

The current study investigates the feasibility of using a small, inexpensive and simple motored engine friction rig to evaluate lube oil performance while approaching fired engine conditions. In conjunction, the feasibility of using the commercial engine design software AVL Excite Power Unit to predict engine friction is also investigated. The motored engine friction rig is constructed using

a small 517 cc single-cylinder, air-cooled engine operated with/without compression and with/without engine auxiliaries with engine temperatures ranging from 20 to 100 °C.

The motored engine friction rig evaluates lube oil performance primarily through friction mean effective pressure (fmep) as function of oil viscosity calculated from measured engine temperatures and motoring torque. Secondarily, lube oil performance and the effect of engine conditions on motoring torque as a function of crank angle are investigated. This is accomplished by measuring motoring torque as a function of engine crank angle using a torque meter and encoder while also measuring engine temperatures and oil pressure. The torque is measured every half degree to create instantaneous torque plots which are averaged for the calculation of friction mean effective pressure. Engine temperatures measured at mid-front of the cylinder liner are used to calculate oil viscosity using Vogel's equation. Engine temperatures are increased to approach fired engine conditions with heaters installed in the oil sump and an enclosure built around the engine. The feasibility of the motored engine rig to evaluate lube oil performance is investigated by testing various lube oils.

The objective for the simulation portion of this study is to predict the motored-engine friction tests using the commercial engine design software AVL Excite Power Unit. This requires the creation of a model of the Hatz 1D50 in the software and oil friction coefficients to be measured experimentally for model input. The friction coefficient for a lube oil is measured using a line contact friction measurement device which can be operated over various speeds, loads, and temperatures. The model considers friction through a friction coefficient equation which expresses the friction coefficient as a function of speed. This equation is fitted to the friction coefficient data measured for oil as a function of

speed for a fixed applied normal load and temperature. A simulation is performed for each friction coefficient curve to predict motored engine friction rig results at the corresponding applied loads and temperatures resulting in several fmep data points at different temperatures and loads. These simulation results are compared to experimental results to examine the friction prediction capabilities of the software.

CHAPTER 2
LITERATURE REVIEW

The current study examines the performance of lube oils experimentally and theoretically. To aid in these endeavors, a background and literature survey is presented in this chapter. A general background of friction and lubrication is provided in Section 2. Section 3 is an overview of engine friction and lubrication. Since the properties of the lubricants play such a pivotal role in engine friction, lubricant properties are discussed in Section 4. Finally, Sections 5 and 6 discuss the measurement and theoretical modeling of engine friction, respectively.

2.1 General background of friction and lubrication

Friction is a part of everyday life that is often taken for granted but mechanical work could not be transmitted without it. Friction has many useful benefits but it has disadvantages as well. Energy is lost to overcome friction and wear from friction shortens the life of materials and machines. In the 1960s, a study performed by the Jost Committee of the British Department of Education and Science showed that approximately £515 million per year was wasted from friction related losses, a significant part of Britain's national annual expenditures in 1966 of approximately £15 billion [19, 30, 31]. Because of this, it was determined by the British government that the study of friction was financially important. Therefore, it was considered useful if the losses could be reduced through a research program on friction, wear, and lubrication, and to accomplish this, the importance of the research had to be conveyed to the public. It was thought that the best way to convey the importance of this research was to unify these classical subjects and to give it a new name — tribology [19].

Friction losses can be lessened through material selection, surface finishes, surface coatings, and lubrication. Lubricants perform several functions

but friction is mainly reduced through hydrodynamic lubrication. Hydrodynamic lubrication occurs as surfaces in relative motion are separated by a lubricant fluid film through pressure generated in the fluid due to the relative motion of the surfaces. Hydrodynamic lubrication is a function of the speed between surfaces, the load pressure on the fluid, and the viscosity of the fluid.

Viscosity is a material property which describes a liquids resistance to shear. Viscosity can be imagined as the shear stress block but with one surface moving as described by Figure 2.1. Viscosity has units of stress multiplied by time or force over area multiplied by time. Poises are typically units for dynamic viscosity, η, but are usually given as centipoise, cP, with one centipoise equal to one milli-Pascal second, mPa.s. Kinematic viscosity, ν, is dynamic viscosity divided by density and has units of Stokes or centistokes, cS. Lubricant viscosity changes very strongly with temperature and pressure [32].

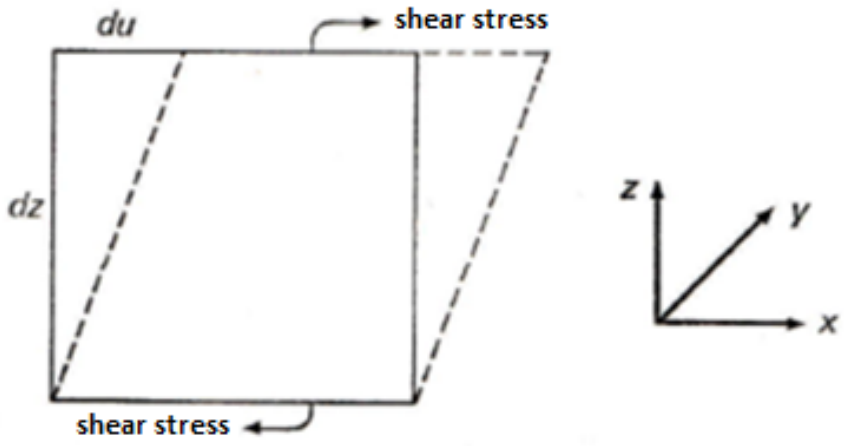

Figure 2.1: Shear stress diagram [32]

2.1.1 General friction theory

Ancient civilizations used primitive bearings to reduce friction, showing some understanding of friction. However, theories explaining the fundamental aspects behind friction were not developed by scientist such as Amontons, Coulomb, and Moring until as early as 1699 [33]. The early theories attributed friction to the interlocking of asperities or surface protuberances similar to the teeth of gears interlocking. This theory was referred to as the roughness hypothesis as the rougher surfaces with larger protuberances would interlock with greater force. The benefit of this theory was that it offered an explanation to why the friction coefficient is independent of apparent surface, i.e., the area of the surface observable with the naked eye.

A more modern theory of the cause of friction is called the adhesion hypothesis which considers friction to be caused by adhesion between the two surfaces. This theory was first postulated long before it came into favor in the 1920s; for it required the understanding of surface chemistry for validation [33]. Initially this theory was considered to be incorrect because at the time the surface area as seen by the naked eye was considered to be the actual area of contact between the surfaces. If this were the case, the friction coefficient should change with area which is easily disproven. However, the area as seen by the naked eye or the apparent area is not the true area of contact because the surfaces are not flat at the microscopic scale. Instead, the surfaces are rough and only contact at asperities. With the realization that the contact at asperities is the actual area, A_r, of contact between surfaces, the adhesion hypothesis was accepted because this allowed for the friction coefficient to be independent of the apparent area, A_a, as can be seen in Figure 2.2. Currently a mix of the roughness and adhesion theories is considered to be more correct, with asperities deforming, shearing, scratching, sliding, and adhering.

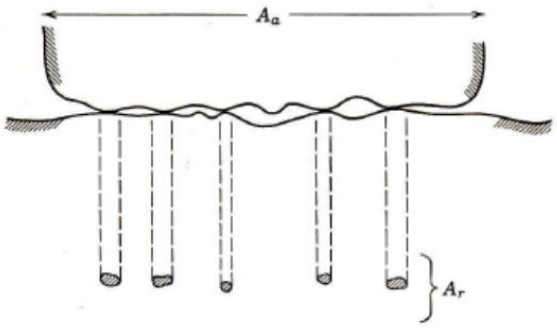

Figure 2.2: Comparison of apparent area (A_a) and actual area (A_r) for surfaces in contact [33]

2.1.2 Wear

Wear occurs as friction causes deformation and breakage in the materials in contact. Lubricants can serve to reduce friction but generally the lubricant preforms better as a wear reducer than friction reducer [19]. This can be related to the nature of wear. Wear can be separated into the following categories: adhesive, abrasive, fatigue, and corrosive [32]. Adhesive wear occurs when asperities contact and weld together. The metal around the adhesive contact becomes work hardened and thus making adhesive contact is stronger than the cohesion of the base metal which causes chunks to be ripped out of the base metal. Adhesion is the reason dissimilar metals are usually chosen to run together as they do not weld together easily [32]. Abrasive wear is akin to sand paper on wood. Relative hard particles rub against softer material and scratches are formed. During this form of wear, polishing can also occur just like sand paper on wood which can lower friction and be favorable in some instances. Fatigue wear occurs as asperities are repeatable deformed and eventually break, like a paper clip being bent over and over. Corrosive wear occurs as chemical reactions break down the wear surface. This can also have positive effects as

some light corrosion can reduce adhesion. Rarely do these forms of wear occur alone but usually all have a compounding effect on each other. Adhesive wear forms particles that cause polishing which reduces the protective oxides on the metal surfaces which can cause further adhesive wear and etc. The prevention of these compounding interactions is the most important role of the lubricant as it flushes away particles to filters where they are removed and chemical compounds are added to the lubricant (additives) to replace the worn protective layers.

2.1.3 Lubricated friction

The friction coefficient for a lubricating oil and the material it separates is usually described using the Stribeck diagram shown in Figure 2.3. The Stribeck diagram has a vertical axis showing the friction coefficient, f, and a horizontal axis of ηU/P, referred to as the Stribeck number; where η is dynamic viscosity, U is speed, and P is pressure load. For small values of the Stribeck number, the friction coefficient is relatively large with a value of approximately 0.1 [19, 20]. This lubrication regime is termed boundary friction and surface to surface contact occurs with the surface to surface contact being the dominant factor in determining the friction coefficient. As the surfaces are in contact and boundary friction occurs, the friction coefficient is stable. Lubrication moves from boundary to mixed lubrication as the Stribeck number increases. Mixed lubrication occurs when there is some surface to surface contact at asperities but there is also surface separation at pockets of lubrication. During mixed lubrication, the friction coefficient drops very sharply to a minimum, on the order of 0.001 to 0.0002 [19, 20]. Beyond mixed lubrication, hydrodynamic lubrication occurs and there is complete separation of the two surfaces by a fluid film. In this regime, the coefficient of friction gradually increases in a log linear rate as a function of hydrodynamic lubrication laws.

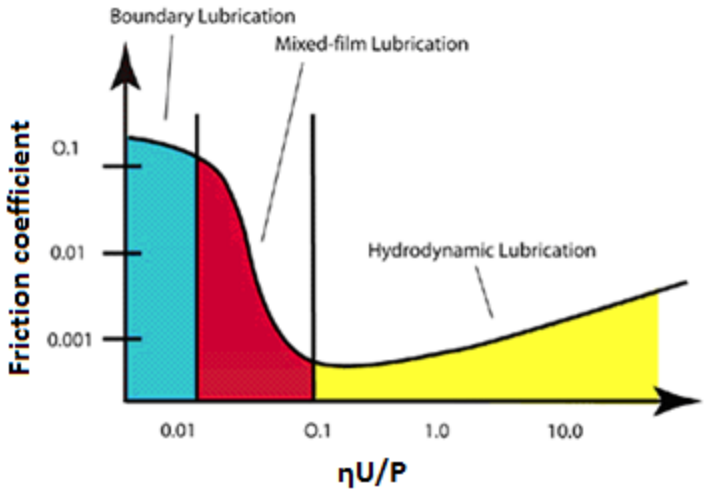

Figure 2.3: Stribeck diagram showing three distinct lubrication regimes: boundary, mixed, and hydrodynamic lubrication [34]

2.1.4 Hydrodynamic friction

Hydrodynamic friction occurs when a lubricating fluid film separates two surfaces in relative motion. The driving forces of the separation can be described by three effects: the wedge, squeeze, and stretch effects [19]. The wedge effect occurs as the liquid lubricant is driven from a large gap into a progressively smaller gap by the surface movement, as seen in Figures 2.4 and 2.5 where h represents the oil film height with $\bar{h}$ being the oil film height at maximum pressure, P_{max}, and U is speed. The wedge effect creates pressure within the fluid and separates the surfaces. This pressure effect was first clarified experimentally by a British railroad engineer Beauchamp Tower in 1883 when he noticed an increase in journal bearing pressure with increasing speed [35, 36]. From Tower's experiments, Osborn Reynolds formulated the mathematical theory of hydrodynamic lubrication in 1886 [24].

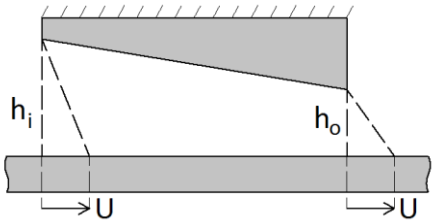

Figure 2.4: Converging wedge velocity profile

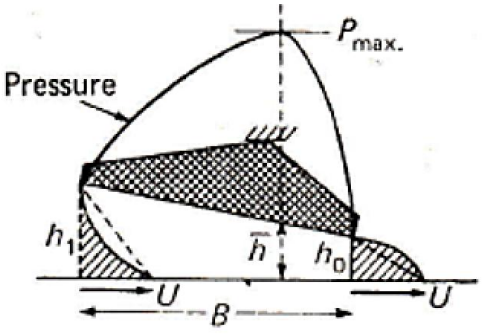

Figure 2.5: Converging wedge velocity profile with pressure [32]

The squeeze effect refers to the generation of pressure as two surfaces are pushed together, thus squeezing the oil film. This form of pressure generation is not sustainable as eventually the surfaces would come in contact or the pressure will slow the surfaces enough to negate the pressure effect. This form of lubrication pressure effect can be seen in small-end bearings [19]. The stretch effect is the pressure generation due to the variation of surface velocity from place to place during deformation of the lubricated surface and can generally be ignored in all but elastic surfaces such as rubber or in some machining applications [19]. These effects and Reynolds work form the fundamental theories behind many engine friction simulations.

2.2 Overview of internal combustion engine friction

2.2.1 Introduction

The frictional characteristics of internal combustion engines are highly dependent on the fundamental aspects of engine operation. Therefore, it is critical to have an understanding of these fundamentals. Common combustion cycles for the automotive engine include the Otto or diesel cycles. The present study focuses on diesel engines but the general friction characteristics are similar for both engines. The ideal air-standard diesel cycle, shown in Figure 2.6, consists of the isentropic compression with work in (1 to 2), reversible constant pressure heating with heat in, q_{in}, (2 to 3), isentropic expansion with work out (3 to 4), and the reversible constant volume cooling with heat out, q_{out}, (4 to 1).

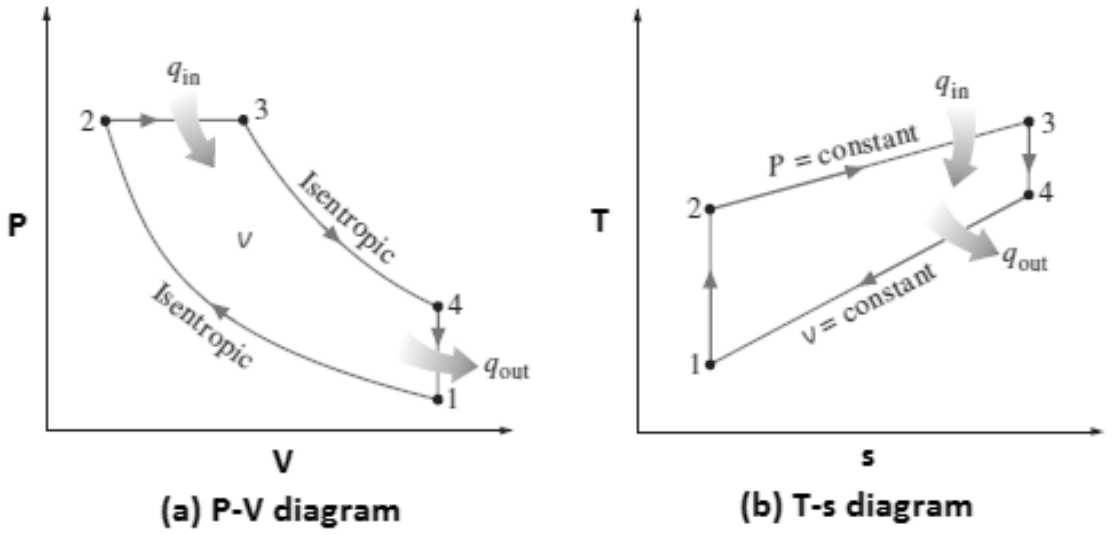

Figure 2.6: P-V (a) and T-s (b) diagrams for ideal air-standard Diesel cycle [37]

The work used to compress the air is provided in the form of kinetic energy of a rotating mass (flywheel). The flywheel transfers energy through a crank-slider to a piston, where the piston moves within the cylinder compressing the air which results in an increase in cylinder temperature. The temperature is high enough that when diesel fuel is injected into the cylinder, it combusts as it mixes with the heated air. The combustion provides energy which pushes the piston downward which rotates the flywheel and driveshaft. In a four-stroke cycle, the piston would then be pushed upwards in the cylinder through the momentum of the flywheel expelling exhaust through a valve. Once the piston reaches the top of its stroke, momentum from the flywheel will pull it back down through the cylinder drawing in fresh air through an intake valve with valves typically opened and closed via a mechanical valve train also driven by flywheel momentum and combustion forces. When the piston returns to the bottom of the stroke, the cycle is ready to begin again.

The slider-crank mechanism previously mentioned consists of a crankshaft, connecting rod (conrod), and the piston. The crankshaft is supported and connected to the conrod with journal bearings. These bearings can experience large loads due to the downward force during combustion but the speed within the bearing is relatively steady during the engine cycle. For the piston to perform the task of compressing air and contain the combustion gases, a tight seal between the piston and liner is required. This seal is made by small clearances between the piston/liner and with flexible rings housed in grooves on the piston. The piston experiences a range of speeds, loads, and temperatures during a cycle making frictional characterization here particularly difficult. The valve train sees relatively slow speed and some high loads. These load and speeds described above determine the mode of friction each component experiences, as listed in Table 2.1 [17].

Table 2.1: Engine components and their respective modes of lubrication

Components	Lubrication Mode	Oil Properties Related to Lubrication Mode
Bearings, bushings	Hydrodynamic	Oil viscosity
Gears, piston rings, and liners	Hydrodynamic to boundary	Oil viscosity, additives
Cam, valve train	Mixed to boundary	Oil additives

Diesel engines are inefficient with only approximately 40% of the total energy produced by combustion being used as work as shown in Figure 2.7. The rest is lost to heat, friction, or auxiliaries such as oil pumps, water pumps, and etc. Friction accounts for approximately 10% of the total loss and, of that, 50% can be attributed to the piston, connecting rod, and rings with the rings being the cause of the majority. Holmberg et al. [21] reported the division of engine friction losses as approximately 45% to piston assembly, 30% to bearings and seals (hydrodynamic lubrication), 15% to valve train (mixed lubrication), and 10% to pumping and hydraulic viscous losses.

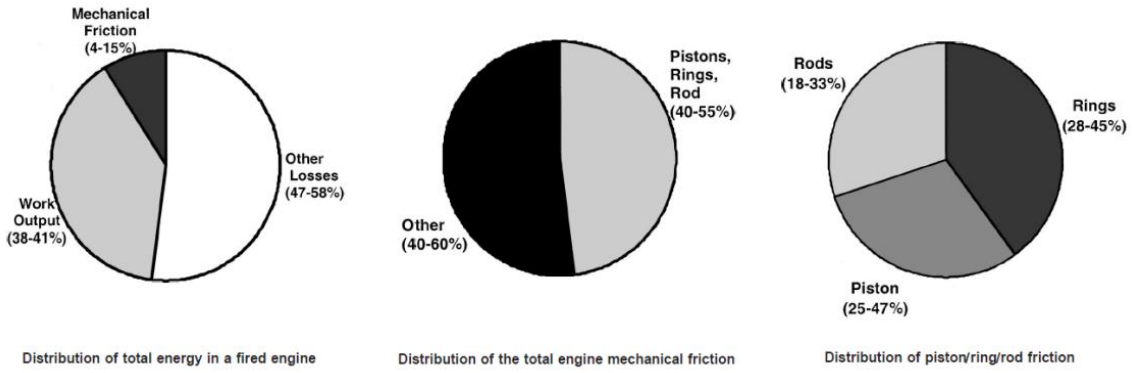

Figure 2.7: Distribution of engine losses and friction (rod = connecting rod) [4]

2.2.2 Friction characterization

A common term used to describe engine friction loss is friction mean effective pressure (fmep). Friction mean effective pressure is a way to characterize engine friction across engines of different sizes through measurement or calculation. To calculate fired engine fmep, the indicated mean effective pressure (imep) and the brake mean effective pressure (bmep) are measured with fmep being the difference between the two. Indicated mean effective pressure is calculated from the cylinder pressure and represents power produced by combustion pressure. Brake mean effective pressure is calculated from the output torque and represents engine output after losses.

Friction mean effective pressure can also be measured as the torque required to spin or motor an engine. Friction mean effective pressure, given as

$$fmep = \frac{4\pi\tau}{V_s}, \tag{2.1}$$

is found by multiplying the measured torque, τ, by 4π and dividing by the swept volume, V_s, of the engine [25]. Friction force and fmep at the mid-stroke have a

linear relationship [38]. Friction mean effective pressure allows for the examination of friction as a function of engine speed, load, or oil viscosity. This also allows for the performance of a lube oil to be plotted as a function of some parameter, typically viscosity.

2.2.3 Engine operation effect on friction and wear

The operation of the engine, type of service, type of fuel, and the characteristic and age of the engine can change oil properties [17]. Engine oil properties are not inherently constant and change for a variety of reasons including shear of polymers in the oil which lowers viscosity, fuel diluting the oil, additives being used, and various forms of deposits. Oil can also nitrate from nitrogen in the air or nitrogen reaction products. Lower molecular weight molecules in the oil can evaporate thereby thickening the oil [17]. For diesel engines, soot is the most detrimental contaminant which is caused by fuel rich pockets during the combustion process from the direct injection of the fuel [17] . The soot is carried to the bulk oil through the oil film under the piston rings. The amount of soot present in used lube oil is likely to rise as longer drain intervals and emission strategies like exhaust gas recirculation (EGR) become increasingly common [17].

Soot has two major effects on the oil; it thickens the oil and increases wear. Oil that is too thick causes flow problems and this leads to improper lubrication. However, the effect of soot on wear remains controversial [17]. Furuhama and Takiguchi [23] showed that frictional forces increased substantially at points as load increased, particularly during the last half of the compression stroke and the first half of the expansion stroke. But these points are relatively brief when considered over the entire cycle.

2.2.4 Engine power cylinder friction and wear

The power cylinder components can be divided into eight tribological systems: liner/ring, ring and ring groove, liner/piston skit, piston pin and piston bore, piston pin and connecting rod, piston skirt/piston pin (articulated piston), piston crown/liner (articulated piston), and oil ring/expander [17]. Wear of these components results in excessive oil consumption and blow-by. Oil consumption is associated with excessive radial wear of the top compression ring and cylinder wear at top dead center (TDC). Properly designed piston skirts will have sufficient oil film between surfaces and often employ coatings for oil film separation break down. Extreme operating conditions can alter clearances and cause changes in the friction [17]. It is now increasingly recognized that transient skirt elastic deformations during the engine cycle are another key factor in piston skirt lubrication. Furthermore, piston deformations and misalignments can deform the rings and increase friction due to a change in the oil film [39].

The piston/ring/liner components account for the majority of the power cylinder losses with the rings account for the majority of the entire piston/ring/liner losses [23]. The piston/ring/liner assembly for a single-cylinder engine was found to contribute approximately 30 to 50% of fmep according to Gauthier et al. [38]; with the percent contribution decreasing with increasing speed. The piston/rings/liner area is the most difficult lubrication area to study and predict. It is also the most important area. The rings serve as a gas seal while removing and applying oil to the liner and also serve as a means to transfer heat away from the piston. The difficulties in predicting piston/ring/liner assembly friction are becoming even more complex as engines evolve to produce more power at a given size while reducing fuel consumption and extending oil drain intervals. To facilitate the prediction of piston/ring/liner assembly friction, it is important that precise knowledge of the lubricant behavior is known [38].

Friction of the piston/ring/liner assembly occurs in every regime. Boundary friction was found to occur over significant parts of the stroke at low RPM and at the dead centers at all RPMs according to Gauthier et al. [38]. Liner design and manufacturing is important for liner wear. Bhushan [17] reports that bore distortion can lead to excessive wear and during boundary lubrication liner surface finishes influence wear. Linear wear occurs mostly through adhesion and abrasion [17]. Adhesive wear occurs mostly at the top ring reversal due to the breakdown of the oil film and boundary lubrication. This can be controlled via the additives in the oil and anti-wear films produced by the additives. Abrasion occurs from particles in the oil film. The rings filter these particles and the size of the particle is related to the thickness of the film as controlled by the ring. Due to all these effects the piston ring and liner tribological interactions are the most difficult to model.

2.2.5 Journal bearing friction and wear

Journal bearings have been reported to account for 25 to 40% of the total mechanical power losses [40]. Journal bearings being used in automotive engines experience a wide range of temperatures, loads, and speeds. Because of this, all forms of lubrication can possibly occur. However, during typical operation, the journal bearings operate in the hydrodynamic regime. It is only at low speeds or high loads where mixed and boundary friction occur, possible during start-up.

2.3 Engine lubricant properties

2.3.1 Introduction

The automotive lubricant performs many vital functions within the engine [17]. Engine lube oils separate surfaces in relative motion. Additives to the oil serve many functions such as providing different surface chemistry for the

tribological surfaces, load capacity of the fluid, viscosity-temperature, and viscosity-pressure dependence [18]. Through a chemical or physical process these additives serve to create a surface layer which protects surfaces, from wear and degradation, and/or reduces the friction coefficient [18]. Wear reduction additives within the lubricant create a surface layer to reduce wear when the oil film can no longer separate these surfaces. There are additives which combat the buildup of varnish, deposits, and sludge. Other additives help prevent rust, corrosion, and various chemical attacks. Friction reduction additives react with engine surfaces to lower friction. The oil also carries heat and debris to locations where they can be removed from the engine [17]. The oil must perform all these functions while remaining stable for long durations. This is accomplished through complex formulations, fitting the correct viscosity range for the application, and understating how the oil performs over the expected range of conditions.

Friction in an engine originates from several components operating at widely different conditions of temperatures, shear rates, loads, and surface speeds. Each component can operate in the boundary, mixed, and hydrodynamic lubrication regimes with the regime being determined by position in the cycle, load, temperature, speed, and etc. Thus, these components may experience various combinations of hydrodynamic, mixed, and boundary lubrication during engine operation. For each of these regimes, the factors that govern friction can be different [41]. The wide variety of tribological conditions in the engine make the selection of the optimal base oil, oil additives, and engine component surface composition and geometry to yield low friction a complex problem [41].

2.3.2 Oil standards

Several oil standards are used to select an oil which is appropriate for a given application. The most basic is the SAE grade [42]. This classification is reported for an oil as SAE XX for single grade oils or SAE XXWXX for multigrade oils, where XX represents a number. Each number represents a range of viscosity at 0°F if the number is attached to the W, which stands for winter, and 210°F if not. Figure 2.8 provides an example of SAE grade viscosities, whereas Table 2.2 provides SAE grade viscosity requirements. The viscosity requirements for an engine lube oil are defined by a set of standards called SAE J300.

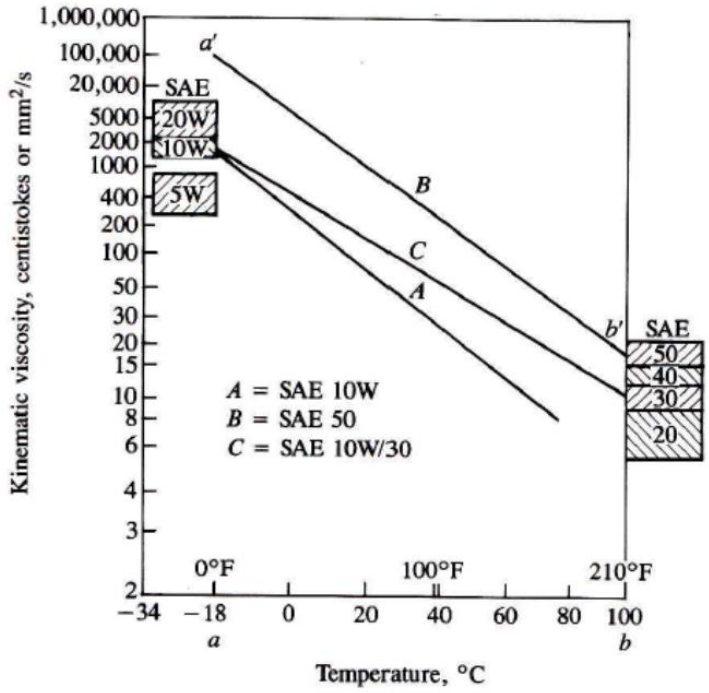

Figure 2.8: Example viscosity ranges of various SAE grades [42]

Table 2.2: Viscosity requirements for SAE grades [32]

SAE viscosity number	Viscosity units	Viscosity range			
		at 0°F		at 210°F	
		min.	max.	min.	max.
5W	Centipoises	–	1200	3·9	–
10W	„	1200[a]	2400	3·9	–
20W	„	2400[a]	9600	3·9	–
20	Centistokes	–	–	5·7	9·6
30	„	–	–	9·6	12·9
40	„	–	–	12·9	16·8
50	„	–	–	16·8	22·7

[a]The minimum measured viscosities at 0°F for 10W and 20W oils can be waived provided the measured kinematic viscosity at 210°F for such oils is not below 4·2 sC and 5·7 cS respectively.

The rheological properties of oil for hydrodynamic lubrication are primarily defined by kinematic viscosity measured at 40°C and 100°C. Oil viscosity is not a function of temperature alone and standard viscosity measurements might not be adequate under extreme conditions. Oil performance at extreme conditions is measured via Cold Cranking Simulator (CCS) and High-Temperature, High-Shear (HTHS) viscosities. These tests follow procedures defined by several ASTM standards with ASTM D5293 and ASTM D4684 defining CCS procedures and ASTM D4683 being the standard test method for HTHS viscosity measurements [17].

Single grade oils of the same SAE grade may not have the same viscosity temperature relationship, i.e., the rate of viscosity change over temperature differs across oils of the same grade. Therefore it is important to have a parameter which provides information of this relationship. For this, the viscosity index was created by Dean and Davis in 1929 [43]. The viscosity index was created by considering two different oils, both with approximately the same

viscosity at 210°F (98.9°C) but different viscosities at 100°F (37.8°C). The oil with a lower viscosity at 100°F, and thus a smaller change in viscosity over temperature, was said to have a viscosity index (VI) of 100. The oil with the higher viscosity at 100°F, and thus a larger change in viscosity over temperature, was said to have a VI of 0. The VI equation, given as

$$VI = 100\left(\frac{\nu_L - \nu_U}{\nu_L - \nu_H}\right), \qquad \textbf{(2.2)}$$

is used to find the VI of an oil. Values in the equation are based on measured viscosity values for the oil of interest and viscosity values of two reference oils taken from a table according to the ASTM D2270 standard [43]. Table values for ν_L (low VI oil viscosity at 100°F) and ν_H (high VI oil viscosity at 100°F) are found by matching viscosities at 210°F (98.9°C). The term ν_U in Equation 2.2 is the viscosity of the oil in question at 100°F. Figure 2.9 provides a graphical representation of this method, whereas Figure 2.10 provides examples of the viscosity temperature relationship of oils with various VIs. Notice there are oils with VI values greater than 100. This is common and is more likely the norm in modern multigrade oils.

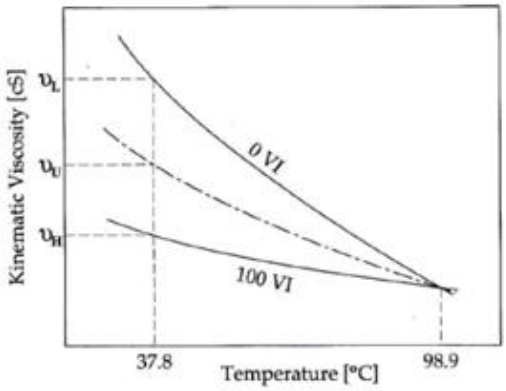

Figure 2.9: Viscosity index calculation [43]

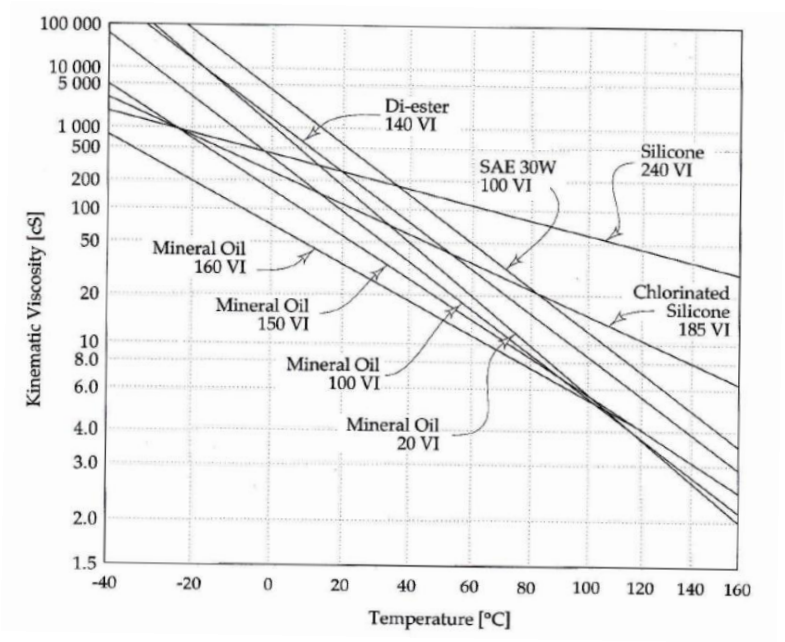

Figure 2.10: Viscosity comparison of oils with various VI values [43]

2.3.3 Oil formulation

The many functions of a modern lubricant are the result of careful blending of chemical additives and carefully refined base stocks [4]. Engine base oils are typically mineral oils, synthetic, or partial synthetic. Mineral oils are produced from crude oil in a distillation process which separates the hydrocarbons in the crude oil by molecular weight. Synthetic oils are lubricants primarily developed from a chemical process to buildup low-molecular-weight hydrocarbons whose molecular-weight distribution range is small and whose chemical structure is resistant to degradation [17]. Partial synthetic oils are oils whose base stocks are enhanced in some degree. The heat transfer properties of synthetic base oils can be very different from mineral oils with synthetic oils being able to sustain higher oil temperatures [17].

To base oils, additives are added which serve a variety of purposes. The antioxidant is the most important oil additive [17]. This is a sacrificial agent that reduces the tendency of the engine oil to oxidize, thicken, and form varnish. Anti-wear additives, like Zinc DialkylDithioPhosphate (ZDDP), in the oil react with the physical surfaces within the engine to create protective layers which prevent wear and corrosion. There are detergents added to the oil which neutralize acids formed during combustion or overheating of the oil, protect engine components from corrosion, inhibit deposits from forming, and help keep surfaces clean [17]. Insoluble contaminants, varnish, and sludge are controlled with dispersants. Friction modifiers are added to reduce engine friction. Defoamers are added to reduce the foaming of oil as foam can alter the oils load carrying and viscometric properties. Viscosity modifiers or viscosity index improvers change the base oils viscosity-temperature relationship so that the oil remains sufficiently fluid when cold but does no become too thin when hot. Pour-point depressants help to keep the oil from solidifying at very low temperatures. All these additives work together to prolong the life of the engine while also seeking to improve efficiency.

Engine oils were originally a single SAE grade but multigrade oils were developed to aid in cold start conditions. Thin oils have a slower rate of change in viscosity over temperature than thicker oil. It is advantageous for the thicker oil to have a flatter slope, like the thinner oil, so that the viscosity does not drop as drastically at lower temperatures. This can be accomplished by thickening a thin oil with polymers, usually methacrylate [32]. This effectively shifts the viscosity-temperature profile of the thin oil upward along the viscosity axis to make a multigrade oil, as shown in Figure 2.11. The addition of a small amount of a long-chain polymer, the length of which may be a million times the diameter of a water molecule, to a Newtonian fluid gives the most desirable lubricant by increasing the fluid film pressure and as a result the load carrying capacity increases and the friction factor decreases [44].

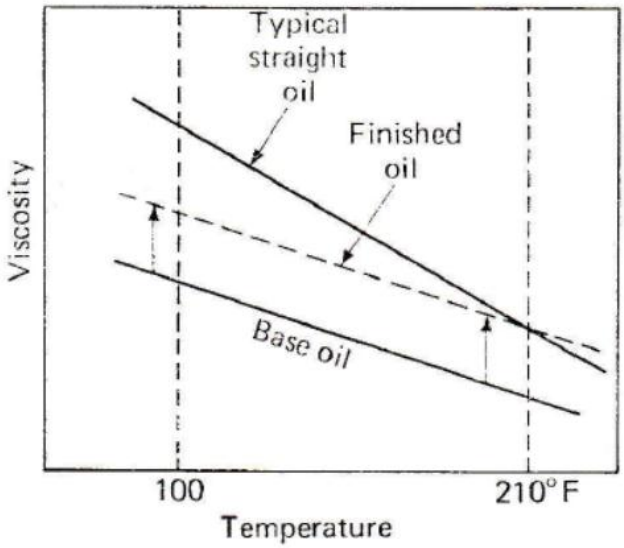

Figure 2.11: Polymer thickened oil viscosity change [32]

2.3.4 Equations for viscosity

A common equation to predict oil viscosity for a given temperature is the Walther's equation [43],

$$(\nu + a) = bd^{1/T^c}, \tag{2.3}$$

where ν is kinematic viscosity, T is temperature, and a, b, c, and d are constants. The four constants in the Walther equation are found by fitting the equation to experimental data for an oil. Another common equation used to predict oil viscosity for a given temperature is Vogel's equation [32],

$$\eta = ae^{\frac{b}{T-c}}, \tag{2.4}$$

where η is dynamic viscosity, T is temperature, and a, b, and c are experimentally-determined constants. The constant a has units corresponding to

viscosity and gives the 'inherent viscosity' of the oil [32]. The constant b, referred to as the 'viscosity-variation' term, influences the rate of change in viscosity with temperature and increases with oil thickness. Although the Walther's equation is the viscosity-temperature conversion used in the ASTM D341 standard, Vogel's equation is generally regarded in literature as more accurate.

The Vogel equation accurately predicts viscosity at low shear rates and atmospheric pressure. However, not all lube oils are Newtonian fluids and viscosity at a given temperature can change due to high shear rates and pressures. This is why limits on cold cranking simulator (CCS) and high-temperature, high-shear (HTHS) viscosities are specified for SAE engine oil viscosity grades [25]. To account for pressure effects on viscosity, Barus's equation [20],

$$\eta = \eta_{atm} e^{\kappa P}, \tag{2.5}$$

can be used. Barus's equation expresses pressure compensated viscosity, η, as a function of pressure, P, viscosity at atmospheric pressure, η_{atm}, and a pressure coefficient, κ, found experimentally. This equation was applied by Coy [20] and Allmaier et al. [28, 40, 45] to account for pressure effects on viscosity when modeling engine friction. Furthermore, Taylor [46] discusses the Barus equation and the Cross equation, used to account for shear rate effects on viscosity, and provides some constants for use with the Barus equation based on base oil, pressure, and temperature.

2.3.5 Oil ageing

Engine oils age as they are used. Some of the aging occurs from such things as temperature and pressure and these effects can be reversible. However, others are not reversible and occur for a variety of reasons. Additives in the oil are depleted as they perform their function. Multigrade oils can shear

thin due to the breakdown of Viscosity Index (VI) improver polymers. Irreversible changes in viscosity are also linked to the formation of oxidation products, soot, base oil evaporation, VI improver degradation, and fuel dilution. The 'in engine' actual oil viscosity is determined not only by temperature, pressure, and shear rate, but also through oil ageing. The various forms of oil aging are summarized in Table 2.3 [47].

Table 2.3: Parameters affecting oil viscosity

Viscosity change	***Reversible***	***Irreversible (oil aging)***
Increase	Pressure	Oxidation products
	-	Soot formation
	-	Base oil evaporation
Decrease	Temperature	VI improver degradation
	Shear	Fuel dilution

The oil aging associated with viscosity index (VI) improving polymers is of particular importance. Viscosity index improving polymers (multi-grade oils) can deform, both temporarily and permanently. Because of this, lube oils typically behave as pseudoplastic fluids, fluids which thin with increase shear rate, which means the oil viscosity can become lower due to shear stresses. This occurs in multigrade oils due to shear stress changing the structure of the VI improver molecules. The polymers chains used as VI improvers can be stretched under shear stress and a reduction of oil viscosity is observed. When the stress is suppressed, this phenomenon can be reversible (temporary shear) or definitive

(permanent shear) if the molecule is broken by the shear stress [38]. These polymers also provide lower friction loss and energy consumption compared to a Newtonian fluid at a given viscosity as calculated from measured temperatures [38]. This is misleading though because the polymer oil will have a decrease in effective viscosity due to shear thinning that was not likely accounted for in normal viscosity measurements.

Gauthier et al. [38] took care to quantify the effective thickening loss in the piston/rings contact area. Gauthier et al. show that friction increases around top and bottom dead centers for polymer thickened oils and attributes this to break-down of the polymer causing an increase in temperature and lower viscosity, boundary friction coefficient modification due to surface effects, and higher efficiency of the scraper ring with the polymer thickened oil. In fact, aged oil can have a friction mean effective pressure (fmep) change of a few percent [25]. This is akin to a temperature change of a few degrees Centigrade. Consequently, a low VI straight mineral oil and a high VI oil containing a metallic dispersant and anti-wear additive both can give less friction than a high VI straight mineral oil of the same viscosity. Similarly, an oil thickened with a polymeric VI improver can give less friction under mild conditions but more friction under sever conditions than a high VI straight mineral oil of the same viscosity as measured at the 80°C test temperature in a capillary viscometer [48].

Shayler et al. [25] showed that a change in viscosity of a few hundred mPa.s at low temperatures which results in fmep change of a few percent. Typically, formulation changes and oil aging over a few hours of engine operation gave rise to friction changes of a few percent. This shows that while two oils may have the same viscosity/temperature relationship under low stress conditions, the same two oils may not have the same viscosity/temperature relationship under the stresses experience in an operating engine.

2.4 Engine friction measurement

2.4.1 Introduction

Engine friction measurement can be categorized into three methods: fired engine tests, engine component tests, and motored engine tests. Fired engine tests measure friction in an engine with combustion. These tests typically measure total engine losses by calculating the difference between indicated work, obtained from a cylinder pressure trace, and measured work, calculated from the output torque of the engine. These calculations require highly accurate measurements of cylinder pressure and output torque, making these tests complex and expensive. Component tests measure friction through setups designed to simulate specific engine components, i.e., a section of a piston ring reciprocated against a cylinder liner section. These tests offer great insight to friction over the conditions in which they are run but actual engine conditions are lost. Motored engine tests are an intermediate between fired engine and component tests. Motored engines directly measure total energy losses for an engine via motoring torque and offer the ability to focus on the friction contribution of various engine components. Fired engine conditions are lost with these tests but with modifications, such as heating the engine, a motored engine can be made to approach fired engine conditions. Lube oil performance measured by a motored engine is typically reported as friction losses versus oil viscosity which is calculated from engine temperatures.

2.4.2 Temperature measurement and control

There are several engine locations which are of key importance when measuring engine temperatures so that oil viscosity can accurately be described. The oil sump, engine case, and liner are some likely places. The liner

temperature or particularly the oil film temperature at the liner can be difficult to measure for several reasons. The temperature of the oil film is not constant throughout the liner and depends on the engine position in the engine cycle. Friction, combustion, ring pressure, and heat transfer from other components all have an effect on the oil film temperature. It is also significant where the temperature is measured. For example, not only will the temperature at the top dead center (TDC) and the mid-stroke be different but the forces and speeds experienced will be different as well. All of this information is important when examining or predicting the performance of the lube oil.

Gauthier et al. [38] measured cylinder oil film temperature in a motored engine directly via two thermocouples embedded in the liner. This was accomplished with thermocouples (T/C) made from two concentric electrodes mounted flush with the liner. As the piston rings travel over the electrodes, wear causes the materials to join and form a thermocouple junction. Measurements taken with this method show significant spikes in temperature for a fired engine as the rings and certain skirt positions pass over the thermocouples as shown in Figure 2.12. However, significant temperature spikes are not observed in a motored engine as seen in Figure 2.13. This is an example of the accuracy lost when measurements are made with a motored engine.

Gauthier et al. [38] attributed the spikes in cylinder oil film temperature for the fired engine to three things: greater heat transfer due to a thinner oil film, metal to metal contact, and heat generation due to oil shearing. It is difficult to quantify actual contributions from the three mentioned causes, but the thinner oil film and close approximation of the hot surface is likely the largest contributor. Some areas of normal gap also show spikes which could be contributed to thermal expansion of parts and wear marks found in these areas support this conclusion [38]. The oil film thickness affects the temperature in several ways.

First, the gap is smaller so there is less insulation between hot engine components. Second, the thinner oil films have more shear which generates heat as well. Gauthier et al. [38] also showed that the oil film temperature was found to be 5°C lower for an oil of lower viscosity, attributing this observation to less oil shear heating effect for the lower viscosity oil. During these tests the coolant was maintained at 80°C and the oil gallery was self-regulated. For a fired engine at half load, the mean oil film temperature was found to be approximately 20°C above the oil gallery temperature of 109.5°C. The motored test produced a mean oil film temperature of approximately 15°C less than this even though oil gallery temperatures were hardly different [38].

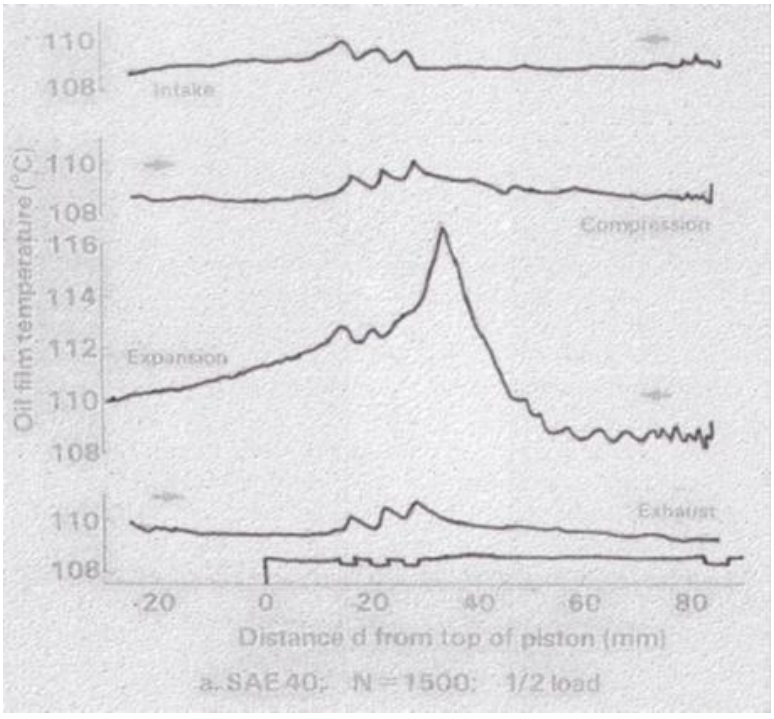

Figure 2.12: Cylinder liner oil film temperature measured via liner embedded T/C for fired engine operating at ½ load [38]

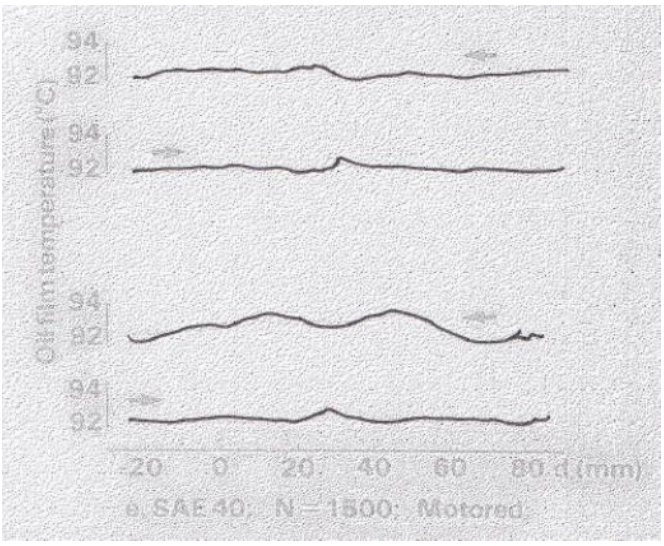

Figure 2.13: Cylinder liner oil film temperature measured via liner embedded T/C for motored engine [38]

Since oil viscosity and thus engine friction is highly dependent on engine temperatures, the ability to operate a motored engine at a desired temperature is important. Shayler et al. [25] housed the test engine in a thermally insulating cell. The engine could be cooled with the cell and by circulating chilled ethylene glycol around the engine coolant circuit and through finned copper tubing inserted in the oil sump to simulate cold starts or cooler engine temperatures. If higher temperatures were desired, the housing could simply be left open. Shayler et al. [25] concluded that with their setup the engine could be chilled from laboratory ambient temperature to a temperature of -25°C in approximately 4 hours.

Leong et al. [49] examined engine friction by cooling and motoring a 2400 cc in-line four-cylinder engine. The engine was cooled to temperatures of -20°C by housing the engine in a cooling enclosure and cooling the surrounding air. The engine was then motored reaching temperatures as high as 60°C. Several

engine temperatures and three cylinder wall temperatures were measured during warm up of the engine, as shown in Figures 2.14(a) and 2.14(b). The oil sump and main oil gallery show a delayed temperature increase; whereas, all other components show an immediate increase in temperature. The cylinder wall mid-stroke temperature was the highest of the three liner temperatures.

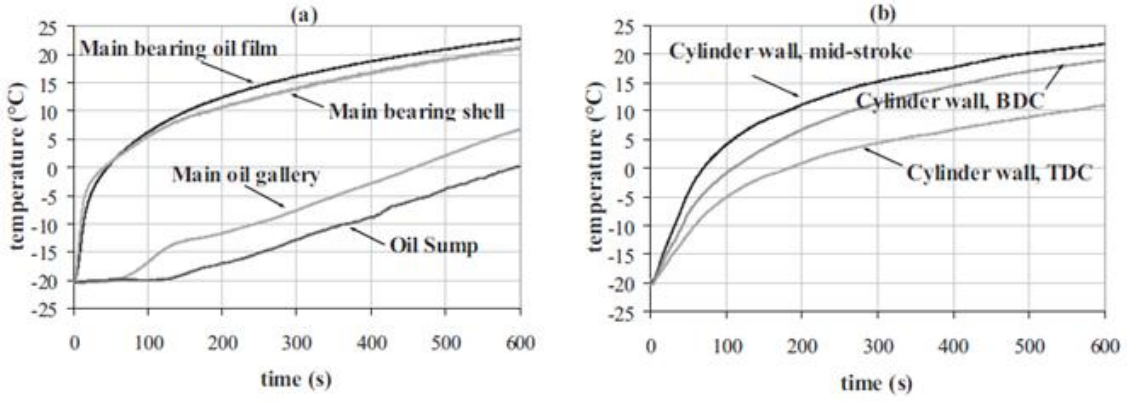

Figure 2.14: Engine temperatures observed in a chilled motored engine [49]

Several of these temperatures were used to calculate oil viscosity and engine fmep was plotted in a log-log plot as shown in Figure 2.15. The delayed temperature rise of the oil sump and oil gallery causes an abrupt decrease in fmep initially and a linear decrease thereafter. The fmep plotted with mid-stroke and main bearing oil film viscosities shows a consistent linear decrease in fmep throughout the test and much higher fmep at a given viscosity. Mid-stroke and main bearing are shown to be the best locations to evaluate fmep as a function of viscosity since the results from the two locations are comparable, showing a consistent decrease, and representing oil temperatures at friction points. Of these two, the mid-stroke is the most important because of the variations of

tribological conditions over the piston stroke and the large contribution to friction by the piston/liner/rings assembly. Furuhama and Takiguchi [23] measured cylinder wall temperatures at the top ring for three crank angle positions as well and likewise found the mid-stroke temperature to be best for characterizing engine friction.

Leong et al. [49] examined the engine fmep as a function of liner mid-stroke viscosity for three oils over three motoring speeds and two initial temperatures of -20 and 0°C. The results shown in Figure 2.16 exhibit a linear decrease in friction mean effective pressure with decreasing viscosity for all conditions and oils examined in a log-log plot. The oils examined follow a similar trend regardless of oil weight and do not show any significant difference in fmep for a given viscosity.

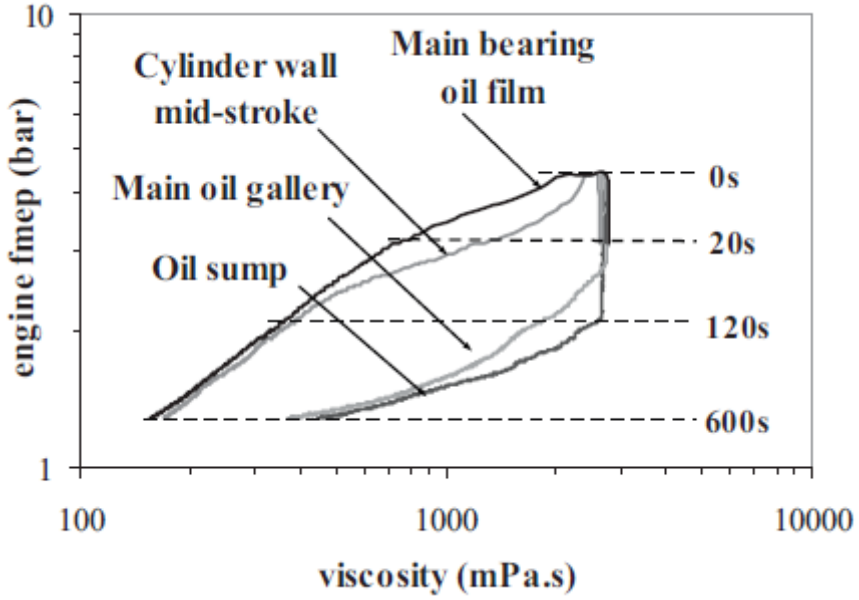

Figure 2.15: Comparison of fmep as function of viscosities calculated from different engine temperatures [49]

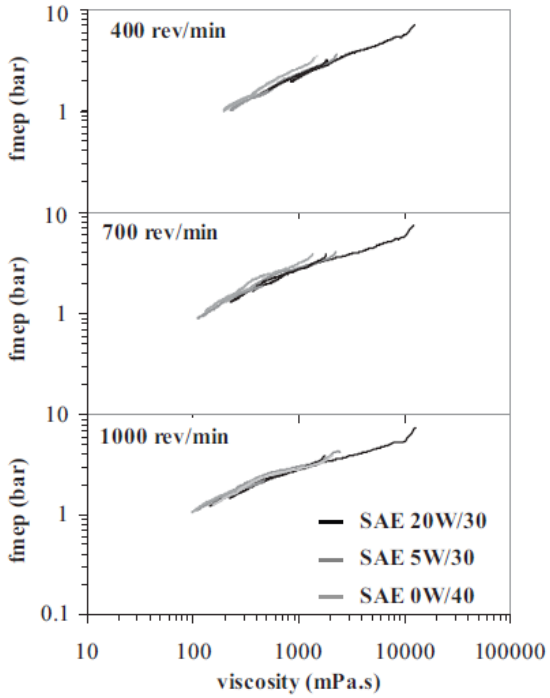

Figure 2.16: Motored engine fmep versus liner mid-stroke viscosity for starting engine temperatures of -20 and 0°C [49]

2.4.3 Motored engine friction rigs

Motoring friction does not include the combustion effects which are vital to engine friction. These include gas pressure loading on the piston, lower piston and cylinder liner temperatures, and the exhaust blowdown phase at the start of the exhaust process [22]. Low gas pressures reduce the load from the piston rings on the liner surface and thus lower rubbing friction. Lower temperatures due to the lack of combustion and the relative temperature differences affect oil viscosity and change friction properties. Exhaust gases are denser than air, and therefore motored pumping loads are less.

There are many types of motored friction tests. Some are used in an attempt to simulate specific tribological parts of the engine, while some are used to measure whole engine friction. One example of the former is reciprocating a liner around a motionless piston in an attempt to simulate piston/ring/liner friction. This method was used as early as 1978 as McGeehan [48] mentioned this method in his literature review. This method offers some advantages such as very well-known tribological conditions. However, the results are not accurate for real engine pressures, loads, and temperatures [38].

Whole engine friction can be simulated by instrumented engines. In fact, such test have been around since the 1980s when several researchers developed instrumented single-cylinder engines to perform direct measurements of piston friction forces in an engine [38]. The piston ring pack friction was examined in these methods using the floating bore as shown in Figure 2.17. The floating bore technique utilizes a liner which 'floats' on load cells. As the piston moves within the liner, friction forces push the liner. These forces are measured via the load cells. The main difficulties to be solved are the water and gas sealing and the lateral stiffness of the liner to bear the normal load due to piston dynamics [38]. Gas pressure in the cylinder can also affect the measurements so compensations must be taken in the design of one of these setups. The liner can also resonate and further disrupt the measured friction signal. Gauthier et al. [38] utilized electronic filters to eliminate a frequency band centered on 1100 Hz, the typical value of resonance frequency of the floating liner. Furuhama and Takiguchi [23] developed several versions of instrumented engines which incorporated the floating bore method. This method allows for direct measurement of engine cylinder friction but setup is complex.

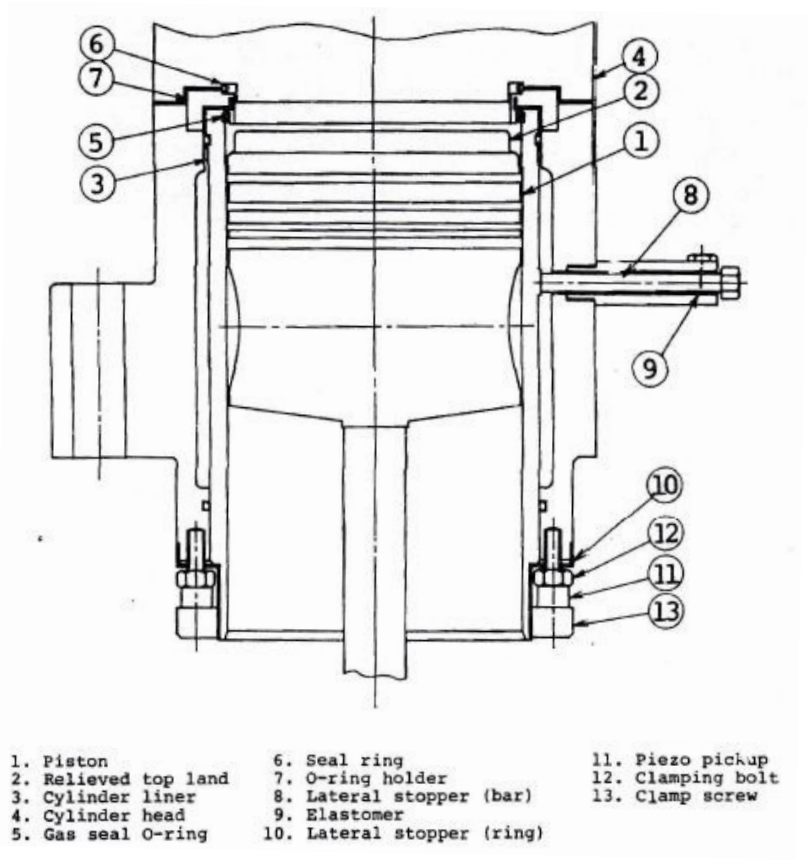

Figure 2.17: Schematic of floating bore piston/ring/liner assembly friction measurement device [23]

Motored tests allow for component removal to isolate the frictional contribution of various components by subtracting measured friction with a component removed from total engine friction. By motoring an engine, and sequentially dismantling it, each component of the mechanical and accessory friction contributions can be determined [22]. While this method offers insight to the contribution of various components, the same general problems with motored test affect this method as well. In fact these problems can be magnified by removing components. In component removal methods, the accuracy is affected

by different test conditions between the two tests such as gas pressure, lubricant oil pressure and temperature, and other operating variables [23]. Engines can be set up with the capability to run both motored and fired conditions. This allows for motoring to be performed at near operation temperatures by running the engine in a fired condition until equilibrium is reached and then shutting off combustion and simply motoring the engine afterwards.

2.4.4 Fired engine friction rigs

One of the simpler fired engine friction measurement methods is the friction mean effective pressure. In this method [50] friction mean effective pressure is calculated as the difference between indicated mean effective pressure (imep) and brake mean effective pressure (bmep), as shown by

$$\text{fmep}\ (\text{N/m}^2) = imep - bmep. \tag{2.6}$$

The imep represents total input energy calculated from measured cylinder pressure, through

$$\text{imep}\ (\text{N/m}^2) = \frac{indicated\ work\ ouput\ (N.m)\ per\ cylinder\ per\ mechanical\ cycle}{swept\ volume\ per\ cylinder\ (m^3)} \tag{2.7}$$

and Figure 2.18. The bmep represents total output energy and is calculated from measured torque at the drive shaft of the engine [50], via

$$\text{bmep}\ (\text{N/m}^2) = \frac{brake\ work\ output\ (N.m)\ per\ cylinder\ per\ mechanical\ cycle}{swept\ volume\ per\ cylinder\ (m^3)}. \tag{2.8}$$

The fmep includes the auxiliary losses as well as friction and is highly dependent on the accuracy of both the pressure and torque measurements. This method provides information about the friction loss of the engine but does not provide detailed information on the performance of the lube oil.

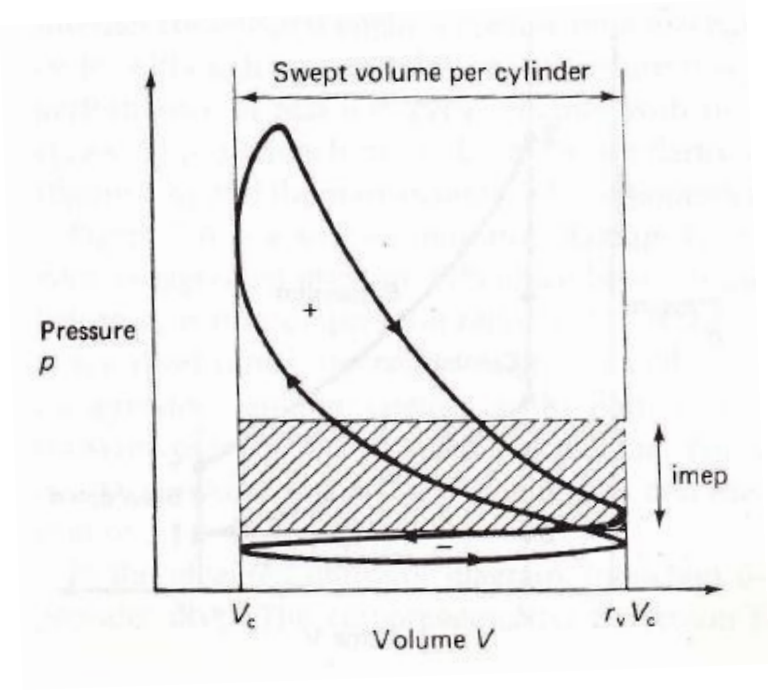

Figure 2.18: Pressure volume graph description of imep [50]

Hot engine shut down and cylinder shut down are methods that can be used to directly measure engine friction. Hot engine shut down cuts the fuel from the engine and engine speed is recorded as the engine slows to a stop. From this, insight to engine friction can be gained. Cylinder shut down cuts fuel to

individual cylinders and an electric motor is used to maintain the engine at a constant speed. The torque required to keep the engine at speed is related to the loss in combustion power and friction required to move the non-fired components.

Sethu et al. [51] used the instantaneous imep method to measure instantaneous in-cylinder friction for a 2.5 liter V6 spark-ignition engine in both fired and motored conditions. The instantaneous imep method calculates in-cylinder friction as function of crank angle by subtracting calculated inertia, F_{ma}, calculated weight, F_W, and measured conrod force, $F_{c,}$ from measured gas pressure, P_g, as described by

$$F_f = P_g A_c - F_{ma} - F_W - F_c, \quad \textbf{(2.9)}$$

where A_c is the area of the cylinder. The force balance for this calculation is diagrammed in Figure 2.19. Inertia values are calculated from the piston, piston pin, and any conrod mass above the measurement point. This method requires highly accurate measurements due to the small size of the calculated friction force compared to the measured forces.

The connection rod force was measured by Sethu et al. [51] via strain gage installed on the connecting rod, and a four-bar linkage is used to transmit the signal from the strain gain to the data acquisition system. Errors in the measurement, such as low signal to noise ratio and strain gauge errors due to temperature, are magnified when calculating friction. Thermal shock errors from the pressure transducer can create errors, and the variable speed of the engine, shown in Figure 2.20, creates difficulties when calculating inertia vales. Accounting for these errors and obtaining the measurements makes the instantaneous imep method complex.

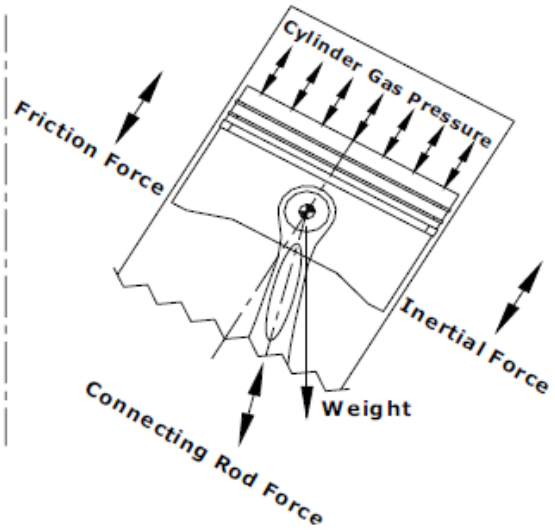

Figure 2.19: Instantaneous in-cylinder friction force balance [51]

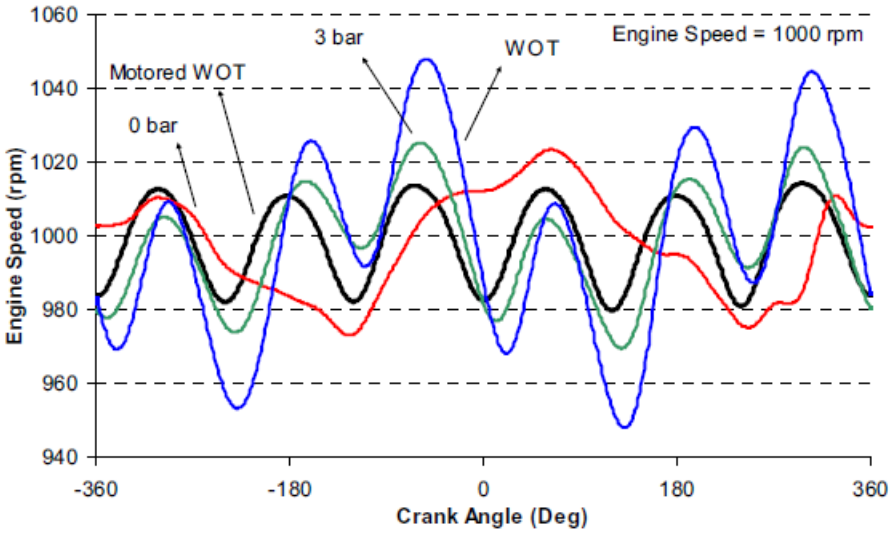

Figure 2.20: Engine speed variation during idle (0 bar), mid-throttle (3 bar), Wide Open Throttle (WOT), and motored WOT for a 2.5 L V6 SI engine [51]

Instantaneous in-cylinder friction was also examined by Sethu et al. [51] as function of temperature at two different engine speeds as can be seen in Figure 2.21. The temperature increase during the lower speed of 100 RPM shows a slight increase in friction but boundary friction still dominates. Examining the results for the higher speed of 1500 RPM shows a decrease in friction with temperature. This is expected as friction is mostly hydrodynamic at this engine speed and hydrodynamic friction decreases with temperature. The down stroke friction at 1500 RPM and 52°C shows lower friction than observed at 100 RPM which indicates mixed friction. This plot shows the importance of measuring the correct temperatures when describing engine friction as function of viscosity. The friction around the dead centers is relatively uneventful; whereas, friction drastically changes during mid-stroke. Thus mid-stroke temperature should be used when examining cylinder fiction and engine friction as well.

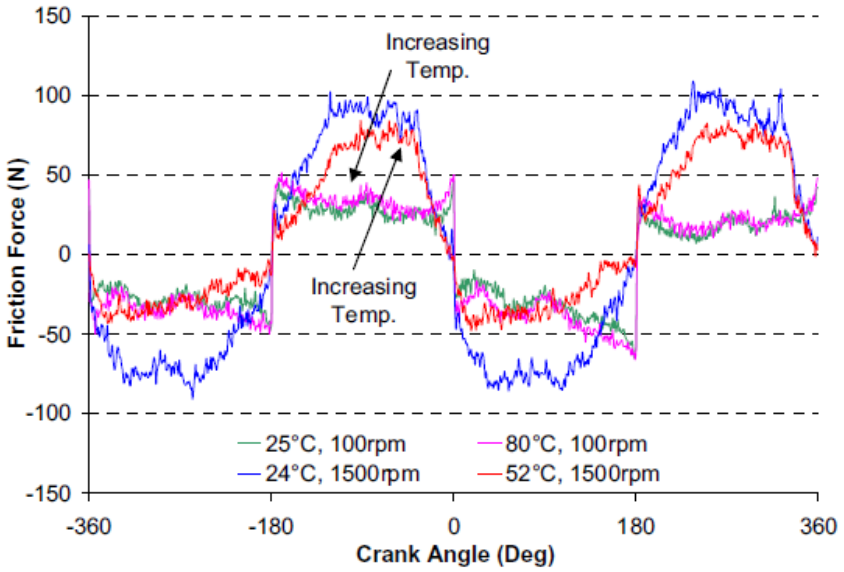

Figure 2.21: Effect of temperature on instantaneous in-cylinder friction [51]

2.4.5 Example motored engine friction results

Shayler et al. [25] examined motored engine friction as a function of oil viscosity. The results presented by Shayler et al. [25] show the relationship between friction mean effective pressure and lube oil viscosity for several oils in Figure 2.22, with information about the oils listed in Table 2.4. Friction mean effective pressure is observed to lower near 1000 mPa.s for most oils. This change in fmep is typical during cold start conditions. As viscosities decrease below 1000 mPa.s, fmep decreases linearly on the log-log scale shown in the plot. This is typical for most oils as well. This method of presenting lube oil performance via friction mean effective pressure as a function of lube oil viscosity is used in the current study as well.

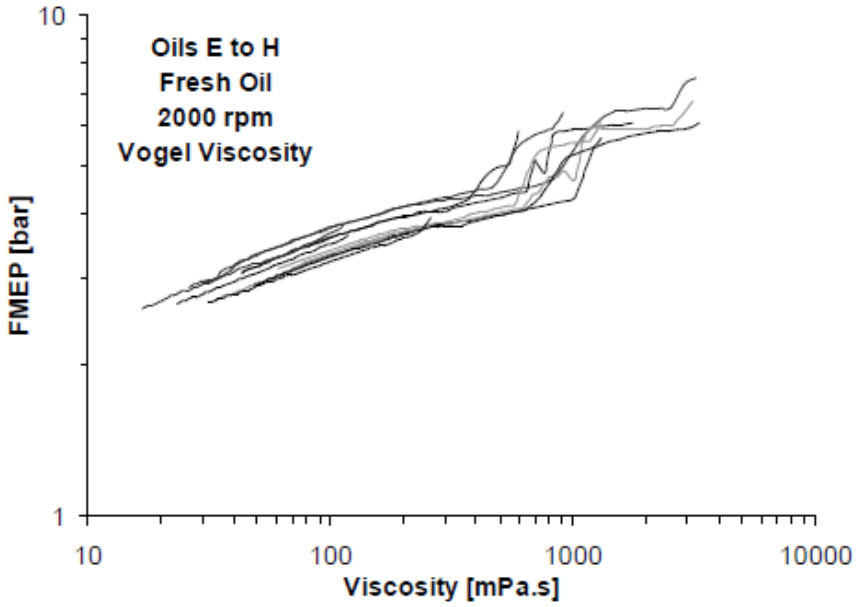

Figure 2.22: Motored engine friction reported as fmep for various oils [25]

Table 2.4: Lube oil viscosities for results presented in Figure 2.22 [25]

Temperature	*Viscosity units*	*Oil Designation*			
		E	*F*	*G*	*H*
-20°C	mm^2/s	2181	2680	4706	5723
0°C	mm^2/s	408.67	451.67	815.63	893.04
40°C	mm^2/s	47.21	48.35	89.60	90.59
100°C	mm^2/s	8.45	8.12	15.33	14.53
CCS @ -30°C	mPa.s	4236	6380	4101	6722
HTHS @ 150°C	mPa.s	2.77	2.74	3.92	4.01

2.5 Theoretical modeling of engine friction

2.5.1 Introduction

Theoretical modeling of lubricated friction began as early as 1886 when Osborne Reynolds first developed the equation for hydrodynamic lubrication in a journal bearing. Modeling engine friction consist of models concerning friction regimes in the engine (boundary, mixed, and hydrodynamic), viscosity changes (temperature, pressure, and shear rate), and the engine components (temperature, dynamics, and mechanics of materials). When all these conditions, regimes, and components are considered together the problem is exceptionally complex. Therefore, models have been developed to focus on specific types of friction or conditions and are used in conjunction to estimate total fiction. In more complex component models, sub-models are used to break

the complexity into more manageable parts and reduce computational time.

The engine is typically broken into its components for modeling with the components usually described as journal bearings or sliding interfaces. Models range in complexity, from simple equations which model friction as a function of velocity only, to intricate models which consider heat generation due to friction and the possibility of asperity contact. As mentioned before, these complex models typically consist of a combination of sub-models working in unison to generate results. When asperity contact is concerned, the Greenwood-Tripp model, discussed in a later section, is usually used in some fashion.

2.5.2 Reynolds equation based simulations

Reynolds work in 1886 [24] is an important part of engine friction simulation especially when hydrodynamic lubrication is concerned. Reynolds created his equation in response to a series of experiments done by Beauchamp Tower where the pressure in a journal bearing was measured for various loads and speeds. In this experiment, Tower concluded that pressure is generated by the oil. Based on Tower's experiments, Osborn Reynolds formulated a theory of lubrication in 1886 [24]. Reynolds original work does have some flaws, namely it lacks variable temperature effects. Because of this, many papers use various modified versions of Reynolds equation. Reynolds theories have continued to be the fundamental basis for simulations which consider the hydrodynamic pressure field in the lubricant.

2.5.3 Surface contact

Greenwood and Tripp [52] created a mathematical model of asperity contact for two rough surfaces in their 1970 paper entitled "The contact of two nominally flat rough surfaces" in which they discuss and derive equations for the total load, area, and number of contacts. The formulas are based on an

assumed Gaussian distribution of asperity heights and uniform asperity shape. The shape of the asperity [52] is described as

$$y = f(\mathrm{x}) = {\mathrm{x}^2}/{2\beta} \qquad \textbf{(2.10)}$$

,where x is horizontal distance, y is vertical distance, and β is the radius of curvature at the peak. Figure 2.23 shows an example asperity shape for two values of β. The one simplifying feature of surface roughness so far found is that, although the height of a particular asperity is random, the distribution of the asperity heights is rather close to Gaussian especially for ground or girt-blasted surfaces [52].

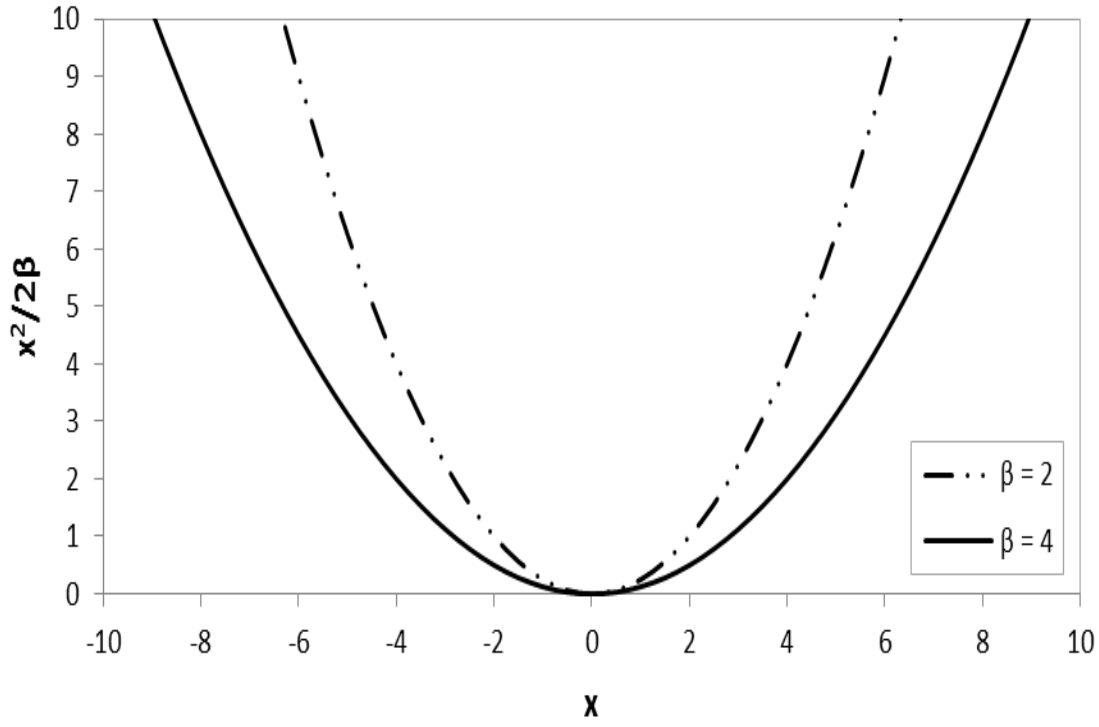

Figure 2.23: Asperity shape for different β values

Greenwood and Tripp [52] derived equations for total load, total area, total number of contacts, and nominal pressure for elastic deformation for an equivalent surface against a plane ($\widetilde{P}_c$, $\widetilde{A}$, $\widetilde{N}$, and p_e respectively). The total number of contacts [52] is calculated as

$$\widetilde{N}(d_a) = 4\pi(ap_\rho\beta\sigma)ap_\rho A_a G_1\left(\frac{d_a}{\sigma}\right), \quad \textbf{(2.11)}$$

where ap_ρ is the surface density of the asperity peaks, β is the radius of curvature at the peak of the asperity, σ is the standard deviation of the Gauss distribution, A_a is the apparent contact area, $G_1\left(\frac{d_a}{\sigma}\right)$ is a Gaussian integral [52], and d_a is the distance between the planes of mean asperity height for the two surfaces. The nominal pressure for elastic deformation [52] is describe as

$$p_e(d_a) = KG_{3/2}\left(\frac{d_a}{\sigma}\right), \quad \textbf{(2.12)}$$

where $G_{3/2}\left(\frac{d_a}{\sigma}\right)$ is a Gaussian integral [52] and K is defined as

$$K = \frac{2\sqrt{2}}{3}(ap_\rho\beta\sigma)E'\sqrt{\frac{\sigma}{\beta}} \quad \textbf{(2.13)}$$

where E' is the composite elastic modulus of the two materials.

Wang et al. [26] modeled the contact between two rough surfaces by taking a composite of the two surfaces and considering it to be in contact with an infinitely large, flat, and rigid surface. The deformation of the surface caused by asperity contact is computed via the influence-coefficient method with the

coefficients obtained from finite element method (FEM). Wang et al. [26] suggested that shaft defection and bearing-shaft misalignment should be taken into account in mixed lubrication analysis as these can lead to surface contact. Surface roughness can have a profound effect in mixed lubrication, especially when roughness approaches the same magnitude as the oil film. The finish of the surface influences the output as well. It was found that the rougher surface results in higher peak contact pressure and larger contact areas, as seen in Figures 2.24 and 2.25. The load also was found to influence the contact area and it was found that for small loads the asperity contact occurred at the edge of the bearing in the presence of either shaft deflection or misalignment. The contact spreads across the bearing width as the load increases. Wang et al. [26] also showed a transition of the contact and a corresponding temperature transition. This transition is shown by a large jump in the maximum temperature in the bearing, which can be a sign of impending bearing failure.

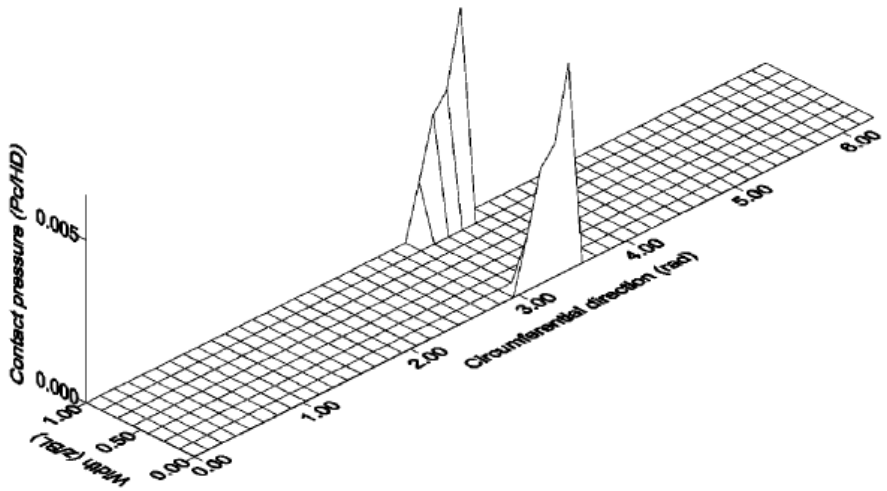

Figure 2.24: Contact pressure distribution over bearing surface for 0.8 μm roughness at 500 RPM and 122 kN load [26]

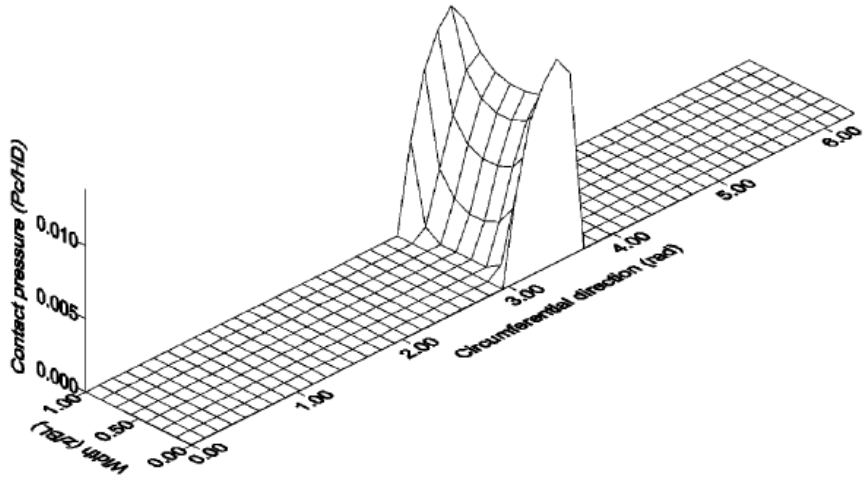

Figure 2.25: Contact pressure distribution over bearing surface for 1.5 μm roughness at 500 RPM and 122 kN load [26]

2.5.4 Piston, piston rings, and liner interface

Complete piston ring-pack lubrication models include both viscosity/temperature and viscosity/shear rate effects but the viscosity/pressure effect can generally be ignored [20]. It is also important to include oil starvation effects around top/bottom dead center and at the top ring due to the lower rings. Some models chose to break the piston/ liner interfaces into sub-models to decrease processing time. Offner et al. [29] accomplished this by using an elastohydrodynamic (EHD) model for piston skirt lubrication and using a simplified multi-body-system with dry piston-to-liner contact. They concluded that predicting piston/liner contact is central processing unit (CPU) intensive but simplifications can lead to incorrect results. However, time saving representations of the effects at these interfaces must be included to provide results at a reasonable rate but care must be taken not to lose accuracy.

Livanos and Kyrtatos [27] modeled the oil film action between the piston ring and the cylinder liner with a one-dimensional Reynolds equation,

$$\frac{\partial}{\partial x}\left(\frac{h^3}{12\eta}\frac{\partial P}{\partial x}\right) = \frac{1}{2}\mathrm{v}_p\frac{\partial h}{\partial x} + \frac{\partial h}{\partial t} \qquad \textbf{(2.14)}$$

which considers sliding and squeezing ring motion [27]; where x direction parallel to liner surface, v_p is the piston velocity, P is the developed pressure, η is the oil viscosity, h is the oil film thickness between ring and cylinder liner, and t is time. This equation and a force balance between oil pressure forces, cylinder gas forces, and ring tension force can be used to solve for the oil pressure, P, minimum oil film thickness, h_{min}, and position of lubricant inlet, x_{inlet}, and outlet, x_{outlet}, over the face of the oil ring with boundary conditions for x at inlet and outlet and pressure at inlet and outlet.

Livanos and Kyrtatos [27] calculated friction force from the piston/ring/liner interface with the sum fluid shear stress forces and asperity contact forces. The shear stress forces are calculated with a double integral of a fluid shear stress equation taken over area; whereas, asperity contact force is calculated with a coefficient multiplied by the double integral of the asperity contact pressure over contact area. For hydrodynamic lubrication, the power loss P_f^{ring} is calculated from [27],

$$P_f^{ring} = \iint \frac{\eta}{\mathrm{h}}\mathrm{v_p}^2\, d\mathrm{A} + \iint \frac{\mathrm{h}^3}{12\eta}(\nabla \mathrm{P})^2 d\mathrm{A} \qquad \textbf{(2.15)}$$

where A is the area over the ring face.

It is important to note that an engine piston is not constrained to move along the cylinder center axis and in fact rotates about the piston pin. Livanos

and Kyrtatos [27] included these effects along with hydrodynamic lubrication models of the piston skirt to calculate skirt friction as a function of engine crank angle. Piston secondary motion such as the small translations and rotations within the confinement of the cylinder clearance were defined as piston eccentricities "e_t" and "e_b" at the top and bottom of the skirt. Equations of motion and a two-dimensional Reynolds equation are used to describe the motion and lubrication of the piston skirt. The solution to this problem coupled equations to provide skirt motion and lubrication pressure field. Friction losses can be calculated after the integration of the developed shear stresses over the piston skirt lubricated area. This same procedure is done for the piston rings. Livanos and Kyrtatos [27] provided several references which provide information regarding the method of solution of the system of coupled differential equations. The Greenwood and Tripp model was used by Livanos and Kyrtatos [27] to model asperity contact as well for the calculation of the contact pressure P_c in a piston/ring model.

2.5.5 Journal bearings modeling

Journal bearings models are extensive and come in a wide variety. These bearing models are often simplified to find analytical solutions and there are equations for short, long, and finite loaded bearings [27]. Numerical models apply finite element methods to solve the Reynolds equation either in the simplified isothermal conditions or in more complex thermo-elasto-hydrodynamic (TEHD) models. These Reynolds-based models solve for pressure distribution, as shown in Figure 2.26. From this, forces acting on the journal and bushing are calculated.

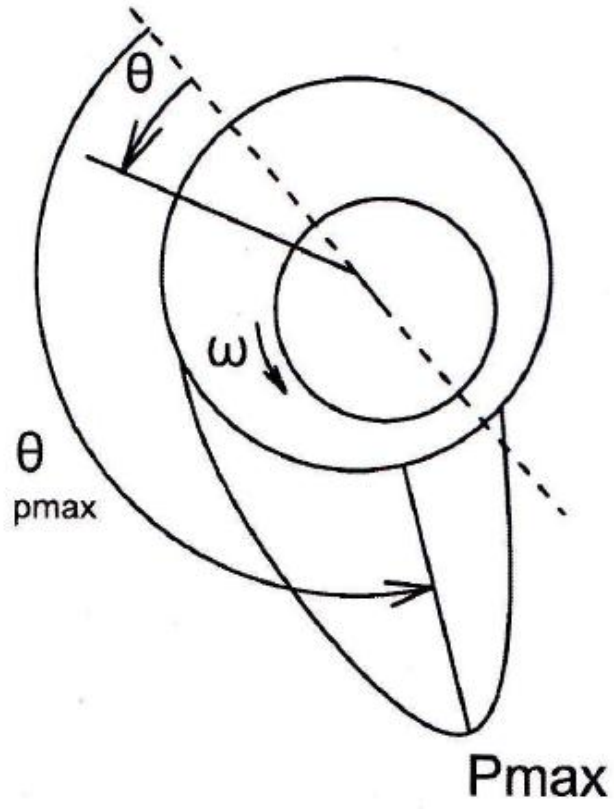

Figure 2.26: Journal bearing pressure distribution [27]

On the other hand, elastohydrodynamic (EHD) fluid film models ignore the varying temperatures within the areas being modeled, and thus have lower accuracy since the change in oil properties are not included. Also, a temperature only viscosity profile does not take into effect the changes on oil properties associated with different pressures. Allmaier et al. [40] avoided some of these problems by running simulations at different operation points or shaft speeds and modeling bearing temperature based on experimental results. The non-Newtonian behavior of the base oils is important under severe EHD conditions as it determines the friction [20].

Allmaier et al. [40] examined a elastohydrodynamic (EHD) journal bearing model in comparison to an experimental journal bearing friction rig with simulations performed with a temperature dependent viscosity, η(T), and with a pressure and temperature dependent viscosity, η(P,T). In a journal bearing, hydrodynamic pressure and oil temperatures are not constant and a peak in pressure over the loaded region occurs, as shown in Figure 2.26. The pressure increases oil viscosity creating higher hydrodynamic pressure. In simulations hydrodynamic losses can be under predicted and surface contact over predicted if the viscosity increase due to pressure is not considered since the underrepresented oil viscosity will not generate enough pressure to support the journal.

This is explored by Allmaier et al. [40] as they showed only a slight increase in simulated friction moment with journal speed when considering viscosity as a function of temperature alone, as seen in Figure 2.27. The temperature values used in the temperature dependent viscosity simulations, 90°C at 2000 RPM and 103°C at 4500 RPM, were calculated from averaged experimental journal bearing temperatures. The simulation for temperature dependent viscosity at 2000 RPM greatly over predicts the surface contact friction but under predicts hydrodynamic losses since it did not take into account oil thickening in the high pressure section of the journal bearing. The surface contact friction is predicted more reasonably for 4500 RPM but hydrodynamic friction is over predicted due to simulation temperatures being lower than true temperature at the high pressure point. The simulation which considers pressure and temperature effects on viscosity predicts friction at 2000 RPM well but under predicts at 4500 RPM, which would be attributed to temperature not accurately being represented across the bearing. This shows the importance of accurately describing the oil properties and conditions in a simulation.

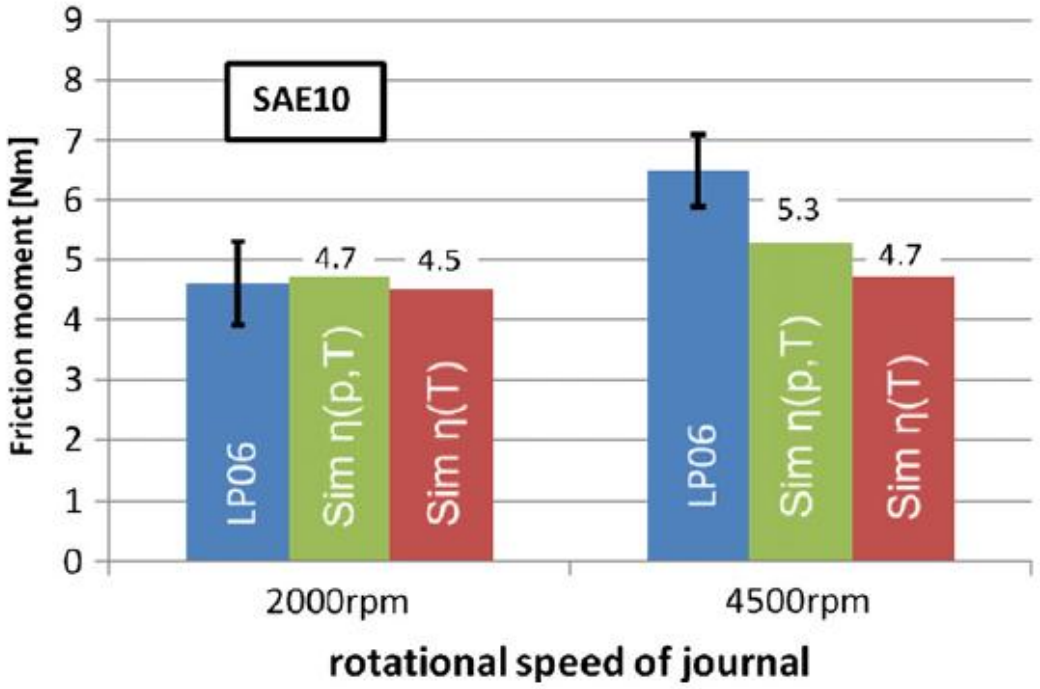

Figure 2.27: Comparison of measured friction moment (LP06) and simulations with temperature dependent viscosity (Sim η(T)) and temperature and pressure dependent viscosity (Sim η(p,T)) [40]

2.5.6 Simulation results with experimental comparison

Durak et al. [18] simulated friction in a journal bearing with a modified Reynolds equation using,

$$\frac{\partial}{\partial\varphi}\left(H^3\frac{\partial P}{\partial\varphi}\right)+\frac{D^2\partial}{B^2\partial Z}\left(H^3\frac{\partial P}{\partial Z}\right)=\frac{6\eta}{\psi^2}\left((\omega_1+\omega_2)\frac{\partial H}{\partial\varphi}+2\frac{\partial H}{\partial t}\right). \qquad \textbf{(2.16)}$$

This modified Reynolds equation is a function of the dimensionless oil film thickness, H, expressed as a function of eccentricity ratio and bearing angle of

location, oil pressure, P, and various geometric, kinematic, and oil parameters. The pressure derivatives in the modified Reynolds equation are represented using a centered finite difference method. With this and boundary conditions for oil pressure, the pressure over the bearing is obtained and used to calculate fiction force.

Durak et al. [18] compared simulation results to experimental results collected with a device built to simulate a journal bearing. This device has a rotating shaft fixed along its rotational axis and a bearing which can move along an axis perpendicular to the rotational axis of the shaft. The movement along this axis allows for a load to be applied to the shaft and bearing. Load was applied to the bearing with hydraulics to simulate engine loads. To measure the friction force, the rotation of the bearing housing was measured through strain gauges mounted on a deflection arm connected to the bearing housing. The mathematical and experimental approach did not completely match but similar trends were observed as shown in Figures 2.28 and 2.29.

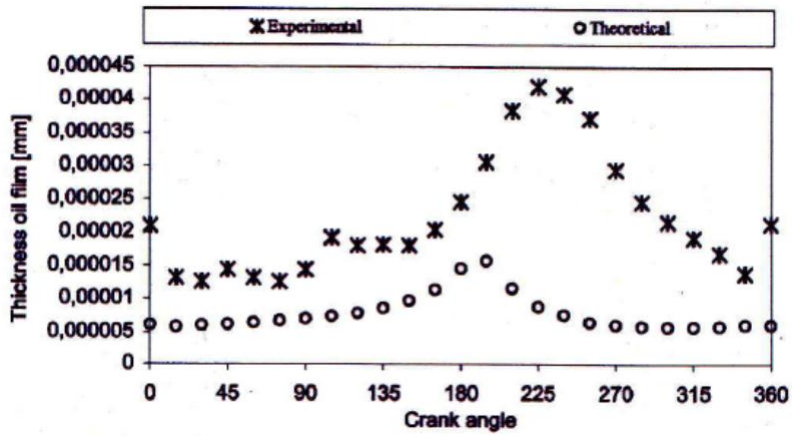

Figure 2.28: Comparison of experimental and theoretical journal bearing oil film thickness as function of crank angle [18]

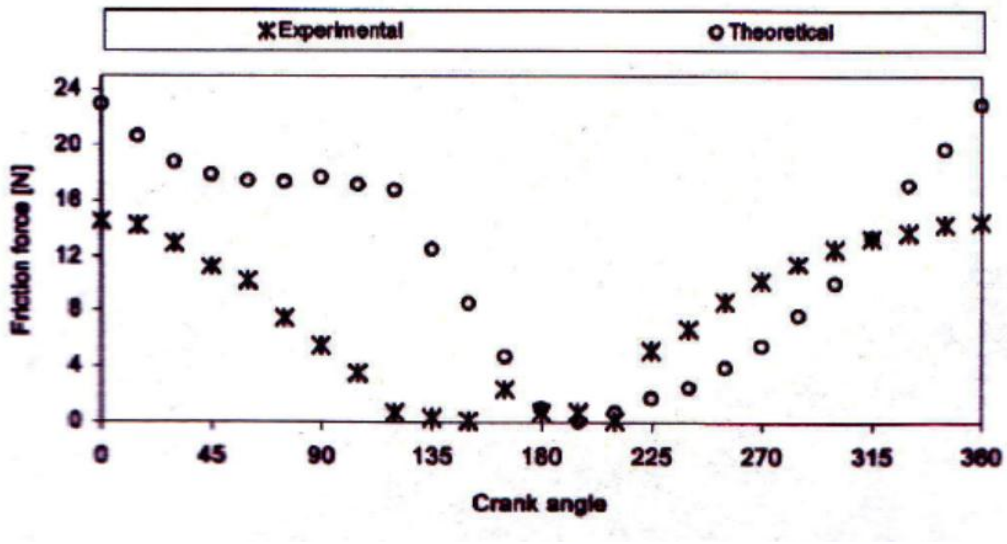

Figure 2.29: Comparison of journal bearing experimental and theoretical friction force as function of crank angle [18]

Livanos and Kyrtatos [27] simulated total engine friction using sub models for piston rings, piston skirt, big end bearings, main bearings, piston pin, and valve train with the piston components and journal bearings being modeled with Reynolds-based equations. The results show that the average friction loss for the piston skirt is the largest, followed by the main bearing. Although the piston skirt has the largest average friction, the piston rings have larger friction peaks. The results also show large friction losses for the piston rings around TDC after firing due to lower speeds and increase load due to gas pressures. Total engine friction mean effective pressure (fmep) is compared to experimental results and results from several semi-empirical models. Simulation results for this model predict result at maximum and minimum load but over predict at intermediate results as shown in Figure 2.30.

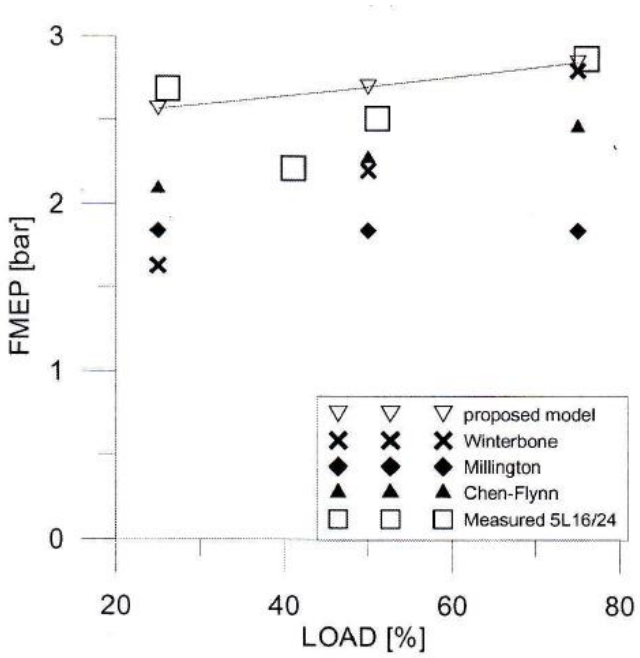

Figure 2.30: Comparison of total engine power loss for three models and measured data at crank shaft speed of 1200 RPM [27]

A wide variety of methods exist for both measuring and simulating engine friction. Typically accuracy to actual fired engine conditions comes at a cost of complexity, cost, and time. The methods presented in the present study examine the feasibility of using relatively simple and quick methods to measure and predict engine friction without a detrimental loss of accuracy to engine conditions so that the performance of lube oils can be examined. The methods and apparatuses used in the present study are presented in the following chapter.

CHAPTER 3
EXPERIMENTAL APPARATUSES, MODELING METHOD, AND PROCEDURES

This chapter describes the experimental apparatuses, experimental procedures, and the software, AVL Excite Power Unit, used for modeling engine friction. Section 3.1 describes the small single-cylinder engine test bench, the data collection system, and any associated experimental procedures. Section 3.2 discusses the measurement of lube oil viscosity and the calculation of Vogel constants. A description of AVL Excite and the simulation to be used in this study is discussed in Section 3.3. Section 3.4 describes a line contact friction measurement device which is used to obtain friction coefficients for use with the AVL Excite Power Unit software.

3.1 Motored engine friction rig

A motored engine friction rig is developed for this study with the objective of measuring lube oil performance in a relatively inexpensive and simple manner while approaching fired engine conditions. To accomplish this, a 517 cc Hatz 1D50 single-cylinder, air-cooled diesel engine is motored by a Leeson 5 hp electric motor at approximately 1800 RPM, as shown in Figure 3.1. Data measured with the motored engine rig include temperatures at various locations of the engine, engine speed, oil pressure, and motoring torque. Throughout the study an effort has been made to increase the usefulness of the motored engine friction rig by improving signal-to-noise ratio of the torque meter and increasing engine temperatures towards fired engine conditions. The improvements of the motored engine rig include: switching from an AC power supply to a 12 VDC battery power supply to reduce 60 Hz noise in the torque signal, installing a torque meter with a larger range to reduce base line drift, extending the engine

operating temperatures, and configuring three different engine setups to reduce errors and to examine the friction contribution of various components.

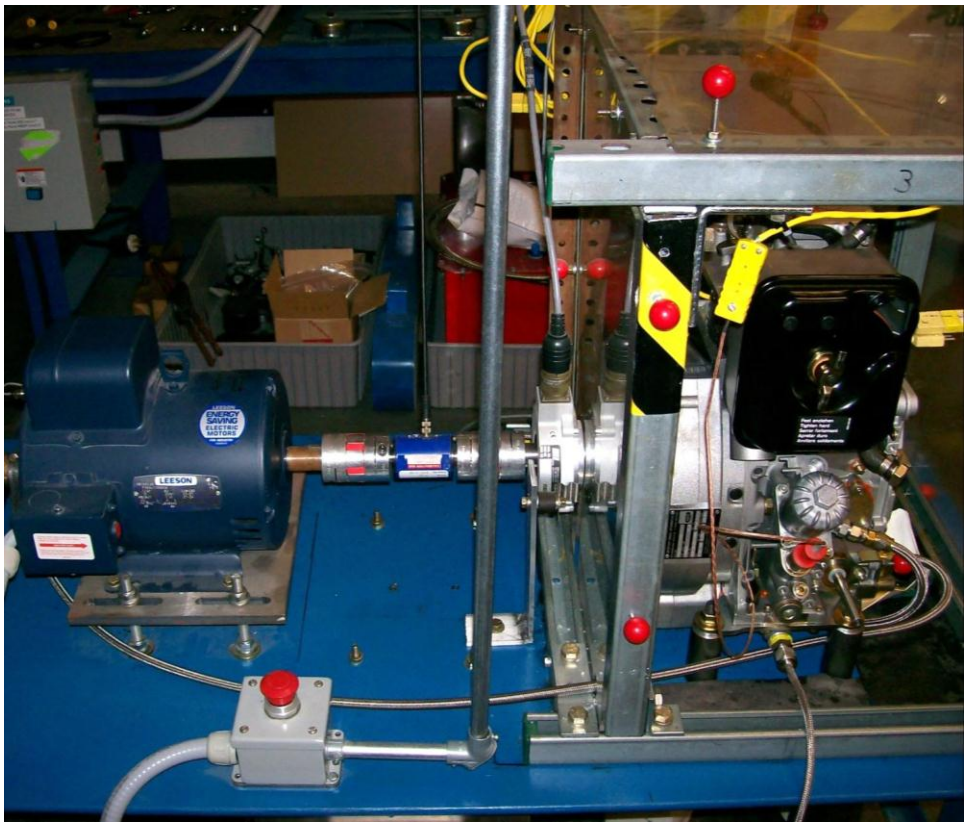

Figure 3.1: Motored engine friction rig located at the National Transportation Research Center (NTRC)

Motoring torque is measured with a torque meter installed between motor and engine shafts at ½ crank angle resolution using a hollow shaft incremental encoder, BEI industrial encoders model number HS45F-112-R2-SS-720-ABZC-28V/5-SM18, installed on the drive shaft of the engine, as shown in Figure 3.2. From this, motoring torque can be plotted as instantaneous torque, i.e., torque

per ½ degree over an engine cycle, or average torque, i.e., average torque per cycle. Instantaneous torque plots allow for the shape of torque over an engine cycle to be observed and frictional differences between oils can be seen at the peaks and troughs of the instantaneous torque curve. However, it is difficult to compare the performance of lube oils as a function of some propriety such as viscosity in this manner. Averaging the instantaneous torque allows for the data to be plotted as a function of time, engine temperature, oil viscosity, oil pressure, and etc., making it simpler to compare lube oils. In the present study, average torque is typically converted to fmep and plotted against oil viscosity calculated from liner mid-stroke temperature.

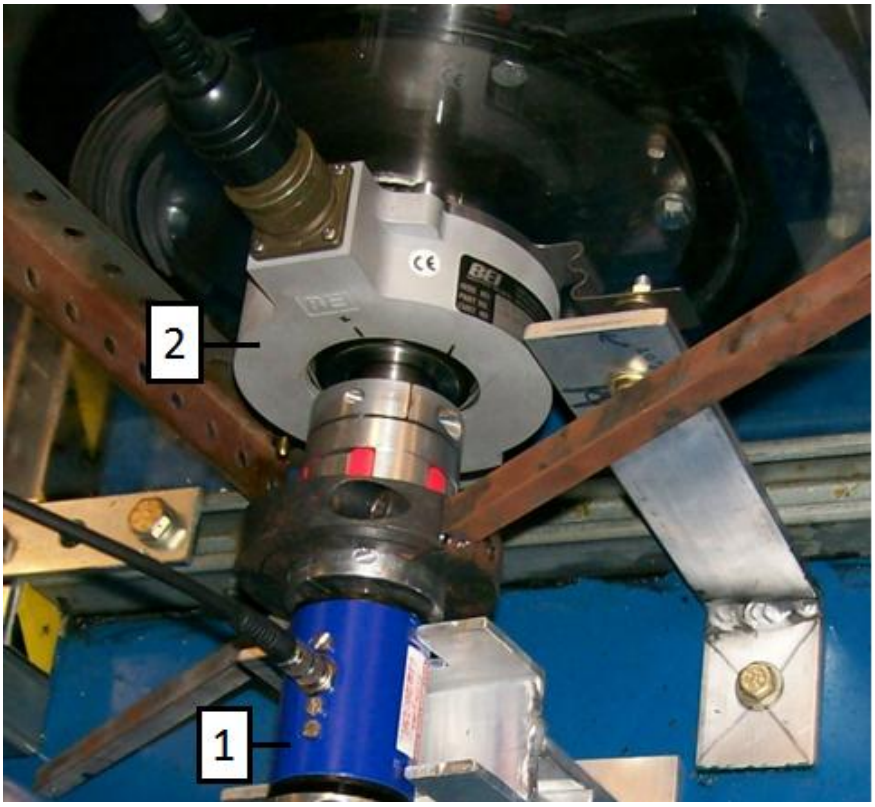

Figure 3.2: Torque meter (1) and engine shaft encoder (2)

3.1.1 Engine configurations

Two engines in three configurations are used in this study as shown in Table 3.1. For the first configurations, the Hatz engine is modified by removing the fuel system, pushrods, tappets, and intake valve. This engine, which operates without compression, is referred to as modified with internal oil pump. In this configuration, the internal oil pump and timing gears were left in the engine. However, during a series of tests an unexpected change in motoring torque occurred for an oil. This change in motoring torque is the results of a drop in oil pressure when the automatic oil pressure relief valve in the engine opened. The oil pump in the engine is directly coupled to the output shaft and thus a change in oil pressure will cause a change in motoring torque. To eliminate this problem, the internal oil pump and the timing gears are removed from the engine. This second engine configuration is referred to as modified with external oil pump.

The external oil pump was installed to eliminate oil pumping torque from motoring torque and to increase the repeatability of tests. The 0.5 hp rotary gear pump, model number GCBN33V, draws oil through the oil sump with a hydraulic hose attached at a drain port. The oil is then pumped through another hydraulic hose to the oil filter housing where the oil is pumped through the filter and into the original engine oil channels. This configuration bypasses the oil pressure relief valve without eliminating any lubricating channels in the engine. With the internal oil pump and timing gears removed, friction torque is limited to the crank bearings and the piston/ring/liner interface.

The last engine configuration is a new Hatz 1D50 engine mostly stock with compression to examine total engine friction. This engine is referred to as the stock engine. The only major modification to this engine is the removal of the original oil pressure relief valve and the installation of a manual screw valve.

This allows the oil pressure in the engine to manually set so that the effect of the oil pressure on engine conditions and motoring torque can be examined.

Table 3.1: Overview of engine configurations examined

Engine configuration	***Parts removed***	***Compression***	***Oil pump***
Modified – internal oil pump	Fuel system, tappets, pushrods, intake valve	No	Internal
Modified – external oil pump	Fuel system, tappets, pushrods, intake valve, timing gears, oil pump	No	External
Stock	Fuel system	Yes	Internal with manual pressure relief valve

3.1.2 Increasing engine temperatures

The temperatures of the motored engine are increased with a variety of methods in an effort to approach fired engine conditions so that results are applicable to fired engines. This is primarily done by restricting the airflow around the engine with a Plexiglas enclosure. The enclosure limits heat loss from the engine by inhibiting the mixing of cool ambient air with the warm air surrounding the engine. Also, the Plexiglas panels are opaque for wavelengths above approximately 2.2 μm and, thus, the enclosure lowers thermal radiation losses as well [53]. The engine is cooled by flywheel which serves as a fan. The flywheel draws air in from under and around the engine and blows air through a cowling across the cylinder jacket to cool the engine. This cowling is reversed to reduce the air flow around the cylinder jacket, thus increase engine

temperatures. A cartridge heater installed in the oil sump is used to heat the engine oil. Several heaters and installation configurations are examined in an effort to approach the temperatures achieved in fired engines. With the combination of the engine enclosure and cartridge heater, the liner temperatures on the engine with compression can be increased to values that fall within the range observed in a fired engine.

The Plexiglas housing is a 2'X2' cube constructed with a Unistrut frame as can be seen in Figure 3.3. The panels can be removed individually to provide some limited control over the maximum temperature reached by the engine. Several holes were cut in the Plexiglas to facilitate the running of wires, heating elements, and etc. Diagonal braces were also installed on several of the panels to prevent bowing when the panels are heated. The panel on the output shaft side of the engine was installed between the engine and the encoder so that the encoder would not be heated.

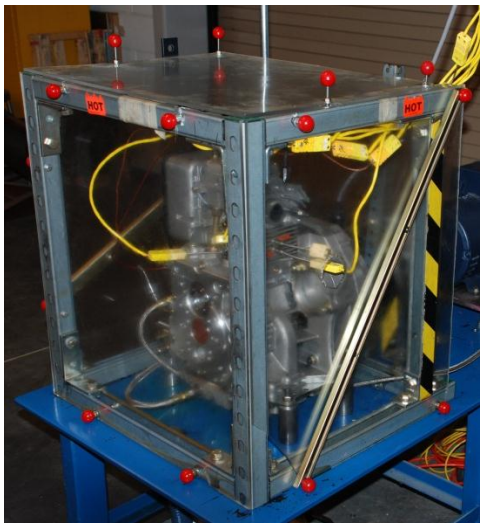

Figure 3.3: Plexiglas engine enclosure

The engine cowling is used in three positions: stock position where the cowling directs air across the cylinder jacket shown in Figure 3.4, reverse position where the cowling directs air away from the engine as seen in Figure 3.5, and the engine cowling removed where limited air flow is directed across the engine. The positioning of the cowling is dependent on the engine configuration used. When there is no compression in the engine, cylinder liner temperatures are lower and the cowling is run in the reverse position so that maximum temperatures are reached. When the engine with compression is used, the cylinder temperatures are much higher and the cowling is adjusted for the engine temperatures desired. If engine temperatures approaching fired engine conditions are desired the cowling is run in the reverse position. For temperatures similar to the engine without compression, the cowling is run in the stock position. When intermediate temperatures are desired the cowling is left off the engine.

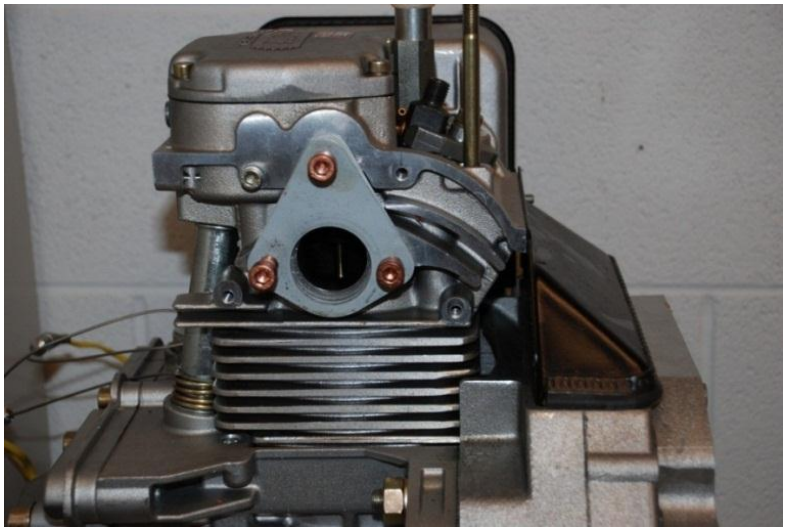

Figure 3.4: Engine cowling stock position

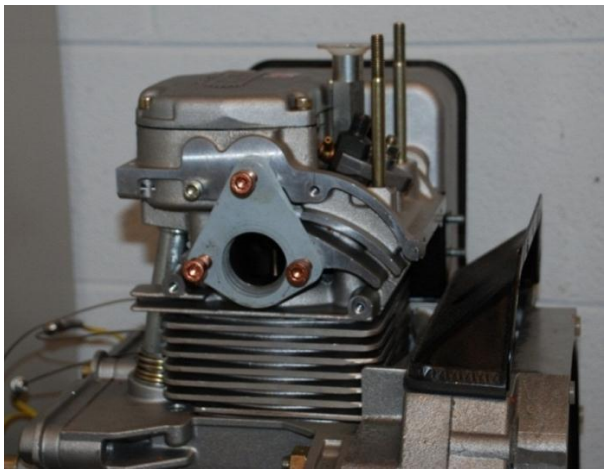

Figure 3.5: Engine cowling reverse position

A cartridge heater is used to heat the oil in the oil sump. Several cartridge heaters of varying power and installation methods were examined. The oil pan was modified by replacing a drain plug with a Swagelok fitting, and the oil sump internal fins were machined down so that the heater could be installed. Initially the heater was simply inserted into the sump through this fitting leaving a gap between the heater and oil pan bottom surface. This installation method was revised to further increase the usefulness of the heater by clamping the heater to the oil pan via brass clips bolted to the oil pan in an effort to transfer more heat to the oil pan and provide more uniform heating of the oil. Great care was taken to reduce leakage by using copper washers and silicone engine sealant. The heater is used to further increase the oil temperatures and provides greater control over the oil temperatures through a temperature controller.

3.1.3 Engine temperature measurements

The engine temperatures measured during this study include cylinder liner, crank case, oil sump, and the valve cover. In addition to the engine

temperatures, the air temperature inside the enclosure and the ambient temperature in the room are measured as well. The outer cylinder liner temperatures are measured with thermocouples installed through the aluminum cylinder jacket with the thermocouple junctions in contact with the outer surface of the liner. Only outer liner temperatures at top dead center and mid stroke on the front and the down stroke, thrust side of the liner are measured. Bottom dead center was not measured due to space limitations.

The accuracy of using the liner outer surface temperature instead of the liner inner surface is investigated by estimating the liner inner surface temperature from the cylinder jacket and liner outer surface temperature using heat flux calculations. The position of the temperature measurements for heat flux calculations is shown in Figure 3.6. In the figure, T_3 is the temperature measured on the outside of the cylinder jacket, T_2 is the temperature measured between the jacket and liner, and T_1 is the liner inner surface temperature. The liner inner surface temperature is estimated using,

$$T_1 = \frac{k_2 L_1}{k_1 L_2}(T_2 - T_3) + T_2 \qquad \textbf{(3.1)}$$

which is derived from,

$$q" = \frac{k_1}{L_1}(T_1 - T_2) = \frac{k_2}{L_2}(T_2 - T_3) \qquad \textbf{(3.2)}$$

where q" is heat flux, k_1 is thermal conductivity of the gray cast iron liner with an assumed value of 63 W/m.K, L_1 is liner thickness of 0.115", k_2 is thermal conductivity of the aluminum cylinder jacket with an assumed value of 273 W/m.K, L_2 is the jacket thickness to the base of the fins of 0.343", T_1 is liner inner wall temperature, T_2 is liner outer wall temperature, and T_3 is cylinder jacket temperature [54, 55]. For these calculations, the temperature distribution is

assumed to be steady state and constant along the vertical axis with the temperature at the base of the fin equal to T_3. Furthermore, the thermal resistance of the oil film is assumed to be negligible and the thermal properties are assumed to be constant. Initially six positions on the liner and jacket were measured with 1/8" type K Omega sheathed and grounded thermocouple probes with an accuracy of 2 °C. Two are installed on the piston trust side of the liner, two on the front side of the engine, and two installed on the outer surface of the jacket as shown in Figure 3.7. The positioning and installation method of liner thermocouples is changed when the engine with compression was used. The engine muffler is required when motoring with compression and this blocks access to the side positions of the liner. Three positions on the front of the liner, top dead center, mid stroke, and a lower position, are measured for this configuration. Type K 1/16" sheathed and grounded thermocouple probes with an accuracy of 2 °C purchased from McMaster-Carr are used in this setup to reduce installation difficulties shown in Figures 3.7. Dimples were also drilled into the liner so that the thermocouple more accurately measures the liner temperature.

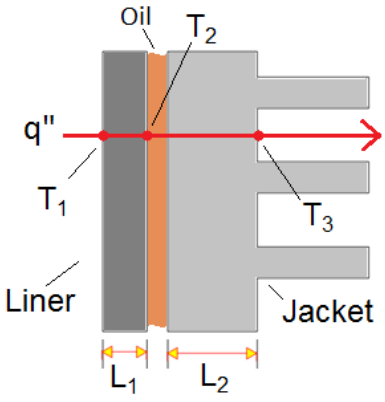

Figure 3.6: Cross-sectional schematic of cylinder liner, oil, and cylinder jacket

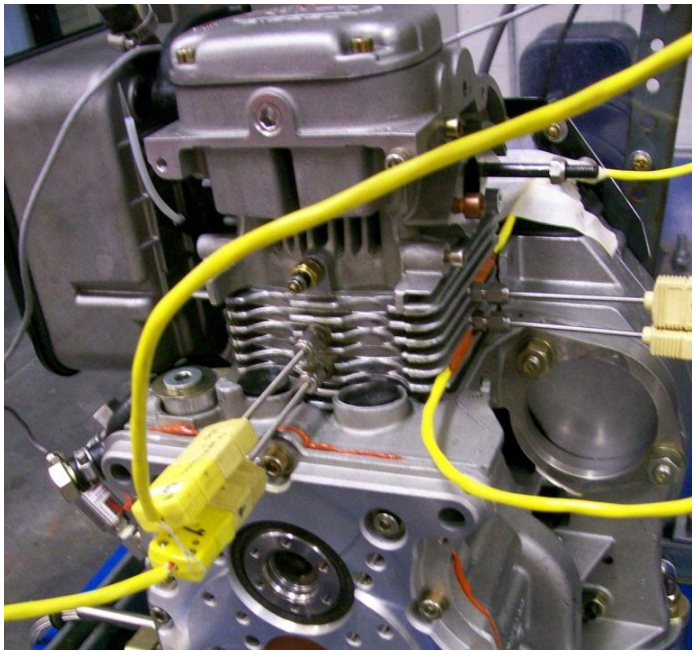

Figure 3.7: Thermocouple position for engine without compression with jacket outer surface thermocouples installed

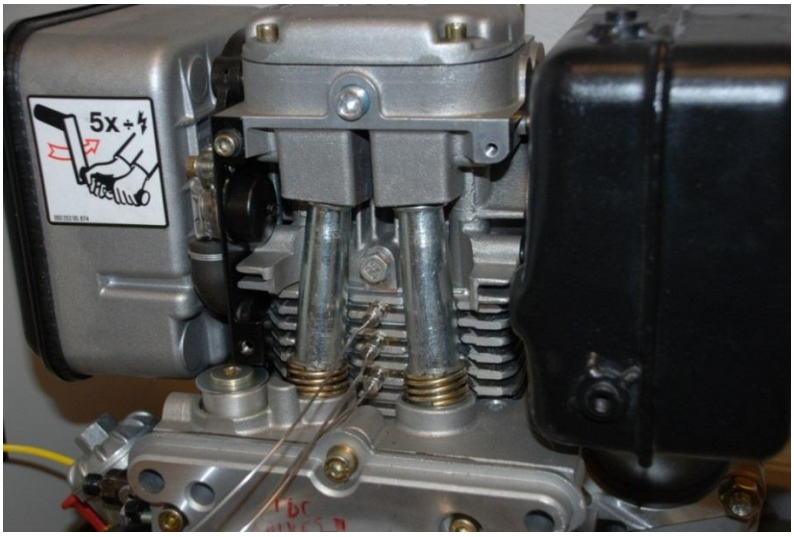

Figure 3.8: Stock engine with compression cylinder thermocouples

3.1.4 Engine oil pressure measurement and control

The Hatz 1D50 has an internal oil pump which is coupled to the output shaft of the engine, and thus motoring torque is coupled to oil pressure. Test repeatability is of great concern, so it is important to have some level of control over oil pressure. The stock Hatz engine uses a spring operated automatic pressure relief valve which can open during a test and skew results. This valve is eliminated using two methods. In the engine with no compression, the internal oil pump is removed and an external oil pump is installed bypassing the oil pressure relief valve. For the engine with compression, the internal oil pump is left in place and the oil pressure relief valve is replaced with a manual screw valve. For both engines, oil pressure is measured using a Cecomp Electronics Inc. pressure gauge, model number F4L100PSIG, with a range of 0 to 100 psig

The stock oil pump system in the engine consists of a gear pump which intakes oil at the sump and pumps oil through oil filter housing to the intake and exhaust valves and the clearance between the jacket and liner. The gear pump is driven by the drive shaft and part of the timing gear system. Thus the oil pump would be difficult to remove without removing the valve train of the engine. The external oil pump, shown in Figure 3.9 (a), is installed by removing the timing system and thus removing the drive system of the gear pump. A hydraulic hose is fitted to one of the drain plugs of the oil sump. The external oil pump draws oil from this hose and pumps the oil through another hydraulic hose to the oil filter housing where the oil is then pumped back into the original oil channels, shown in Figure 3.9 (b). This solution was not feasible for the engine with compression since the oil pump is coupled to the timing gears of the engine. Thus the stock pressure relief valve is removed and a screw valve is installed providing control over engine oil pressures. This also allows for a range of oil pressures to be run to examine the effect of oil pressure on motoring torque.

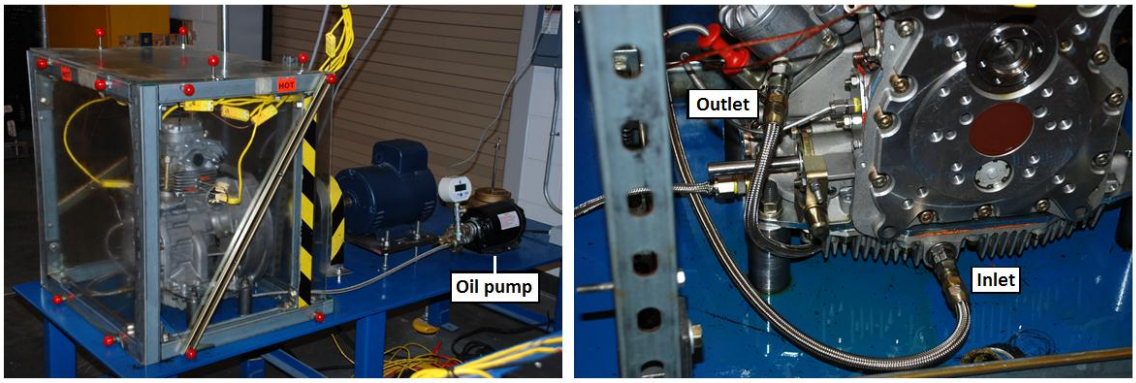

Figure 3.9: (a) External oil pump overview with (b) inlet and outlet

3.1.5 Motored engine friction rig data acquisition

The data acquisition system (DAQ) used in this study is comprised of an encoder, a torque meter, thermocouples, pressure transducers, power supplies, signal conditioners, connector blocks, DAQ cards, a PC, and LabVIEW™ programs. The DAQ is used to collect, process, display, and save data. This is accomplished by first obtaining the signals from the measurement devices then routing it through other components, as shown schematically in Figure 3.10, to the LabVIEW™ program where the data are processed. The DAQ hardware consists of high speed and low speed components. The high speed component is based on a National Instruments PCI-6284 card with a SCB-68 connector block measuring torque signal based on a digital trigger from the encoder. The low speed data consists of a NI cDAQ-9172 USB chassis with three NI 9221 analog input modules which measures temperatures and oil pressure. This allows for the separation of the instantaneous and average torque measurements.

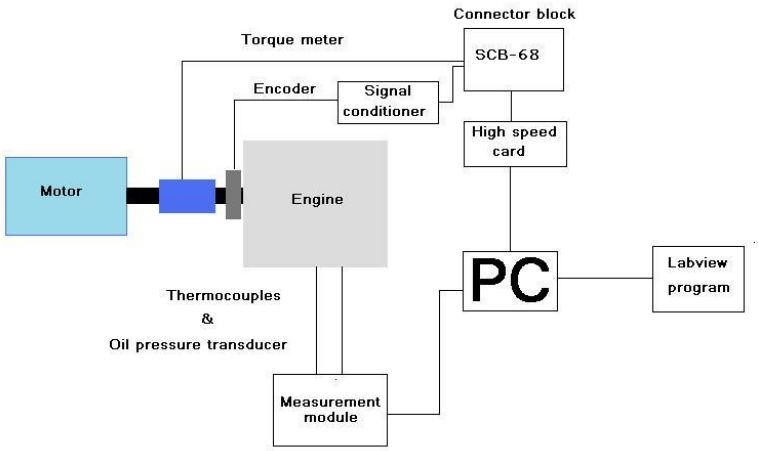

Figure 3.10: DAQ hardware wiring diagram

Motoring torque is measured as a function of engine crank angle with engine position measured using an encoder mounted on the engine drive shaft. The torque is measured every ½ degree and processed into two data sets. The first data set, called instantaneous torque, is motoring torque per ½ degree crank angle over an engine cycle with a maximum, minimum, and average value calculated for each ½ degree from a data set of 300 engine cycles. This number of engine cycles is selected to provide a large enough data set to reduce errors from cycle-to-cycle variation without the total time of data collection being too long. The max, min, and average instantaneous torque curves are each averaged to calculate the second data set, referred to as average torque. This process is shown schematically in Figure 3.11. The average torque provides an overview of the lube oil performance over a longer time period than the instantaneous torque. These average torque data are collected in conjunction with time, engine temperatures, oil pressure, and engine speed. Combining these data provide an overview of the lube oil performance.

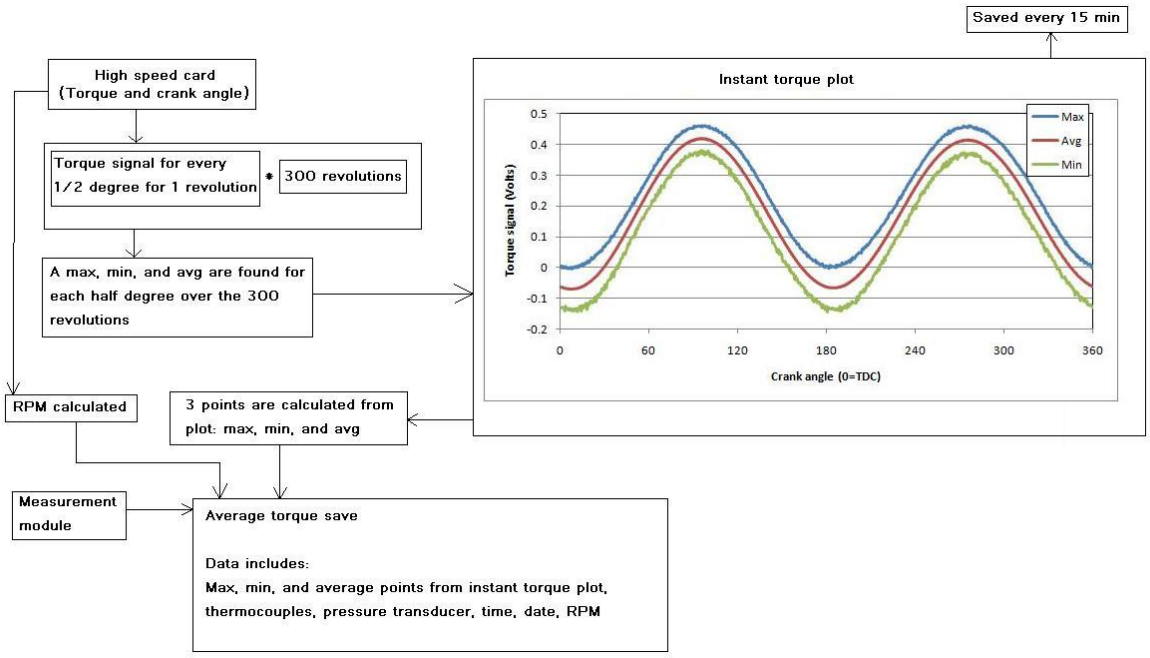

Figure 3.11: Motored engine friction data processing

3.1.6 Oil flushing procedure

Residual oil is left in the oil sump when an oil is drained and additive deposits can be left on the surfaces of the components when switching to new oils. Thus, it is important to devise an oil flushing procedure when examining lube oil performance with a motored engine rig. The oil drainage procedure used in the present study is as follows. The oil is first drained from the oil sump and the oil filter housing. The oil is also flushed out of the pumping system either by turning the engine by hand when the compression engine is used or by disconnecting the external oil pump output hose from the engine and using the pump to flush the oil out of the system. With the oil sump drain plug still removed, a portion of the new oil is poured into the oil sump to flush some of the residual oil from the oil pan. This concludes the oil drainage procedure and the

engine is then filled with the new oil sample. After the first test with the new oil sample, the oil drainage procedure is repeated and this concludes the oil flush procedure.

3.1.7 Calibrations

Over the course of the present investigation two torque meters were used. Initially, a Cooper Instruments and System LXT 971 torque meter with a range of 0 to 75 N.m and accuracy of 1% full scale output was installed between the motor and engine shafts via two flexible couplings, as shown in Figure 3.12 (a). The second torque meter, installed in the same manner as shown in Figure 3.12 (b), is an Omega TQ514-2K with a range of 0 to 226 N.m and linearity and hysteresis errors of 0.1 % of full scale output. The Omega torque meter has a larger range because a zero drift was observed with the previous torque meter which could be attributed to over extending the range during start-up. Excitation power is provided by a 12 VDC automotive battery for both torque meters.

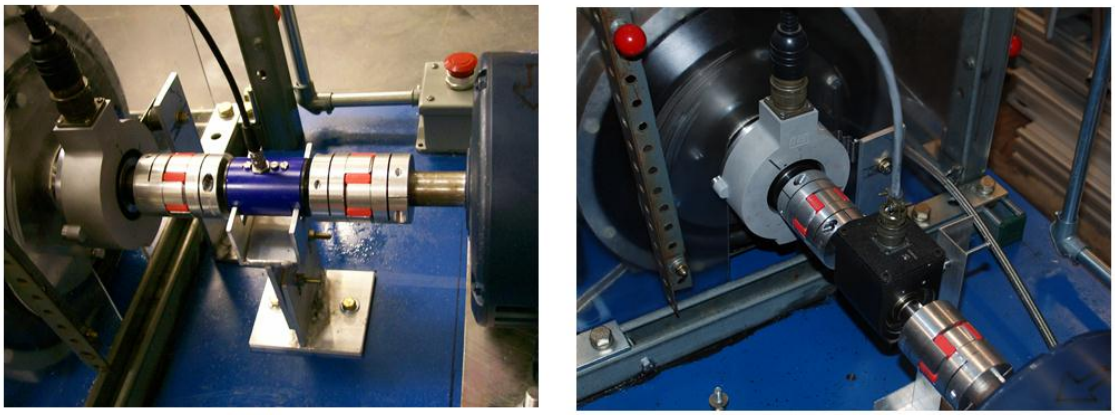

Figure 3.12: (a) Cooper Instruments and (b) Omega torque meters installed between the motor and engine

Both torque meters are calibrated using torque arms fabricated with two-piece clamp shaft collars and square bar stock. Bar stock of equal size was welded to each side of a clamp so that the torque arms are counter balanced and do not produce a moment as can be seen in Figure 3.13. Weights hung from the torque arms produce a moment on the torque meter for calibration. Weight is added until the maximum is reached and then individually removed to provide a measure of hysteresis. The Cooper torque meter is calibrated with 1 foot torque arms and weight up to 1.7 kg to produce a maximum moment of approximately 5 N.m, as shown in Figure 3.14 (a). The Omega torque meter is calibrated with torque arms of 1.5 feet and weight up to 8 kg to produce a moment of 36.4 N.m, as shown in Figure 3.14 (b). A calibration is performed before and after each experiment to observe any changes in calibration constants.

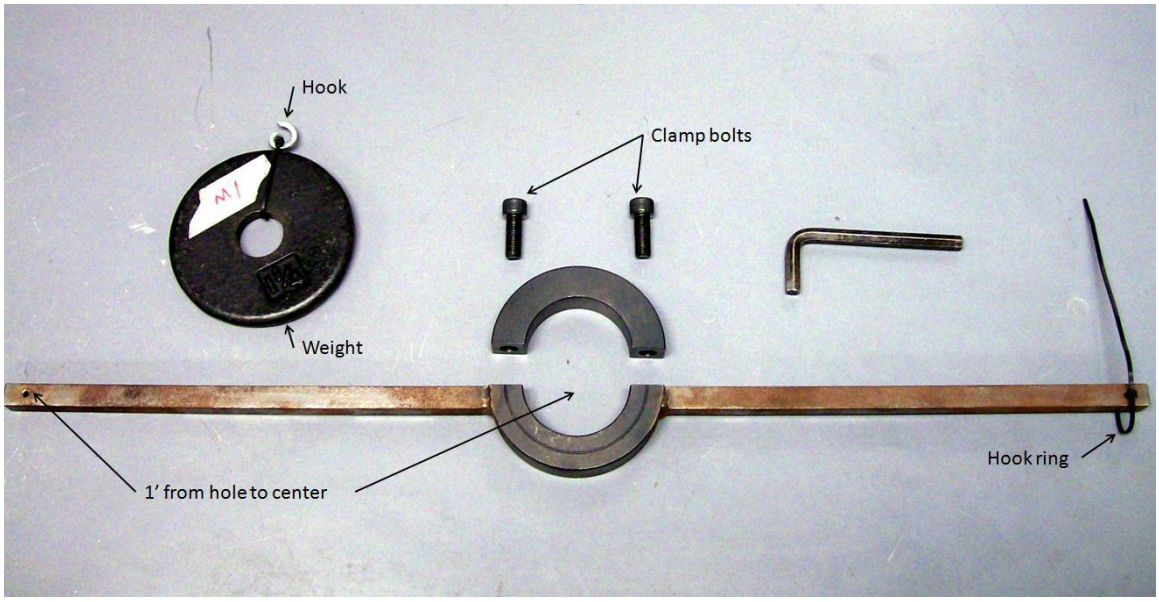

Figure 3.13: Torque meter calibration torque arm

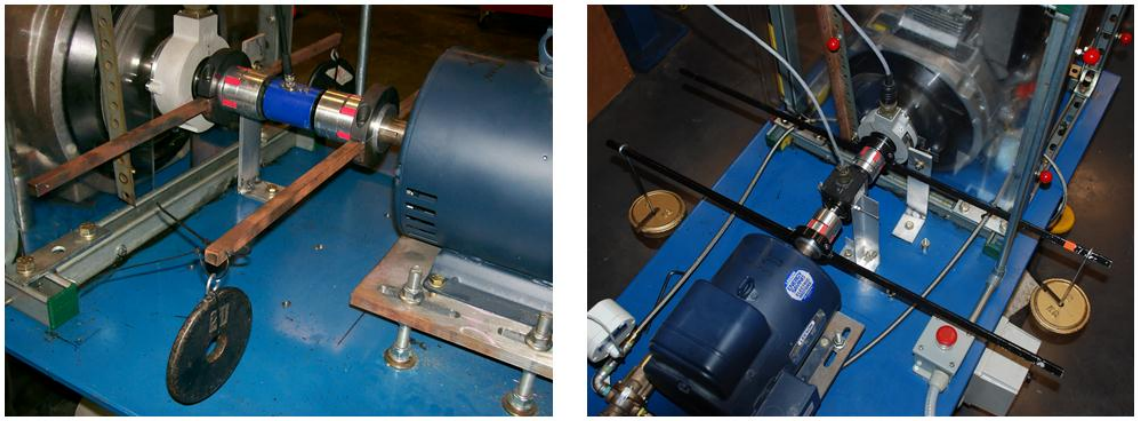

Figure 3.14: (a) Cooper Instruments and (b) Omega torque meter calibrations

3.2 Lube oil viscosity analysis

The motored engine friction rig developed in this study is used to evaluate lube oil performance through motoring torque or fmep as function of oil viscosity. Lube oil viscosity is calculated based on cylinder liner mid stroke temperature. Vogel's equation, shown as Equation 2.4, is used to determine lube oil dynamic viscosity, η, from engine oil temperature, T. The Vogel equation is a function of oil temperature and three constants. The constants, a, b, and c, are specific to a particular oil and are found using experimentally measured viscosities.

Lube oil viscosity is measured using the Petrolab Minivis II falling ball viscometer. This viscometer measures the time it takes a ball to fall a set distance through the oil sample and uses this information to calculated oil viscosity at a particular temperature via Stoke's law,

$$\eta = \frac{2gr_{ball}(\rho_{ball} - \rho_{oil})}{9\mathrm{v}} \qquad \textbf{(3.3)}$$

where η is dynamic viscosity, g is gravity, r_{ball} is the radius of the falling ball, ρ_{ball} is the density of the ball, ρ_{oil} is the density of the oil, and v is velocity. The density of the oil is required for the calculations but an initial value can be guessed for measurements and Stoke's law can be resolved to account for actual density. For a given oil, viscosity measurements are typically taken from 0 to 100 °C in increments of 20 °C. To calculate Vogel coefficients for an oil only three viscosities and temperatures are required. Typically, measurements at 20, 60, and 100 °C are used to solve Vogel's equation and the rest of the data points are used for reference to check Vogel predicted viscosities after calculation of the coefficients.

As seen in Equation 3.3, lube oil density is used in the measurement of lube oil density but the change in density over the temperatures measured is small. Therefore, the oil density change should not affect viscosity measurements and oil density at room temperature should be sufficient when measuring viscosity. To test this assumption, the density of an oil is examined over a range of temperatures and the effect of oil density on the Vogel predicted viscosity is investigated. If constant density proves to be acceptable, then room temperature density is used for all viscosity measurements.

Lube oil density is obtained by filling a 100 cc volumetric flask at room temperature and measuring the weight of the oil sample. The oil sample in the flask is then heated up to 100 °C in an oven with oil volume measured approximately every 5°C. These data are used to calculate a linear fit of oil density as a function of temperature so that oil density can be calculated for viscosity measurements. Vogel coefficients are then calculated for an oil using viscosities measured with constant density and temperature-dependent density. The results predicted by the two sets of Vogel coefficients are then compared.

3.3 AVL Excite Power Unit software

The theoretical investigation in this study is performed using AVL Excite Power Unit software. AVL Excite Power Unit is primarily a noise, vibration, and harshness engine design software but also simulates friction. Mathematically, the engine is modeled in two main groups called “Body equations” and “Joints” which model the engine components and the interactions between components, respectively. The model is based on engine parameters such as bore and stroke, component parameters such as mass and geometry, cylinder pressure over a cycle, and engine speed. The component interactions require various inputs depending on the sub-model or Joint being used. These inputs range from spring/damper coefficients to surface roughness, bearing clearances, mean asperity height, and etc.

The cylinder pressure trace and speed are the driving forces of the model. As a precursor to simulation, a kinematic analysis is performed which calculates the forces and torques on the bodies in the system. An average torque on the crank shaft is calculated during this analysis which equivalent to the losses in the pressure trace. This average torque is applied to the engine during the simulation so that gas pumping losses are balanced. Simulation results include the dynamics of the components and loads on the components. For this study, the angular acceleration of the crankshaft is the primary output of interest. This is multiplied by engine system inertia to calculate instantaneous torque on the crankshaft and average torque for comparison to experimental results.

3.3.1 Overview of basic mathematical models

AVL Excite Power Unit models the complex engine system as coupled systems. The mathematical models are divided into linear elastic or rigid models of engine components and non-linear contact between engine components,

referred to as Body Equations and Non-linear Contact Equations (Joints) respectively. The mathematical models of the Body Equations are capable of modeling both small motions (vibrations) and big (global) motions of the engine components. Excite accomplishes this through a discretization of the component (body) into a sufficiently high number of rigid sub-bodies (partial masses). The partial masses are modeled using Newton's equation of momentum and Euler's equation of angular momentum. The interaction between the partial masses is considered through damping and stiffness coefficients and any external forces from Joints or loads on the body.

The non-linear contact equations (Joints) range in complexity from non-linear spring damper models to thermo-elasto-hydrodynamic models which consider hydrodynamic pressure and hydrodynamic friction and the effect temperature and pressure on oil viscosity and density. For this study, friction is modeled using a modified Stribeck curve equation shown,

$$f = \frac{\mathrm{v}}{A\mathrm{v}^2 + B|\mathrm{v}| + C} + D\mathrm{v} \qquad \textbf{(3.4)}$$

where *f* is the friction coefficient, *v* is surface velocity, and A, B, C, and D are experimentally determined constants.

3.3.2 Overview of motored Hatz model

The AVL Excite model is created based on basic engine specifications, engine components models, models of the connections between engine components, and a cylinder pressure trace. The basic engine specifications of the Hatz engine are listed in Table 3.2. The engine components considered in this model are the engine block, crankshaft, flywheel, conrod, piston pin, and piston. These components are either considered as lumped masses or the body is modeled as a lumped mass system. The piston, piston pin, and flywheel are

considered as lumped masses with the piston and piston pin added to the small end of the connecting rod and the flywheel mass added to the crankshaft model. The connecting rod and crankshaft are modeled using the built-in sub-programs conrod modeler and shaft modeler respectively. The components modeled and the associated mass values are listed in Table 3.3, and the AVL Excite 2-D representation of the Hatz model is shown in Figure 3.15. The engine block is a component which must be included in the model as well. Excite requires a finite element model of the block; however, any model of an engine block can be used if the block is considered as rigid and the nodes moved to fit the specifications of the engine being modeled. This is done for this study by using a finite element model of an engine block from an AVL single-cylinder engine example model. This finite element model from AVL is modified by adjusting bearing and cylinder nodes to be consistent with the Hatz engine. This process does not affect the simulation since the engine is considered to be rigid. If the engine is considered to be flexible this would not be possible.

Table 3.2: Excite Hatz model basic engine specifications

Engine speed, RPM	1791
Number of cylinders	1
Bore, mm	97
Stroke, mm	70
Conrod length, mm	115
Engine Type	4-Stroke
Rotation axis	e1
Vertical axis	e3

Table 3.3: Engine components considered in Excite Hatz model

Component	*Modeled as*	*Measured mass values, grams*	*Excite mass values, grams*
Piston	Lumped mass	649.8	650
Piston Pin	Lumped mass	202.8	200
Connecting rod	Lumped mass system	638.5	640.021
Crankshaft and Flywheel	Lumped mass system	30454	30426.3

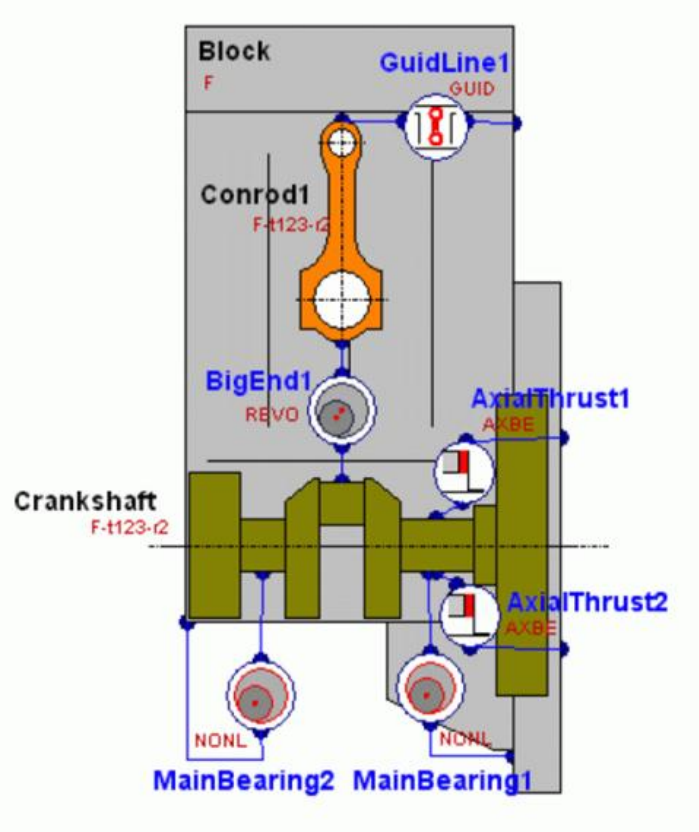

Figure 3.15: 2-D view of Hatz model with components and joints

The conrod modeler models the connecting rod based on material properties and geometry. Figures 3.16 and 3.17 show the material properties and geometry of the conrod of the Hatz single-cylinder engine, respectively. The density of the connecting rod is calculated by measuring connecting rod mass and adjusting density in Excite so that the connecting rod mass calculate in the program is equal to measure mass. The Young's Modulus and Poisson's Ratio are the default steel material properties used by AVL Excite.

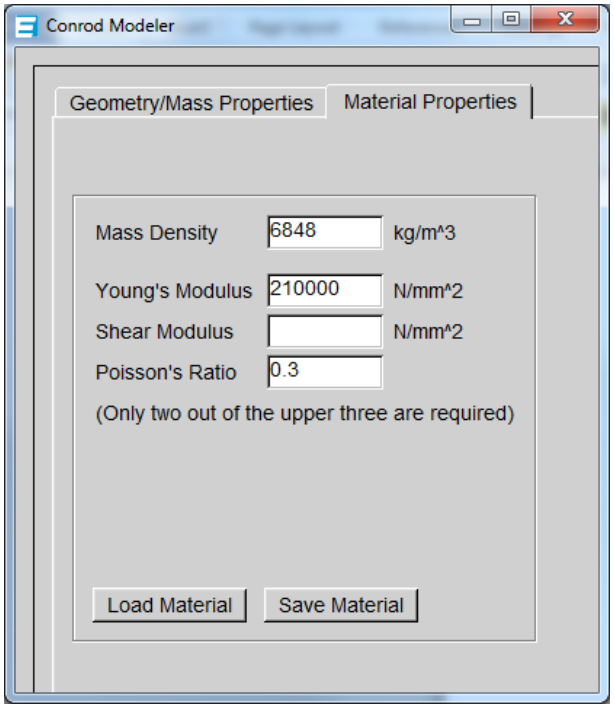

Figure 3.16: Conrod Modeler Material Properties – input

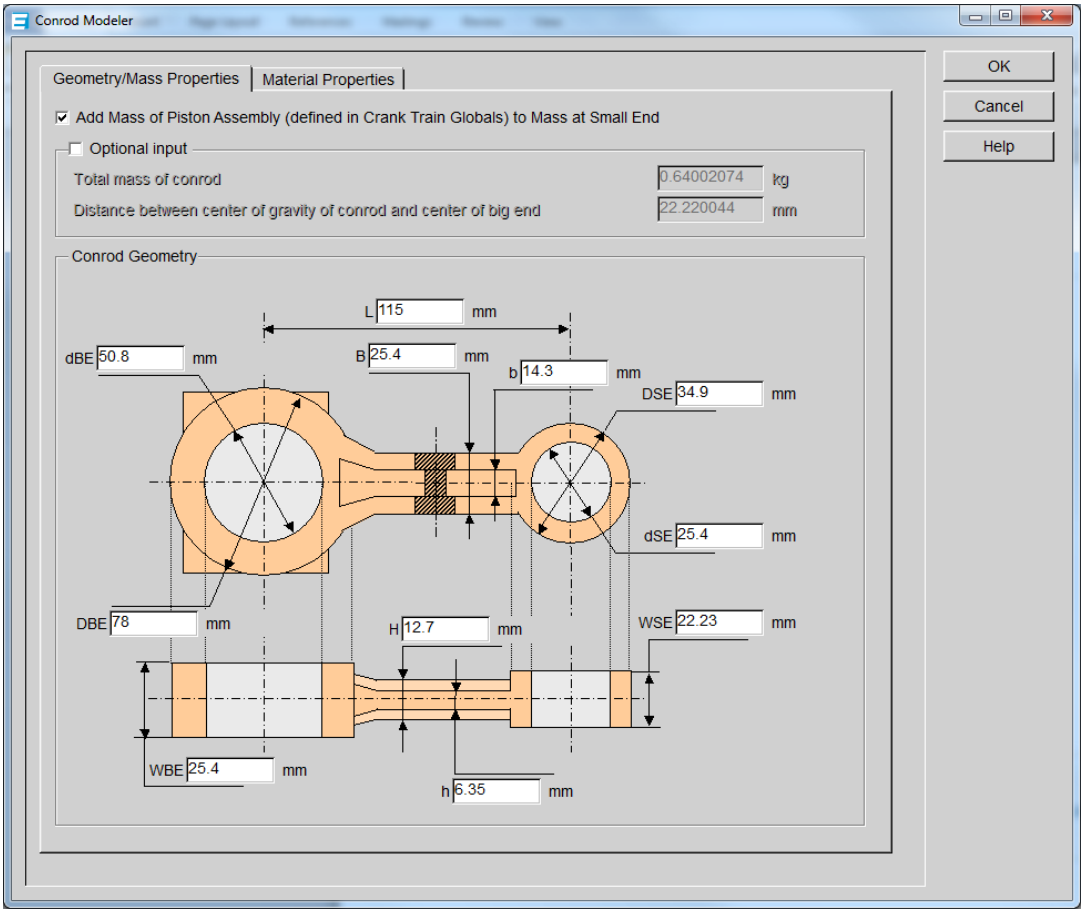

Figure 3.17: Conrod Modeler dimensional inputs

The crankshaft is modeled using the built-in Excite subprogram shaft modeler. For this model, a CAD drawing of the crankshaft without the flywheel is used to create a sterotithograph file (STL) for input into the shaft modeler sub-program as shown in Figure 3.18. The flywheel is added to the crankshaft in the shaft modeler program based on a measured mass value and a moment of inertia calculated using a basic cylinder inertia equation. Shaft modeler uses the geometric data from the STL file, shaft material density, and the flywheel inputs to create a lumped mass system representative of the crankshaft and flywheel.

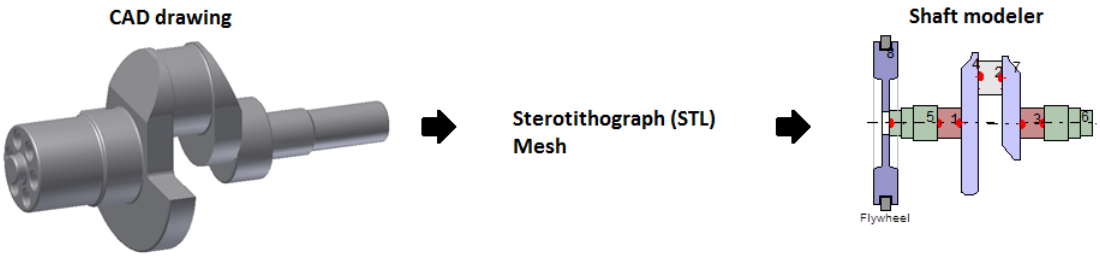

Figure 3.18: Geometric shaft modeler input

The connections between each component are modeled using spring-damper models. The piston/liner contact is modeled as connections between a node representing the small-end of the connecting rod and several nodes on the trust sides of the liner. The connecting rod and crankshaft connections are modeled as a connection between the center of the big-end of the connecting rod and center of the crank-pin. The two main bearing models which connect the crankshaft and engine block are each modeled as a set of 5 nodes along the crankshaft center axis and 5 sets of nodes arranged in circles which represent the bearing surface. The axial thrust bearings are generic connections to provide resistance to axial movement of the crankshaft. The connections for these joints are made between a node from the crankshaft bearing and a node from the engine block. A 3-D model of the lumped mass systems, nodes, and connections is shown in Figure 3.19, where the crankshaft is green, the connecting rod is red, and joint connections are dark and light blue. Only one main bearing is shown in this figure and the axial thrust bearings are excluded.

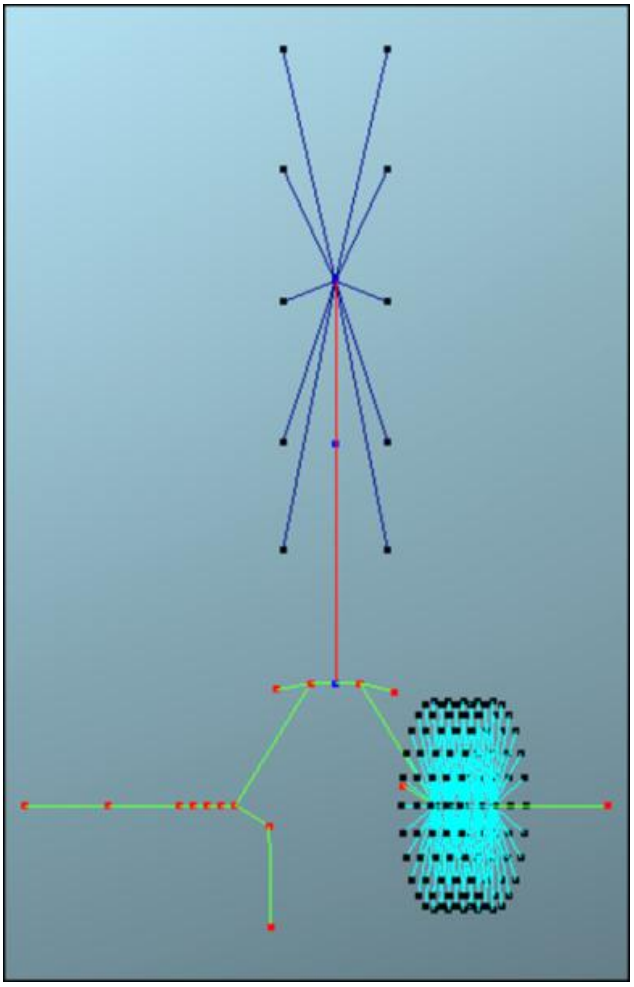

Figure 3.19: 3-D view of Hatz Excite model

Two pressure traces are used in this study to model a compression and a no-compression motored engine. The compression pressure traces, shown in Figure 3.20, are obtained from a Hatz 1D50 engine used in another study while being motored at 1791 RPM. A no-compression pressure trace, shown in Figure 3.21, was created from the compression pressure trace by copying and repeating the intake/exhaust section so that the data set is 720 degrees long which is a requirement of AVL Excite.

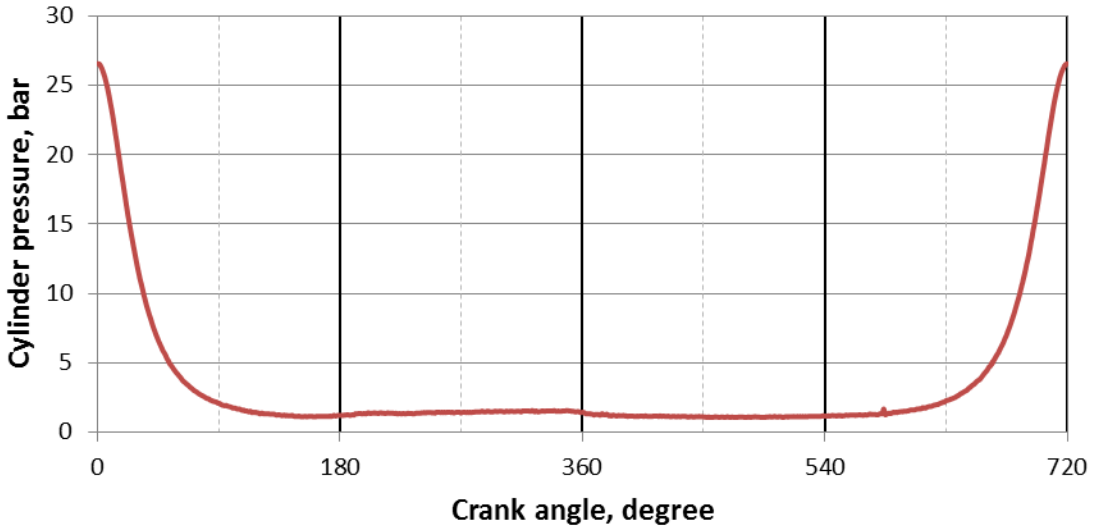

Figure 3.20: Cylinder pressure trace for motored Hatz 1D-50 with compression (0 = TDC)

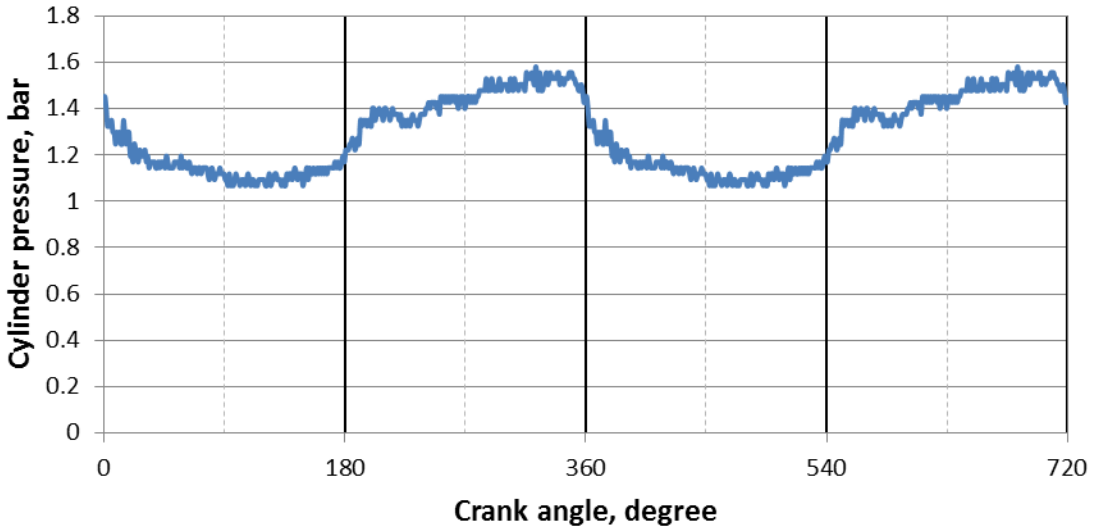

Figure 3.21: No compression cylinder pressure trace

3.3.3 AVL Excite Hatz model output

Simulation outputs include forces, positions, velocities, and accelerations of the bodies in all coordinates. However, friction losses are not directly calculated and have to be evaluated through crankshaft angular acceleration. Excite accounts for any losses in the pressure trace by using kinematics to calculate the average torque on the crankshaft pre-simulation and applying this load during simulation. This load is equivalent to pressure trace losses since the other loads in the kinematic calculations created by mass-acceleration forces are conservative over the engine cycle.

When friction is applied in simulation, the average angular velocity of the crankshaft decreases from cycle-to-cycle and, if fiction losses are consistent from cycle-to-cycle, the average angular acceleration of the crankshaft is constant. Friction torque losses are found by multiplying the angular acceleration of the crankshaft by system inertia. This can be done to the instantaneous or average angular acceleration of the crankshaft for comparison to experimental instantaneous and average torque. Typical crankshaft angular acceleration output from a simulation is shown in Figure 3.22.

The system inertia is calculated by creating a model with zero cylinder pressure and thus zero average torque when no friction is considered in the model. A load is manually applied to the crankshaft and the change in average angular acceleration is observed. This is done for several loads. The loads and the corresponding average angular accelerations are plotted. The slope of this plot is the system inertia. Calculated average friction torque is checked by manually applying the calculate friction torque and checking that the average velocity of the simulation remains constant

PREVIEW

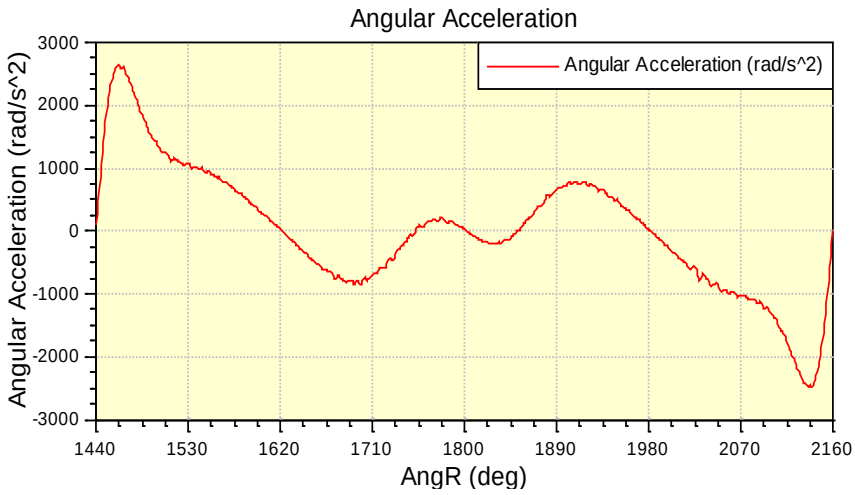

Figure 3.22: Excite crankshaft output based on compression pressure trace

3.4 Line Contact Friction Rig

The theoretical portion of this study requires measurement of the friction coefficient for the oils simulated. A line contact friction measurement device is used to obtain friction coefficients for a given oil as a function of speed, temperature, and applied normal load. Line contact friction rig results are used as input for the AVL Excite Power Unit software to predict engine friction for a given oil.

The line contact friction rig consists of a cylinder, rotated by a variable speed electric motor, with a plate forced against it to create friction. The 3.5” diameter by 2.5” long cylinder is enclosed in a housing which also holds the oil sample. The bottom of the cylinder is submerged in the oil and as it rotates oil adheres to the cylinder. The cylinder housing has a rectangular opening which allows the 1” X 2” flat plate to be pushed against the rotating cylinder. The plate is mounted to a carriage which gives the plate 3 degrees of freedom. The plate

can move in a horizontal-perpendicular plane to the cylinder axis, a vertical-perpendicular plane to the cylinder axis, and rotate about an axis vertical-perpendicular to the cylinder axis. The horizontal movement allows for the plate to be moved to and from the cylinder and allows for an oil film to form between the surfaces. A cable connected to the plate housing carriage is used to force the plate against the cylinder via calibration weights. The vertical movement of the plate housing allows for friction to force the housing downwards against a load cell. Thus with the friction force measured with the load cell and the known applied load, the friction coefficient can be calculated. The third degree of freedom allows for corrections in misalignment. A picture of the line contact friction rig is shown in Figure 3.23.

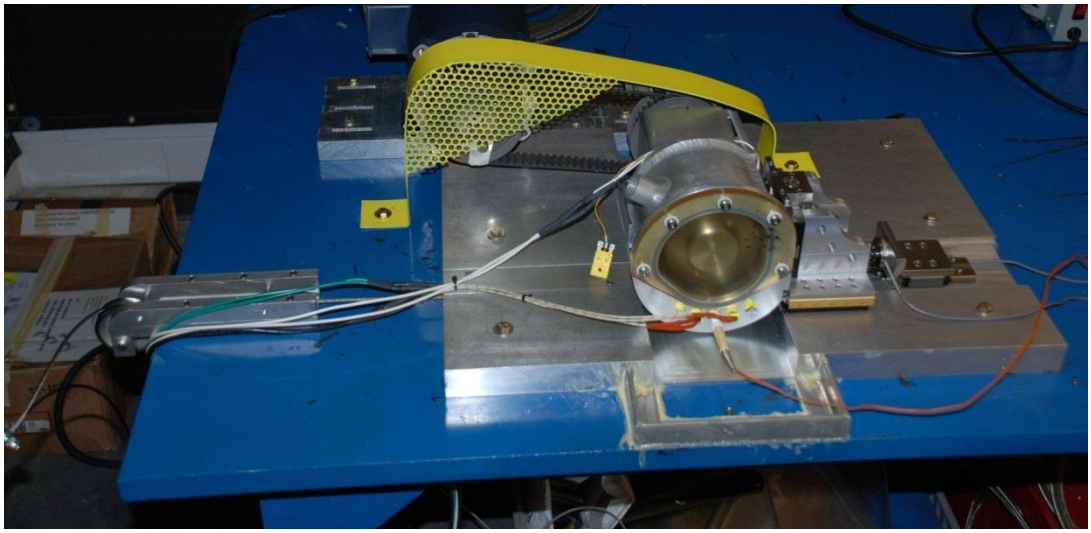

Figure 3.23: Line contact friction rig

Surface contact is measured using electrical contact resistance (ECR). ECR consist of an electrical circuit between the plate and the cylinder. For metal to metal contact, the resistance between the cylinder and plate will be at a minimum and voltage at a maximum. As a surface layer starts to form the resistance will increase and voltage will drop in the circuit. Eventually, as the oil film layer will build to the point where there is no surface contact and the voltage will drop to zero.

During these experiments: friction load, temperature, rotating speed, and surface contact are measured with temperature measured by a type K Omega thermocouple with an accuracy of 2 °C and speed measured with a US digital encoder, model number HB6MS-2048-625. The normal load produced via calibration weights and friction load, measured by a LCGC-5 Omega load cell with a range of 5 lbs and linearity and hysteresis errors of 0.1 % full scale output, are used to find a friction via,

$$F_f = f F_n \tag{3.5}$$

where F_f is friction force, f is the friction coefficient, and F_n is the normal force. This information is plotted as a function of sliding velocity for a particular load and temperature so that the constants in the friction coefficient equation from AVL Excite, shown as Equation 3.4, can be calculated. These constants are then used as inputs to AVL Excite to examine the lube oil performance prediction capability of the software. Temperatures in the oil sump are increased with two 100 W cartridge heaters.

CHAPTER 4
MOTORED ENGINE FRICTION RIG RESULTS AND DISCUSSION

This chapter presents and discusses the development of and results from the motored engine friction rig used in the current study. The development of the motored engine friction rig is described in Section 4.1. The results for the calculation of Vogel's constants and the validity of using a constant density when measuring lube oil viscosity are discussed in Section 4.2. The instantaneous motoring torque results for the motored engine friction rig are presented Section 4.3 with a comparison for the different engine configurations. Finally, the average torque or friction mean effective pressure results are discussed in Section 4.4.

4.1 Motored engine friction rig development

In order to approach the temperatures achieved in a fired engine and to reduce errors in results, the motored engine friction rig in the present study has gone through several stages of development. These stages of development included three engine configurations: the modified engine with internal oil pump, modified engine with external oil pump, and stock engine. The development and impact of the various methods used to increase engine temperatures are described in Section 4.1.1. The accuracy of using cylinder liner wall outer temperature in lieu of liner wall inner temperature is discussed in Section 4.1.2. The reduction of torque meter signal noise by switching to a 12 VDC automotive battery and implementing a torque averaging procedure is presented in Section 4.1.3. Torque meter calibration constants are evaluated over time and the difference in results measured with the Cooper Instruments and Omega torque meters is shown in Section 4.1.4. Finally, the effect of the external oil pump on motoring torque described in Section 4.1.5.

4.1.1 Increasing engine operating temperatures

Engine temperatures are increased with an enclosure, an oil sump heater, and engine cowling. The installation of the enclosure around the engines has the most significant effect, increasing temperatures from approximately 45°C for the unheated engine without compression to approximately 70°C as shown in Figure 4.1. While this increase is significant, motored engine temperatures are still 20°C below fired engine temperatures. Therefore a 500 W Watlow firerod cartridge heater is installed in the oil sump to further increase temperatures, resulting in an increase of only approximately 5°C. To further increase the engine operating temperature, the 500 W heater is replaced by 1000 W heater of the same type. However, the 1000 W heater was installed at the same time as the external oil pump and the effect of the higher power heater is diminished due to heat losses from oil pump supply hoses. Because of these losses, engine temperatures with 1000 W heater modification are similar to temperatures for the enclosure alone. Thus the maximum engine temperatures for the modified engine (without compression) are approximately between 70 and 75°C.

The engine with compression can be operated at higher temperatures as compression adds heat to the system as shown in Figure 4.2. The results shown in this figure are performed over a range of engine temperatures which are varied by adding or removing enclosure panels, adjusting heater set point, and adjusting the position of the engine cowling. The lowest liner temperature of approximately 70°C occurs with the cowling in the stock position, the heater off, and an enclosure panel removed. The highest liner temperature of approximately 100°C occurs with the oil sump heater set to a temperature of 120°C, cowling in reverse position, and the full enclosure in place. The lowest temperature is comparable to temperatures for the modified engine without compression; whereas, the highest temperatures are similar to fired engine temperatures.

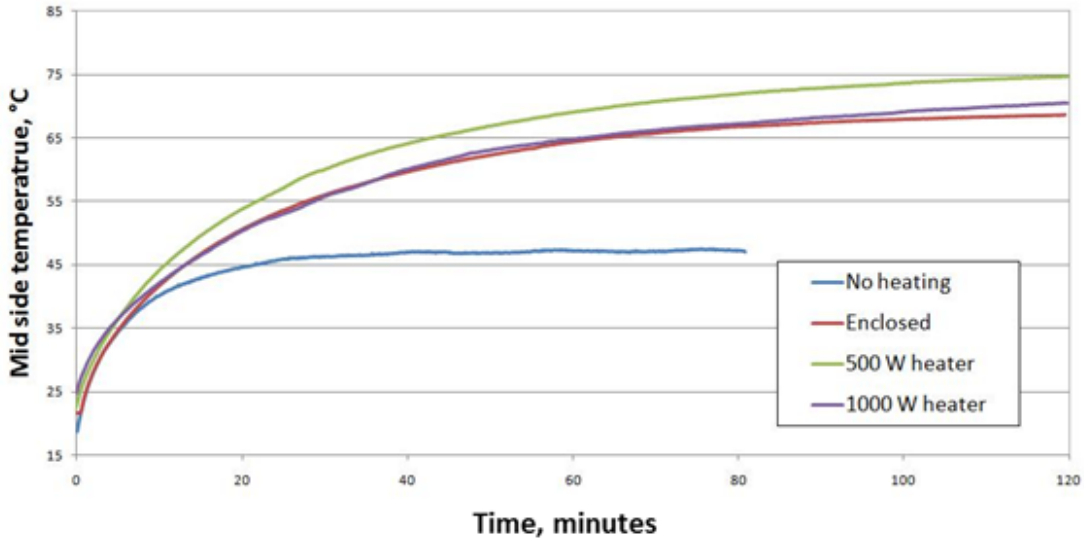

Figure 4.1: Effect of different methods used to increase temperatures in the motored engine without compression measured at cylinder liner mid-stroke

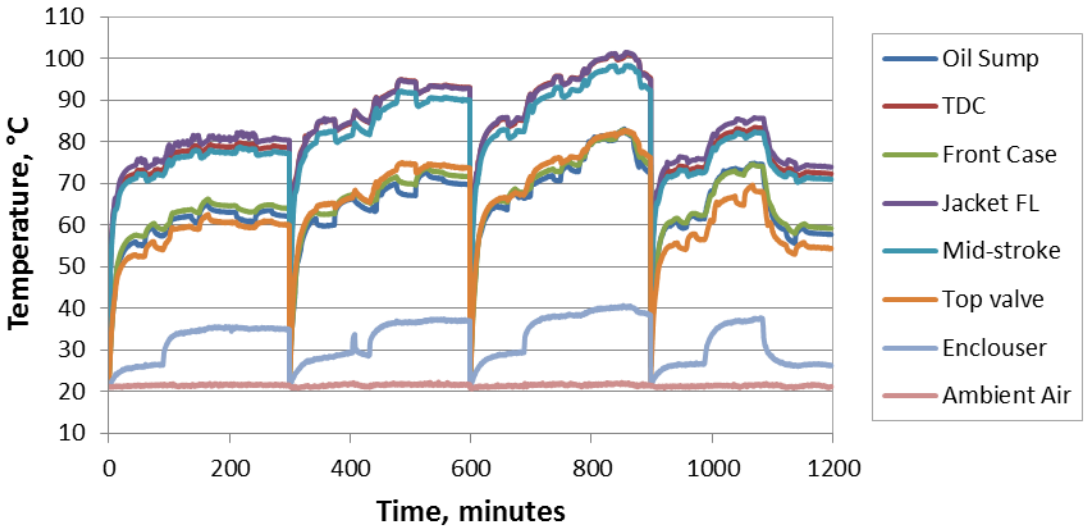

Figure 4.2: Temperatures at different engine locations for Mobil-1 5W30 test run in the stock motored engine with compression over 4 tests

4.1.2 Comparison of estimated of inner cylinder liner and outer cylinder liner temperatures

The validity of using the external cylinder liner temperature for lube oil viscosity calculations instead of the inner wall temperature is examined in this section with the liner inner surface temperature estimated using Equation 3.1 with the assumptions listed in Section 3.1.3. The temperature difference between the inner and outer surfaces of the liner generally decrease with time with the average difference being 1.6°C for the first 10 minutes and 0.6°C for the rest of a 2 hour test. When comparing fmep plots for piston liner inner and outer surface temperatures the effect is more noticeable during the first 10 minutes of the test as can be seen in Figure 4.3. However, the curves are similar during the rest of the test. Because the curves are so similar, the same conclusions would be drawn when comparing results from different oils regardless of if the inner or outer liner surface temperature is used. Consequently, it was decided that either temperature would be acceptable for determining lube oil viscosity and the outer liner temperature was chosen for use in this study.

4.1.3 Reduction of torque meter noise via battery power supply

Initial tests with the motored engine friction rig show evidence of 60 Hz noise in the output of the torque meter as seen in Figure 4.4. A major portion of the noise originates from an AC to DC power converter with a smaller noise contribution from power cords near the signal cable. To eliminate these sources of noise, a new signal cable is used and the torque meter excitation source is switched from the AC/DC converter to a 12 VDC battery. This produces a much cleaner signal as can be seen in Figure 4.5. The effect of the battery can also be seen in the frequency domain as shown in Figure 4.6.

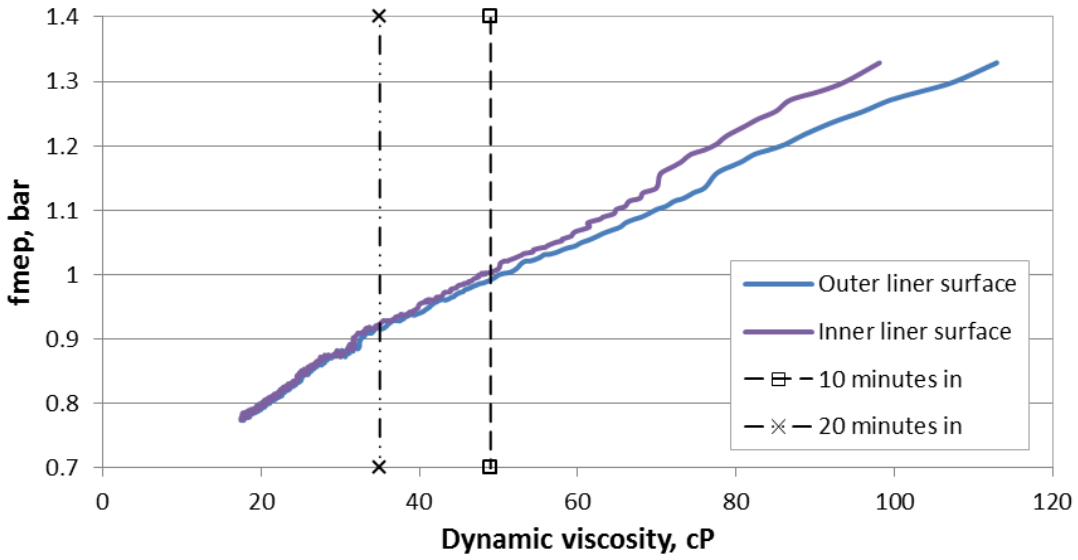

Figure 4.3: Comparison between fmep data plotted with viscosities calculated from inner and outer liner surface temperatures

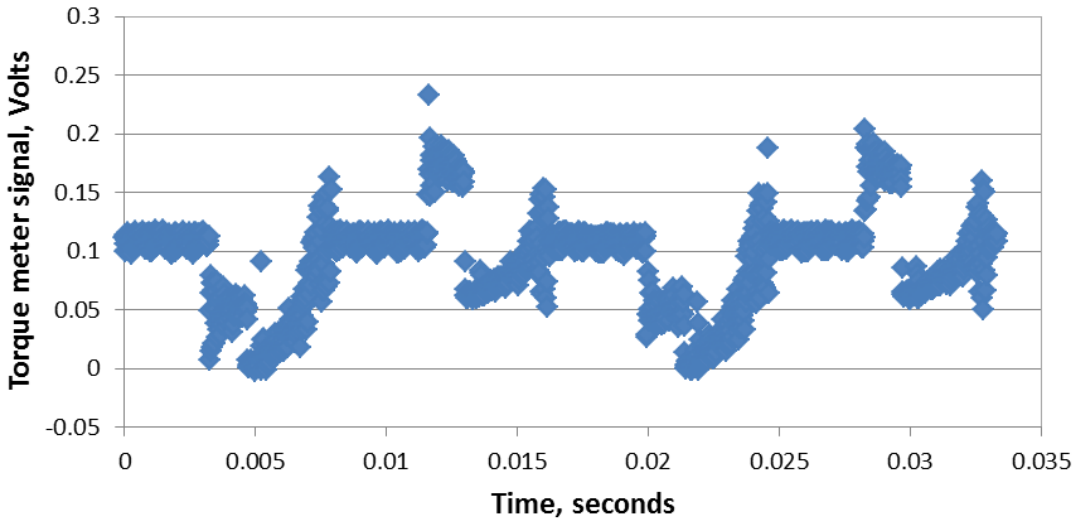

Figure 4.4: Signal from torque meter when powered by A/DC converter sampling at 60 kHz

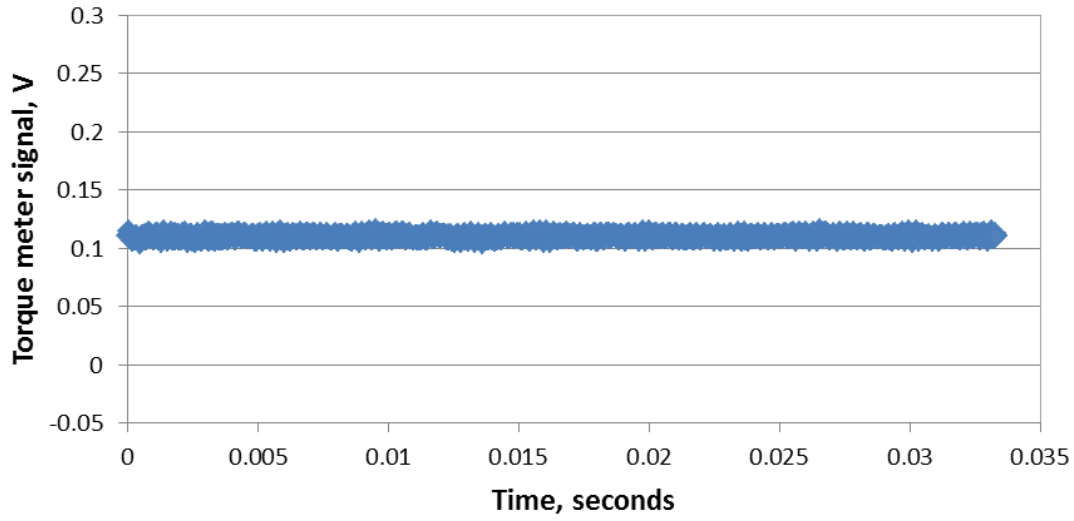

Figure 4.5: Signal from torque meter when powered by 12 VDC battery sampling at 60 kHz

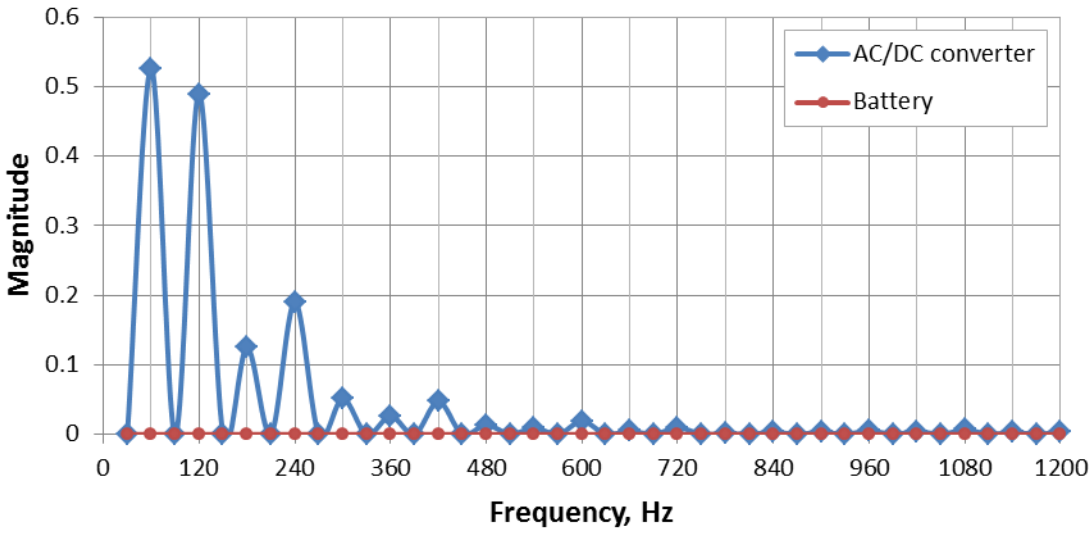

Figure 4.6: Comparison of frequency domain plots for torque meter signal powered by AC/DC converter and battery

Engine vibrations during motoring and cycle-to-cycle variations can also produce noises in the torque output. These effects are considerably reduced by measuring torque every ½ degree for 300 cycles and calculating a maximum, minimum, and average value each ½ degree crank angle. The torque signal before switching to battery power and averaging the torque over 300 cycles produced noisy results, as can be seen in Figure 4.7. By, switching the torque meter to a battery power supply and averaging the data produces much cleaner results as illustrated in Figure 4.8. The effect of cycle to cycle variations obtained is still observed in this figure in the maximum and minimum instantaneous curves; i.e., the larger the separation between these curves, the larger the cycle variations. From the average instantaneous torque results, friction mean effective pressure is calculated for the evaluation of lube oil performance.

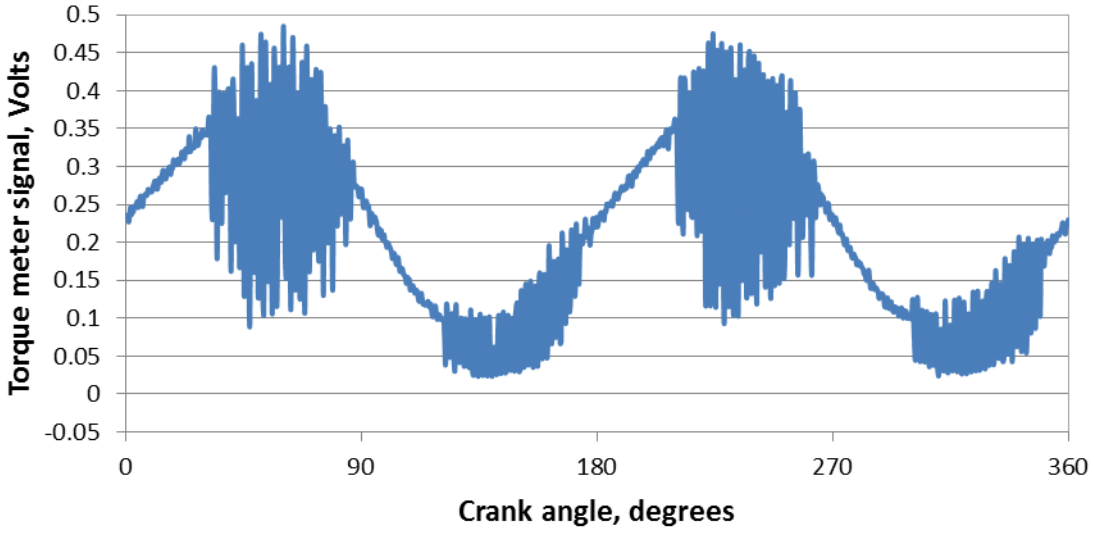

Figure 4.7: Instantaneous torque with torque meter excited by AC/DC converter

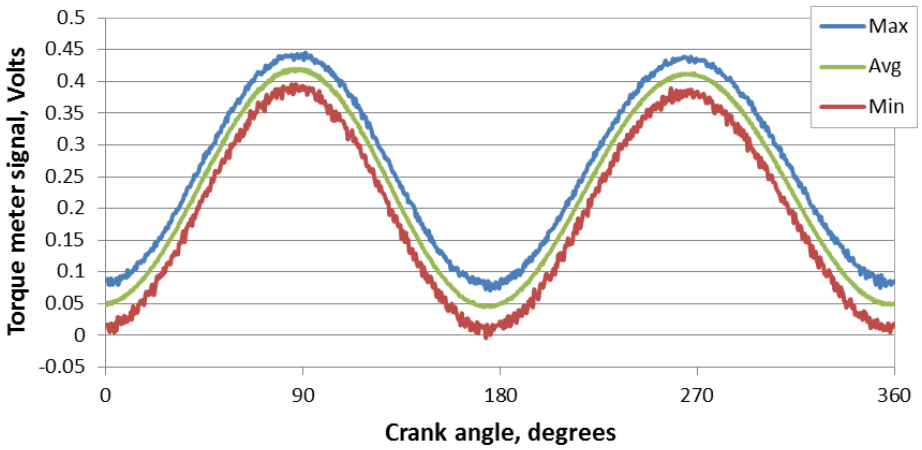

Figure 4.8: Instantaneous torque with torque meter excited by 12 VDC battery and averaged over 300 crankshaft revolutions

4.1.4 Torque meter calibrations and comparison of results from the two torque meters

The effects of instrument drift and changes in the calibration curve of the torque meter can be minimized by performing torque meter calibrations before and after each test. Calibration curves of a Cooper Instruments torque meter are shown in Figure 4.9. The averaged calibration curve in the figure is used for data reduction and is obtained by averaging the slope and intercepts from the pre and post calibrations. The Cooper Instruments torque meter, with a range of 0 to 75 N.m, is used for the first stage of the study. The calibration slope for this torque meter varies from 48 to approximately 52 N.m/Volt as shown in Figure 4.10. The y-intercept of the calibration curves shows greater consistency than the calibration slope as can be seen in Figure 4.11, with the exception of calibrations 33 and 34. The calibration arms were not removed between calibrations 33 and 34, so the anomaly likely stems from some calibration arm setup error.

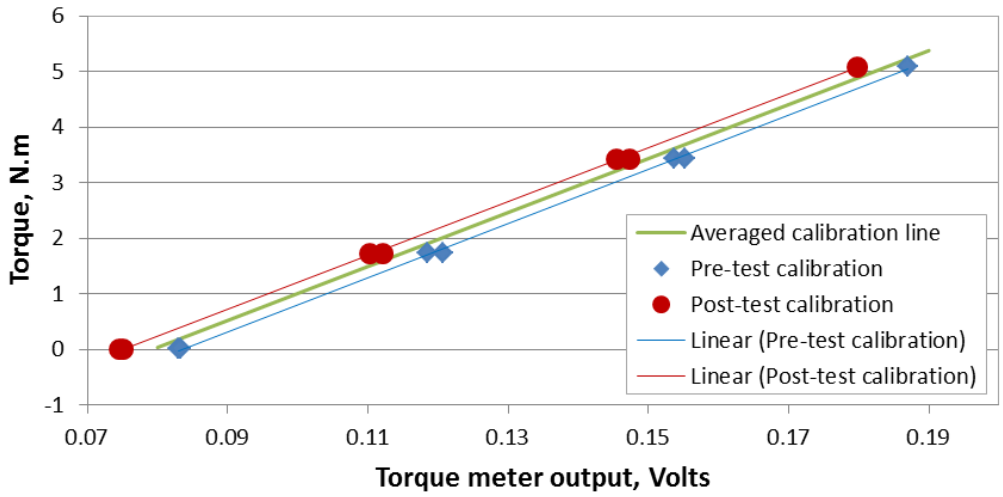

Figure 4.9: Example calibration plot for Cooper Instruments torque meter

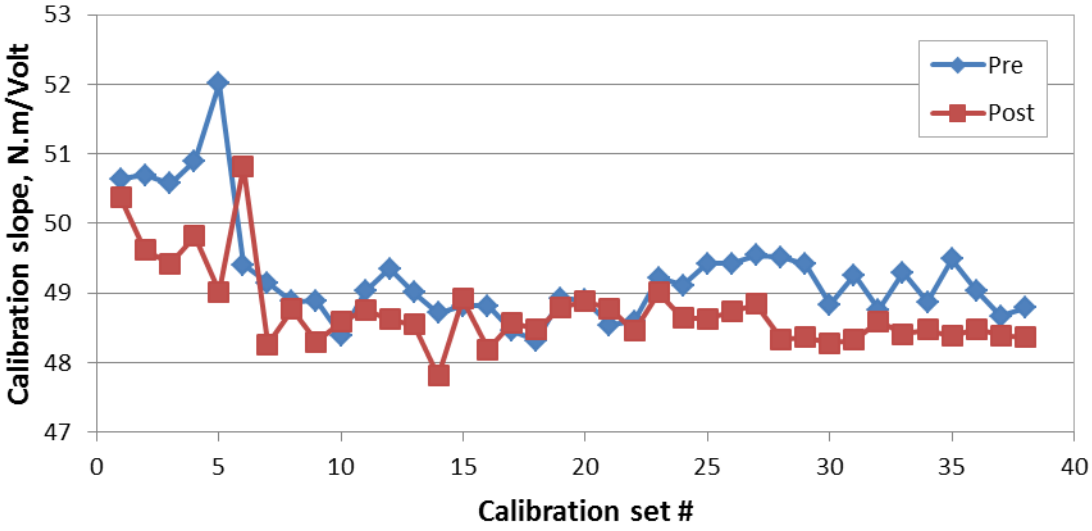

Figure 4.10: Cooper Instruments calibration equation slope over time

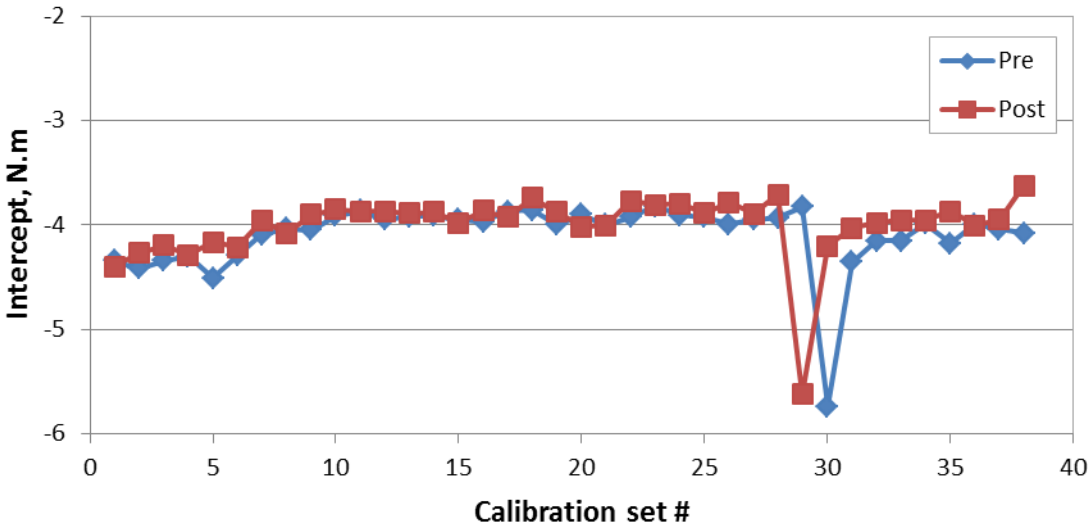

Figure 4.11: Cooper instruments calibration equation y-intercept over time

The calibration slope and y-intercept for the Omega TQ514-2K torque meter with a range of 0 to 226 N.m appear to be much more consistent than the Cooper Instruments torque meter as can be seen in Figures 4.12 and 4.13. A slight upward shift is noticed in the y-intercept for the Omega torque meter which occurred after a dip in battery voltage due to normal decrease in voltage over time and use. Even though the battery is fully charged after this dip, the shift in the calibration y-intercept remains. The better performance of the Omega torque meter is attributed to the larger range as the smaller range Cooper Instruments torque meter may have been subjected to larger excursions during start-up causing errors in the sensor. This shows the importance of correctly sizing a torque meter for the intended use. Since single-cylinder engine motoring and fired torques vary significantly over a cycle, over-sizing the torque meter for single-cylinder engines is appropriate and care should be taken when selecting the torque meter.

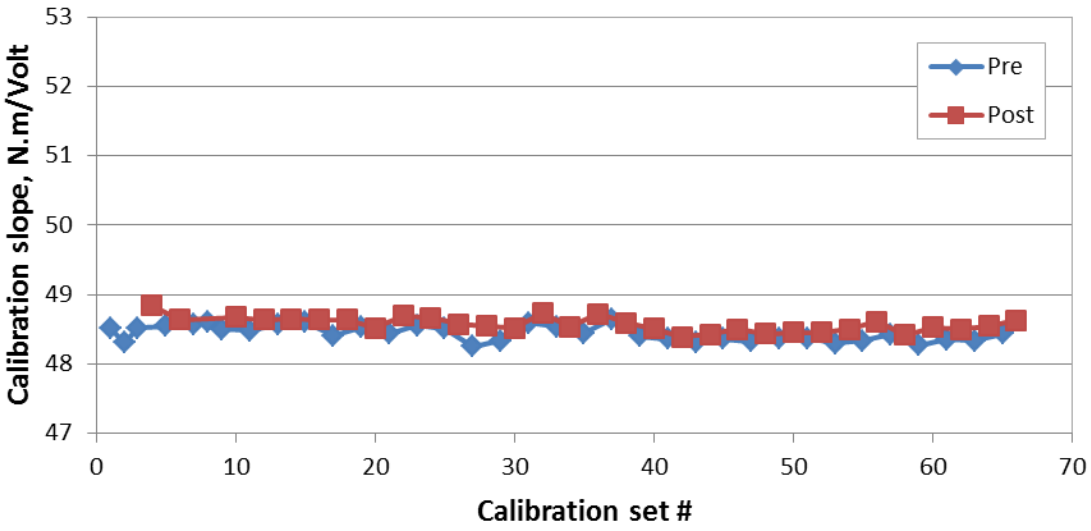

Figure 4.12: Omega torque meter calibration equation slope over time

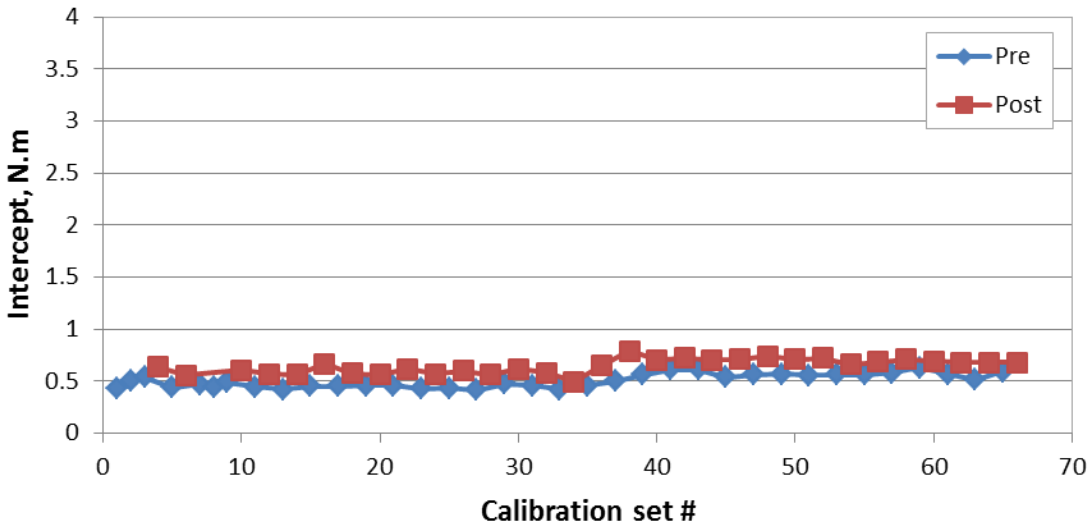

Figure 4.13: Omega torque meter calibration equation y-intercept over time

4.1.5 Engine oil pressure

Since the oil pump in the engine is coupled to the drive shaft a change in oil pressure can affect the motoring torque. Therefore, it is important to have methods in place to prevent unexpected changes in oil pressure. The effect of oil pressure on motored engine friction rig results is observed during a set of tests with a 10W30 base oil as can be seen in Figure 4.14. The oil pressure units are expressed in volts as initially the oil pressure was not deemed important for the evaluation of lube oil performance and is measured mainly as a safety check. The oil pressure profile for experiment 1, blue data, is typical but a significant increase in oil pressure is observed in experiment 2, red data. This increase in oil pressure directly results in an increase in fmep as seen in Figure 4.15.

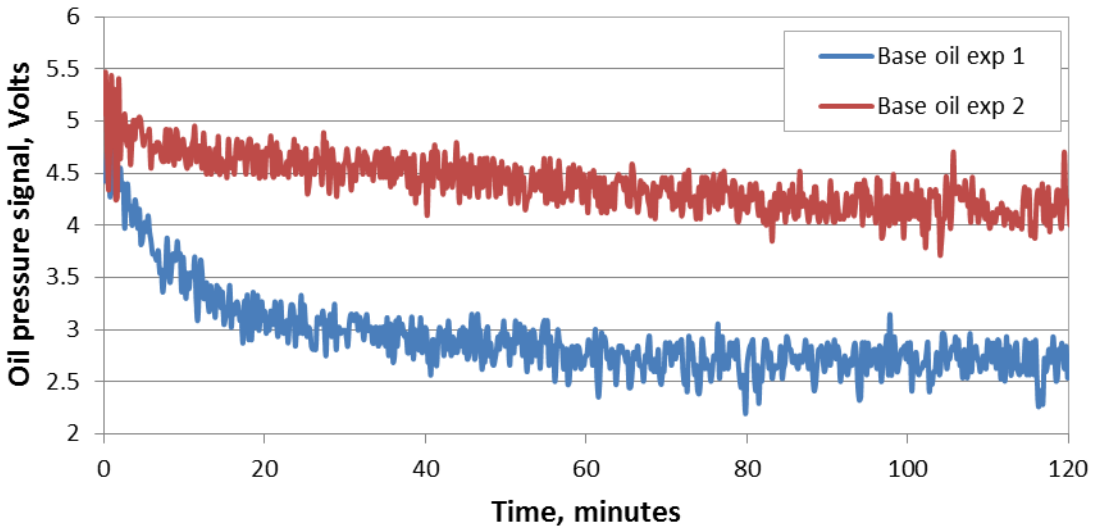

Figure 4.14: Oil pressure over two SAE 10W30 base oil experiments

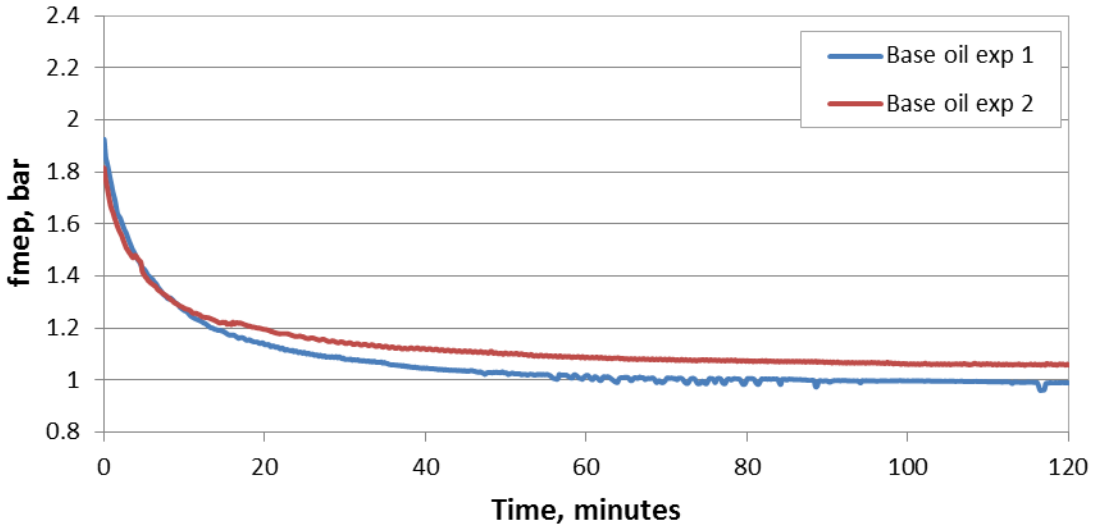

Figure 4.15: Increase in fmep due to increase in oil pressure for 10W30 base oil

To prevent oil pressure from affecting the motoring torque, the internal oil pump is removed and an electrically driven external oil pump is installed on the modified engine without compression. For the engine with compression, the internal oil pump was not removed since the timing gears required for valve operation are linked to the gear pump. Instead, the automatic pressure relief valve was replaced with a manual oil pressure valve. As seen in Figure 4.16, the removal of the internal oil pump results in a lower fmep since the AC drive motor for the motored engine friction rig is no longer pumping the oil. The difference in fmep for the two cases is approximately 0.37 bar and is largest at the beginning of the test. For the stock engine, oil pressure is varied from approximately 25 to 72 psi producing a change in fmep of approximately 0.08 bar which is similar to the difference seen in Figure 4.15. These methods of controlling and eliminating oil pressure increase the usefulness of the motored engine friction rig by improving repeatability of experiments.

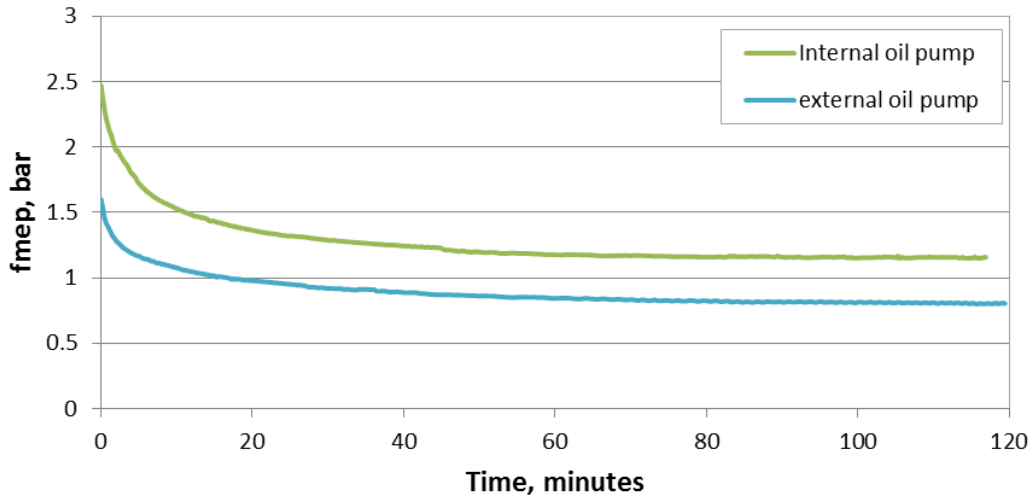

Figure 4.16: Fmep for a SAE 15W40 lube oil before and after installing external oil pump

4.2 Lube oil viscosity as a function of temperature

Vogel's equation involves temperature and three experimentally-determined coefficients. These coefficients are unique to a given oil and are found by fitting Vogel's equation to lube oil viscosity measured using a falling ball viscometer. Lube oil density, which is temperature-dependent, is required to use this viscometer. However, the oil density change over the range of temperatures measured has a small effect on the measured viscosities. Thus, a constant density measured at room temperature can be assumed when measuring lube oil viscosity. The validity of a constant density assumption is explored in Section 4.2.1 in which viscosity measured with constant density are compared to those measured with temperature-dependent density. Section 4.2.2 provides an overview of the viscosity measurements and Vogel coefficients for all the oils examined in this study.

4.2.1 Effect of lube oil density on viscosity measurements

Viscosity for a lube oil is measured using a falling ball viscometer which calculates viscosity with Stoke's law shown in Equation 3.3. Stoke's law expresses dynamic viscosity as a function of gravity, the radius of the falling ball, density of the ball and the liquid, and the terminal velocity of the ball. Since the density of the ball is much larger than of the liquid, i.e., 7.88 compared to 0.85 g/cc, the change in lube oil density over the temperatures investigated should not have a significant impact on viscosity measurements. Consequently, a constant density assumption for lube oils is acceptable for use in the determination of viscosity.

To test the validity of using constant oil density when measuring lube oil viscosity, results measured using constant oil density are compared to lube oil viscosity measured using temperature-dependent oil density. The effect of temperature on oil density is found by measuring the change of lube oil volume in a flask while being heated. Figure 4.17 shows density as a function of temperature measured for a 15W50 lube oil denoted by blue diamonds with a linear curve fit represented by a black line. The linear curve fit predicts the viscosity well for temperatures below 70°C. Above this temperature, the results become less predictable due to difficulty in heating the oil consistently and accurately. However, the linear fit has a coefficient of determination value of 0.9949 and therefore is acceptable for the prediction of lube oil density in viscosity measurements. These results are expected for the other oils in the as well since the densities are similar and thermal expansion coefficients for lube oils are small.

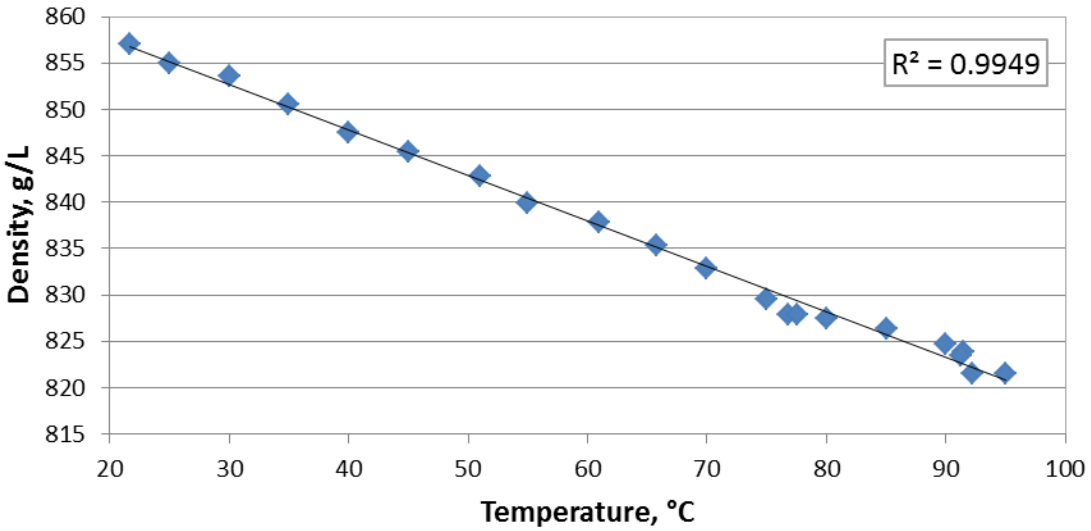

Figure 4.17: Effect of temperature on density for Mobil-1 15W50 lube oil

Initially viscosity measurements are made with a constant density measured at room temperature and then a viscosity based on temperature-dependent density is calculated from,

$$\frac{\eta_2}{\eta_1} = \frac{(\rho_{ball} - \rho_{liquid_2})}{(\rho_{ball} - \rho_{liquid_1})} \qquad \textbf{(4.1)}$$

This equation, which was derived from Stoke's law, calculates a new viscosity value, η_2, based on a new density value, ρ_2, the initial viscosity, η_1, the initial density, ρ_1, and the density of the ball, ρ_{ball}. A comparison of viscosity data for Mobil-1 15W40 using a constant oil density and temperature-dependent oil density is shown in Tables 4.1and 4.2. A small difference of 0.56% is observed in both the measured viscosities and Vogel predicted viscosities at 100 °C. Figure 4.18 shows Mobil-1 15W40 lube oil viscosity as a function of temperature calculated with the Vogel's equation for constant oil density denoted by a solid

blue line and temperature-dependent oil density denoted by a red dashed line. As seen in the figure, no deviation is observed between viscosities. From this, it is concluded that temperature-dependent density did not have a detrimental effect on the viscosity measurements. Consequently, constant oil density measured at room temperature will be used for viscosity measurements and calculations throughout the current investigation.

Table 4.1: Vogel coefficients for constant and temperature-dependent density for Mobil-1 15W40

		Constant Density	*Temp.-Dependent Density*	*% difference*
Vogel constants	***a***	0.0640336	0.0657728	2.68
	b	1135.33	1129.22	0.54
	c	-113.221	-112.921	0.27

Table 4.2: Comparison of viscosity results using constant and temperature-dependent oil density

	Temperature, °C	*Constant Density*	*Temp.-Dependent Density*	*% difference*
Density, g/cc	20	0.8580	0.8580	0.00
	60	0.8580	0.8384	2.31
	100	0.8580	0.8188	4.67
Measured viscosity, cP	20	321.77	321.77	0.00
	60	44.97	45.09	0.28
	100	13.15	13.22	0.56
Viscosity calculated with Vogel eq., cP	20	321.76	321.78	0.01
	60	44.96	45.09	0.28
	100	13.15	13.22	0.56

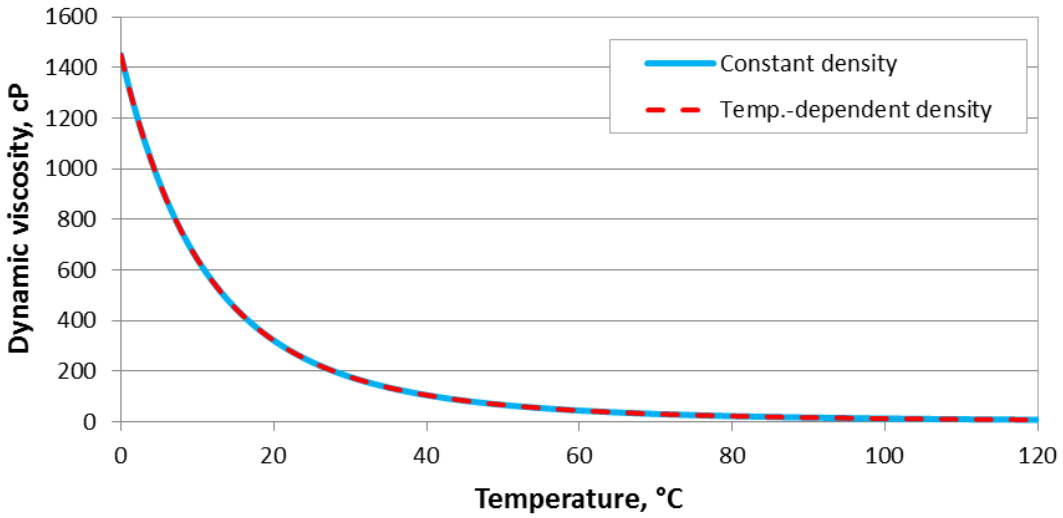

Figure 4.18: Comparison of viscosity temperature relationship calculated with Vogel's equation for constant and temperature-dependent density

4.2.2 Obtaining Vogel equation for oils of different formulations

The relationship between lube oil viscosity and temperature is determined by using Vogel's equation, shown as Equation 2.4, where dynamic viscosity (η in cP) is a function of the three constants, a, b, and c, and temperature. The units of constant a are cP while the units of b and c are dependent on the units of temperature used when the constants are calculated. For this study, temperature is expressed in °C and thus the constants are expressed in °C as well. If temperature values in units of Kelvin are used, the constant c can be adjusted to account for the difference between °C and Kelvin. Values of these constants are unique to a specific oil and are found with viscosities measured at three different temperatures. This section presents measured oil density, measured viscosities, and calculated Vogel constants. The viscosity-temperature relationships for several oils are presented as well.

The Vogel constants and density for eleven commercial oils investigated in the present study are listed in Table 4.3. The density of the oil, measured at room temperature, is considered constant for viscosity measurements. Density values range from 0.841 to 0.880 g/cc. Vogel constants for all the oils are general similar with the exception of Mobil Delvac-1 5W40. However, the measured and predicted viscosities for Mobil Delvac-1 5W40 are not significantly different, as seen in Figure 4.19. Therefore, the difference in the Vogel coefficients between Mobil-1 5W40 and the other oils is not a problem. The viscosities predicted by the Vogel equation for several of the oils are shown in Figures 4.20 and 4.21.

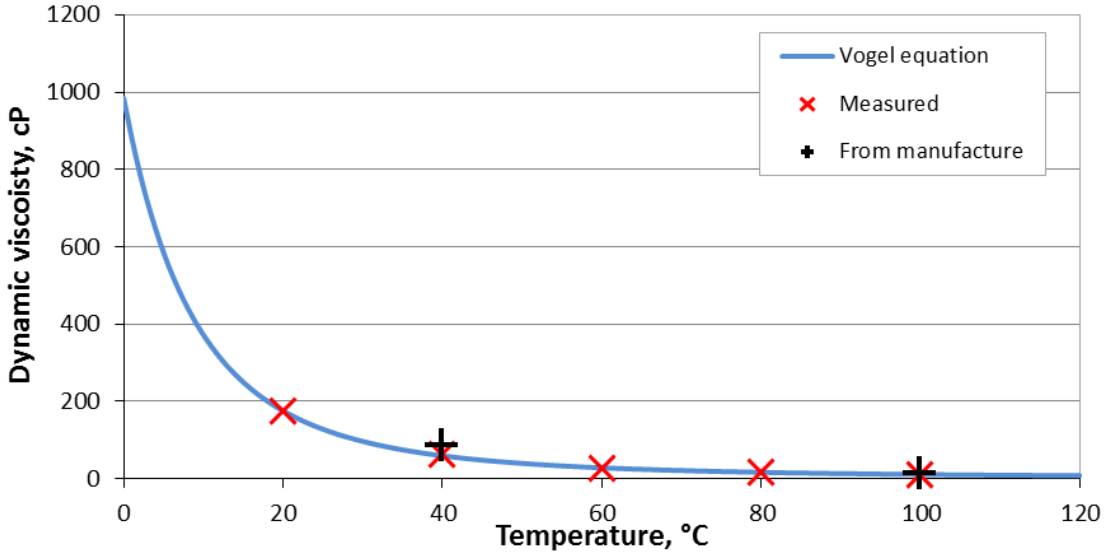

Figure 4.19: Comparison of measured and Vogel predicted viscosities for Mobil Delvac 1 5W40

Table 4.3: Measured density and calculated Vogel constants for some commercial oils

Oil	*Weight*	*density (g/cc)*	*Vogel constants*		
			a (cP)	*b (°C)*	*c (°C)*
Shell Rottela T	30	0.869	0.06789	954.87	-96.57
Royal Purple	0W-10	0.870	0.05653	941.09	-118.53
Mobil-1 Fully Synthetic	0W-30	0.841	0.09370	953.72	-113.98
Mobil-1 Fully Synthetic	5W-20	0.851	0.09014	878.22	-105.73
Mobil Super	5W-30	0.850	0.03089	1259.30	-131.49
Mobil-1	5W-30	0.855	0.02739	1358.35	-139.31
Mobil Delvac 1	5W-40	0.850	0.51103	511.78	-67.67
Fresh Pennzoil	10W-30	0.880	0.03050	1252.64	-126.76
Shell Rottela T	15W-40	0.873	0.07600	1030.99	-104.85
Quaker State Universal HDX	15W-40	0.875	0.08666	990.60	-102.40
Mobil-1 Fully Synthetic	15W-50	0.858	0.06404	1135.34	-113.22

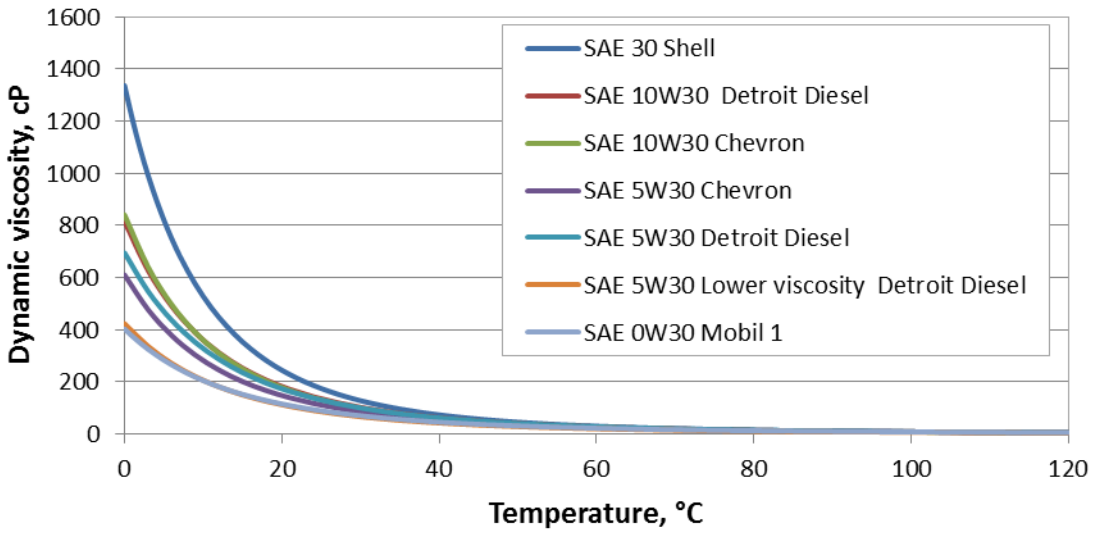

Figure 4.20: Effect of temperature on Vogel predicted viscosity for SAE 30 grades

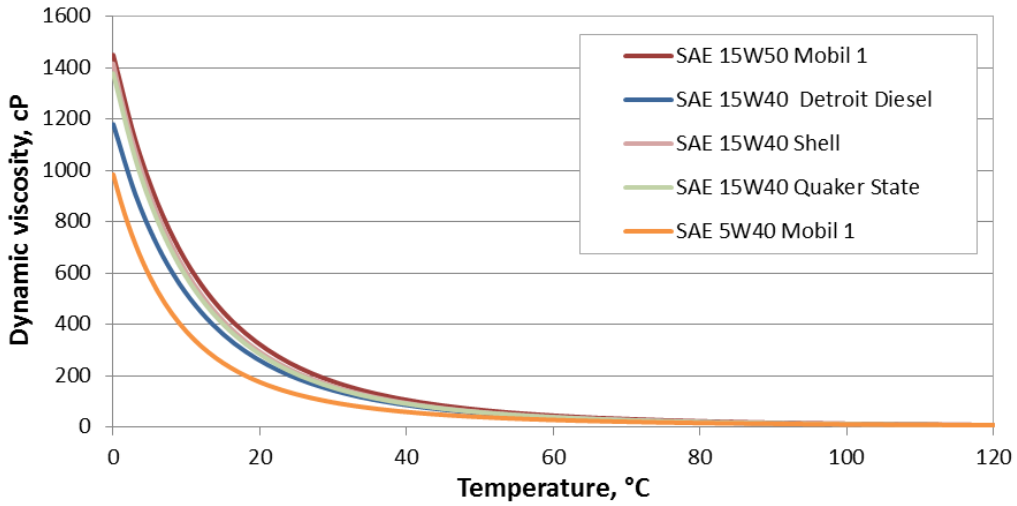

Figure 4.21: Effect of temperature on Vogel predicted viscosity for SAE 40 and 50 grades

The Vogel constants for two different oils, Chevron 5W20 and Chevron 10W30, in three different stages of production, base oil, commercial without additives, and commercial oil, are presented in Table 4.4. While there is significant difference between viscosities of the base oils and the commercial oils, there is no observable change in viscosities between commercial oils with and without additives as can be seen in Figures 4.22 and 4.23. The viscosities of the commercial oils are approximately double those of the base oil between 0 and 20°C.

Multigrade oils are manufactured by thickening low viscosity oils with polymers. This is done because low viscosity oils have a slower rate of change in viscosity over temperature. When these oils are thickened, the rate of change in viscosity with temperature remains the same while the whole viscosity profile is shifted up along the viscosity axis. This is desirable so that the oil remains sufficiently thick at high temperatures while remaining sufficiently thin at cold

temperatures. When examining the viscosity of the 5W20 oils on log scale the shape of the curves are identical and a shift is observed just as previously described, as can be seen in Figure 4.24.

Table 4.4: Comparison of calculated Vogel constants for two oils in three stages of production (b – base oil, w/o – without additives, and c – commercial)

Weight	*density (g/cc)*	*Vogel constants*		
		a (cP)	*b (°C)*	*c (°C)*
5W20-b	0.850	0.07498	753.61	-95.77
5W20-w/o	0.853	0.08272	871.66	-102.86
5W20-c	0.849	0.08712	862.27	-102.35
10W30-b	0.856	0.06993	806.26	-93.11
10W30-w/o	0.867	0.08062	918.35	-99.44
10W30-c	0.868	0.08620	904.97	-98.52

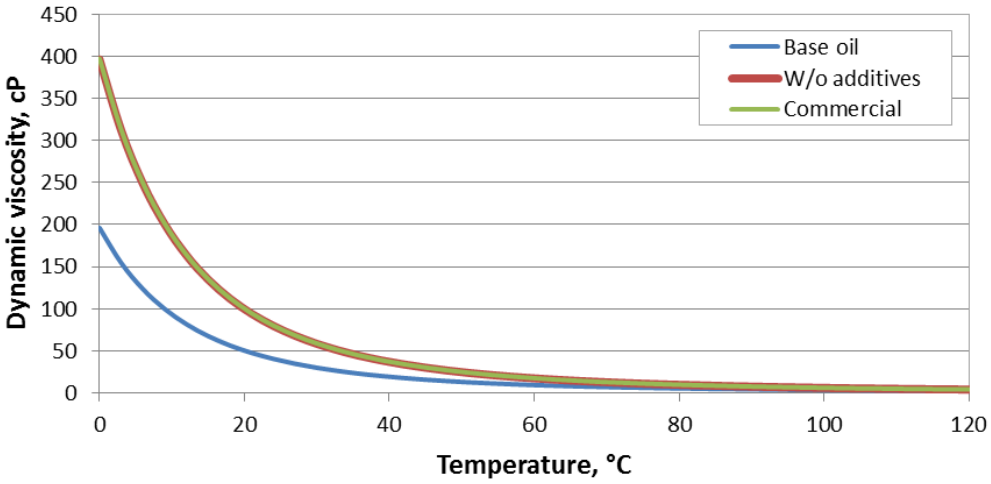

Figure 4.22: Vogel predicted viscosities for Chevron 5W20 in three different stages of production

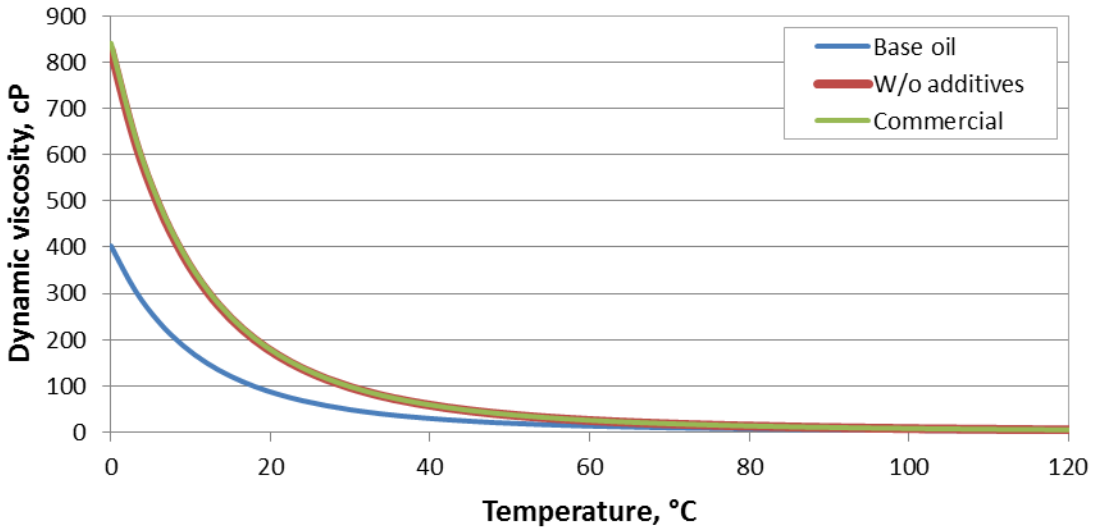

Figure 4.23: Vogel predicted viscosities for Chevron 10W30 in three different stages of production

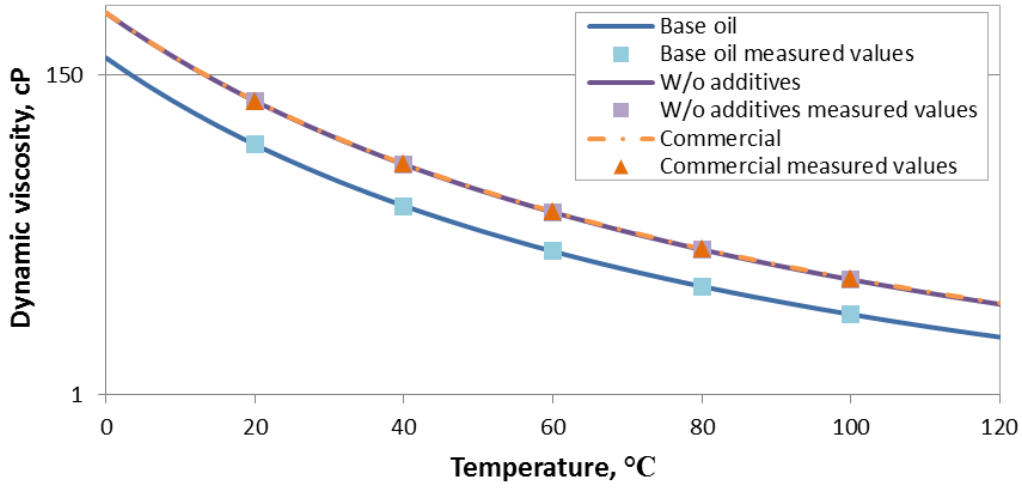

Figure 4.24: Log-viscosity plot of 5W20 oil in three different stages of production

The Vogel constants for fresh and used oils are shown in Table 4.5. Significant differences in predicted viscosity at temperatures below 20°C are observed but the differences become negligible above 20°C as can be seen in Figure 4.25. Since the vast majority of data collected in this study is above 25°C, the Vogel constants calculated for fresh oil are acceptable to be used for the evaluation of lube oil performance.

Table 4.5: Comparison of calculated Vogel constants for fresh and used oils

Oil	*Weight*	*density (g/cc)*	*Vogel constants*		
			a (cP)	*b (°C)*	*c (°C)*
Fresh Pennzoil	10W-30	0.880	0.03050	1252.64	-126.76
Used Pennzoil 10W-30	10W-30	0.880	0.02617	1290.15	-126.30
Royal Purple	0W-10	0.870	0.05653	941.09	-118.53
Used Royal Purple	0W-10	0.875	0.09443	740.59	-97.18

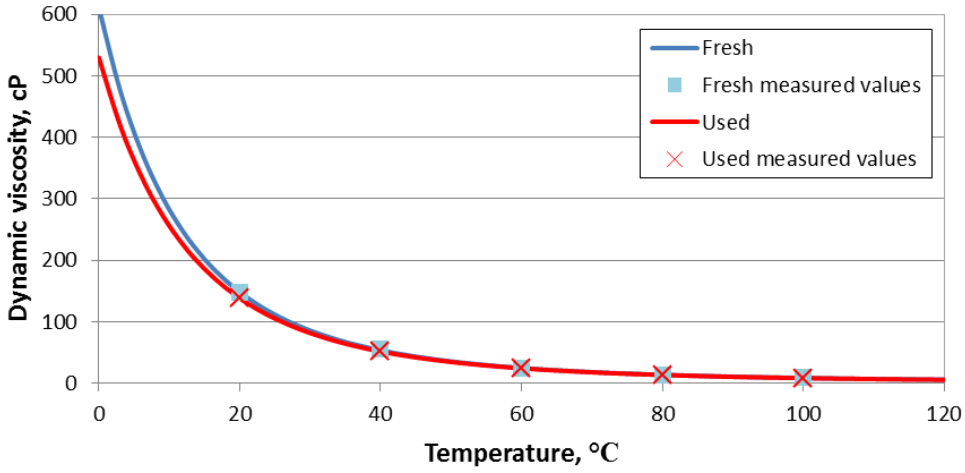

Figure 4.25: Comparison of viscosities between fresh and used 5W30 oil

4.3 Instantaneous motoring torque

By displaying instantaneous torque, i.e, motoring torque as a function of crank angle over an engine cycle, information about the dynamics of the engine and some limited information concerning the modes of friction can be observed. For this study, instantaneous torque results are typically presented as averaged instantaneous torque plots created from a data set of typically 300 engine cycles to reduce cycle-to-cycle variations. However, some information concerning engine dynamics and vibrations are lost by averaging the data. Thus, the raw data and averaged instantaneous torques for the various engine configurations are examined in Section 4.3.1. The effect of lube oil viscosity on averaged instantaneous torque is discussed in Section 4.3.2. Effects of lube oil formulation on averaged instantaneous torque are instigated for an oil in three stages of production — base oil, commercial oil without additives, and commercial oil — in Section 4.3.3.

4.3.1 Instantaneous torque for different engine configurations

The instantaneous torque plot for the modified engine (no compression) with internal oil pump measured using the Cooper Instruments torque meter is a curve which resembles a sine wave and has little cycle-to-cycle variation as shown in Figure 4.26. What cycle-to-cycle variations are present occur primarily as changes at the peaks and troughs of the curves. Figure 4.27 presents the averaged instantaneous torque over 300 revolutions for this engine configuration with maximum and minimum bounds that represent the differences across the 300 revolutions due to cycle-to-cycle variations. Overall, the average curve is smooth and the variance due to cycle-to-cycle variations is relatively small. This is due to the engine being balanced as the timing gears and counter weights are left intact for this engine configuration.

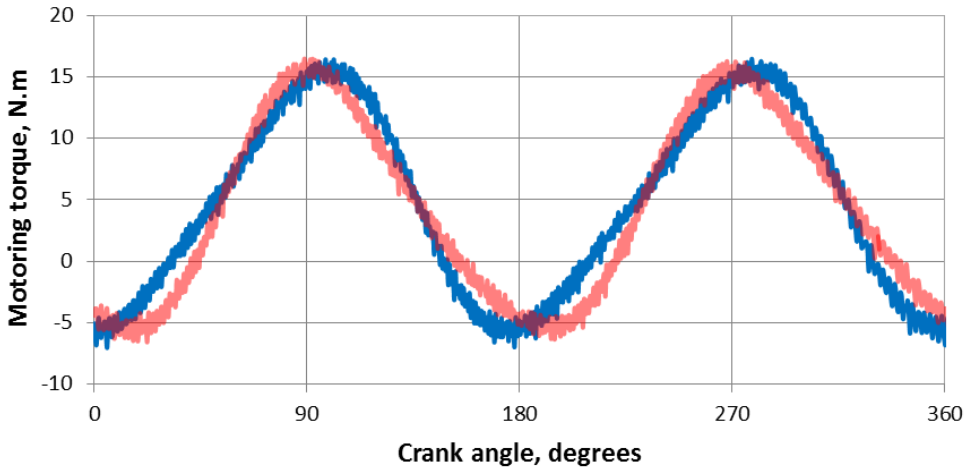

Figure 4.26: Instantaneous torque curves measured approximately 3 seconds apart for modified engine with internal oil pump (no compression) with the Cooper instruments torque meter and a 15W40 weight oil

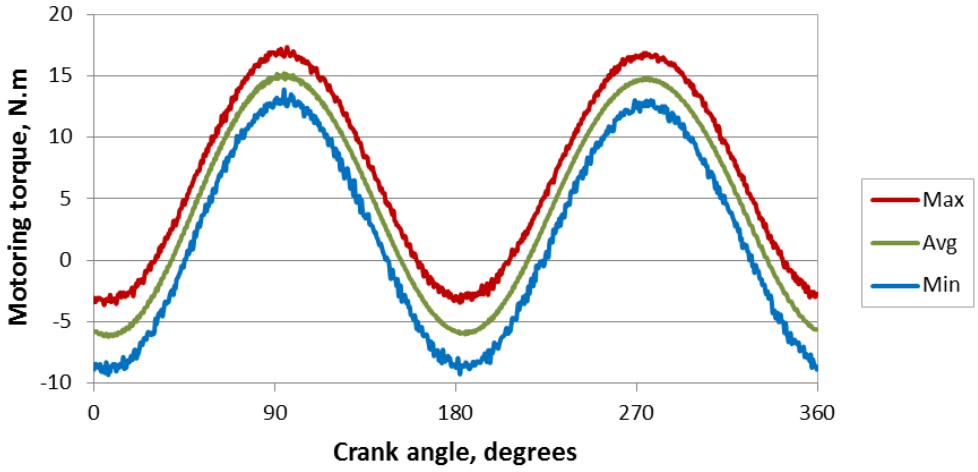

Figure 4.27: Averaged instantaneous motoring torque with maximum and minimum bounds for modified engine with internal oil pump (no compression) using the Cooper Instruments torque meter and a 15W40 oil

Instantaneous torque over four revolutions for the modified engine with external oil pump using the Omega torque meter and Mobil-1 5W30 oil is seen in Figure 4.28. At the first look, no significant cycle-to-cycle variations seem to be present in the instantaneous torque when shown at this scale. However there are vibrations present in the data and one such vibration is denoted by red dashed circle. These vibrations are caused by engine an engine unbalance which is a consequence of removing the balancing masses from the engine when removing the oil pump. The vibrations are periodic and shift from cycle-to-cycle which is more clearly seen when the motor torque is plotted over 28 crankshaft revolutions as done in Figure 4.29. In this plot, the vibrations are shown to have a frequency different than the crankshaft causing the vibrations and the peak torques to change periodically. Similar results are observed for the Cooper Instruments torque meter although noise causes the vibrations to be unclear.

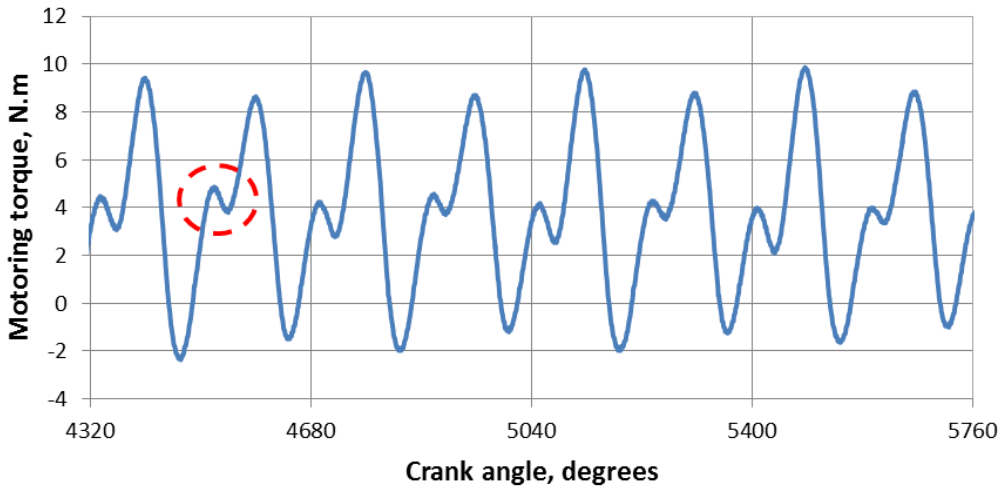

Figure 4.28: Instantaneous torque over four crankshaft revolutions for modified engine with external oil pump (no compression) using Omega torque meter and Mobil-1 5W30 oil (red circle highlights an engine vibration)

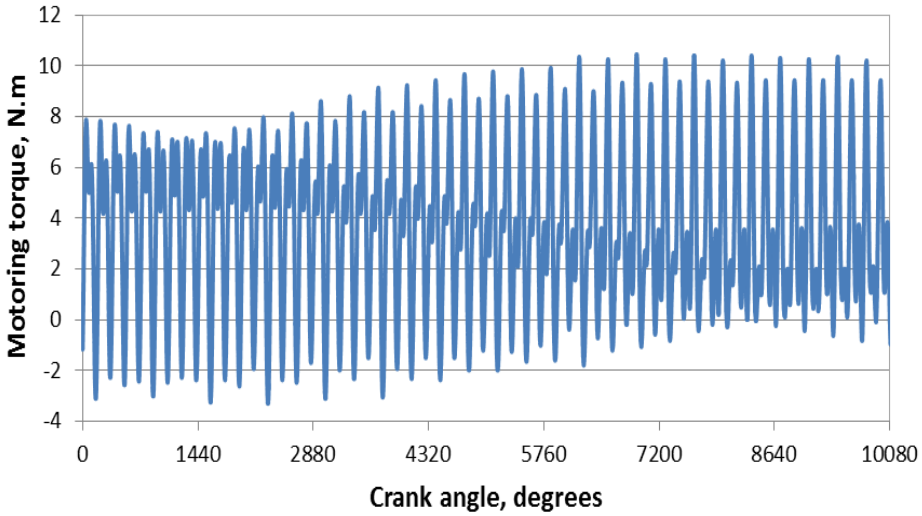

Figure 4.29: Instantaneous torque over 28 crankshaft revolutions for modified engine with external oil pump using Omega torque meter and Mobil-1 5W30 oil

The instantaneous torque for the modified engine with external oil pump (no compression) using the Omega torque meter and Mobil-1 5W30 oil presented as average, maximum, and minimum torque curves over 300 revolutions is shown in Figure 4.30. The engine vibrations create a large difference between the maximum and minimum curves while the vibrations are filtered from the average curve. The shape of the average curve is primarily driven by the acceleration of the piston and connecting rod masses with the peaks and troughs corresponding to accelerations and decelerations, respectively. Since the vibrations are periodic, averaging the torque does not adversely affect the calculations of fmep.

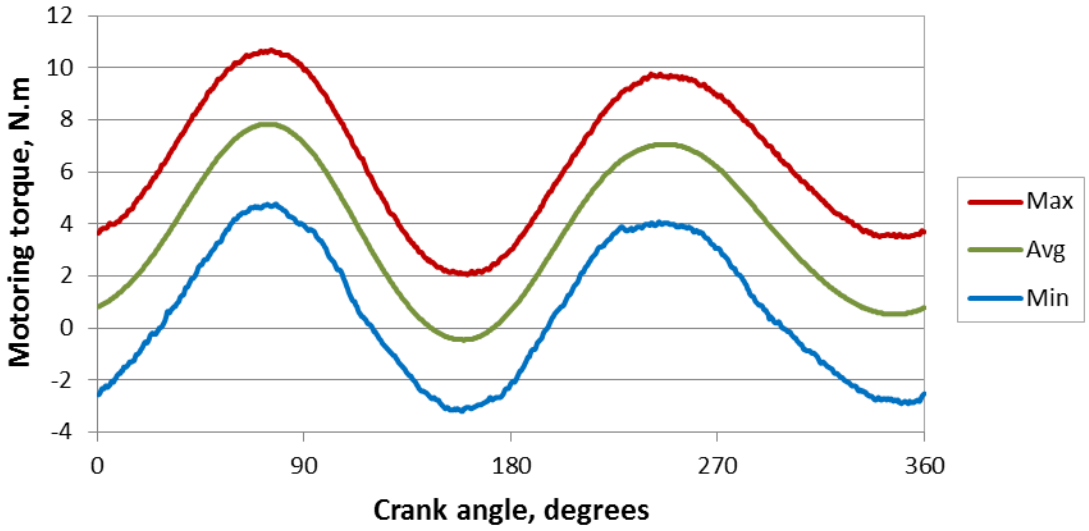

Figure 4.30: Averaged instantaneous motoring torque with maximum and minimum bounds for the modified engine with external oil pump (no compression) with the Omega torque meter and a 5W30 oil

The instantaneous torque measured with the Omega torque meter for the stock engine (with compression) and Mobil-1 5W30 oil produces a distinctly different shape as can be seen in Figure 4.31. This is due to the added toque on the crank shaft caused by increased cylinder pressure during compression and expansion. The compression effects can be observed between the crank angles of 540 and 720 degrees as the majority of torque is above the median line due to positive torque required to counter compression forces. A peak negative torque is observed at approximately 90 degrees during the expansion stroke of approximately 0 to 180 degrees. This occurs as the motoring torque is slowing the piston and counteracting expansion forces. A peak positive torque is seen near 180 degrees. The exhaust valve opens near 130 degrees which is approximately where the torque crosses the median line. Thus, the peak positive

torque is caused by the sum of the torques required to open the exhaust valve, accelerate the piston and connecting rod, and force the gasses out to the cylinder. The difference between the maximum and minimum instantaneous torque plots is generally small which indicates little cycle-to-cycle variation and a balanced engine. This is expected since the stock engine does not have any engine components removed.

4.3.2 Effect of lube oil viscosity on instantaneous torque

The effect of viscosity on the shape of the instantaneous torque curve is investigated by comparing instantaneous torque curves measured during an experiment with a 5W30 oil on the modified engine (no compression) with external oil pump and Cooper Instruments torque meter at different times during the test and thus at different oil viscosities. A total of nine instantaneous torque curves are obtained during the test with one being recorded every fifteen minutes. As each curve is measured at a different time, each curve has a different viscosity than the other curves as can be seen in Table 4.6.

Table 4.6: Instantaneous torque curves over an experiment with a 5W30 oil

Curve #	*Min into test*	*Liner mid-stroke temperature, °C*	*Lube oil viscosity, cP*	*Avg Torque, N.m*		
				Max	*Avg*	*Min*
1	0	24.46	114.71	7.75	5.35	2.76
2	15	47.07	39.74	6.73	3.91	0.95
3	30	56.85	27.58	6.51	3.58	0.53
4	45	63.10	22.34	6.36	3.38	0.28
5	60	66.43	20.09	6.32	3.31	0.18
6	75	68.36	18.93	6.28	3.27	0.15
7	90	69.83	18.11	6.24	3.25	0.14
8	105	71.14	17.41	6.27	3.22	0.06
9	120	72.13	16.91	6.26	3.19	0.00

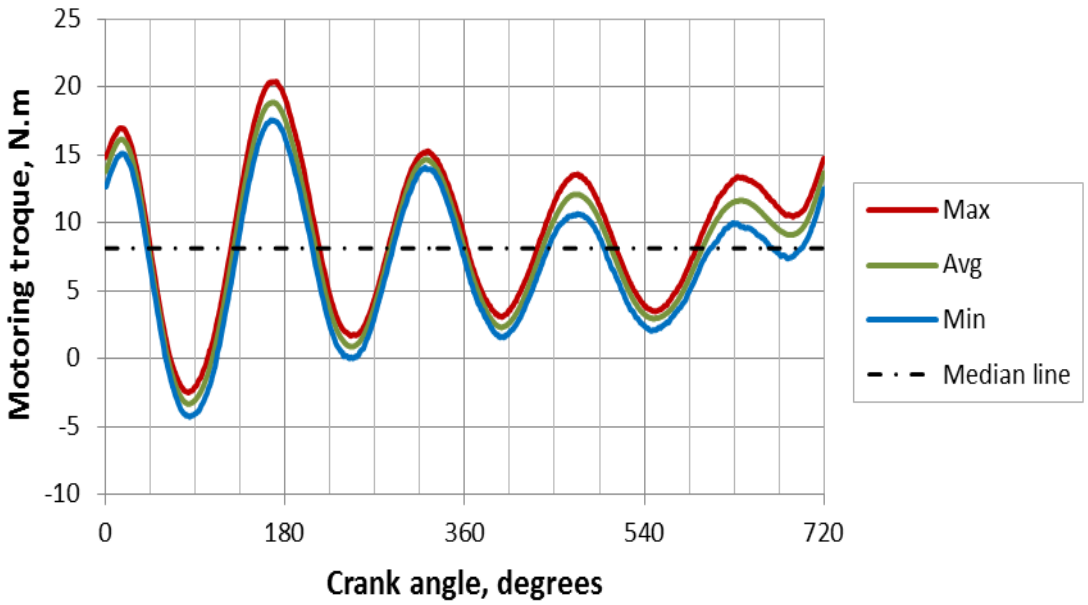

Figure 4.31: Instantaneous torque for stock engine (compression) using the Omega torque meter and Mobile 1 5W30 oil

To measure the change in the cycle-to-cycle variation over the experiment for the 5W30 oil, the difference between the maximum and minimum instantaneous motoring torque curves is plotted in Figure 4.32. There is a slight change from the first data set, but as this data set was collected during start-up it can be ignored as the engine is not yet in dynamic or thermal equilibrium. There is little change for the remaining data sets. This shows that the viscosity of the oil does not have an effect on the cycle-to-cycle variation of the instantaneous torque; and thus, the variations are attributed to engine/motor system dynamics and vibrations.

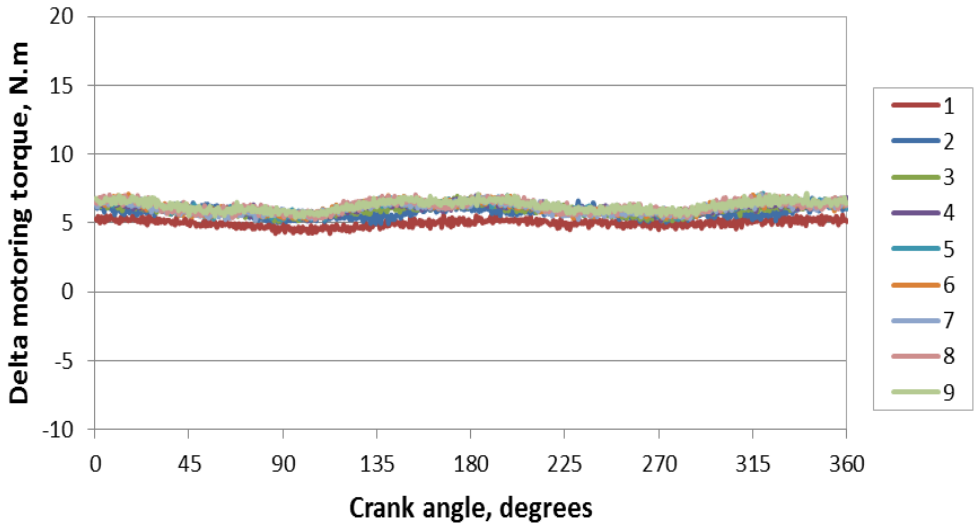

Figure 4.32: Difference between maximum and minimum instantaneous torques curves collected every 15 minutes for an experiment with the during a 5W30 run

Examining the average instantaneous torque over the duration of the experiment for the 5W30 oil shows changes around the peaks of the instantaneous torque curves as can be seen in Figure 4.33. The difference between the first average torque curve and the rest of the curves is due to the transient nature of the engine when this data set was collected at the very beginning of the test. The rest of the series changes around the peaks and the troughs, both of which are becoming lower in magnitude with lowering viscosity. The difference between the maximum torque for curves 2 and 9 is 3 N.m which is 30% of the amplitude for curve 2. The peaks and troughs represent accelerations and deceleration, respectively. Also, the effect of lower friction due to lower viscosity should be more significant since friction will be opposing the positive torque. Thus, the effect is more significant at the peaks than at the troughs.

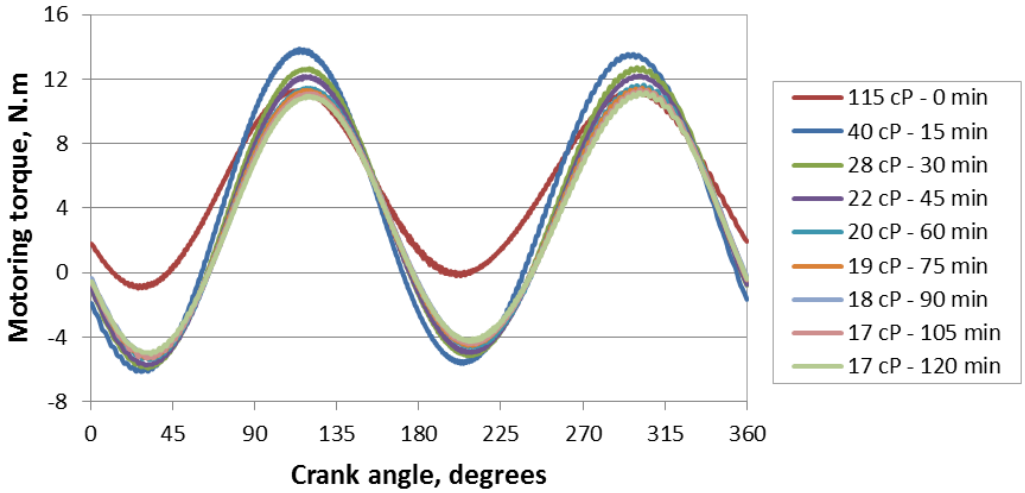

Figure 4.33: Instantaneous torques over the duration of an experiment the modified engine with external oil pump with Cooper Instruments torque meter and a 5W30 oil

4.3.3 Effect of oil additives on instantaneous torque

The effect of the oil formulation on the instantaneous torque is studied for a 5W20 oil in three different stages of production — base oil, commercial oil without additives, and commercial oil — using the modified engine with external oil pump and Cooper Instruments torque meter. Instantaneous torques are examined for the oil samples at a viscosity of approximately 16 cP so that viscosity does not cause differences between the curves. The base oil reaches this viscosity at approximately 15 minutes into the test, while the other oils do not reach this viscosity until approximately 45 minutes into the test. Cycle-to-cycle variations, examined as the difference between maximum and minimum instantaneous torques, do not drastically change during the test as can be seen in Figure 4.34.

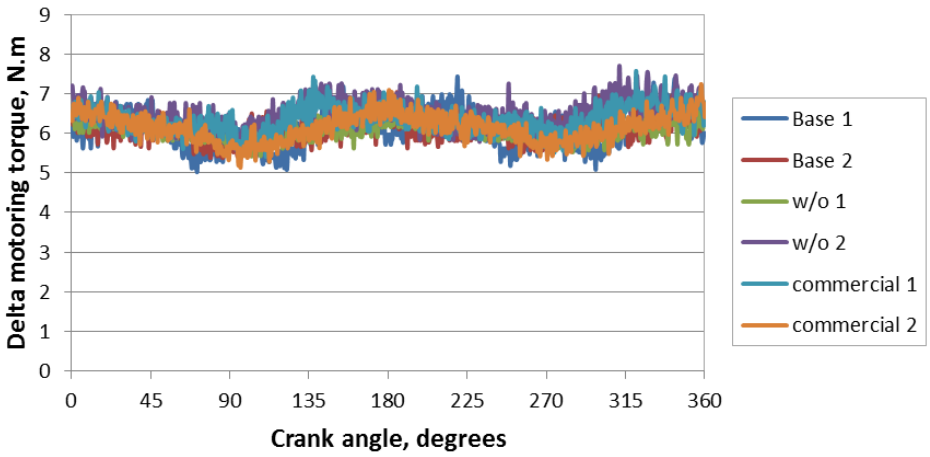

Figure 4.34: Difference between maximum and minimum instantaneous torque curves measured for an oil in three stages of production (base oil, commercial oil without additives (labeled w/o), and commercial oil)

When the instantaneous torque curves for the oil in three stages of production are plotted together, the results are similar with small differences at the peaks and troughs as can be seen in Figure 4.35. The slight difference the Base oil 1 and Base oil 2 curves and all other curves can be attributed to these data being measured during the beginning of a test which would still include some transient effects. Data measured for the base oil at the end of a test, shown in Figure 4.35 as Base 2 – 120 min in, fits with the other curves further showing the effect of start-up on the instantaneous torque curve. The peak torque for the oil w/o additives is slightly less than the commercial oil even though these oils have very similar viscosities which could indicate friction from additives. The differences between these instantaneous torque curves are approximately 6% of maximum curve amplitude and are much smaller than the differences observed between viscosities for the 5W30 oil showing that it is difficult to observe additive effects in instantaneous torque curves.

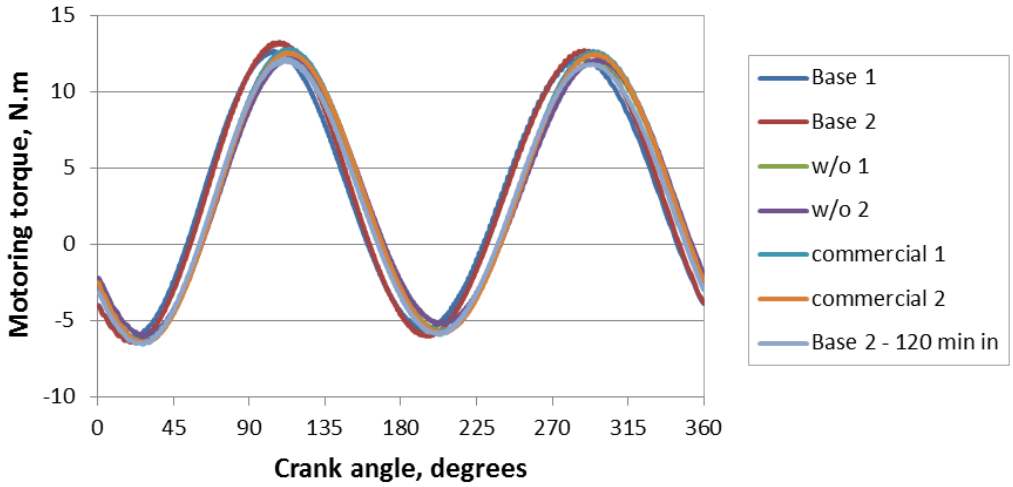

Figure 4.35: Instantaneous torque for a 5W20 oil in three stages of production (base oil, commercial oil without additives (labeled w/o), and commercial oil)

4.4 Average torque and friction mean effective pressure

Examining lube oil performance over a large range of data is cumbersome with instantaneous torque plots. By averaging the instantaneous torque friction mean effective pressure (fmep) can be obtained, from which lube oil performance can be more easily examined as a function of viscosity. The fmep results for this study are presented in this section. The validity of using the oil flushing procedure described in the previous chapter is examined in Section 4.4.1. The results for the modified engine with internal oil pump (no compression) using the Cooper Instruments torque meter are discussed in Section 4.4.2, which also includes results from a test performed using a 10W30 oil in three different stages of production. The average torque results for the modified engine with external oil pump (no compression) are presented in Section 4.4.3 with results from the Cooper Instruments and Omega torque meters. The stock engine (compression)

results are shown in Section 4.4.4. The average torque results across the engine configurations are reported in Section 4.4.5. These results show the usefulness and repeatability of the developed motored engine friction rig.

4.4.1 Oil residuals effects on average torque

The effect of lube oil left in the engine when switching to different lube oil formulations is examined by comparing the average motoring torque over several runs with different oils and is shown in Figure 4.36. The experiments shown on the x-axis are in chronological order, the blue bar represents oil viscosity at approximately 35°C, and the red bar represents the fmep output at approximately 35°C. As seen in the figure whenever there is a large increase or decrease in oil viscosity, as observed in the first three tests, there is a corresponding change in fmep for the next oil across the tests. The results stabilize after the first test and second oil flush, showing that the flush procedure used in this study is acceptable in minimizing the effect of oil residuals on average torque.

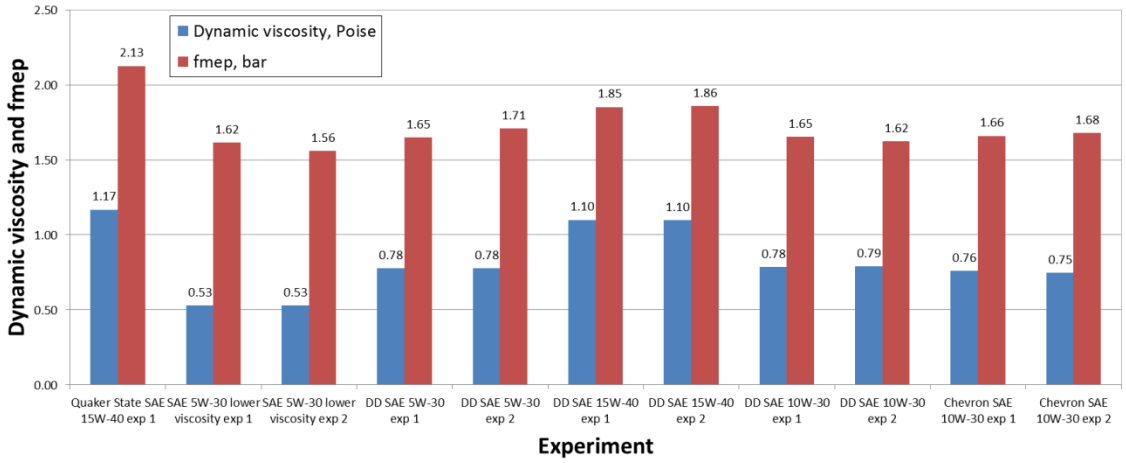

Figure 4.36: Oil sump residual effect on test results

4.4.2 Modified engine with internal oil pump (no compression)

The performance of several oils are evaluated on the modified engine with internal oil pump (no compression). These oils include four oils of different weights: 15W40, 10W30, 5W30, and 5W30 lower viscosity, all referred to as Detroit Diesel oils. The performance of the oil is compared by plotting fmep versus the dynamic viscosity. Results for the 15W40 and 10W30 oil are similar with 10W30 having slightly lower fmep at a given viscosity as shown in Figure 4.37. Surprisingly the 5W30 oil has higher fmep at a given viscosity than the two heavier oils. The lower viscosity 5W30 oil has the highest fmep at any given viscosity. This shows that generally oils of have similar friction for a given viscosity but very thin oils can have a higher friction at a given viscosity.

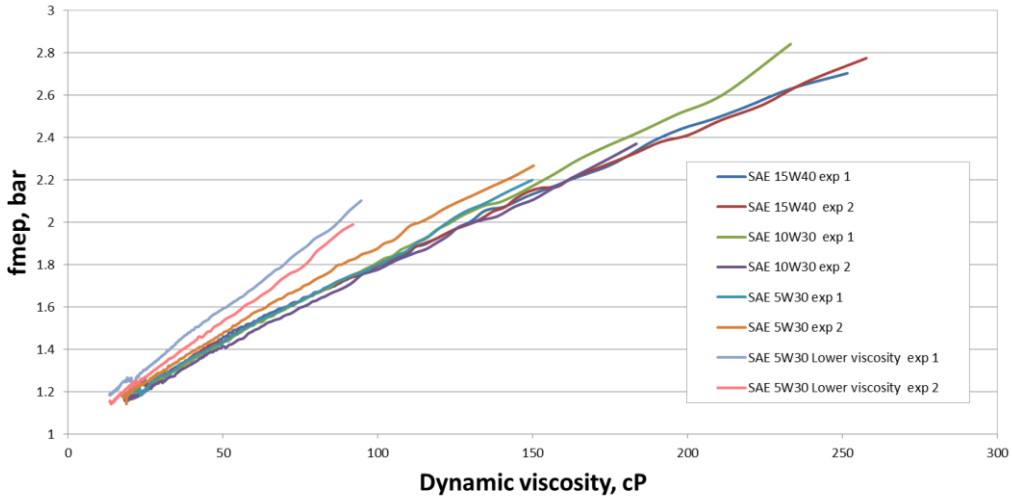

Figure 4.37: fmep versus viscosity for Detroit Diesel oils using the Cooper instruments torque meter

A different 10W30 oil in three different stages of production — base oil, finished oil without additives, and finished commercial oil — is investigated. Comparing fmep results in Figure 4.38 shows very similar friction mean effective pressure for the commercial oil with and without additives with a slight increase in friction for the commercial oil. The base oil has significantly higher fmep and the results for this oil are not very repeatable at low viscosity. The differences between the base oil tests at low viscosities are caused by a change in oil pressure as shown in Figure 4.39. The difference in oil pressures is due to the automatic oil pressure relief valve malfunctioning during the second experiment for the base oil, which results in increased oil pressure. As the internal oil pump is coupled to the crank shaft, the increased oil pressure increases fmep as well. This is unacceptable in terms of accuracy and repeatability; thus, it was decided to remove the internal oil pump to prevent the problem from occurring again.

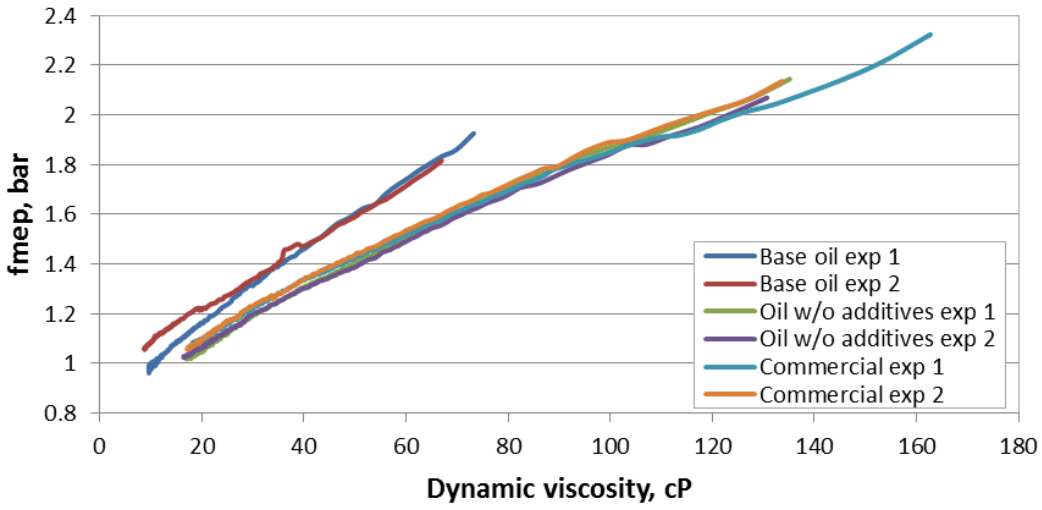

Figure 4.38: Comparison of fmep for a 10W30 oil in three different stages of production using Cooper Instruments torque meter

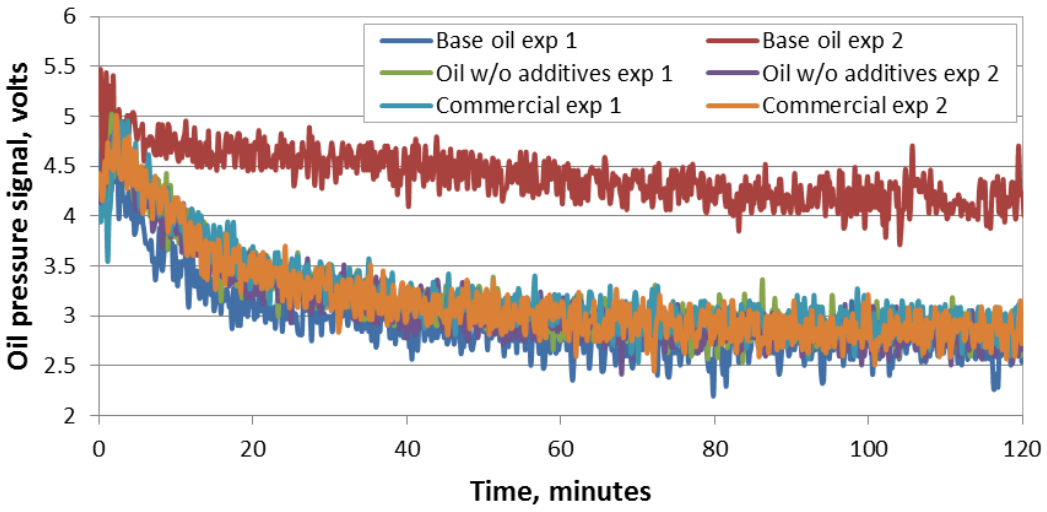

Figure 4.39: Engine oil pressures for a 10W30 oil in three different stages of production for the modified engine with internal oil pump and Cooper Instruments torque meter

4.4.3 Modified engine with external oil pump (no compression)

4.4.3.1 Comparison of friction mean effective pressure for a 5W20 oil in three different stages of production

Friction mean effective pressure for a 5W20 oil in three stages of production — base oil, commercial oil without additives, and commercial oil — is investigated using the Cooper Instruments torque meter with the modified engine with external oil pump (no compression). Each oil was tested three times with an oil flush protocol implemented after the first run. The results show the base oil has the highest fmep at a given viscosity as shown in Figure 4.40. Also, the finished oil has a slightly higher measured fmep at a given viscosity than the finished oil.

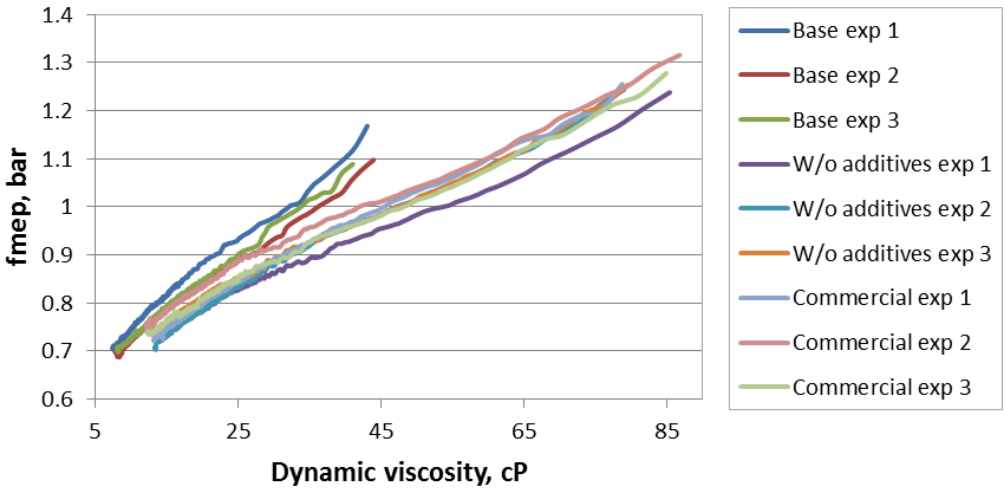

Figure 4.40: Chevron 5W20 series fmep measured using Copper Instruments torque meter for modified engine with external oil pump (no compression)

The differences between the oils are difficult to discern when all tests are plotted together so a linear fit with 95% confidence and prediction intervals is performed for each sample. When the fits and prediction intervals are compared for the series, there is a noticeable difference between the linear fits for the three oils, as can be seen in Figure 4.41. However, the prediction intervals overlap with both the mid oil and commercial oil falling within the prediction values. The confidence intervals in Figure 4.41 do not overlap though and thus the motored engine friction rig shows the effect of additives on engine friction, with the base oil having the highest friction and the oil without additives having the lowest. The results show that very thin lube oil can increase friction, especially during start-up. The lube oil additives are likewise shown to increase friction consistently over the oil without additives.

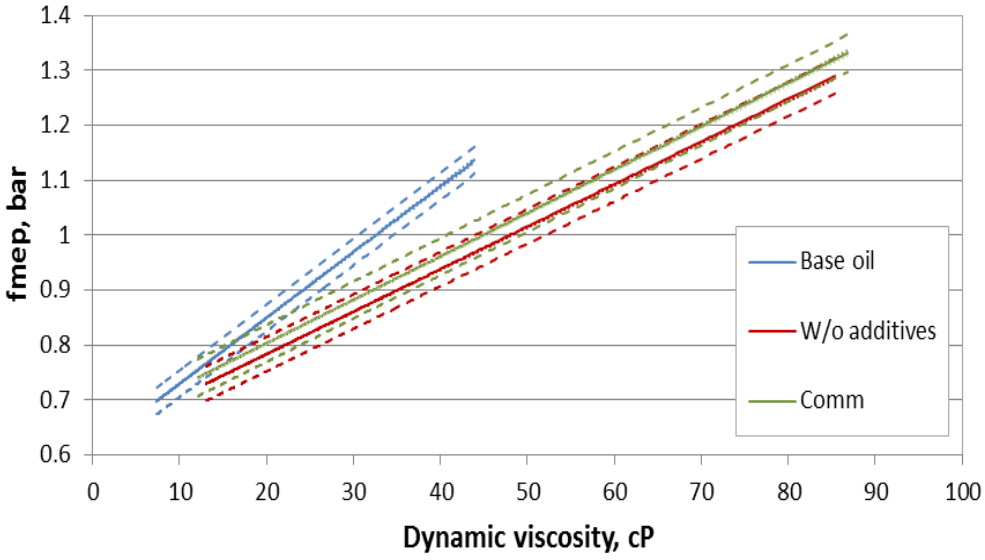

Figure 4.41: Chevron 5W-20 series linear fit with prediction interval (dashed line) and confidence interval (dotted line)

4.4.3.2 Friction mean effective pressure change over several successive runs for a 5W30 oil

The repeatability of friction mean effective pressure measurements are investigated by performing two series of test with a 5W30 oil: one with an oil change before each test and one without oil change. For each series a total of 5 runs are performed. The 5W30 oil is first examined with an oil change after each test. The first two tests, shown as the dark blue and red lines in Figure 4.42, show a significant difference when compared to the other results for this series of runs. The rest of the runs produced similar results.

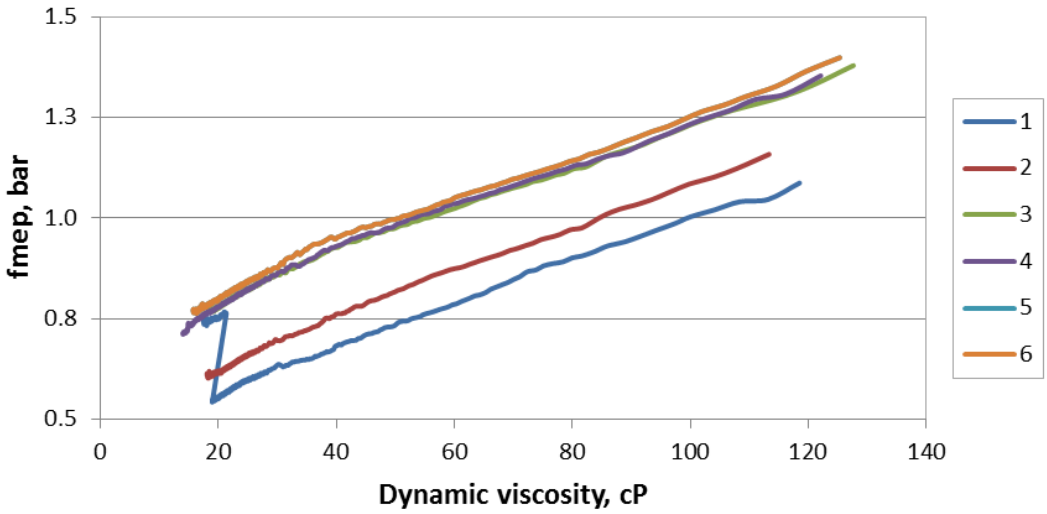

Figure 4.42: Friction mean effective pressure with oil changes after each test using Cooper Instruments torque meter for modified engine with external oil pump and a 5W30 oil

The differences observed in the first two runs are directly related to the torquemeter. The torque meter calibration intercepts corresponding to runs 1 and 2 are outliers from the typical calibration intercepts as cab be seen in Figure 4.43. The first error occurs for the post-run calibration for run 1 and continues to following calibration which is the pre-run calibration for run 2. The torque meter calibration arms were not removed between these two calibrations. This indicates that the error is caused by some setup error during the calibration. However, the sharp increase in fmep during the first run is due to a power outage with the lower fmep data being measured before the power outage and the rest after. It is not clear why the fmep increases after the power outage especially, since the error continues during the second run. Since the calibration constants differ from the mean value by approximately 5 times the standard deviation, these tests are considered as outliers and ignored due to calibration errors.

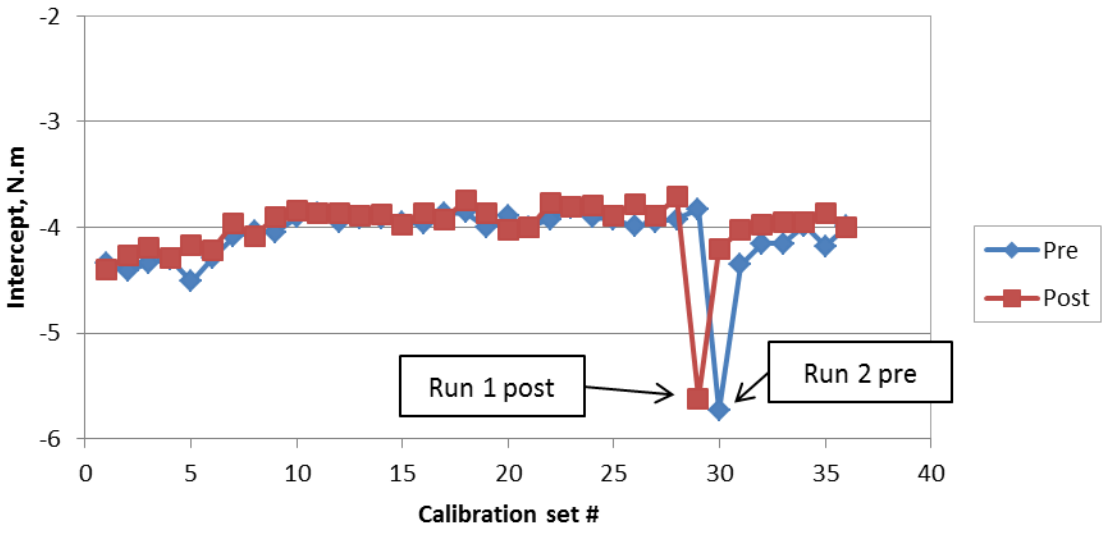

Figure 4.43: Cooper Instruments torque meter calibration y-intercept over time

Runs 1 and 2 are consider as outliers and are not included in analysis. The rest of the data, runs 3, 4, and 5, are combined into one set and a linear fit with a 95% prediction interval and a 95% confidence interval is created. Key values for this fit are shown in Table 4.7 and the data with fit are plotted in Figure 4.44. The prediction interval has a maximum margin of 0.0863 fmep, which is approximately 12% of the minimum measured fmep for the series. The max confidence interval is approximately 1.5% of the minimum measured fmep.

Table 4.7: Change in fmep for 5W30 with oil change key values

max prediction margin (fmep)	0.0863
max CI margin (fmep)	0.0106
Max fmep	1.3985
Min fmep	0.7111
%+/- PI error from min fmep	6.07%

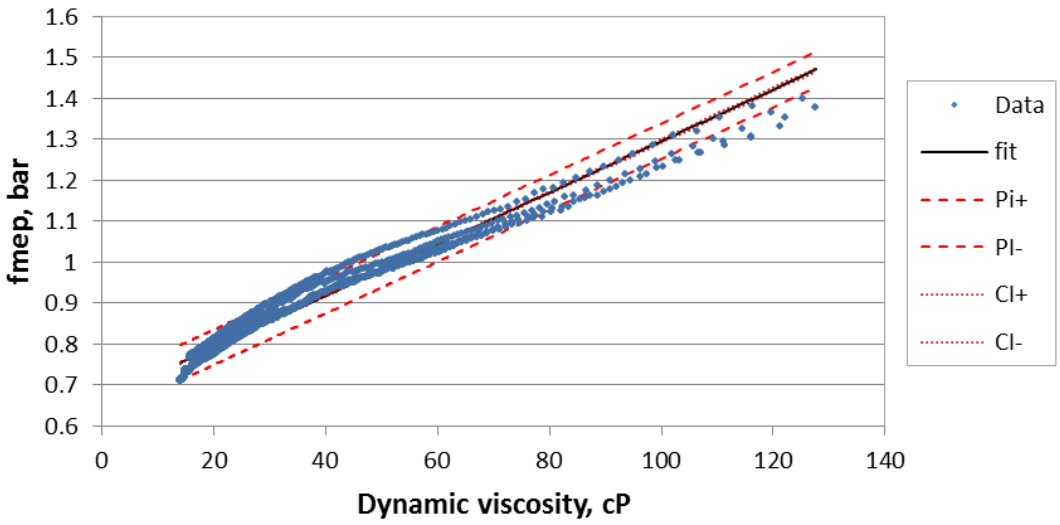

Figure 4.44: Friction mean effective pressure fit with 95% confidence intervals with oil changes after each test using Cooper Instruments torque meter for modified engine with external oil pump and a 5W30 oil (outliers deleted)

No outliers are present in the 5W30 series without oil changes and a linear fit with a 95% confidence interval, CI, and 95% prediction interval, PI, are also calculated and plotted for this series, as can be seen in Table 4.8 and Figures 4.45 and 4.46. The maximum prediction margin, the difference between the maximum and minimum prediction intervals at a given dynamic viscosity, for this series is 0.0774 which is approximately 10.3% of the minimum measured fmep for this series. The maximum confidence margin, which is the difference between the maximum and minimum confidence intervals at given dynamic viscosity, is 1.1% of the minimum measured fmep.

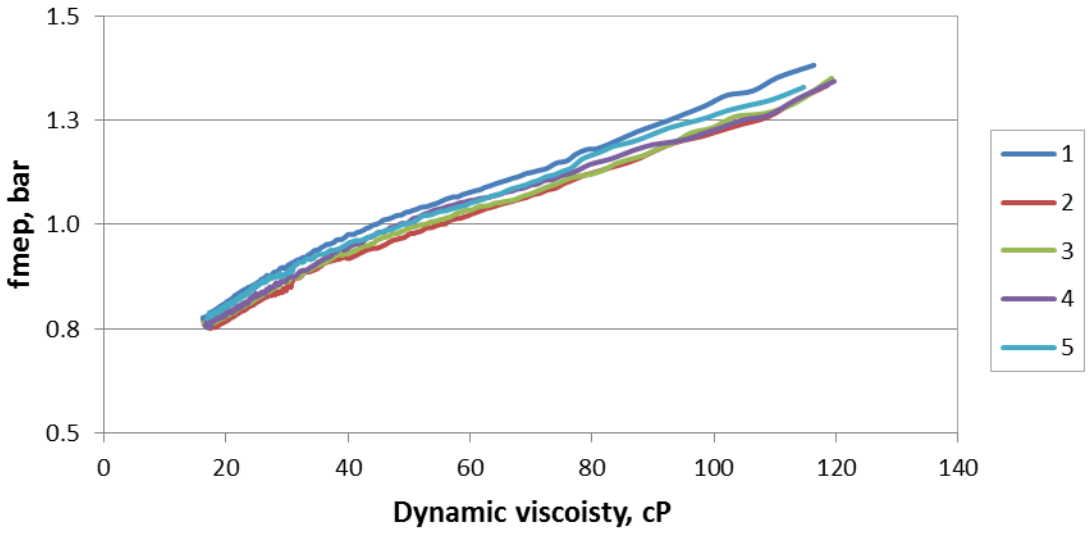

Figure 4.45: Friction mean effective pressure without oil changes after each test using Cooper Instruments torque meter for modified engine with external oil pump and a 5W30 oil

Table 4.8: Change in fmep for 5W30 without oil change key values

max prediction margin (fmep)	0.0774
max CI margin (fmep)	0.0083
Max fmep	1.3816
Min fmep	0.7510
%+/- PI error from min fmep	5.15%

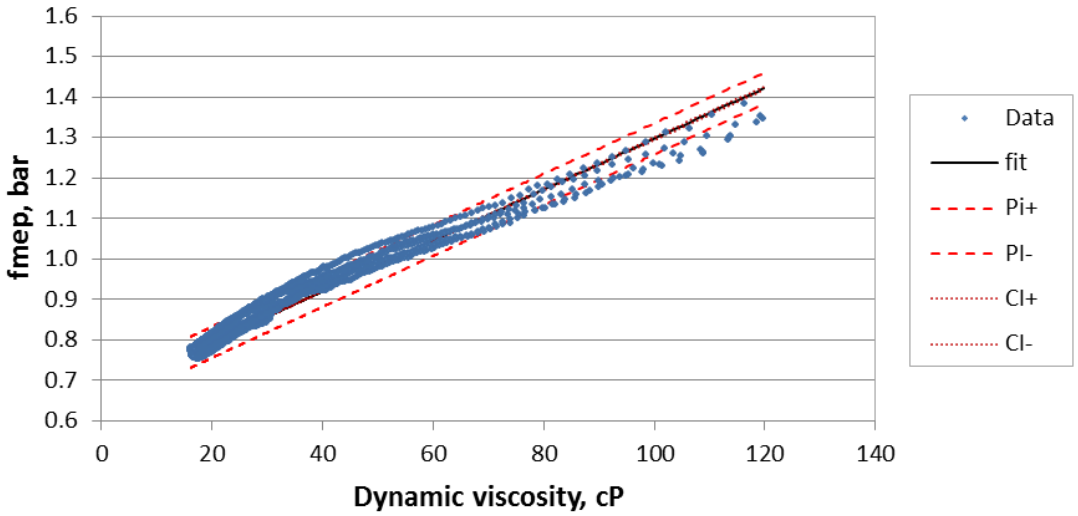

Figure 4.46: Friction mean effective pressure fit with 95% confidence and prediction intervals with oil changes after each test using Cooper Instruments torque meter for modified engine with external oil pump and a 5W30 oil

The two linear fits show that there is no significant difference between the tests with and without oil changes as can be seen in Figure 4.47. The prediction interval for the test series without oil changes generally falls within the prediction interval of the series with oil changes. Confidence intervals generally overlap with some separation at very low viscosity. This separation is mostly likely caused by a narrowing of the confidence interval due to the large amount of data for each series at low viscosity compared to the higher viscosities. The separation between the confidence intervals is approximately 0.2% of the fmep measurement and thus can be ignored. This shows that the tests from the rig are acceptably repeatable but care should be taken to record calibration constants so that outliers may be identified.

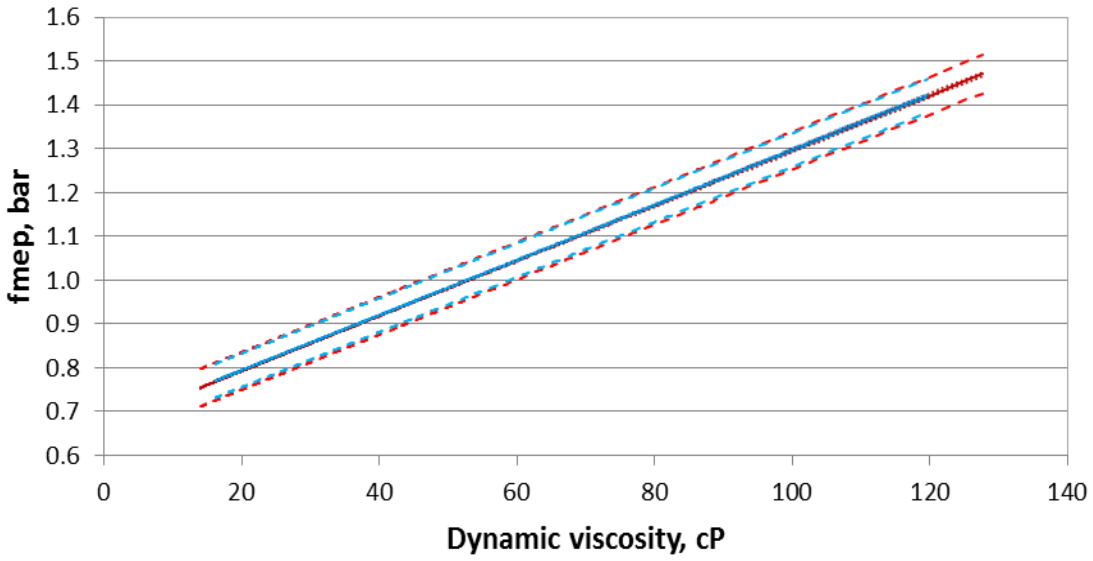

Figure 4.47: Comparison of linear fits for 5W30 tests with oil changes (red) and without oil changes (blue) with confidence and prediction intervals

4.4.3.3 Modified engine with external oil pump and Omega torque meter

Several oils are evaluated on the modified engine with external oil pump using the Omega torque meter to compare base and finished oils and to compare results between the modified and stock engine configurations. The oils are evaluated with the modified engine with external oil pump and Omega torque meter. The evaluated oils include a 15W40 weight oil and its associated base oil, a 0W30 weight oil and its associated base oil, and Mobil-1 5W30. Mobil-1 5W30 was also evaluated with the stock engine using the Omega torque meter. The results for the two oils in two stages of production are presented first with Mobil-1 5W30 results following.

The difference in friction mean effective pressure as a function of viscosity between a finished oil and its associated base oil is examined for two sets of oils; 15W40 and 0W30, using the modified engine with external oil pump and the Omega torque meter. Three runs are performed for each oil with an oil change after the first run. The results for the 15W40 and its base oil can be seen in Figure 4.48. The fmep varies very little from test to test for a given oil and showing high repeatability. There is a clear difference observed between the base and finished oil which shows the base oil has higher fiction.

Similar observations are made for the 0W30 oil and its base oil, as shown in Figure 4.49, with only a slight variation occurring during the first run of the 0W30 base oil. This could be attributed to residual 0W30 finished oil remaining in the engine as this oil was run before the 0W30 base oil, but the difference is negligible. Friction mean effective pressure for the 0W30 oils is more linear than the 15W40 series oils. This is likely due to the much smaller change in overall viscosity for the 0W30 oils when compared to the 15W40 oil. Both base oils are shown to have higher friction at a given viscosity which agrees with previous results.

A commercial oil, Mobil-1 5W30, is evaluated using the modified engine with external oil pump and Omega torque meter. The results shown in Figure 4.50 are similar to the previously shown results with good repeatability overall. The results from run 2 and 3 are very similar but a slight difference in the first run is observed. This is due to some residual 0W30 weight oil being in the engine when switching to the 5W30. The friction for all three tests are similar but the viscosity values for the first run are over predicted since residual 0W30 base oil is in the engine, thus causing a slight shift right in fmep at a given viscosity. This error is acceptable and the first run could be excluded.

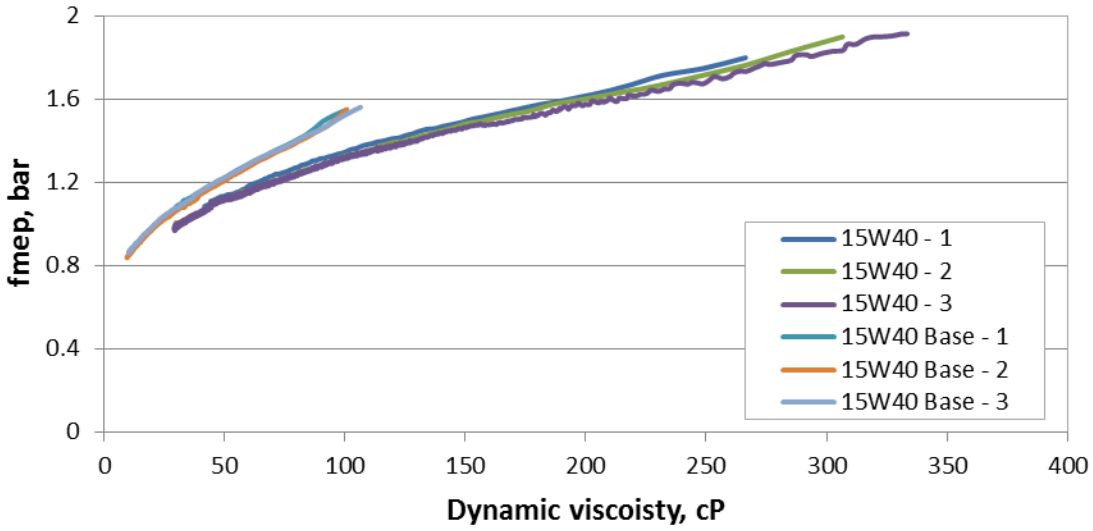

Figure 4.48: Friction mean effective pressure for 15W40 oil and its base oil measured on modified engine with external oil pump using Omega torque meter

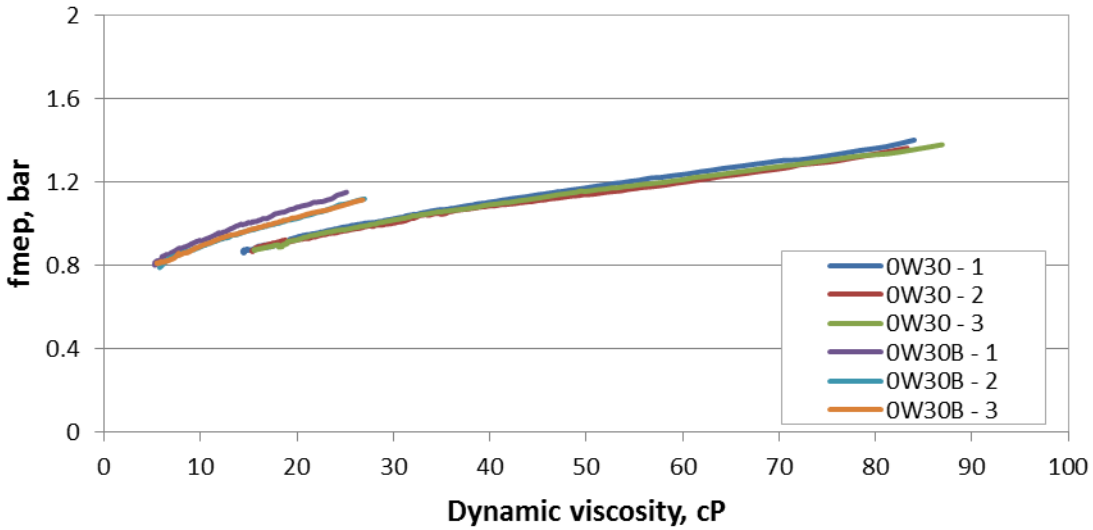

Figure 4.49: Friction mean effective pressure for 0W30 oil and its base oil measured on modified engine with external oil pump using Omega torque meter

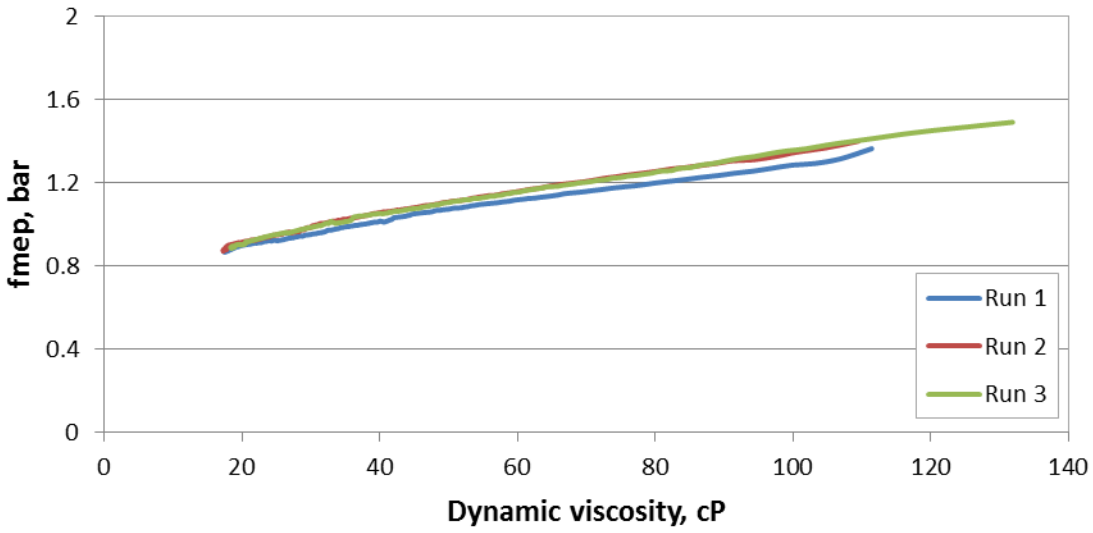

Figure 4.50: Friction mean effective pressure for Mobil-1 5W30 in the modified engine with external oil pump using the Omega torque meter

4.4.4 Stock engine with compression

The only minor modification to the stock engine with compression is the removal of the fuel system and the installation of a manual oil pressure relief valve. With this modification the contribution of engine auxiliaries and valve train components to fmep can be investigated. The Omega torque meter is used during these tests to evaluate four different oils — a base oil, base oil with a typical additive (ZDDP), base oil with a "developmental" additive, and Mobil-1 5W30 weight oil. These oils are run in the stock motored engine friction rig over a wide range of engine temperatures and oil pressures. Tests on this engine are performed in conjunction with a separate wear study in which a new cylinder linear and piston assembly are installed with each new oil sample. For this wear study, tests are run for a total of 20 hours in typically runs.

The stock engine tests include a wide range of temperatures so that the engine conditions approach temperatures of the modified engine without compression and a fired engine. A range of oil pressures are also varied during these tests in order to examine the contribution of the oil pump to motoring torque. The base oil test series is comprised of five runs due to an oil leak during the first run. During this series of tests for the base oil, the oil pressure is set to 20, 35, 37, 50, and 72 psi as seen in Figure 4.51. The maximum temperatures range from 70 to almost 100°C as seen in Figure 4.52. Motoring torque over the test is shown in Figure 4.53. The start-up of each test is observed in these plots as a large spike in measured pressure, temperature, or motoring torque. At early times of the temperature plot there are several spikes showing the quick start and stop in the first test due to an oil leak. The direct effect of oil pressure on motoring torque is evident in motoring torque over time and is seen as small steps in torque in Figure 4.53.

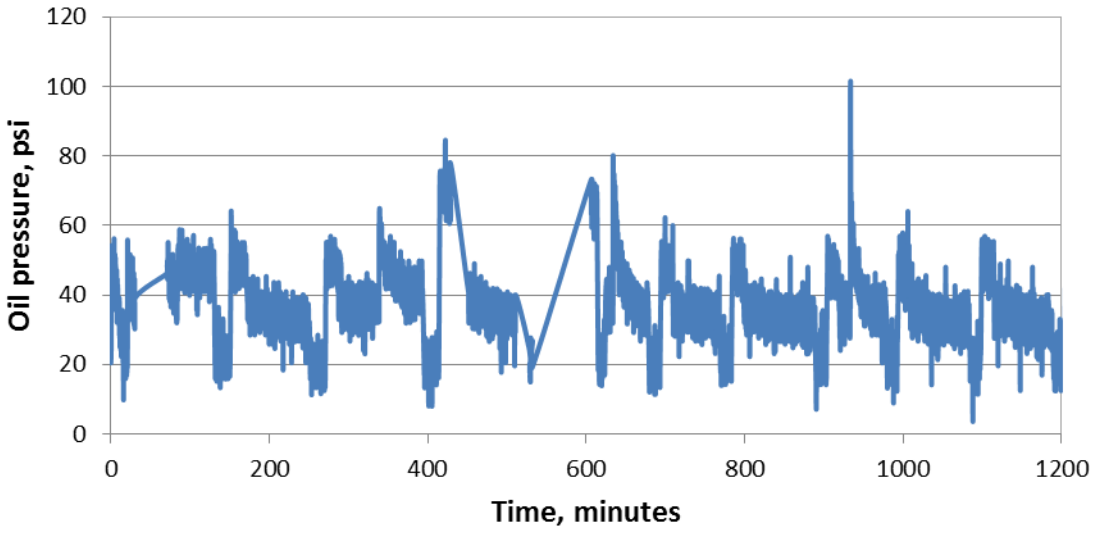

Figure 4.51: Stock engine (compression) oil pressure over time for base oil

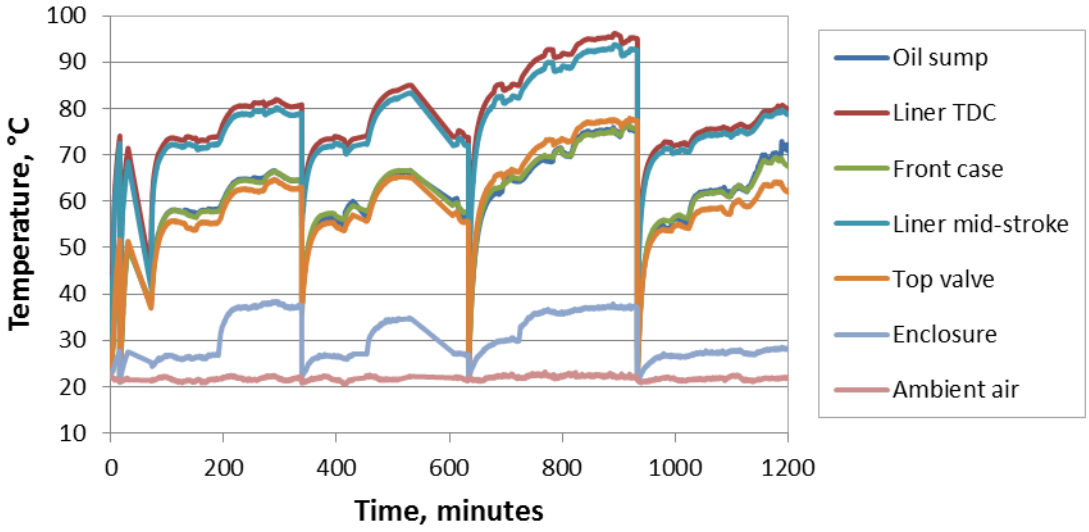

Figure 4.52: Stock engine (compression) temperatures over time for base oil

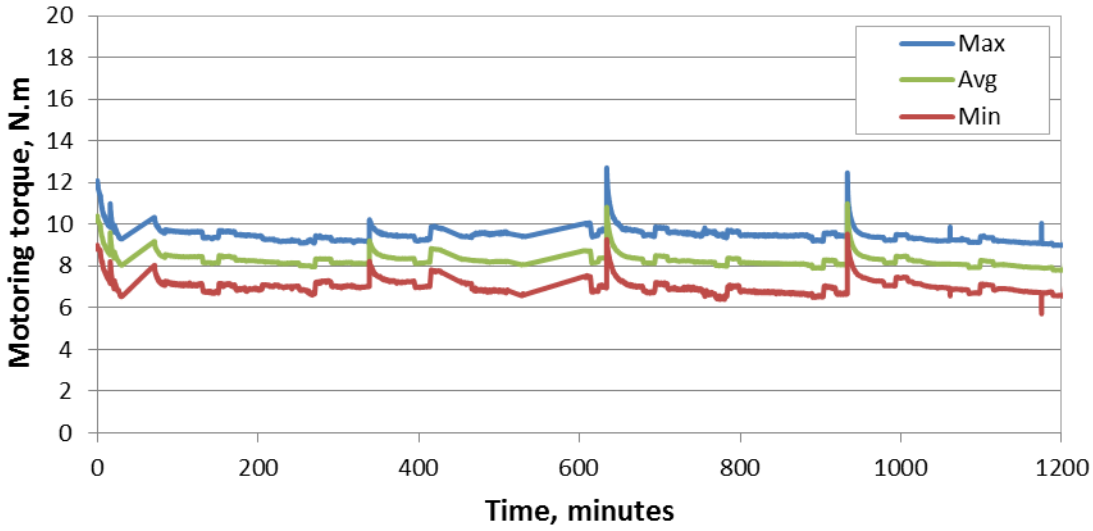

Figure 4.53: Stock engine (compression) motoring torque over time for base oil

The different oil pressures, engine temperatures, and large number of data for the stock engine tests makes creating fmep plots difficult. Results must be presented over a certain run number and oil pressure. This is in Figure 4.54 by plotting the last two runs of the base oil, runs 4 and 5, for three different oil pressures of 20, 35, and 50 psi. The figure shows that fmep increase with increasing oil pressure and decreases with run number. The difference in fmep between the two runs could indicate some wear in of the liner with polishing causing lowering friction. The difference in fmep could also be due to different modes of friction caused by the significant difference in engine temperatures. The valve temperature, for example, is almost 20°C lower than run 4 for run 5. The lower temperature could increase the viscosity and thus decrease boundary friction at the valves. The differences in fmep across the data shows the importance of engine conditions when lube oil performance.

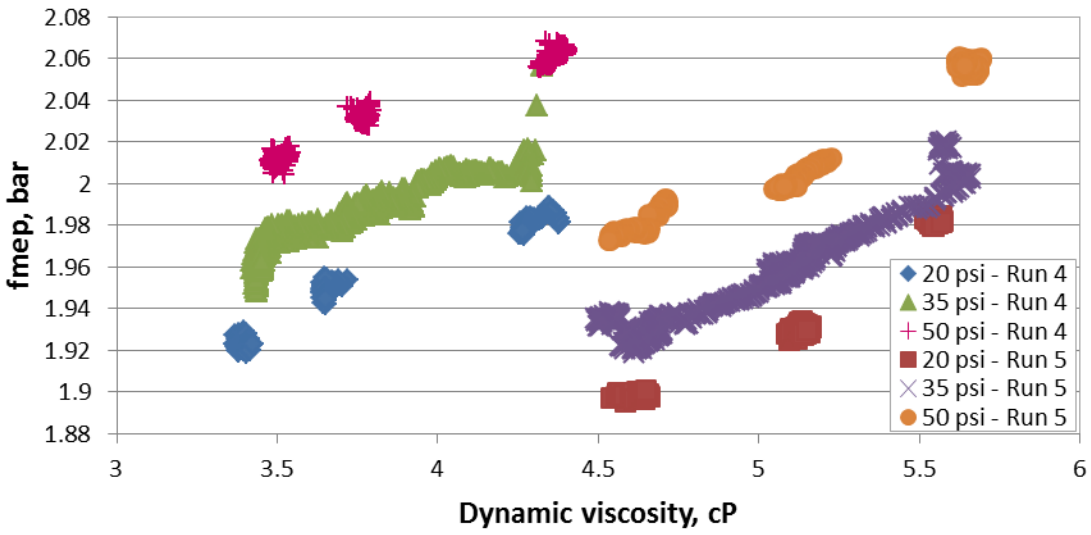

Figure 4.54: Friction mean effective pressure at various oil pressures and runs on stock engine (with compression) for Omega torque meter and base oil

The base oil with the developmental additive is also investigated over a similar range of oil pressures and engine temperatures. Plots of temperature and oil pressure are very similar to base oil plots so and are therefore excluded. The maximum and minimum average torques for the second run are much larger for than for the rest of the tests as seen in Figure 4.55. This was caused by accidently processing data over one revolution instead of two, distorting maximum and minimum torques but not adversely affecting average torque. The effect of liner wear in is observed for this oil by examining the data at 20 psi for each run as can be seen in Figure 4.56. Presenting the results in this manner shows a decrease in motoring torque for each run, indicating linear wear in and polishing of the liner.

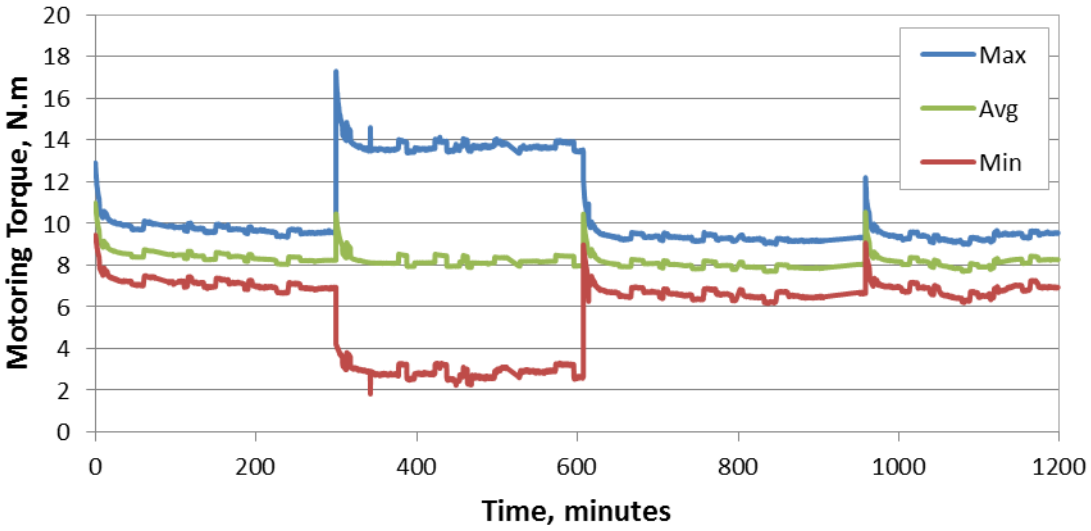

Figure 4.55: Stock engine (compression) motoring torque for base oil with developmental additive using Omega torque meter

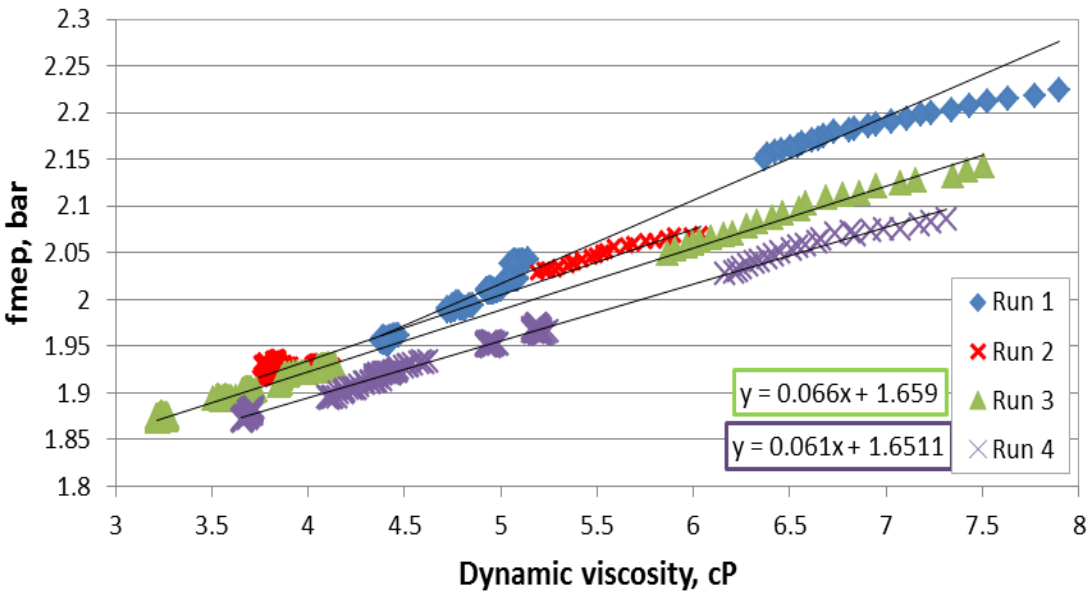

Figure 4.56: Stock engine (compression) fmep for base oil with developmental additive over 4 successive runs at an engine oil pressure of 20 psi

The results for the oil with the typical additive are similar to the base oil with and without developmental additive. A large increase in maximum and minimum torque are not observed in this series, although a single spike in maximum and minimum torque did occur due to noise. Results from the oil must be compared for the same run number and at the same oil pressure. This is done as shown in Figure 4.57 with results for the oils from the fourth run at 35 psi being compared. The base oil with the developmental additive shows the highest motoring torque and the base oil with the typical additive showing the lowest. This shows the developmental additive performs worse than the typical additive when considering friction alone.

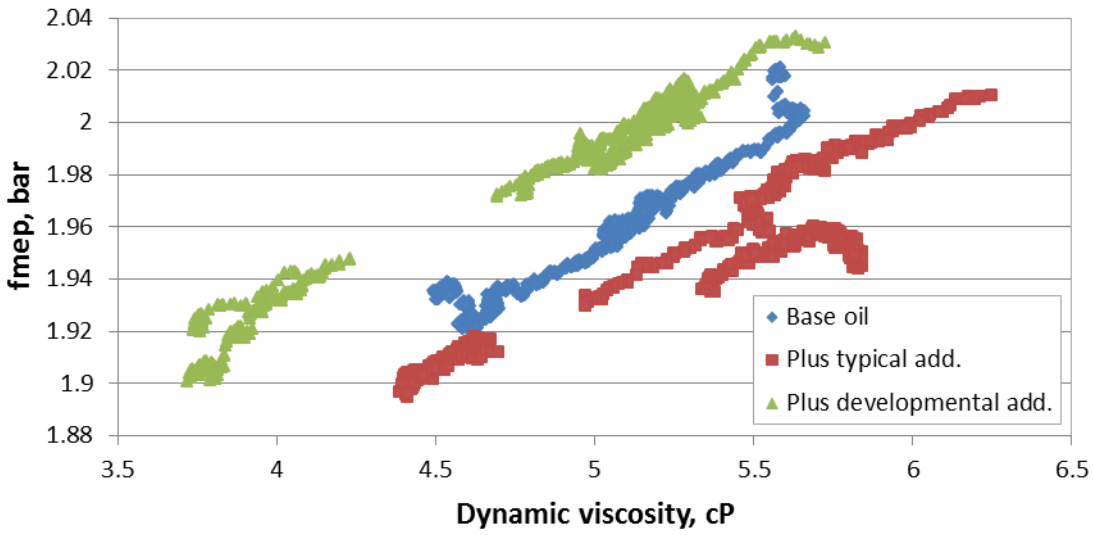

Figure 4.57: Comparison of friction mean effective pressure for a base oil, base oil plus typical additive, and base oil with developmental additive for the stock engine (compression) at 35 psi using the Omega torque meter

4.4.5 Comparison of average torque results across the different engine configurations investigated

Average torque results for several 5W30 oils are obtained for the modified with internal oil pump (no compression), modified with external oil pump (no compression), and stock (compression) engine configurations. These results are compared from which the friction contribution of the internal oil pump and valve train can be determined. The 5W30 oils tested include three oils from an unknown manufacture, referred to as 6Y90, 6Y94, and BL0, and commercial Mobil-1 5W30. The 6Y90 and 6Y94 oils were run on the modified engine with internal oil pump using the Cooper Instruments torque meter. The BLO oil was run in the modified engine with external oil pump using the Cooper Instruments torque meter. Mobil-1 5W30 was run in the stock engine with compression and

the modified engine with external oil pump, both using the Omega torque meter. The viscosities of the oils as predicted by Vogel's equation are shown in Figure 4.58. The viscosities of all the oils investigated significantly differ at temperatures below 40°C but the differences over the tested temperatures are small and thus should not prevent the comparison of results.

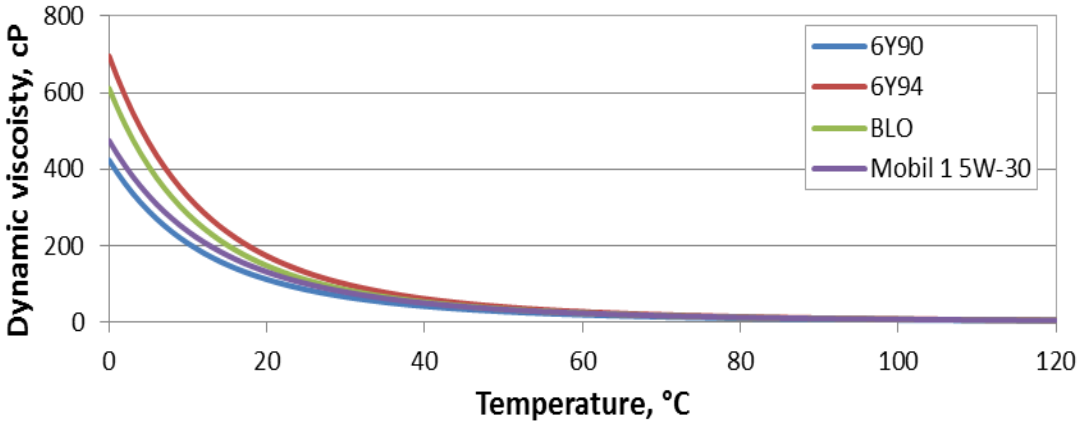

Figure 4.58: Comparison of viscosity for 5W30 oils investigated

Comparing fmep results for the 5W30 oils across engine conditions shows a distinct difference between engine configurations as can be seen in Figure 4.59. The modified engine with external oil pump using the Cooper Instruments torque meter and BLO oil has the lowest fmep with the Mobile 1 oil run on the same engine using the Omega torque meter falling slightly above. The Omega torque meter measures higher torque for the same oil. Thus the difference between the BLO and Mobil-1 oils is caused by the torque meters and is ignored for this discussion. The fmep for the modified engine with internal oil pump and Cooper instruments torque meter for the 6Y94 and 6Y90 oils is approximately 1.2 bar at 20 cP. Friction mean effective pressure for the modified engine with

internal oil pump using the Cooper Instruments torque meter and the BLO oil is approximately 0.8 bar at 20 cP. This shows that the oil pump contributes approximately 0.4 bar to total fmep.

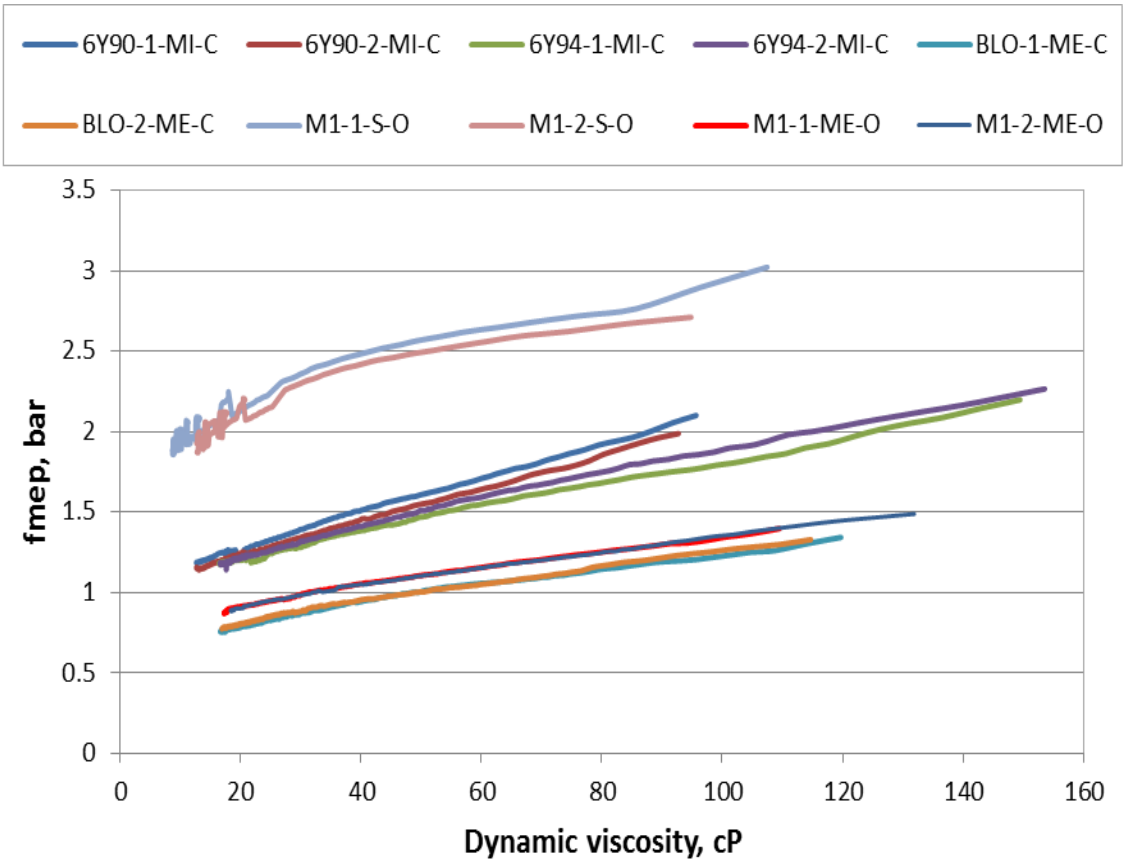

Figure 4.59: Friction mean effective pressure for several 5W30 oils over engine configurations and torque meters (Oil-Run-Configuration-Torque meter, M = Mobil-1, MI = modified internal oil pump, ME = modified external oil pump, S = stock, C = Cooper Instruments, O = Omega)

The stock engine with compression using the Omega torque meter and Mobil-1 oil produces the highest fmep of approximately 2 bar at 20 cP. The modified engine with external oil pump using the Omega torque meter and Mobil-1 oil has a fmep value of approximately 0.9 bar at 20 cP. The difference between fmep of 1.1 bar for these engine configurations is significant. In fact the difference between the two configurations is larger than the measured value for the modified engine with external oil pump. However, this is reasonable. The pumping losses are approximately 0.4 bar which result in 0.7 bar fmep contributed by the valve train, friction from piston rings due to compression, and friction between timing gears. This is reasonable since the piston, the piston rings, and the connecting rod contribute to about half of engine friction. Overall there is a distinct and measureable difference between the engine configurations.

CHAPTER 5
ENGINE FRICTION SIMULATION RESULTS AND DISCUSSION

The feasibility of using AVL Excite Power Unit to predict friction in a Hatz single-cylinder diesel engine is examined in this chapter. The development of the model with a description of the various inputs used to create the Hatz model is detailed in Section 5.1. Pre-simulation kinematic results are examined to help understand the instantaneous torque results produced by the simulation in Section 5.2. A description of the process used to estimate system inertia for the calculation of crankshaft torque from angular acceleration is provided in Section 5.3. Experimentally measured friction coefficients for the lube oils investigated and the fitting of these results to the Excite friction coefficient equation is presented in Section 5.4. The feasibly of predicting motored engine friction rig results using AVL Excite is evaluated in Section 5.5

5.1 Development of model

The model of the Hatz 1D50 a single-cylinder diesel engine is based on the following engine physical components: the piston, piston pin, conrod, crank, and engine block. The block is considered to be rigid and is in the model to provide connection points for the joints between components. Kinetic analysis is performed based on information about these components, engine cylinder pressure over a cycle, and engine speed. The kinetic calculations are discussed by first examining the inputs and then each of the calculations.

The first inputs into the model are the “crank train globals” which are model global inputs that include values such as the number of cylinders, bore, stroke, conrod length, important axes (rotational and vertical), and simple mass properties. General data for the crank train globals are shown in Figure 5.1 and mass properties for the crank train globals are shown in Figure 5.2.

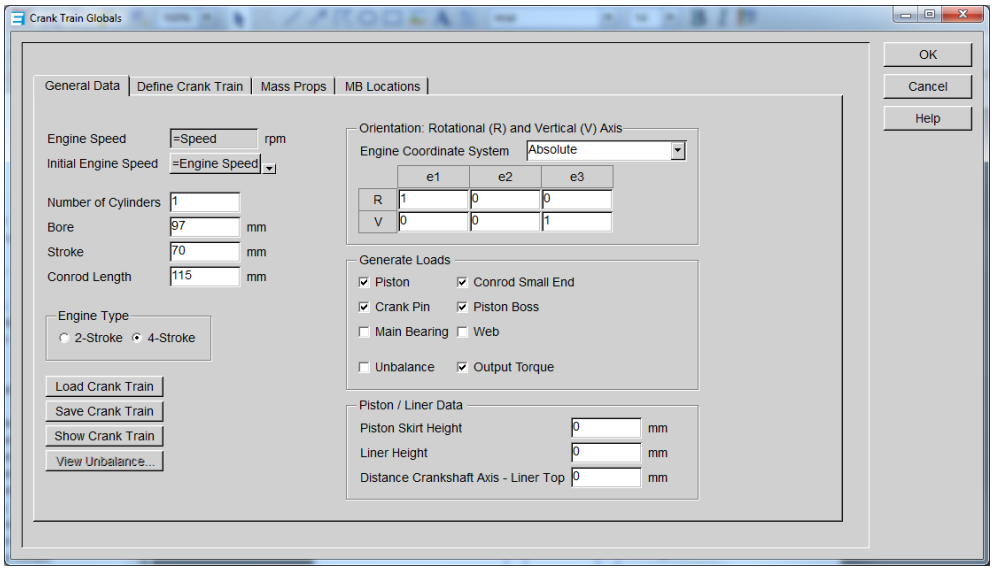

Figure 5.1: General data for crank train globals

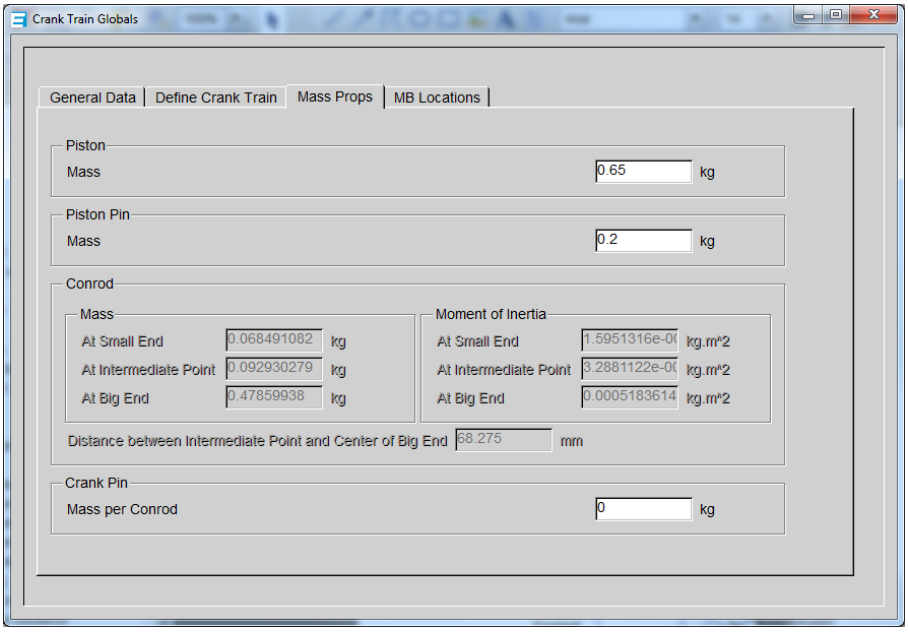

Figure 5.2: Mass properties for crank train globals

The Excite program offers several levels of detail in terms of component modeling. The simplest being a simple mass input to the most complex being a full finite element model of a flexible body. In this model, the piston and piston pin fall on the simple side and are mass values inputted into the program. During simulation these values are lumped onto the small-end of the conrod.

The conrod model falls somewhere in the middle of modeling complexity. This model is created using a subprogram within Excite called the conrod modeler. This subprogram creates a model of the conrod based on geometry and material properties. The conrod modeler mass inputs and conrod modeler with geometric inputs used in the model are shown in Figures 5.3 and 5.4, respectively. The density shown in Figure 5.3 was used to reach a total conrod mass equal to a Hatz conrod mass measured experimentally. The other material properties are Excite defaults and are typical values for steel. The mass and inertia values calculated by Excite are shown in Figure 5.5. The values are shown for the x, y, and z axis with units of Mega-gram (Mg) for mass, milli-meter (mm) for distance, and $Mg(mm)^2$ for inertia.

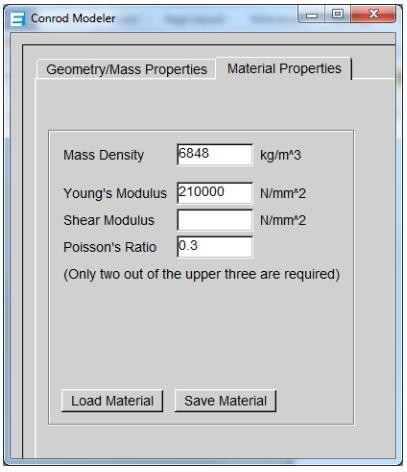

Figure 5.3: Conrod modeler material properties – input

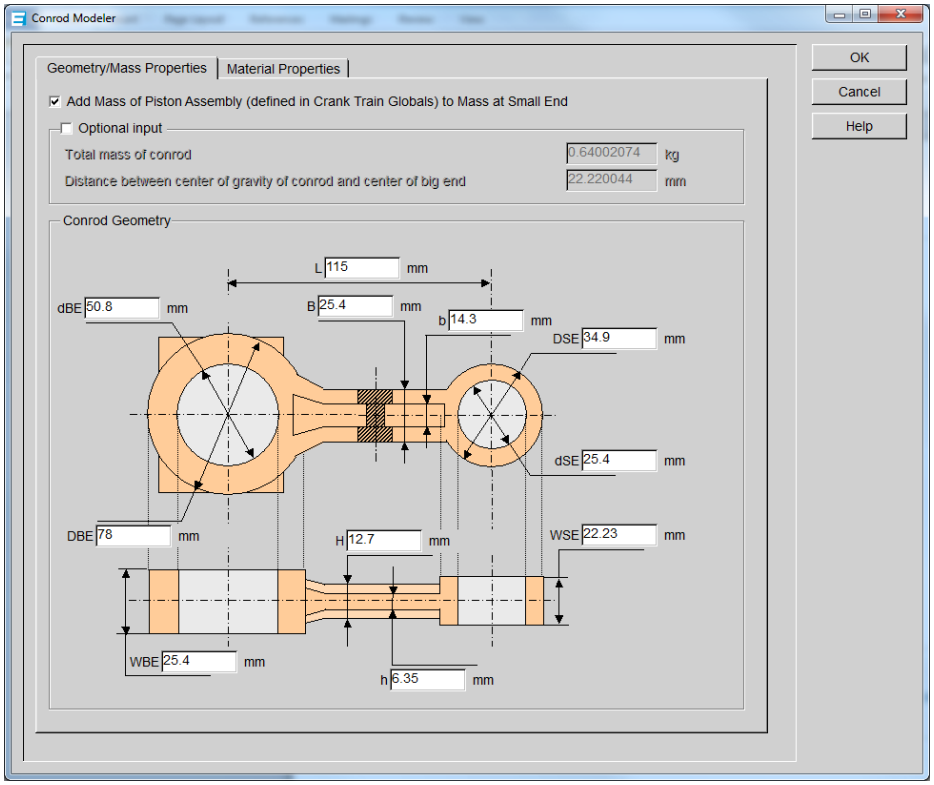

Figure 5.4: Conrod modeler dimensional inputs

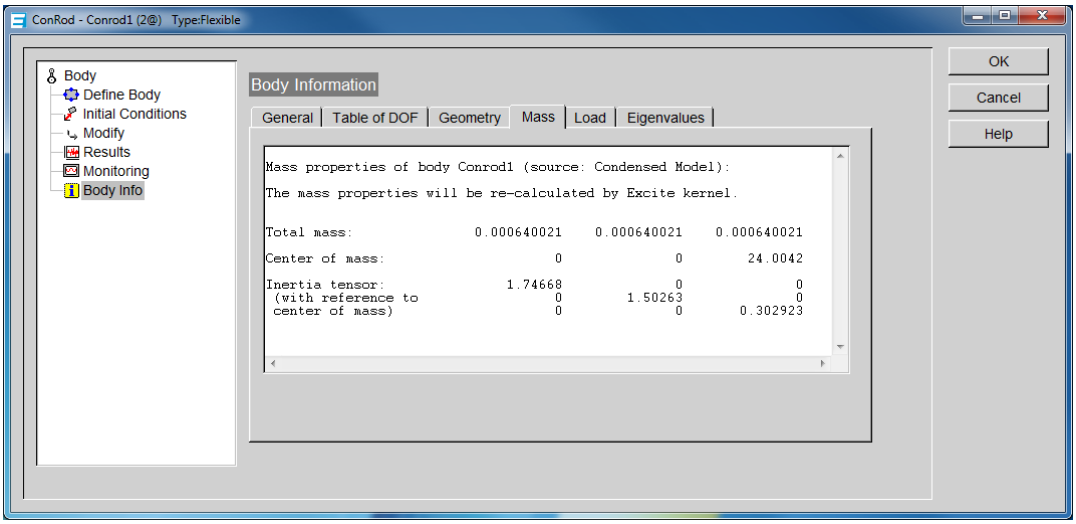

Figure 5.5: Conrod mass properties as calculated by conrod modeler

The crankshaft is also modeled using a built-in Excite subprogram, the shaft modeler. For this model, a CAD drawing of the crankshaft without the flywheel is created. The crankshaft material properties and CAD drawing are used by the subprogram to create a partial mass system representing the crank as seen in Figures 5.6 and 5.7, respectively. Again, a density value is chosen to produce a total mass equal to the measured mass of the crankshaft. The flywheel is not included in the CAD drawing and is lumped to the end of the shaft in shaft modeler allowing for direct input of flywheel mass and inertia. The mass of the flywheels is obtained by weighing the Hatz flywheel. The inertia value is estimated using the inertia formula for a simple disk and general dimensions of the flywheel. The various inputs and the Excite mass outputs for the crank are shown in Figures 5.6 to 5.9.

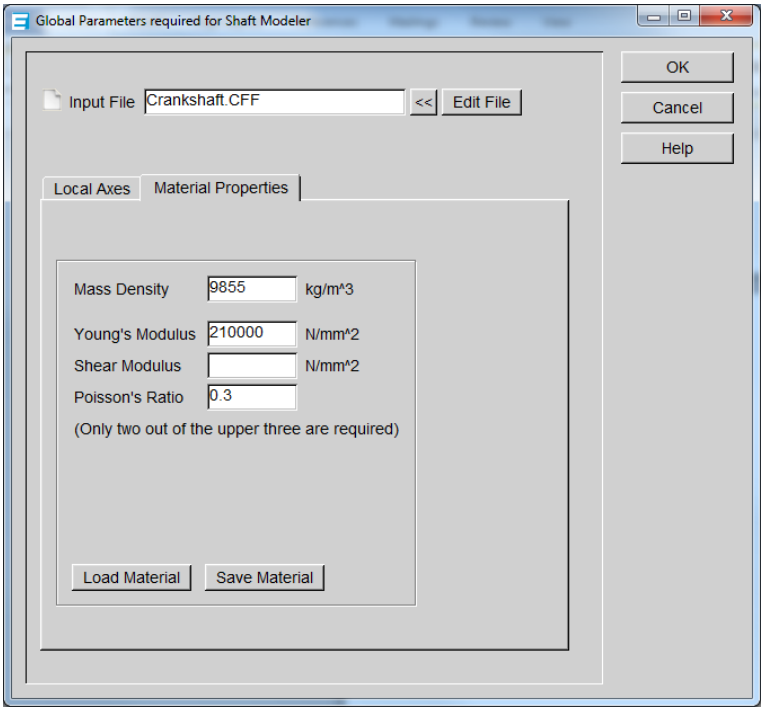

Figure 5.6: Shaft modeler global parameters – material properties

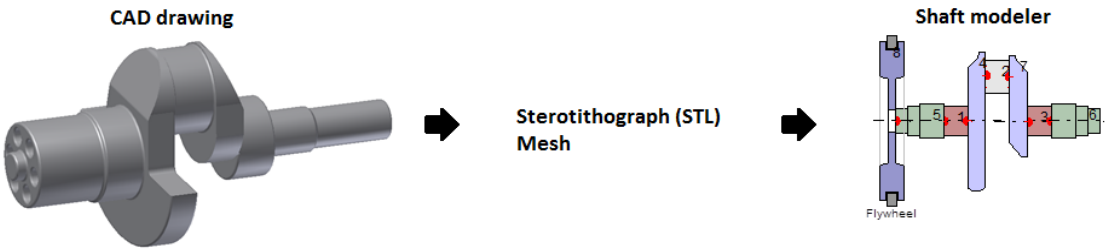

Figure 5.7: CAD drawing of crankshaft and shaft modeler 2-D representation

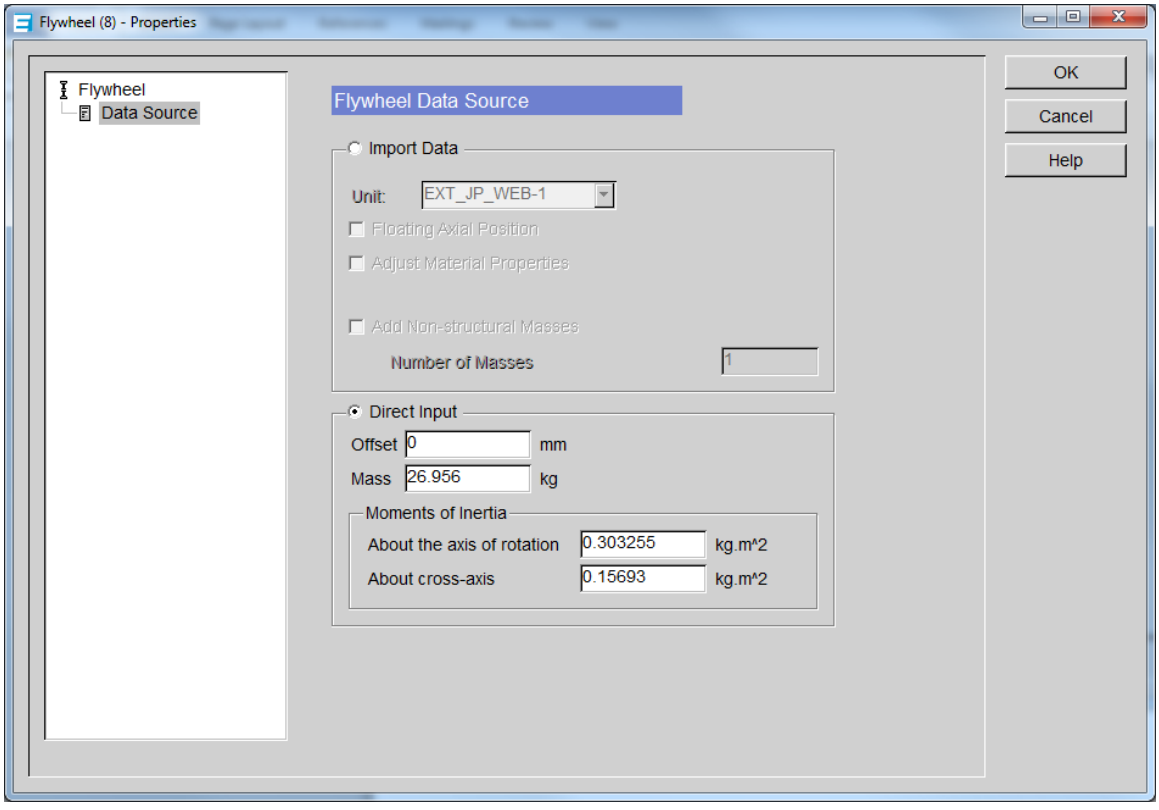

Figure 5.8: Shaft modeler flywheel direct inputs

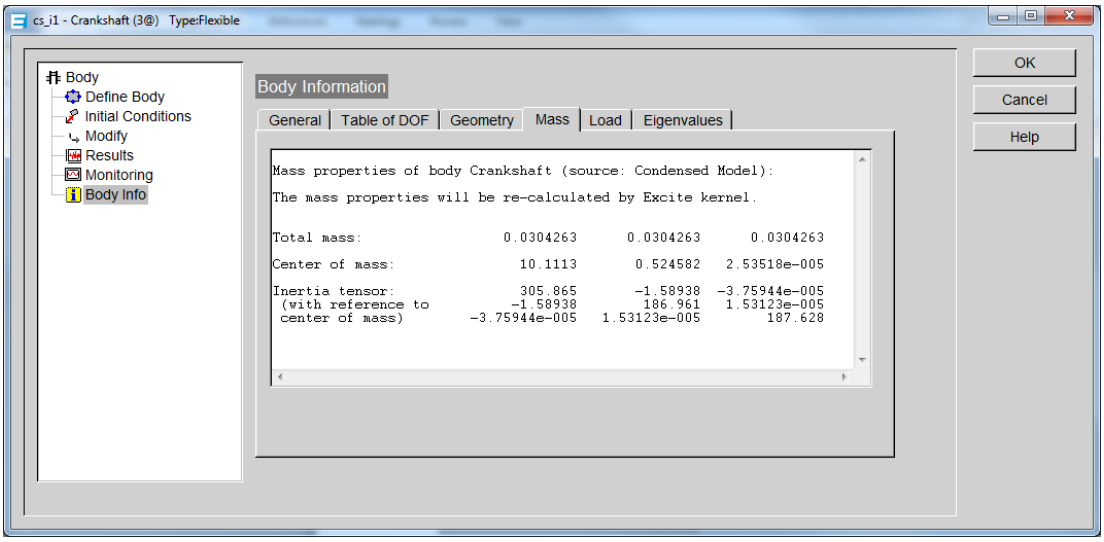

Figure 5.9: Crankshaft mass and inertia values calculated through Shaft Modeler (Mg, mm, and $Mg(mm)^2$)

The final inputs required for the model, besides the friction coefficient data, are the cylinder pressure trace and engine speed. The pressure trace experimentally obtained at a speed of 1791 RPM from a motored Hatz 1D50 engine with compression is shown in Figure 5.10. This information is used as input for Excite to model engines with compression. To model the engine without compression, a no compression pressure trace is created from the measured compression pressure trace by removing the intake and exhaust sections as can be seen in Figure 5.11. In the plot the intake and exhaust sections are repeated so that 0 to 720 crank angle degrees are represented in the plot. This was done because AVL Excite Power Unit requires cylinder pressure trace over two revolutions, a typical engine cycle, for input into the program.

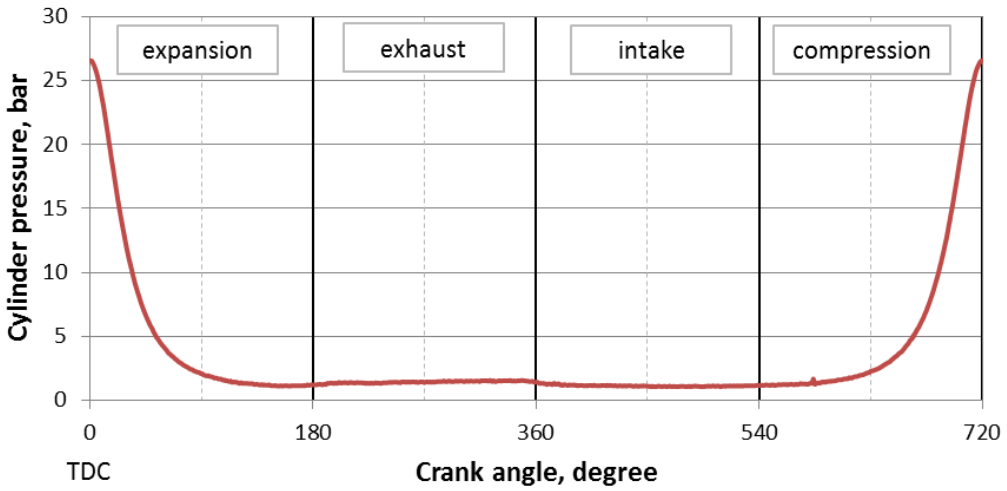

Figure 5.10: Hatz motored pressure trace with compression, 1791 RPM

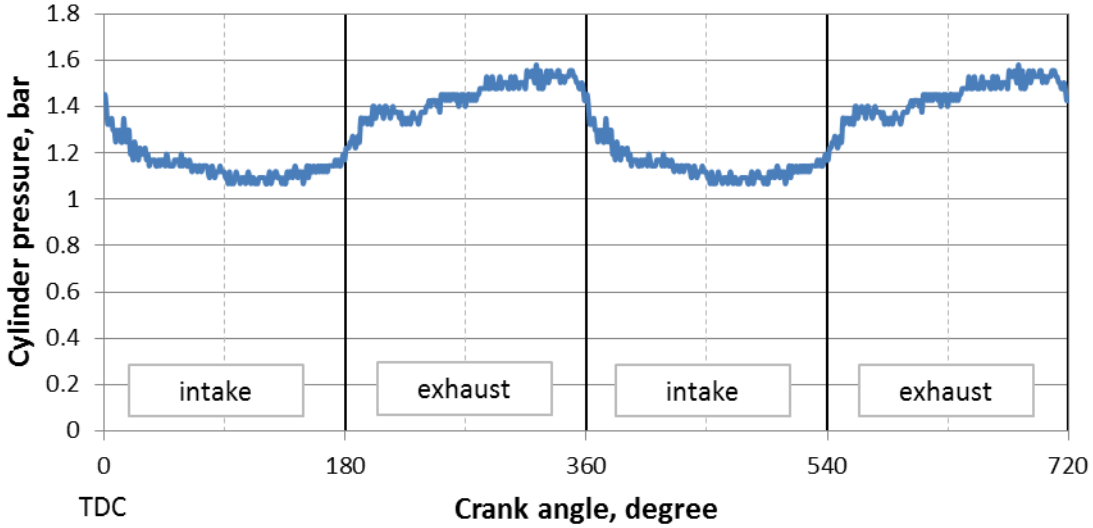

Figure 5.11: No compression pressure trace obtained from Hatz motored pressure trace at 1791 RPM

5.2 Pre-simulation component loads and torques with no friction and no instantaneous speed change of crankshaft

The pre-simulation results calculate the loads and torques on the engine components based on cylinder pressure and component mass, geometry, and acceleration without considering any friction or any instantaneous speed change of the crankshaft. Understanding these calculations helps to explain the shape of the instantaneous torque curves from the motored engine friction rig and the results obtained from Excite. In these calculations the axis along the crankshaft center is labeled as axis 1, the horizontal axis perpendicular to the crankshaft center is labeled axis 2, and the vertical axis along the cylinder center is labeled axis 3. The mass values of the actual Hatz 1D50 diesel engine components and the Excite mass values are shown in Table 5.1. Piston and piston pin masses are rounded and directly inputted into Excite. Conrod and crank/flywheel masses are calculated by Excite based on geometric and material property inputs.

.

Table 5.1: Mass properties of engine components examined in kinetic calculations

Component	*Measured Values*	*Excite Model Values*
Piston Mass, grams	649.8	650
Piston Pin mass, grams	202.8	200
Conrod mass, grams	638.5	640.021
Crank and Flywheel mass, grams	30454	30426.3

The kinetic outputs produced by Excite include: cylinder force, piston pin force, conrod small-end forces, crank pin forces, crank variable torque, and crank average torque. The forces examined are in the z and y direction with z being vertical and y horizontal. The cylinder force is simply calculated based on the

pressure and the piston area based on engine bore. The engine is considered to be at a constant RPM and thus a constant rotational velocity about the crank rotational axis. Since the angular velocity is considered to be constant for these calculations, crank angle and time are equivalent with crank angle of 1 degree equal to approximately 0.093 ms. For this simulation, the pressure trace with compression is used. The force on the piston calculated from the piston size and the pressure trace produces a curve similar in shape to the pressure trace only with all negative values, as shown Figure 5.12.

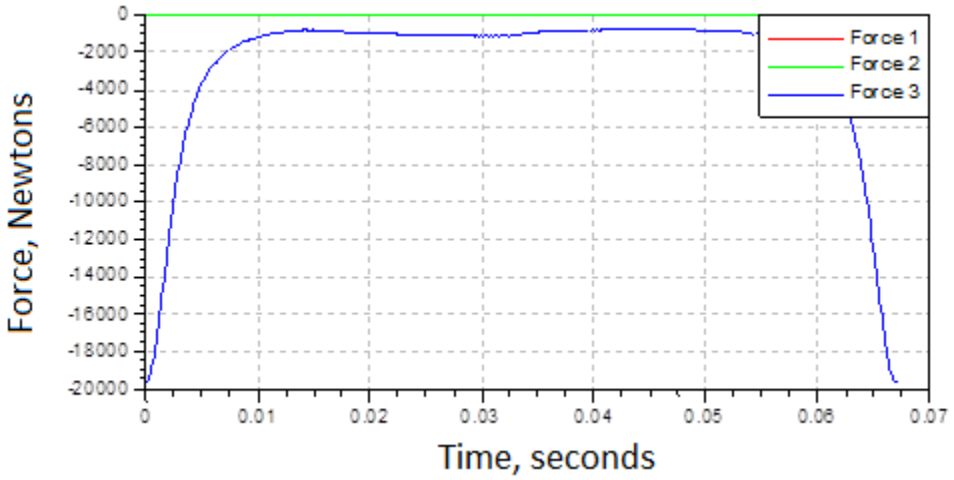

Figure 5.12: Piston force calculated by Excite simulation for Hatz model with compression where Force 3 is the vertical force and Forces 1 and 2 are the horizontal forces both equal to zero

The piston boss is the bearing in the piston which houses the piston pin. The vertical forces on the piston boss are calculated based on the acceleration of the piston and the force on the piston from the cylinder pressure; whereas, horizontal forces are equal to zero at the piston boss. The acceleration of the piston can be found by taking the second derivative with respect to time of the

piston displacement. The piston boss force curve has a similar shape as the piston with differences occurring around mid-stroke as can be seen Figure 5.13.

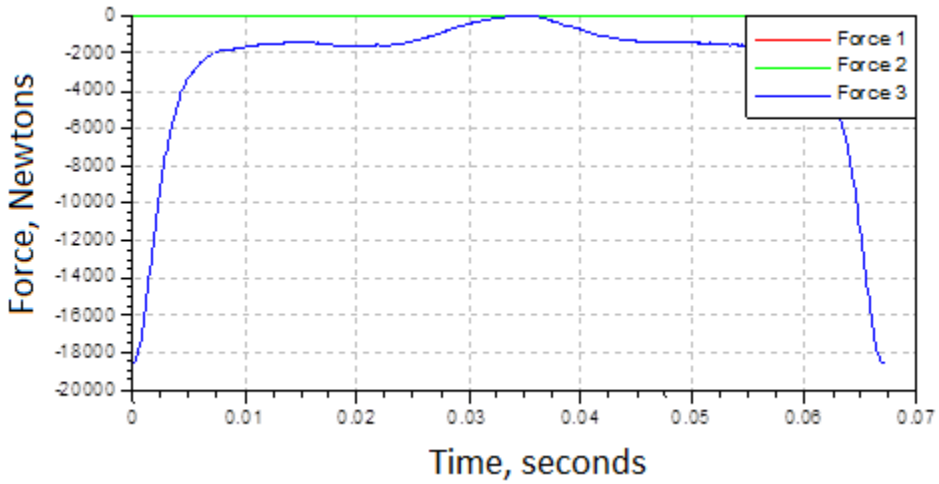

Figure 5.13: Forces on piston boss calculated by Excite simulation for Hatz model with compression (Force 1 = Force 2 = 0)

The force on the piston boss and the mass/acceleration of the piston pin are used to calculate the vertical force on the small end of the connecting rod, i.e., the piston pin bearing end of the connecting rod. The horizontal force on the conrod small end, is more difficult to find and requires a sum of moments about the conrod center of gravity. The sum of moments includes the vertical and horizontal forces at the small end, the inertia moment of the conrod, and vertical and horizontal forces at the big end of the conrod where the big end is the crank shaft pin bearing. The vertical force on the big end is found using the previously mentioned method of summing the vertical forces on the small end with the vertical acceleration force of the conrod. The acceleration of the conrod is found by taking the second derivative with respect to time of the conrod center of

gravity displacement. The remaining unknowns are the horizontal force on the big end, the horizontal force on the small end, and the angular acceleration of the conrod. The two horizontal forces can be equated with the sum of forces and the angular acceleration can be found by taking the second derivative with respect to time of the angular displacement of the connecting rod. The remaining unknown, the horizontal force on the small end, can be solved by the sum of moments. The vertical forces on the small end (shown in blue) have a shape similar to the piston boss forces and horizontal force is now included (shown in green), in Figure 5.14. The connecting rod small end forces include force on the horizontal because the connecting rod is accelerating both vertically and horizontally. The piston, as far as the these ideal calculations are concerned, only accelerates along the vertical axis which is why Force 2 is zero for the piston and piston boss.

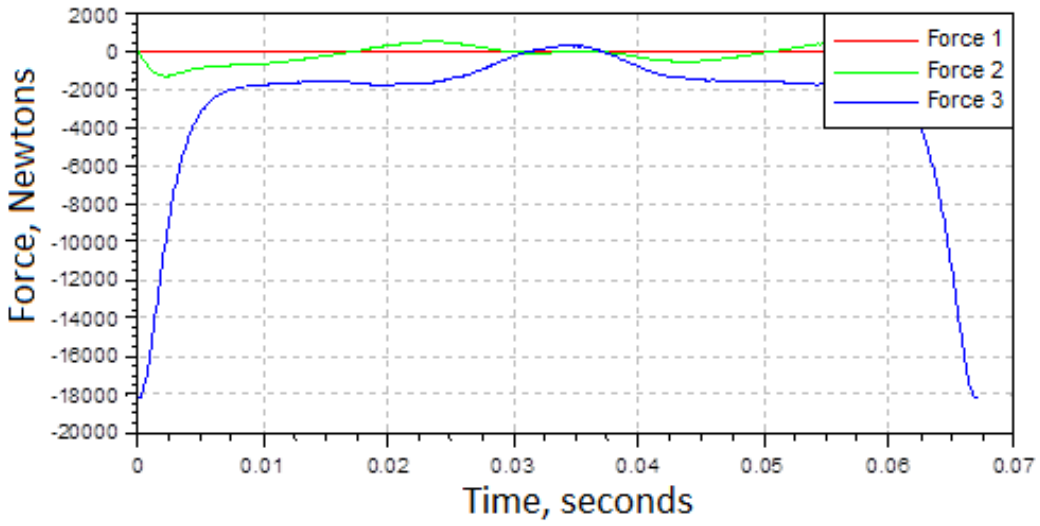

Figure 5.14: Forces on conrod small-end calculated by Excite simulation for Hatz model with compression

The calculated forces on the small end of the connecting rod are used along with the connecting rod center of gravity acceleration to find the forces on the big end via sum of forces. From the crankpin forces, which are equal in magnitude to big end forces, the torque on the crankshaft over an engine cycle or variable torque is calculated. Since the angular acceleration of the crank is considered to be zero for these calculations; this sum of moments is based simply on the forces, engine stroke, and engine crank angle. The crankshaft torque is then averaged over an engine cycle. The calculated average torque is the net torque on the crankshaft over the cycle and is equal to the losses in the cylinder pressure trace since the acceleration forces of the engine components are conservative and friction is not considered here. The forces and moments on the crankshaft are shown in Figures 5.15 to 5.17. In Figure 5.15, the sharp peaks at the beginning and end of the plot are the result of compression and expansion forces in the cylinder and the hump in the middle is caused by acceleration forces of the engine components.

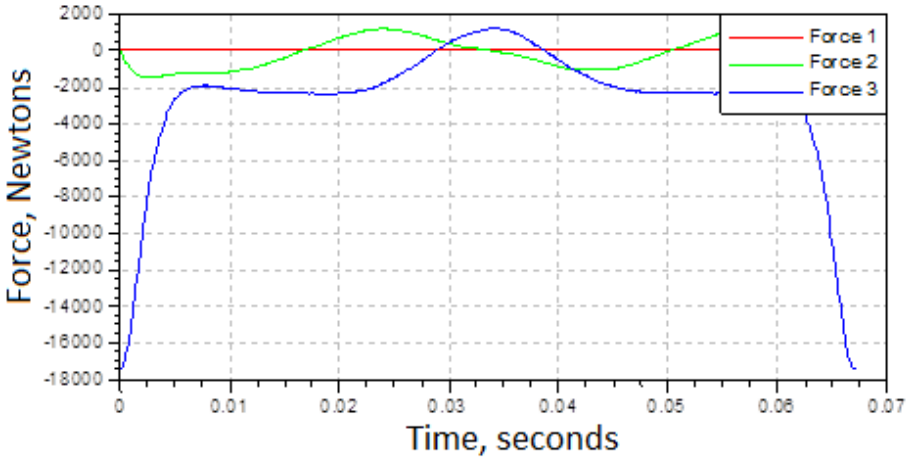

Figure 5.15: Crankpin forces, equal in magnitude to big-end forces, calculated by Excite simulation for Hatz model with compression

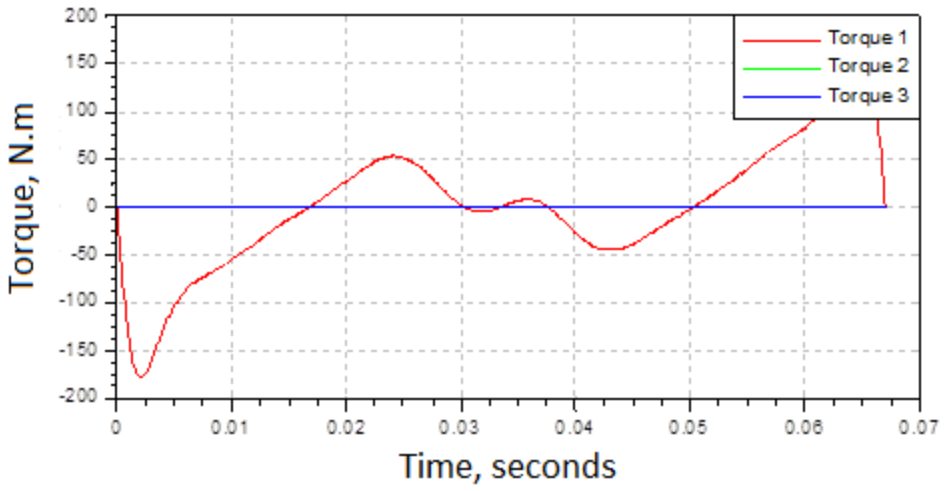

Figure 5.16: Variable torque on crankshaft calculated by Excite simulation for Hatz model with compression (Torque 2 = Torque 3 = 0)

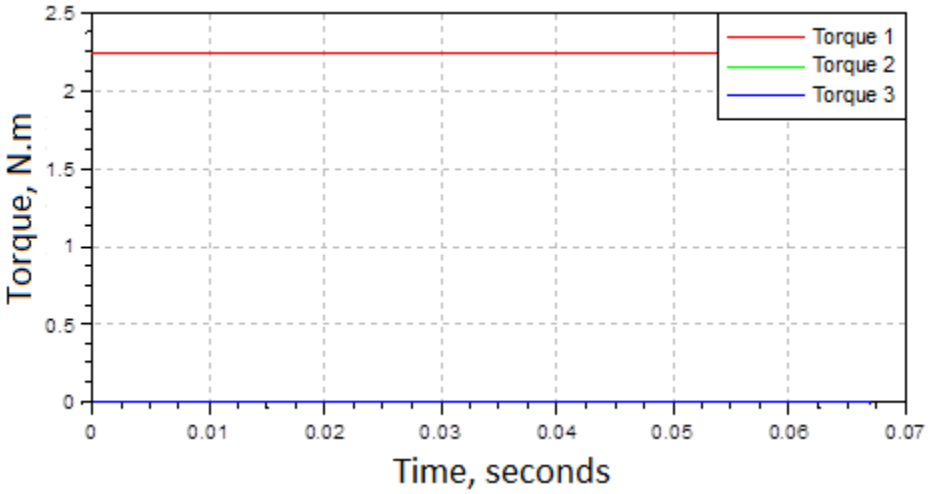

Figure 5.17: Averaged torque on crankshaft calculated by Excite simulation for Hatz model with compression (Torque 2 = Torque 3 = 0)

The variable torque over the cycle can be separated into its components to further examine each component's contribution to the total torque and the pressure force contribution to the average torque. To examine how each section of the engine cycle contributes to average torque, the torque data are split into two data sets of one revolution each. The absolute values of these two data sets are taken and the second revolution is mirrored to allow for comparison with the first. When plotted this way, compression and exhaust are shown to have greater torque than expansion and intake as can be seen in Figure 5.18. To help understand why this is occurring and understand the shape of the curve, the results for pressure torque, torque produced by component masses, and total torque are plotted together in the same fashion as before in Figure 5.19. This plot shows that pressure torque is greater over compression and exhaust, while the bumps at 315-360 degrees in Figure 5.18 arise from the torque produced by the masses overtaking the torque produced by the pressure.

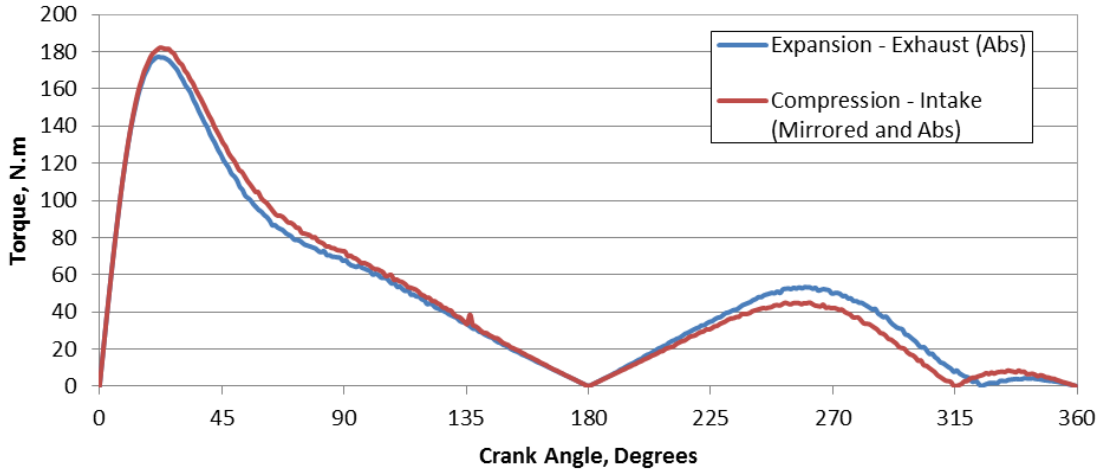

Figure 5.18: Torque on crankshaft for expansion-exhaust and compression-intake revolutions (TDC = 0)

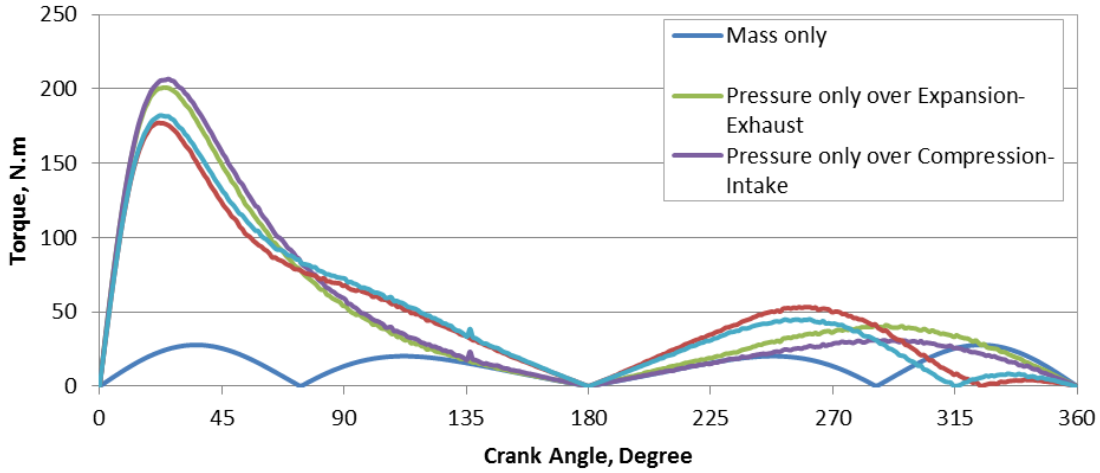

Figure 5.19: Torque on crankshaft for expansion-exhaust and compression-intake revolutions with mass and pressure torque separated (TDC = 0)

The contribution of cylinder pressure to torque can be further examined by plotting the pressure trace in an absolute and mirrored fashion like the previous plots in Figure 5.20. This plot shows greater pressure during compression and exhaust than during expansion and intake. Since both of these points occur when the pressure force is opposing the direction of the piston, a net torque is acting against the rotation of the crankshaft. The pressure trace peak occurs approximately 0.1 degrees into the expansion stroke but this alone does not account for the differences between the compression and expansion strokes. The most likely and most significant source of these differences is heat loss or energy loss during compression and expansion. The difference between the exhaust and intake can be attributed to atmospheric pressure effects.

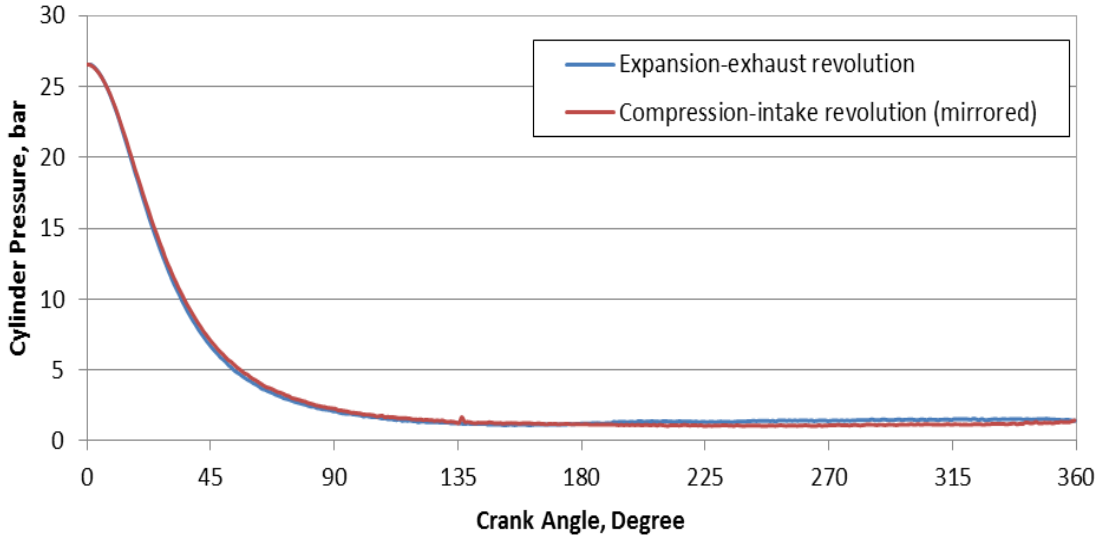

Figure 5.20: Cylinder pressure for Hatz 1D50 with compression separated into expansion-exhaust and compression-intake sections (TDC = 0)

5.3 Estimating system inertia for calculation of friction torque

The simulation results do not include crankshaft torque, and thus torque must be calculated based on the angular acceleration of the crankshaft and the engine system inertia. This inertia is calculated by running the simulation at various torque loads from 0 to 10 N.m applied to the crankshaft with the cylinder pressure set to zero. The output produced a linear increase in average angular acceleration, α_m, of the crankshaft with load. The applied loads are then divided by the average angular accelerations to estimate the inertia of the system, I_s, which is found to be approximately 0.308 kg.m^2/rad as shown in Table 5.2.

Table 5.2: Calculation of system inertia, I_s, over various applied torques

Torque load, N.m	α_m, *rad/sec*^{2}	I_s, *kg.m*^{2}*/rad*^{2}
≈0	-0.01	0
2.5	8.12	0.308
5	16.28	0.307
7.5	24.27	0.309
10	32.59	0.307

5.4 Lube oil friction coefficient measurement using line contact friction rig

Simulating engine friction with AVL Excite Power Unit via the modified Stribeck equation requires fitting this equation to experimental friction coefficient data for a given oil. This is done for a 15W40 base oil and the associated commercial 15W40 oil. The base oil is a thin single grade oil used to produce the fully formulated commercial 15W40 which includes a full additive package. The friction coefficients for the 15W40 base oil shown in Figure 5.21 are measured as a function of speed at several applied normal loads and oil temperatures. The typical shape of the Stribeck curve can be seen in the results with friction coefficients dropping sharply from a high value near zero speed to a minimum value around 0.25 m/s and steadily increasing thereafter. This indicates boundary/mixed lubrication at speeds below approximately 0.5 m/s and hydrodynamic lubrication above this speed.

The friction coefficients in the hydrodynamic regime decrease with increasing load which agrees with the Stribeck curve since load is in the denominator of the Stribeck number and a lower Stribeck number corresponds to a lower friction coefficient in this regime. Temperature has the opposite effect in the hydrodynamic regime with friction coefficients decreasing with increasing temperature which also agrees with the Stribeck curve.

The results at low speeds seem to indicate that higher temperatures increase boundary friction which is not true since the friction coefficient in the boundary regime should be constant regardless of temperature. The results appear this way due to the limitations of the line contact friction rig. There is a minimum speed obtainable with the line contact friction rig and at this speed full boundary friction is not reached for the oil at lower temperatures due to higher viscosities. At higher temperatures, the oil is thinner and is in the boundary/mixed lubrication regime for a larger range of speeds. Furthermore, surface contact is more likely at low speeds and high temperatures. Because of these effects the measured friction coefficients are higher at low speed for higher temperatures but this does not mean that boundary friction is higher. Some of the friction coefficients measured at minimum speed could also be over predicted. This is due to the cylinder and plate sticking at very low speed causing starts and stops and inconsistent cylinder speed. These same errors are present when investigating the effect of applied load on friction coefficient at very low speeds. Generally the friction coefficient decreases with load but this does not mean that boundary friction is lower at lower loads.

The two friction coefficient sets measured for a 1 kg applied normal load and average oil temperatures of 24 and 43°C — the two temperatures being the average of the oil sump and friction plate temperatures over the test for given load applied load — become nearly constant at speeds above 2.5 m/s whereas the friction coefficient should continually increase with speed. This is attributed to an increase in the oil film temperature due to hydrodynamic friction. However, the plate temperature increases with the speed over the test as can be seen in Figure 5.22. As this happens, the oil viscosity in the oil film is decreasing with speed, and thus the effect of speed on the friction coefficient is negated.

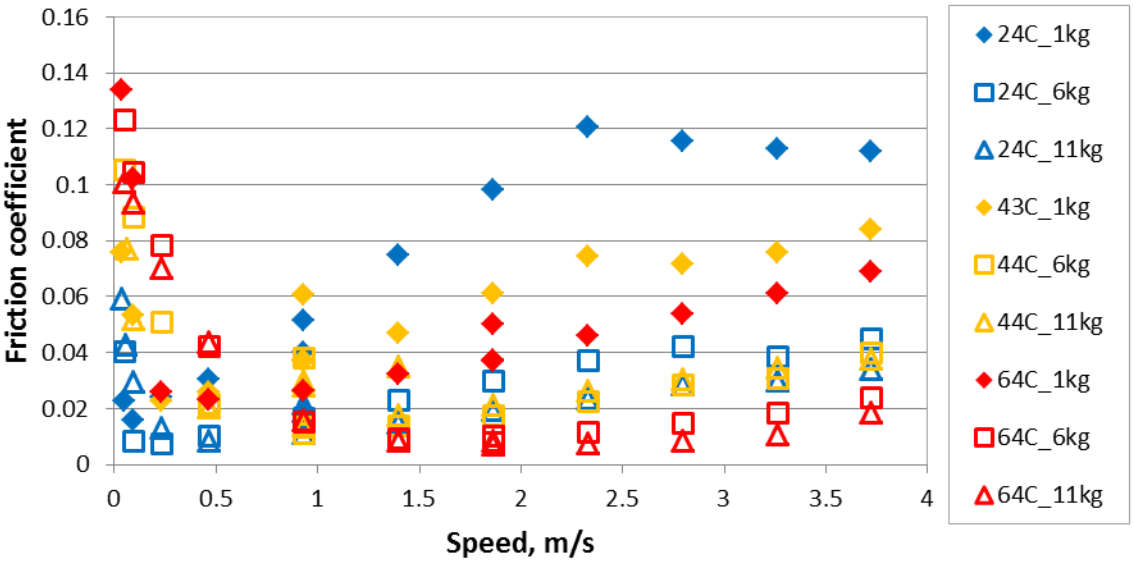

Figure 5.21: Friction coefficient as function of speed at several applied loads and oil temperatures for 15W40 Base oil

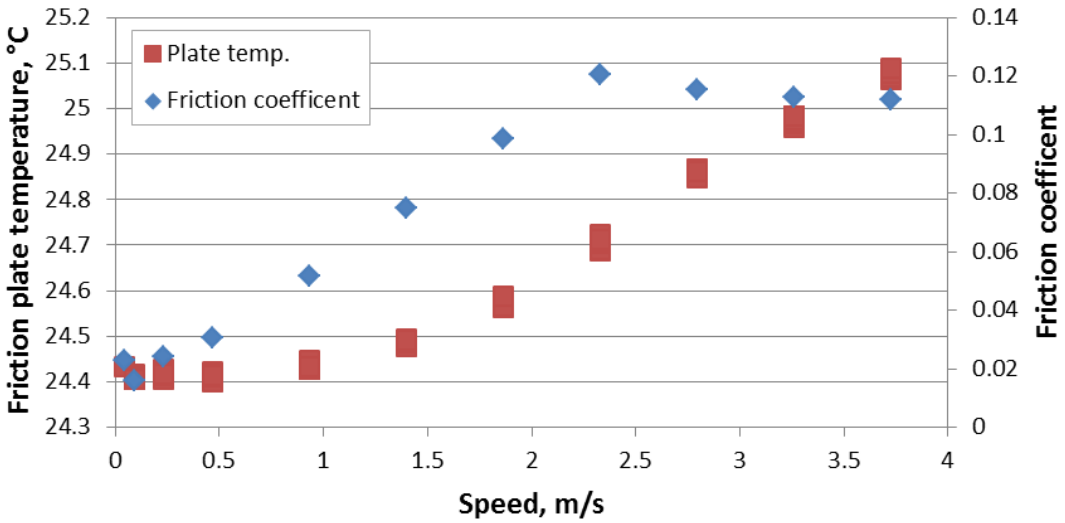

Figure 5.22: Effect of speed on friction plate temperature and friction coefficient at 24°C average oil temperature and 1 kg applied normal load

Results for the commercial 15W40 oil are similar to the base oil as shown in Figure 5.23. For this oil, the friction coefficients do not change as drastically with temperature. This result does not agree with the Stribeck curve since the viscosity of the commercial 15W40 has a greater rate of change with temperature than the base oil. It is not clear why this is occurring and may have to do with some effects not consider in a typical Stribeck curve such as a new plate and cylinder being used for the base oil, whereas the plate and cylinder for the commercial oil have more run time. The friction coefficients decrease with increasing load for the 15W40 commercial oil which agrees with the results from the base oil.

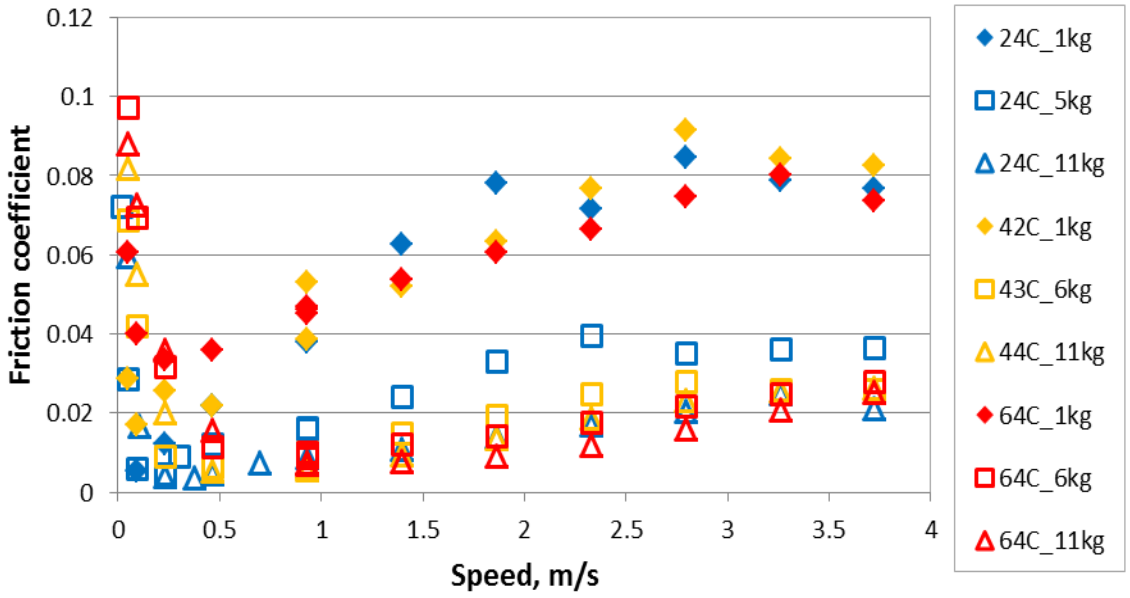

Figure 5.23: Friction coefficient as function of speed for 15W40 weight oil at various average oil temperatures and applied normal loads

Using the FindFit command in Mathematica, the friction coefficients obtained from the line contact rig are fitted to the modified Stribeck curve equation described by Equation 3.4. Some of the fits seen in Figure 5.24 however produce negative friction coefficients caused by a zero denominator in the modified Stribeck equation at certain speeds (see Equation 3.4). With negative friction coefficients the fit is unusable as this causes a failed simulation. To eliminate this problem, several methods to manipulate the data before fitting are employed which include: trimming data, interpolating data, and/or setting conditions to the fit. The method used is dependent on the data and requires trial and error to obtain the best fit. An example of a fit created by eliminating the first data point and then interpolating to provide more points for the fit is shown in Figure 5.25.

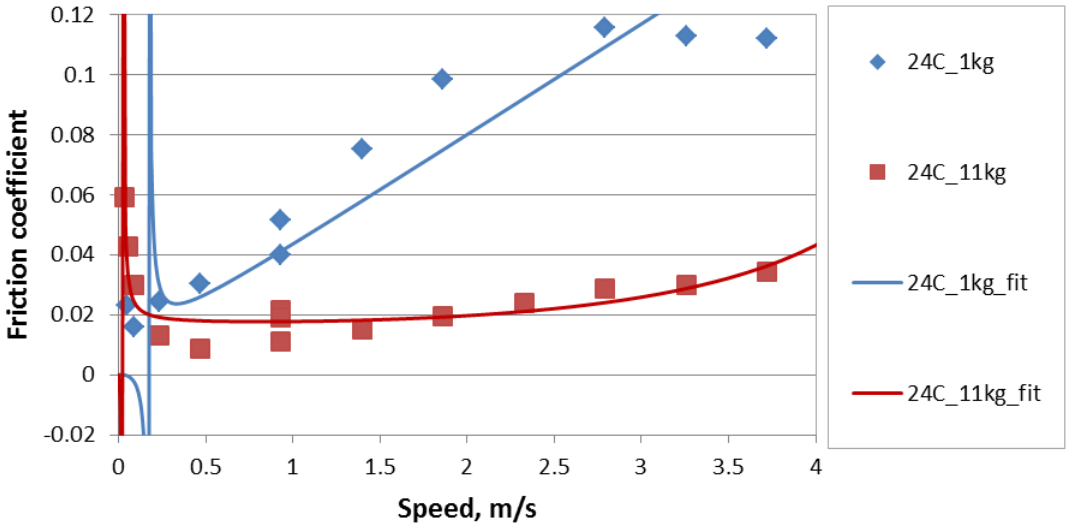

Figure 5.24: Example of modified Stribeck curve fits with negative friction coefficients

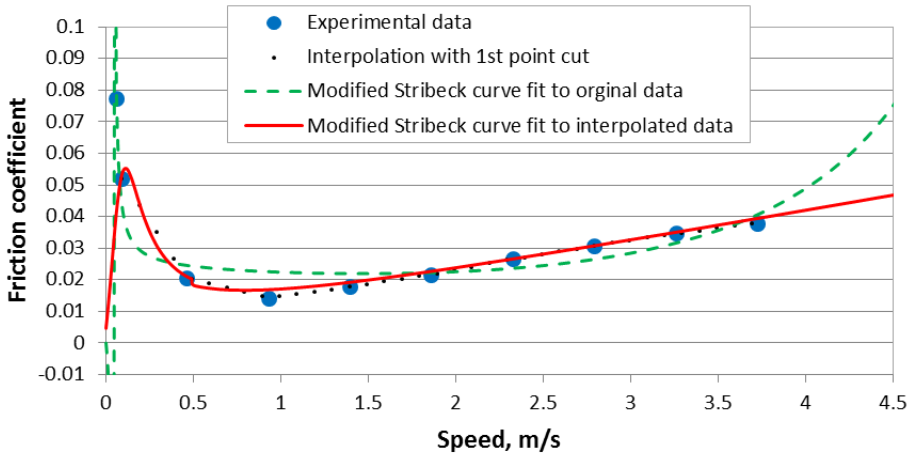

Figure 5.25: Comparison of fits without and with editing original data for 15W40 base oil measured at 44C and 11kg load

To simulate engine friction, six friction coefficient curves are selected for each oil. These curves are selected to represent minimum and maximum friction coefficients over a range of temperatures and loads in order to reduce simulation time. Figure 5.26 shows seven fits for the 15W40 base oil which are calculated at normal loads of 1 and 11 kg and temperatures of 24, 36, and 64°C. Only the data set at 64°C with applied normal load of 1 kg shown in purple is fitted without any manipulation. The rest of the data are focused on the hydrodynamic section of the curve (abbreviated as hydro), the data trimmed, and/or interpolated (abbreviated as interp.) so that a fit can be created. The 24°C and 1 kg results are significantly trimmed so that the fit follows the linear increase during the initial points of the hydrodynamic regime. This was done since hydrodynamic friction should consistently increase and the constant friction coefficients at high speeds are likely due to a localized temperature increase in the oil film caused by hydrodynamic friction. Hysteresis errors can be seen in the experimental data for 43°C and 1 kg at 0.93 m/s. The outlier is measured at the end of the experiment

transitioning from a higher speed; whereas, normally data is taken sequentially starting at the lowest speed.

Similar results are obtained for the 15W40 commercial oil as seen in Figure 5.27. As with the base oil, only the data set at 64°C with applied normal load of 11 kg shown in red is fitted without any manipulation. Data sets at 24 and 36°C and 1 kg normal load are significantly trimmed to eliminate the constant friction coefficients at high speed. With this trim, the curve fit for the 24 and 36°C and 1 kg normal load data sets are basically linear producing friction coefficients above the boundary friction coefficient of 0.1 at speeds over 2 m/s. Figure 5.27 shows a comparison between a hydrodynamic curve fit and a curve fit of all the data for the 24°C and 11 kg load data. The hydrodynamic curve fit is not required for this data set and is included so that simulated friction for the two fit methods can be compared. The comparison is discusses later in this chapter.

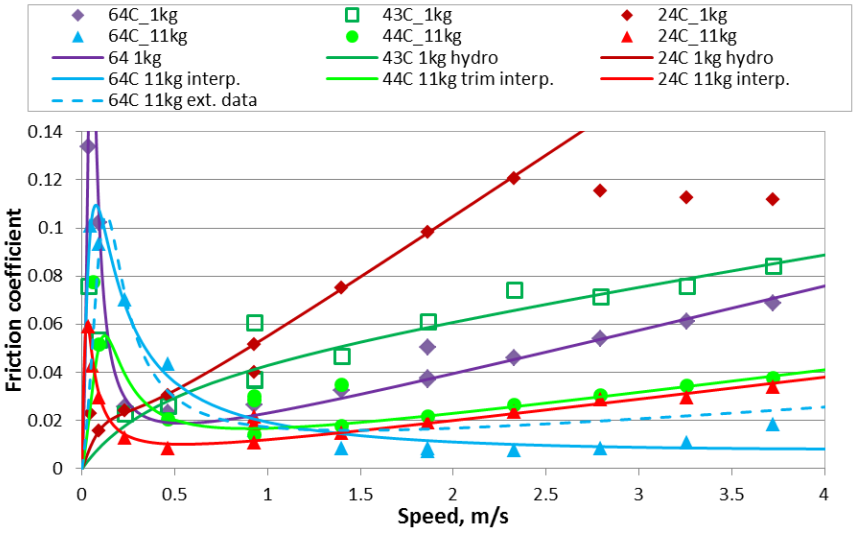

Figure 5.26: 15W40 base oil experimental friction coefficients and friction coefficients predicted by fits to modified Stribeck curve

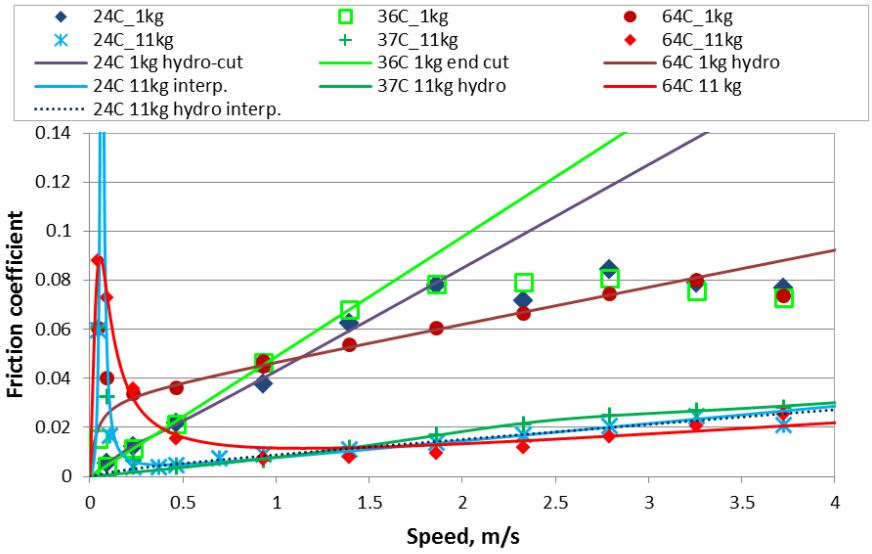

Figure 5.27: 15W40 experimental friction coefficients and friction coefficients predicted by fits to modified Stribeck curve

5.5 Simulation results using measured friction coefficients with comparison to motored engine results

The feasibility of using AVL Excite Power Unit to predict lube oil performance is examined by comparing simulation results to those obtained from the modified Hatz engine with external oil pump. Simulations are performed for 15W40 base and its associated commercial 15W40 oil using fits to the modified Stribeck curve as described in the previous section. For each oil, three different temperatures and two loads are simulated.

The simulation results for the 15W40 base oil shown as single data points generally under predict measured fmep shown as numerous blue diamonds in Figure 5.28. Results for an applied normal load of 11 kg shown as open symbols

are not significantly different than the fmep corresponding to simulated cylinder gas pumping losses shown as a dotted and dashed line which is representative of the losses in the engine without considering friction. Simulated fmep for 24 and 44°C at 11 kg are virtually identical which is due to very similar friction coefficient fit curves for these two conditions as shown in Figure 5.26. The influence of the hydrodynamic regime of the friction coefficients fits on the simulated results is clearly seen in the 64°C/1kg data. For this condition, the friction coefficients are nearly double the others for the same load at low speed but the simulated fmep is lower than the other results due to lower friction coefficients in the hydrodynamic regime. Furthermore, adjusting the fit to increase the friction coefficient in the hydrodynamic regime produces increased simulated fmep shown as a red bar in Figure 5.28.

Simulated fmep for the base oil at an applied load of 1 kg is significantly higher than the results for the 11 kg applied load at 24 and 64°C. The simulated fmep for 43°C and 1kg does not match the other results at the same load. This is again related to the hydrodynamic section of the fit. For this data point, the slope of the fit is decreasing and intersects the fit for 64°C and 1 kg at 6 m/s. Thus the simulated results are very similar since the engine journals bearings operate at approximately 4.5 m/s and piston at average speed of approximately 4 m/s and maximum of 7 m/s.

Simulated result for the 15W40 commercial oil are similar with simulated fmep shown as single data points generally under predicting measured fmep shown as the blue diamond data points in Figure 4.29. Like the base oil, simulations for 11 kg applied load shown as open data points are not significantly different from the cylinder gas pumping losses shown as a dashed and dotted line. The lack of influence by the boundary friction portion of the fit to simulated results is shown by the two data points corresponding to 24°C and 11 kg. The

data point shown as a bar corresponds to a fit to the hydrodynamic portion of the friction coefficients shown as a dotted line in Figure 5.27 which does not include the boundary section of the data as the fit shown as a solid blue line shown in the same figure does. However, even though there is a significant peak in friction coefficient at low speed for one of the fits the simulated fmep is nearly identical since the hydrodynamic sections of the fit are so alike. This is due to the relationship between piston speed and piston/cylinder force with the piston force approaching zero as speed approaches zero. The simulation results for 36 and 64°C at 1 kg load are much closer to measured values and indicate a trend. However, this trend does not continue with the results for 24°C and 1 kg. The result follows the fit though with the fit for 24°C and 1 kg predicting lower friction coefficients versus speed than the same load at 36°C. Whether 36°C and 1 kg friction coefficients are over predicted or 24°C and 1 kg is under predicted is not clear. Therefore, which of the two simulated fmeps are likewise over or under predicted is unclear as well.

Regardless of the oil the simulated, fmep generally under predicts measured results and simulated results are inconsistent. However, this is directly caused by the modified Stribeck curve fits to measured friction coefficients and particularly the hydrodynamic regime of the fit. Furthermore, friction coefficients with higher measured friction coefficients do not necessarily correspond to a steeper hydrodynamic slope for the fit. This can cause predicted friction coefficients for one data set to become lower than another when the measured friction coefficients are higher. Simulated results could be improved by improving friction coefficient measurement and fitting the data. A curved plate instead of flat could improve results from the line contact friction rig. The rings are not included in this model which accounts from some of the under prediction. Therefore, including the rings in the model or accounting for them in some way may make simulated results more accurate.

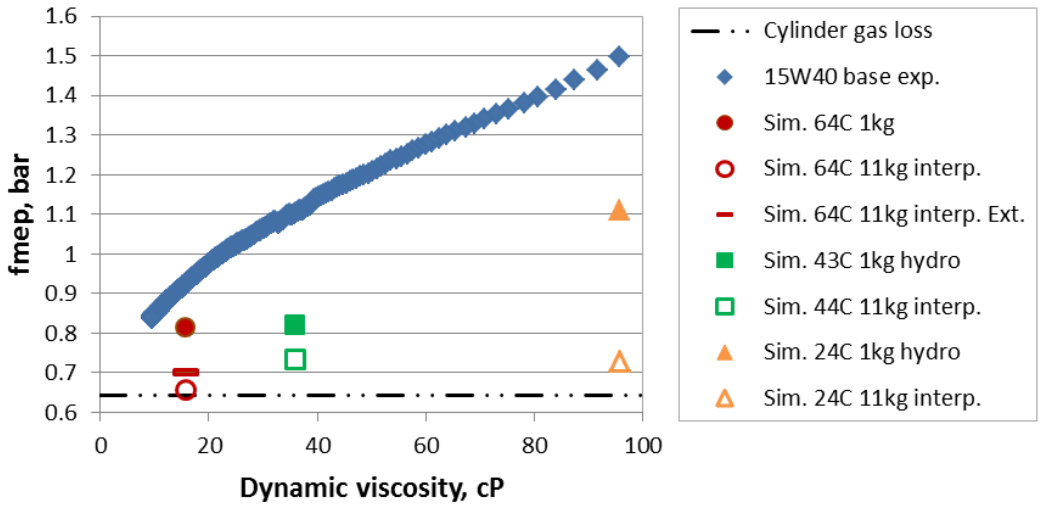

Figure 5.28: Comparison of 15W40 base oil experimental and simulation results

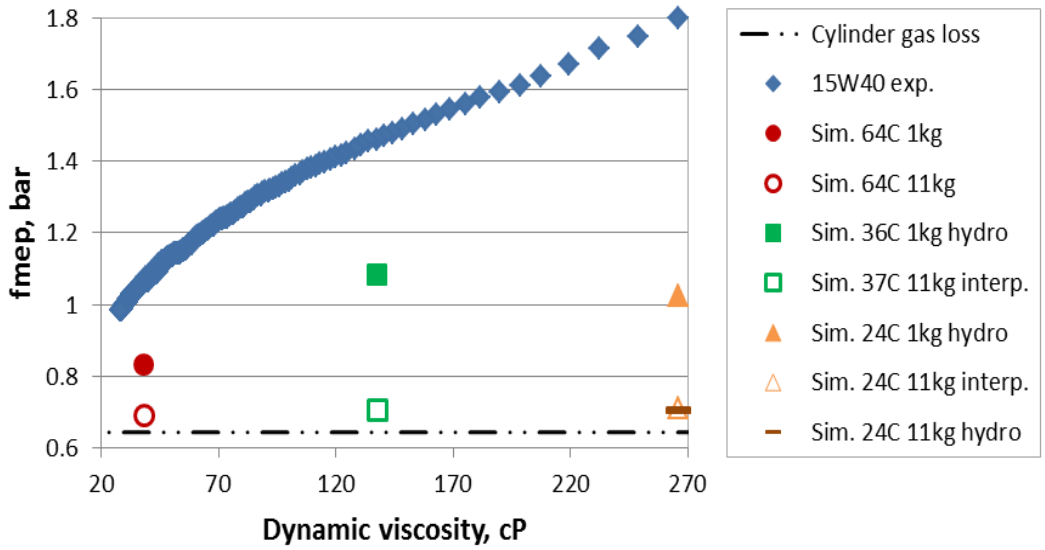

Figure 5.29: Comparison of 15W40 experimental and simulation results

CHAPTER 6
CONCLUSIONS

The feasibility of using a small, single-cylinder motored engine to evaluate lube oil performance at a reduced complexity and cost while approaching fired engine conditions is investigated. The motored engine friction rig is based on an air cooled 517cc single-cylinder diesel engine operated in three different configurations. The first engine configuration which operates without compression and has the push rods and intake valve removed is referred to as the modified engine with internal oil pump. The second engine configuration, referred to as the modified engine with external oil pump; this engine is also operated without compression as well and with the push rods, intake valve, timing gears, and internal oil pump removed. For the final configuration an unmodified engine with compression is used and referred to as the stock engine. By using a combination of an engine enclosure, oil sump heater, and engine cowling the engine temperatures can be increased to approximately 75°C for the modified engine and 100°C for the stock engine. Lube oil performance is evaluated either through motoring torque over an engine cycle (instantaneous motoring torque) or friction mean effective pressure (fmep). For the latter, the lube oil performance is evaluated by plotting the fmep as a function of lube oil dynamic viscosity calculated using the Vogel's equation with mid-stroke cylinder liner temperature; at a given dynamic viscosity the lube oil formulation which results in a lower fmep produces lower engine friction.

The feasibility of using the motored engine friction rig to evaluate lube oil performance is investigated by examining instantaneous motoring torques produced by a commercial 5W30 oil and a 5W20 oil in three stages of production — base oil, commercial oil with additives, and commercial oil without additives. For the commercial 5W30 oil the instantaneous motoring torques are obtained

over a range of viscosities, from which the effect of viscosity on the instantaneous motoring torque can be observed. These instantaneous motoring torques are obtained using the modified engine without compression equipped with external oil pump at a constant speed of 1800 RPM. The peaks in the instantaneous motoring torque curves are found to decrease during the duration of the test for the 5W30 oil. The reduction in the peak torques can be attributed to an increase in the engine temperature over the duration of the test, resulting in a decrease in the oil viscosity. The peak motoring torque produce by the 5W30 oil is reduced by approximately 3 N.m between the beginning and the end of the test, which is 30% of the maximum instantaneous motoring torque. The effect of additives on engine friction is investigated through the evaluation of instantaneous motoring torque plots for the 5W20 oil in three different stages of production at a viscosity of approximately 16 cP. The instantaneous motoring torque curves obtained for the base oil cannot be compared to those obtained for the two commercial oil — with and without additives — due to the base oil being much thinner and thus reaching the viscosity of 16 cP much earlier in the test where start-up effects can strongly affect the instantaneous torques curves. For the commercial oil with additives, a slight increase of 6% in peak instantaneous motoring torques is observed over the oil without additives.

The motored engine friction rig is also used to evaluate lube oil performance via friction mean effective pressure (fmep) using the modified engine with external oil pump (no compression). A 5W20 oil in the three different stages of production — base oil, commercial oil without additives, and a commercial oil — is investigated. At a given viscosity the base oil is found to produce higher friction than the two commercial oils (with and without additives), which can be attributed to increased boundary friction due to the thinner oil, particularly during start-up. Furthermore, the commercial oil without additives is shown to have lower friction than the commercial oil. Additive effects on engine

friction are also observed for the stock engine (with compression) using a base oil, base oil with typical additive, and a base oil with developmental additive. The base oil with developmental additive is shown to increase friction over the base oil, whereas the base oil with typical additive is observed to reduce friction. In summary, based on the results obtained from the motored engine friction rig show it is feasible to evaluate lube oil performance and additive effects using fmep. The frictional contribution of several engine components is also investigated by comparing friction mean effective pressures for 5W30 oils and the various engine configurations. The piston, piston rings, and journal bearings are found to contribute the most at approximately 45% of total fmep, the valve train approximately 35%, and the engine oil pump roughly 20%. Thus, it is possible to use the motored engine friction rig to evaluate lube oil performance and additives effects through the instantaneous motoring torques and the fmep.

The feasibility of using the commercial engine modeling software AVL Excite Power Unit to simulate the effect of lube oil formulation on the friction of the Hatz 1D50 engine is also investigated. Friction is predicted by the software via a modified Stribeck curve obtained with a line contact friction rig for two different oils, a 15W40 base oil and commercial 15W40 oil. The engine friction results predicted by the modeling software AVL Excite Power Unit are similar for the two oils and approximately 26% lower than those from the motored Hatz single-cylinder engine, showing that simulation results are highly dependent on the measured friction coefficients and the fit of the modified Stribeck curve.

BIBLIOGRAPHY

[1] "Who Invented the Automobile?," The Library of Congress, [Online]. Available: http://www.loc.gov/rr/scitech /mysteries/auto.html. [Accessed 12 2012].

[2] J. Sousanis, "World Vehicle Population Tops 1 Billion Units," WardsAuto, 15 Aug. 2011. [Online]. Available: http://wardsauto.com/ar/world_vehicle_population_110815. [Accessed 8 12].

[3] "2010 World Population Data Sheet," Population Reference Bureau, [Online]. Available: http://www.prb.org/pdf10/10wpds_eng.pdf.

[4] D. E. Richardson, "Review of Power Cylinder Friction for Diesel Engines," *Journal of Engineering for Gas Turbines and Power,* 2000.

[5] R. Giannelli, E. Nam, K. Helmer, T. Younglove, G. Scora and M. Barth, "Heavy-Duty Diesel Vehicle Fuel Consumption Modeling Based on Road Load and Power Train Parameters," *SAE Technical Paper,* no. 2005-01-3549, 2005.

[6] "EPA's Fuel Economy Programs," Environmental Protection Agency, [Online]. Available: http://www.epa.gov/fueleconomy/420f09067.pdf. [Accessed November 2012].

[7] Environmental Protection Agency, [Online]. Available: http://www.epa.gov/fueleconomy/guzzler/420f12068.pdf. [Accessed November 2012].

[8] "CAFE - Fuel Economy," National Highway Traffic Safety Administration, [Online]. Available: http://www.nhtsa.gov/fuel-economy. [Accessed November 2012].

[9] whitehouse.gov, "Driving Efficiency: Cutting Costs for Families at the Pump and Slashing Dependence on Oil," [Online]. Available: http://www.whitehouse.gov/sites/default/files/fuel_economy_report.pdf. [Accessed November 2012].

[10] R. LaHood, "The White Hose Blog - Historic Fuel Efficiency Standards for Cars and Light Trucks," [Online]. Available: http://www.whitehouse.gov/blog/2012/08/28/historic-fuel-efficiency-standards-cars-and-light-trucks. [Accessed November 2012].

[11] "whitehouse.gov - Obama Administration Finalizes Historic 54.5 MPG Fuel Efficiency Standards," [Online]. Available: http://www.whitehouse.gov/the-press-office/2012/08/28/obama-administration-finalizes-historic-545-mpg-fuel-efficiency-standard. [Accessed November 2012].

[12] "Table 4-23: Average Fuel Efficiency of U.S. Light Duty Vehicles," Research and Innovative Technology Administration (RITA), [Online]. Available: http://www.bts.gov/publications/national_transportation_statistics /html/table_04_23.html. [Accessed November 2012].

[13] M. Priest and C. Taylor, "Automobile Engine Tribology - Approaching the Surface," *Wear,* vol. 241, no. 2, pp. 193-203, 31 July 2000.

[14] T. Miller, "The Road to Improved Heavy Duty Fuel Economy," Directions in Engine-Efficiency and Emissions Research, 2010.

[15] S. I. Tseregounis, M. L. McMillan and R. M. Olree, "Engine Oil Effects on Fuel Economy in GM Vehicles -- Separation of Viscosity and Friction Modifier Effects," *SAE Technical Paper,* no. 982502, 1998.

[16] "Summary of Fuel Economy Performance (Public Version)," US Department of Transportation, 2011.

[17] B. Bhushan, Modern Tribology Handbook, vol. Two, CRC Press, 2001.

[18] E. Durack, C. Kurganoglu, A. Biyiklioglu and H. Kaleli, "Measurement of Friction Force and Effects of Oil Fortifier in Engine Journal Bearings Under Dynamic Loading Conditions," *Tribology International, Volume 36, Issue 8, ISSN 0301-679X, 10.1016/S0301-679X(02)00263-3,* pp. 599-607, August 2003.

[19] Y. Hori, Hydrodynamic Lubrication, Springer, 2005.

[20] R. Coy, "Practical Applications of Lubrication Models in Engines," *Tribology International,* vol. 31, no. 10, pp. 563-571, October 1998.

[21] K. Holmberg, P. Andersson and A. Erdemir, "Global Energy Consumption Due to Friction in Passenger Cars," *Tribology International,* vol. 47, pp. 221-234, 2012.

[22] D. Sandoval and J. Heywood, "An Improved Friction Model for Spark-Ignition Engines," *SAE Technical Paper,* no. 2003-01-0725, 2003.

[23] S. Furuhama and M. Takiguchi, "Measurement of Piston Frictional Force in Actual Operating Diesel Engine," *SAE Technical Paper,* no. 790855, 1979.

[24] O. Reynolds, "On the Theory of Lubrication and its Application to Mr. Beauchamp Tower's Experiments, Including an Experimental Determination of the Viscosity of Olive Oil," *Philosophical Transactions of the Royal Society, Part I.,* pp. 228-310, 1886.

[25] P. Shayler, A. Allen, D. Leong, I. Pegg, A. Brown and J. Dumenil, "Characterizing Lubricating Oil Viscosity to Describe Effects on Engine Friction," *SAE Technical Paper,* no. 2007-01-1984, 2007.

[26] Y. Wang, C. Zhang, Q. J. Wang and C. Lin, "A mixed-TEHD Analysis and Experiment of Journal Bearings Under Severe Operating Conditions," *Tribology International,* vol. 35, pp. 395-407, 2002.

[27] G. Livanos and N. Kyrtatos, "A Model of the Friction Losses in Diesel Engines," *SAE Technical Paper,* no. 2006-01-0888, 2006.

[28] H. Allmaier, C. Priestner, F. Reich, H. Priebsch and F. Novotny-Farkas, "Predicting Friction Reliably and Accurately in Journal Bearings - Extending the EHD Simulation Model to TEHD," *Tribology International,* vol. 58, pp. 20-28, 2013.

[29] G. Offner, H. Herbst and H. Priebsch, "A Methodology to Simulate Piston Secondary Movement under Lubricated Contact Conditions," *SAE Technical Paper,* no. 2001-01-0565, 2001.

[30] P. Jost, "Tribology: How a Word was Coined 40 Years Ago," *Tribology and Lubrication Technology,* pp. 24-28, March 2006.

[31] "Multiyear Download of UK Government Spending," [Online]. Available: http://www.ukpublicspending.co.uk/download_multi_year_ 1960_2015UKp_10c1li011mcn_F0t. [Accessed March 2013].

[32] A. Cameron and C. Ettles, Basic Lubrication Theory, 3rd ed., Horwood Ltd., 1981.

[33] E. Rabinowicz, Friction and Wear of Materials, Wiley, 1995.

[34] "Basics of Lubrication," Society of Tribologists and Lubrication Engineers (STLE), [Online]. Available: http://www.stle.org/resources/lubelearn/lubrication/default.aspx. [Accessed November 2012].

[35] B. Tower, "First Report on Friction Experiments (Friction of Lubricated Bearings)," *Proceedings of the Institution of Mechanical Engineers,* pp. 58-70, 1883.

[36] B. Tower, "Second Report on Friction Experiments (Experiments on Oil Pressure in Bearings)," *Proceedings of the Institution of Mechanical Engineers,* pp. 58-70, 1885.

[37] Y. Cengel and M. Boles, Thermodynamics an Engineering Approach, 5th edition, McGraw-Hill, 2006.

[38] A. Gauthier, B. Constans, H. Perrin and F. Roux, "Lubricants Effects on Piston/Rings/Liner Friction in an Instrumented Single Cylinder Diesel Engine," *SAE Technical Paper,* no. 872034, 1987.

[39] R. R. Malagi, S. N. Kurbet and R. Krishnakumar, "A Comprehensive Model to Study the Dynamic Motion of Piston and Friction and Lubrication in I.C. Engine," *SAE Technical Paper,* no. 2008-28-0061, 2008.

[40] H. Allmaier, C. Priestner, F. Reich, H. Priebshc, C. Forstner and F. Novotny-Farkas, "Predicting Friction Reliably and Accurately in Journal bearings - The Importance of Extensive Oil Models," *Tribology International,* vol. 48, pp. 93-101, April 2012.

[41] J. Sorab, S. Korcek and C. Bovington, "Friction Reduction in Lubricated Components Through Engine Oil Formulation," *SAE Technical Paper,* no. 982640, 1998.

[42] J. B. Heywood, Internal Combustion Engine Fundamentals, McGraw-Hill, 1988.

[43] G. W. Stachowiak and A. W. Batchelor, Engineering Tribology, Third ed., Butterworth-Heinemann, 2005.

[44] U. Mokhiamer, W. Crosby and H. El-Gamal, "A Study of a Journal Bearing Lubricated by Fluids with Couple Stress Considering the Elasticity of the Liner," *Wear,* vol. 224, no. 2, pp. 194-201, February 1999.

[45] H. Allmaier, C. Priestner, C. Six, H. Priebsch, C. Forstner and F. Novotny-Farkas, "Predicting Friction Reliably and Accurately in Journal Bearings - A Systematic Validation of Simulation Results with Experimental Measurements," *Tribology International,* vol. 44, no. 10, pp. 1151-1160, September 2011.

[46] R. Taylor, "Lubrication, Tribology & Motorsport," *SAE Technical Paper,* no. 2002-01-3355, 2002.

[47] S. Bukovinik, N. Dorr, V. Caika, W. J. Bartz and B. Loibnegger, "Analysis of Diverse Simulation Models for Combustion Engine Journal Bearings and the Influence of Oil Condition," *Tribology International,* vol. 39, no. 8, pp. 820-826, August 2006.

[48] J. McGeehan, "A Literature Review of the Effects of Piston and Ring Friction and Lubricating Oil Viscosity on Fuel Economy," *SAE Technical Paper,* no. 780673, 1978.

[49] D. K. W. Leong, P. J. Shayler, I. G. Pegg and M. Murphy, "Characterizing the Effect of Viscosity on Friction in the Piston Assembly of Internal Combustion Engines," *Journal of Engineering Tribology.*

[50] R. Stone, Introduction to Internal Combustion Engines, 3rd ed., SAE International and Macmillan Press, 1999.

[51] C. Sethu, M. E. Leustek, S. V. Bohac, Z. S. Filipi and D. N. Assanis, "An Investigation in Measuring Crank Angle Resolved In-Cylinder Engine Friction Using Instantaneous IMEP method," *SAE Technical Paper,* no. 2007-01-3989, 2007.

[52] J. Greenwood and J. Tripp, "The Contact of Two Nominally Flat Rough Surfaces," *Proceedings of the Institution of Mechanical Engineers,* vol. 185, pp. 625-623, 1970.

[53] ALTUGLAS, "Plexiglas: Optical and Transmission Characteristics," [Online]. Available: http://www.atoglas.com/literature/pdf/81.pdf. [Accessed 9 4 2013].

[54] "Thermal Conductivity of Metals," Engineeringtoolbox.com, [Online]. Available: http://www.engineeringtoolbox.com/thermal-conductivity-metals-d_858.html. [Accessed 10 4 2013].

[55] P. Incropera, D. Dewitt, T. Bergman and A. Lavine, Fundamentals of Heat and Mass Transfer, Sixth Edition, John Wiley and Sons, 2007.

[56] P. J. Shayler, D. K. W. Leong and M. Murphy, "Contributions to Engine Friction During Cold, Low Speed Running and the Dependence on Oil Viscosity," *SAE Technical Paper,* no. 2005-01-1654, 2005.

APPENDIX

APPENDIX A: Nomenclature

Abbreviations

AC	alternating current
BDC	bottom dead center
bmep	brake mean effective pressure
CAD	computer-aided design
CAFÉ	Corporate Average Fuel Economy
CCS	cold cranking simulator
conrod	connecting rod
CPU	central processing unit
DAQ	data acquisition system
DC	direct current
DOE	United States Department of Energy
ECR	electrical contact resistance
EHD	elastohydrodynamic
EPA	United States Environmental Protection Agency
FEM	finite element method
fmep	friction mean effect pressure
HTHS	high-temperature, high-shear
ICE	internal combustion engine
imep	indicated mean effective pressure
NTRC	National Transportation Research Center
PC	personal computer
STL	sterotithograph file
T/C	thermocouple
TDC	top dead center
TEHD	thermo-elasto-hydrodynamic
U.S.	United States of America
VDC	Volts direct current
VI	viscosity index
WOT	wide open throttle
ZDDP	Zinc DialkylDithioPhosphate

Symbols

£	pound sterling
A	Area
$\widetilde{A}$	total contact area
A_a	apparent area
A_c	cylinder area
ap_ρ	surface density of asperity peaks
A_r	actual area
d_a	distance between mean asperity height
E'	composite elastic modulus of two materials
e_b	piston eccentricity at bottom of skirt
e_t	piston eccentricity at top of skirt
f	friction coefficient
F_c	conrod force
F_f	friction force
F_{ma}	inertia force
F_n	normal force
F_W	weight
G	Gaussian integral
g	gravity
h	oil film height
H	dimensionless oil film thickness
I_s	system inertia
K	nominal pressure for elastic deformation coefficient
k	thermal conductivity
L	thickness
$\widetilde{N}$	total number of contacts
P	Pressure
$\widetilde{P}_c$	total contact load
p_e	nominal pressure for elastic deformation
P_f^{ring}	Power loss from ring friction
P_g	cylinder gas pressure
q	heat energy
q''	heat flux

r_{ball}	radius of ball
r_v	compression ratio
s	entropy
t	time
T	temperature
U	Surface speed
V	Volume
v	velocity
V_c	clearance volume
v_p	piston velocity
V_s	Engine cylinder swept volume
W	Watt
α	angular acceleration
β	asperity radius of curvature at peak
η	dynamic viscosity
θ	angular position
κ	Barus equation pressure coefficient
ν	kinematic viscosity
ν_H	viscosity at 100°F of a high viscosity index oil
ν_L	viscosity at 100°F of a low viscosity index oil
ν_U	test oil viscosity at 100°F
ρ	density
σ	standard deviation
τ	torque
ω	angular velocity

Units

°C	degrees Celsius
°F	degrees Fahrenheit
cc	cubic centimeter
cP	centipoise
cS	centistokes
g	gram
hp	horse power
Hz	Hertz

m	meter
Mg	mega-gram
mm	millimeter
mPa.s	milli-Pascal second
mpg	miles per gallon
N	Newton
rad	radians
RPM	revolution per minute
s	seconds

Subscripts

i	inlet
m	mean
max	maximum
o	outlet

APPENDIX B: Friction coefficient curve fits

Table B.1: Modified Stribeck curve coefficients for 15W40 oil using data collected with 5lb range load cell

Applied load, kg	Average temp., °C	A, sec^2/m^2	B, sec/m	C, unitless	D, unitless
1	24	1866.06	-492.623	102.829	0.0423498
11	24	1811.74	-228.37	7.48888	0.00714175
11	24	0	267.309	71.7872	0.00594216
1	36	30396.6	326621	-15265.9	0.0488803
11	37	334.095	-1523.53	2130.81	0.00681152
1	64	0	30.7401	0.997223	0.0150182
11	64	158.589	-6.20237	0.47558	0.00509021

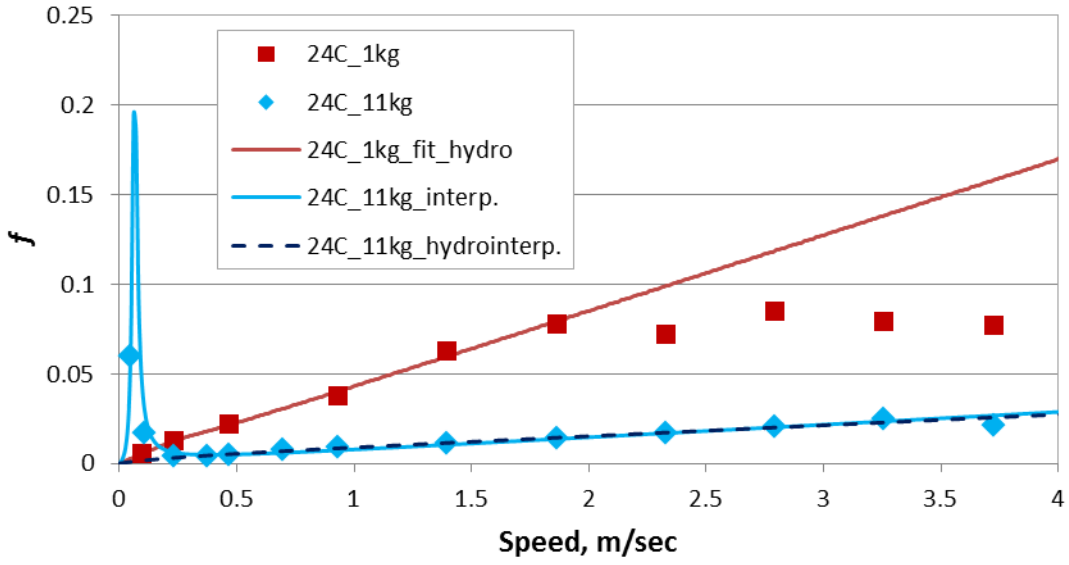

Figure B.0.1: Experimental data and modified Stribeck curve fits for 15W40 oil using 5lb load cell at 24°C

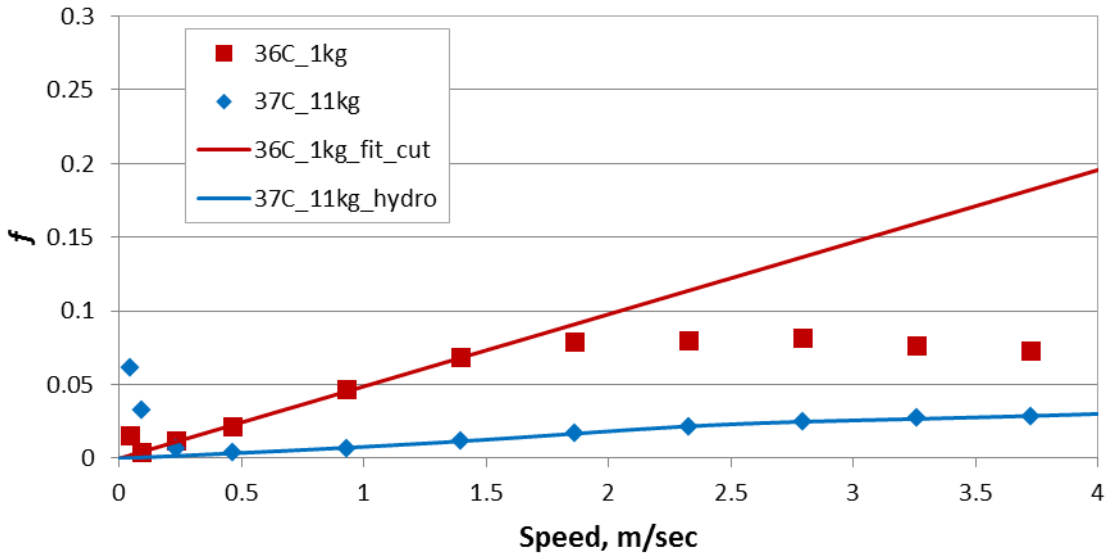

Figure B.0.2: Experimental data and modified Stribeck curve fits for 15W40 oil using 5lb load cell at 36°C

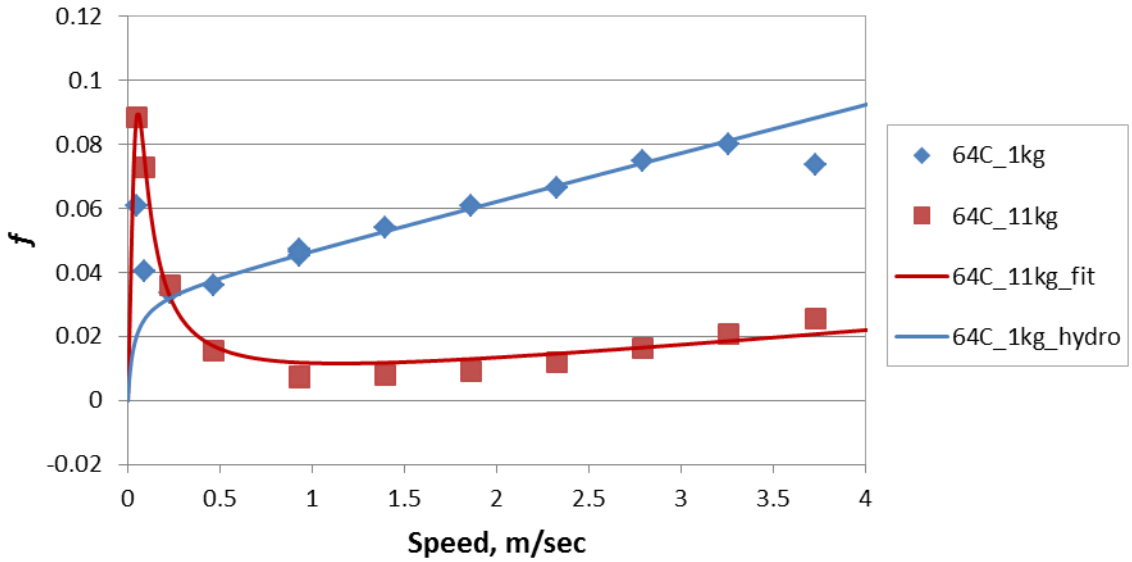

Figure B.0.3: Experimental data and modified Stribeck curve fits for 15W40 oil using 5lb load cell at 64°C

Table B.2: Modified Stribeck curve coefficients for 15W40 base oil using data collected with 5lb range load cell

Applied load, kg	Average temp., °C	A, sec^2/m^2	B, sec/m	C, unitless	D, unitless
1	24	274.633	-2.10063	6.23613	0.0515531
11	24	367.652	-3.23051	0.261636	0.0093463
1	43	0	22.2051	10.2808	0.0121143
11	44	162.766	-20.8022	2.37067	0.00988225
1	64	245.494	-19.5638	0.621467	0.0187188
11	64	52.5922	1.3103	0.291227	0.000868544
11	64	101.996	-16.9741	1.72677	0.00577179

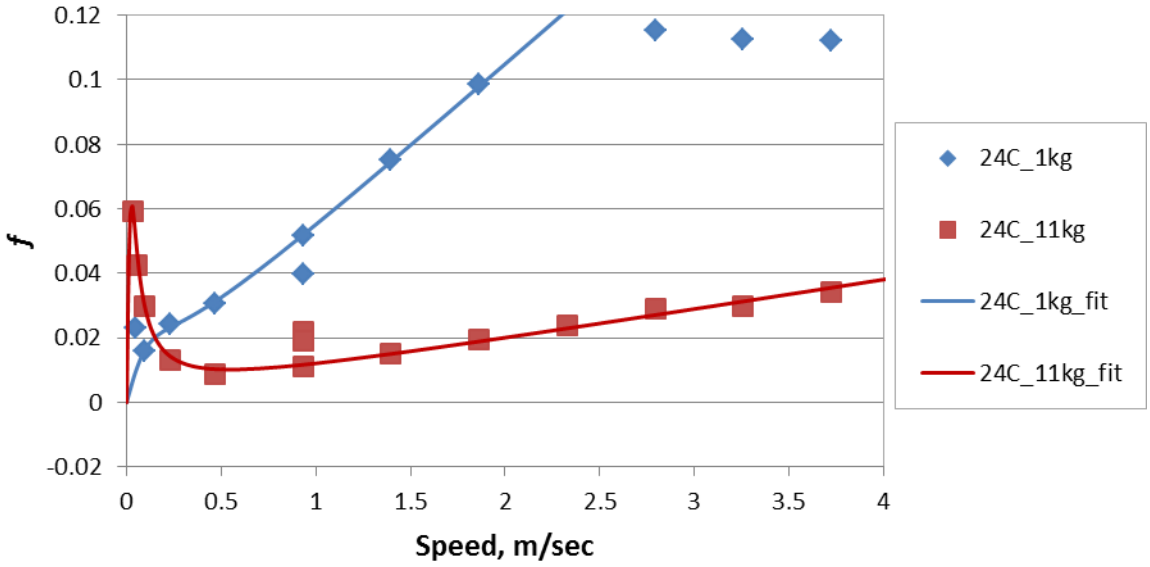

Figure B.0.4: Experimental data and modified Stribeck curve fits for 15W40 base oil using 5lb load cell at 24°C

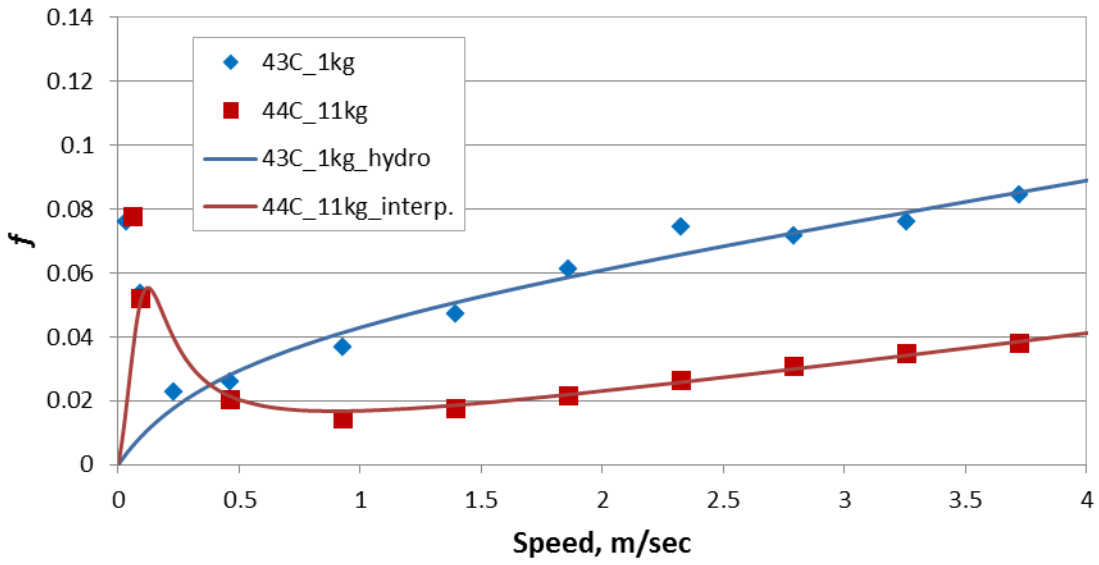

Figure B.0.5: Experimental data and modified Stribeck curve fits for 15W40 base oil using 5lb load cell at 43°C

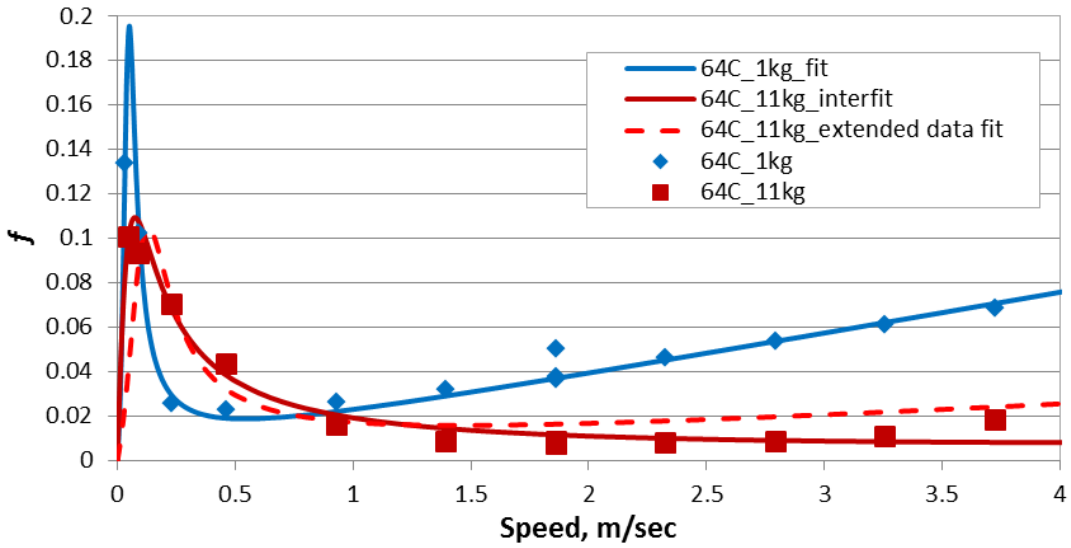

Figure B.0.6: Experimental data and modified Stribeck curve fits for 15W40 base oil using 5lb load cell at 64°C

VITA

William Rohr was born in Tupelo, MS on July 21, 1983. He grew up in Corinth, MS where he lived until moving to Paris, TN at the beginning of high school. While attending the University of Tennessee, Knoxville as a student in mechanical engineering he worked in Circleville, OH for Flour; El Paso, TX for DuPont; and Chattanooga, TN for Wrigley as a maintenance and reliability intern. Mr. Rohr was a member of the University of Tennessee Mini Baja team for three years and competed with the team at two events. The team won first place in the towing event the second year they competed. He graduated with a Ph.D. in mechanical engineering from the University of Tennessee, Knoxville in May 2013.